

**STAR CLUSTERS AS AGE TRACERS OF THE
AGE-METALLICITY RELATION OF THE SMALL
MAGELLANIC CLOUD**

Inauguraldissertation

zur

Erlangung der Würde eines Doktors der Philosophie

vorgelegt der

Philosophisch-Naturwissenschaftlichen Fakultät

der Universität Basel

von

KATHARINA GLATT

aus Känerkinden (Schweiz)

Basel, 2009

Genehmigt von der Philosophisch-Naturwissenschaftlichen Fakultät

auf Antrag von

Prof. Dr. Eva K. Grebel und Prof. Dr. John S. Gallagher

Basel, den 25. November 2008

Prof Dr. Eberhard Parlow
Dekan

**STAR CLUSTERS AS AGE TRACERS
OF THE AGE-METALLICITY RELATION OF THE
SMALL MAGELLANIC CLOUD**

KATHARINA GLATT

Submitted for the Degree of Doctor of Philosophy

Department of Physics and Astronomy
University of Basel, Switzerland

Basel, July 2009

Für meine Familie.

And death shall have no dominion.
Dead men naked they shall be one
With the man in the wind and the west moon;
When their bones are picked clean and the clean bones gone,
They shall have stars at elbow and foot;
Though they go mad they shall be sane,
Though they sink through the sea they shall rise again;
Though lovers be lost love shall not;
And death shall have no dominion.

And death shall have no dominion.
Under the windings of the sea
They lying long shall not die windily;
Twisting on racks when sinews give way,
Strapped to a wheel, yet they shall not break;
Faith in their hands shall snap in two,
And the unicorn evils run them through;
Split all ends up they shan't crack;
And death shall have no dominion.

And death shall have no dominion.
No more may gulls cry at their ears
Or waves break loud on the seashores;
Where blew a flower may a flower no more
Lift its head to the blows of the rain;
Through they be mad and dead as nails,
Heads of the characters hammer through daisies;
Break in the sun till the sun breaks down,
And death shall have no dominion.

Table of Contents

Chapter 1. Motivation	1
Chapter 2. Introduction	3
1. The Small Magellanic Cloud	3
1.1. The Formation and Evolution	5
1.2. The Clouds' Star Clusters	7
2. The Color-Magnitude Diagram	8
3. Age Determination Methods	13
3.1. Isochrones	13
3.2. Relative Ages	16
3.3. The Second Parameter Problem	16
Chapter 3. NGC 121	19
1. Introduction	20
2. Observations and Reductions	21
3. The Color-Magnitude Diagram	24
4. Age of NGC 121	26
4.1. Age Based on Isochrone Fits	26
4.2. Empirical Age Estimates	30
5. Summary and Discussion	33
Chapter 4. Age Determination of Six Intermediate-age SMC Star Clusters with HST/ACS	35
1. Introduction	36
2. Observations and Reductions	38
3. The Color-Magnitude Diagrams	39
3.1. Lindsay 1	41
3.2. Kron 3	43
3.3. NGC 339	43
3.4. NGC 416	45
3.5. Lindsay 38	47
3.6. NGC 419	47
4. BSS candidates	49
5. Cluster Ages	51
5.1. Age of Lindsay 1	53
5.2. Age of Kron 3	54
5.3. Age of NGC 339	56
5.4. Age of NGC 416	57
5.5. Age of Lindsay 38	59
5.6. Age of NGC 419	62
6. Distances	63
7. Discussion	68
7.1. Comparison of our age determination with previous studies	68

7.2. Age range and spatial distribution	71
7.3. Age distribution and cluster formation history	74
7.4. Age-Metallicity Relation	76
7.5. Evolutionary history of the SMC as a whole	77
8. Summary	81
Chapter 5. Structural Parameters of Seven SMC Intermediate-age and Old Star Clusters	83
1. Introduction	84
2. Observation	86
3. Structural Parameters	87
3.1. Centers	87
3.2. King profile	88
3.3. EFF profile	90
3.4. Angular distribution and ellipticity	93
4. Discussion	94
4.1. Comparison of the core radii with previous studies	94
4.2. Age-radius relation	100
4.3. Cluster evolution	101
4.4. Ellipticities	103
5. Summary	104
Chapter 6. Ages of Young SMC Star Clusters	107
1. Introduction	108
2. Literature Data	109
3. Metallicity, Distance Modulus, Depth Extent	109
4. Cluster Age Distribution	110
4.1. Method	110
4.2. Comparison of our age determination with previous studies	111
4.3. Age Distribution	114
4.4. Spatial Age Distribution	116
4.5. Dissolution Effects	117
5. The Cluster Luminosities	120
6. Summary	121
Chapter 7. Summary/ Zusammenfassung	123
Appendix	131
Important Abbreviations	145
Bibliography	147
Acknowledgements	155
Curriculum Vitae	157

Table of Figures

2.1	The Local Group	4
2.2	An interacting triple system	7
2.3	Important features of a CMD	9
2.4	Theoretical evolutionary tracks for different masses	10
2.5	Comparison of Dartmouth isochrones	14
2.6	Age indicators	17
3.1	Photometric errors of NGC 121	23
3.2	CMD of NGC 121	24
3.3	CMD plotting a bona fide sample of NGC 121	25
3.4	CMD with best fitting Padova and Teramo isochrones	26
3.5	CMD with best fitting Dartmouth isochrones	27
3.6	Zoom on MSTO, SGB, and lower RGB region with overplotted Padova and Teramo isochrones	29
3.7	Zoom on MSTO, SGB, and lower RGB region with overplotted Dartmouth isochrones	30
4.1	Spatial Distribution in 2D of SMC star clusters	38
4.2	Photometric errors of Kron 3	40
4.3	CMD of Lindsay 1	41
4.4	CMD showing the central region of Lindsay 1	42
4.5	CMD of Kron 3	42
4.6	CMD showing the central region of Kron 3	43
4.7	CMD of NGC 339	44
4.8	CMD showing the central region of NGC 339	44
4.9	CMD of NGC 416	45
4.10	CMD showing the central region of NGC 416	46
4.11	CMD of Lindsay 38	46
4.12	CMD showing the central region of Lindsay 38	47
4.13	CMD of NGC 419	48
4.14	CMD showing the central region of NGC 419	48
4.15	BSS candidates of Kron 3	50
4.16	Cumulative radial distribution of BSS candidates for NGC 121, Lindsay 1, Kron 3, and NGC 339	51
4.17	Cumulative radial distribution of BSS candidates for NGC 416, Lindsay 38, and NGC 419	52
4.18	CMD with best fitting Padova and Teramo isochrones for Lindsay 1	54

4.19	CMD with best fitting Dartmouth isochrone for Lindsay 1	55
4.20	Zoom on MSTO, SGB, and lower RGB region for Lindsay 1 with overplotted Padova and Teramo isochrones	55
4.21	Zoom on MSTO, SGB, and lower RGB region for Lindsay 1 with overplotted Dartmouth isochrones	56
4.22	CMD with best fitting Padova and Teramo isochrones for Kron 3	57
4.23	CMD with best fitting Dartmouth isochrone for Kron 3	58
4.24	Zoom on MSTO, SGB, and lower RGB region for Kron 3 with overplotted Padova and Teramo isochrones	58
4.25	Zoom on MSTO, SGB, and lower RGB region for Kron 3 with overplotted Dartmouth isochrones	59
4.26	CMD with best fitting Padova and Teramo isochrones for NGC 339	60
4.27	CMD with best fitting Dartmouth isochrone for NGC 339	61
4.28	Zoom on MSTO, SGB, and lower RGB region for NGC 339 with overplotted Padova and Teramo isochrones	61
4.29	Zoom on MSTO, SGB, and lower RGB region for NGC 339 with overplotted Dartmouth isochrones	62
4.30	CMD with best fitting Padova and Teramo isochrones for NGC 416	63
4.31	CMD with best fitting Dartmouth isochrone for NGC 416	64
4.32	Zoom on MSTO, SGB, and lower RGB region for NGC 416 with overplotted Padova and Teramo isochrones	64
4.33	Zoom on MSTO, SGB, and lower RGB region for NGC 416 with overplotted Dartmouth isochrones	65
4.34	CMD with best fitting Padova and Teramo isochrones for Lindsay 38	66
4.35	CMD with best fitting Dartmouth isochrone for Lindsay 38	67
4.36	Zoom on MSTO, SGB, and lower RGB region for Lindsay 38 with overplotted Padova and Teramo isochrones	67
4.37	Zoom on MSTO, SGB, and lower RGB region for Lindsay 38 with overplotted Dartmouth isochrones	68
4.38	CMD with best fitting Padova isochrone for NGC 419	69
4.39	CMD with best fitting Teramo isochrones for NGC 419	70
4.40	CMD with best fitting Dartmouth isochrone for NGC 419	71
4.41	Zoom on MSTO, SGB, and lower RGB region for NGC 419 with overplotted Padova isochrones	72
4.42	Zoom on MSTO, SGB, and lower RGB region for NGC 419 with overplotted Dartmouth isochrones	73
4.43	Age vs distance to the sun	74
4.44	3D distribution for SMC star clusters	75
4.45	Age-metallicity Relation of the SMC	78
4.46	Age-histogram of 15 intermediate-age and old SMC star clusters	80
5.1	Completeness Curves for the F555W and F814W photometry of NGC 339	85
5.2	Star selection to calculate the King and EFF profiles for NGC 339	86
5.3	Number density profiles for the seven SMC clusters in our sample	90
5.4	As for Fig. 5.3 but for NGC 419	91

5.5	Surface-brightness profiles for the seven SMC clusters in our sample	94
5.6	As for Fig. 5.5 but for NGC 419	95
5.7	Difference between $r(\text{King})-r(\text{EFF})$ as a function of c	95
5.8	Surface-brightness profiles for the seven SMC clusters in our sample using stars brighter than the 50% completeness limit and fainter than the MSTO	96
5.9	As for Fig. 5.7 but for NGC 419	97
5.10	Angular distribution for the seven clusters in our sample	98
5.11	Core radii vs distance from the SMC center	99
5.12	Age vs core radius	100
5.13	Age vs ellipticity	103
6.1	CMD of NGC 376	112
6.2	CMD of H86-23	113
6.3	Comparison of the V-band magnitudes found in this study to literature data	114
6.4	Cluster age distribution	115
6.5	Spatial distribution of young SMC star clusters	116
6.6	Spatial distribution of young SMC star clusters in different age bins	118
6.7	Age vs radius	118
6.8	Comparison between V-band magnitudes derived in this study to RZ05	119
6.9	V vs $\log(\text{age})$ and V vs radius using the luminosities adopted from RZ05	120
6.10	V vs $\log(\text{age})$ and V vs radius using the luminosities computed in this study	121

CHAPTER 1

MOTIVATION

“Lasciate ogni speranza, voi ch’entrate!”

Dante Alighieri

The analysis of star clusters is a major tool to obtain information on galaxy formation and evolution. A star cluster is a gravitationally bound concentration of stars having a common chemical and dynamical history. Globular clusters (GCs) are among the oldest objects in the Universe and were studied in all morphological types of galaxies spanning the full Hubble sequence. A typical GC is a very compact object having a mass $\sim 10^4$ - $10^6 M_{\odot}$, which corresponds to a luminosity of $\sim M_V = -5$ to -10 mag. Their properties reflect the conditions of their host galaxies in the earliest stages. The young star clusters, on the other hand, provide information about the galaxy’s present day conditions. The clusters age range and their chemical composition yield information about the evolution of the galaxy. Therefore, star clusters are excellent probes of a galaxy’s chronology. Virtually all stars have originally formed in star clusters, but only a small percentage of old stars are found in a bound system today. Cluster disruption and cluster formation are concurrent in the cluster’s evolution process, where the morphology of the host galaxy has a major influence on the evolution of a star cluster.

Because all stars in a star cluster are of the same age, chemical composition, and distance, conclusions on the formation and evolution of a galaxy can be drawn. The Small Magellanic Cloud (SMC) is a low-mass dwarf galaxy with active star formation that forms, together with the Large Magellanic Cloud (LMC) and the Milky Way (MW), an interacting triple system. The Magellanic Clouds (MCs) are among the closest neighboring galaxies of the MW, which makes them excellent laboratories to study star formation histories and the associated chemical evolution. Since the beginning, the conditions for and the efficiency of star formation have been very different in these three galaxies. The SMC is the only known dwarf galaxy that formed and preserved its star clusters continuously over its entire lifetime. Therefore, these single stellar populations offer a unique possibility to study the age-metallicity relation of this galaxy in detail. However, one has to emphasize that some star clusters seem to be more complex as initially assumed. An increasing number of multiple stellar population objects were discovered in the last five years such as the Galactic globular clusters NGC 2808 (D’Antona et al. 2005; Piotto et al. 2007), NGC 6388 (Piotto 2008), and Omega Centauri (e.g., Bedin et al. 2004; Piotto et al. 2005), as well as some intermediate-age MC clusters (e.g., Mackey & Broby Nielsen 2007; Mackey et al. 2008; Milone et al. 2008, Sabbi et al., in prep.).

The SMC hosts only one ‘true’ globular cluster, which is still several Gyr younger than the ‘typical’ old globular clusters of the LMC, the MW, and all other Galactic companion dwarf galaxies with globulars. It is also intriguing that this cluster is not as metal-poor as the oldest LMC and MW globulars. The SMC must have experienced substantial enrichment prior to the formation of its oldest object. Furthermore, the SMC cannot have experienced a simple chemical evolution where abundances uniformly rose over time: clusters of similar age differ by several tenths dex in metallicity. Only for a few clusters space-based observations are available and cluster ages were mostly performed on ground-based imaging surveys that are limited by crowding and depth and therefore come along with large uncertainties. The extraordinary appearance of the SMC’s age-metallicity relation could be a result of insecure age determination, whereas the wide spread in the metallicity distribution was confirmed by recent chemical abundance measurements (e.g., Da Costa & Hatzidimitriou

1998, Kayser et al., in prep). Since the interstellar medium (ISM) of dwarf galaxies is chemically well-mixed, proving or disproving that clusters of significantly different metallicity exist at a given age is important for constraining the galaxy evolution models.

The main goal of this Thesis was to determine accurate ages of seven key star clusters of which some have similar ages (which can differ by several Gyr in previous studies) but differ by several tenths dex in metallicity. For my approach I use metallicity information and theoretical isochrones fitting of main-sequence turn-offs, subgiant branches, and red clump/horizontal branches simultaneously. The clusters have been observed with the Advanced Camera for Surveys (ACS) aboard the Hubble Space Telescope (HST) as part of a program focussed on star clusters and field stellar populations in the SMC. In the course of this work, a homogeneous set of fiducial ridgelines was provided that can be compared to stellar evolution theories. The capability of the HST/ACS provides an improvement both in depth as well as in angular resolution, which is essential for the reliable photometric age determination in these dense star clusters. The derived ages were combined with cluster ages and spectroscopically derived metallicities from the literature to obtain an accurate age-metallicity relation of the SMC. From our photometry, accurate distances from the Sun were calculated, which confirmed the SMC's large depth extent along the line-of-sight. Structural parameters were determined such as core radius, tidal radius, and ellipticity, which we can compare with previous results from the literature and to structure parameters of clusters in other galaxies to draw conclusions on their evolution.

Recent studies have suggested that the MCs only entered the vicinity of the MW fairly recently (e.g., Kallivayalil et al. 2006a/b) and the most recent proper motion measurements indicate that the MCs are currently on their first passage around the MW. Because the SMC is part of a triple system, its star formation can be triggered by interactions with the MW and the LMC. Evidence for episodic star formation was found by analyzing the age distribution of SMC star clusters younger than 1 Gyr (Chiosi et al. 2006) based on data from the Optical Gravitational Lensing Experiment (Udalski et al. 1998a). The MCs host massive, intermediate-age, *populous* clusters, which are not found in the Milky Way. The reason for this difference in star formation pattern in low density galaxy disks lies presumably in the different structure and star formation histories of these three galaxies. Compact, long-lived star clusters can only form in very dense ISM environments where star formation proceeds with high efficiency. Such conditions were common in the first few billion years after the Big Bang, but present-day globular cluster formation seems to occur most frequently in starburst galaxies and/or in galaxies undergoing violent interactions. In these cases massive, compact star clusters are believed to be produced through strong shock compressions of the ISM induced by the collision of their host galaxies which causes enhanced star formation during close encounters; e.g., the case of M82. In order to trace the age distribution and luminosities of young SMC clusters, we made use of the public catalogues from Bica et al. (2008a) and Zaritsky et al. (2002). For the first time, we are able to provide a large, accurate, and homogeneous large sample of SMC clusters containing ages *and* luminosities that can be used to compare e.g., the theoretically determined cluster disruption timescale for SMC clusters with observations.

INTRODUCTION

“In the beginning, the Universe was created. This has made a lot of people very angry and has been widely regarded as a bad move.”

Douglas Adams

1. THE SMALL MAGELLANIC CLOUD

The *Small Magellanic Cloud* (SMC) is an irregular dwarf galaxy (dIrr) that forms together with the *Milky Way* (MW) and the *Large Magellanic Cloud* (LMC) an interacting triple system. These three galaxies are part of a larger structure, the so-called *Local Group* (LG), which is a group of gravitationally bound galaxies that currently contains more than 40 galaxies (see Fig. 2.1). Besides the MW, the LG hosts a second large spiral galaxy, Andromeda (M 31), each of which has a system of satellite galaxies. The LG is part of the Virgo-Supercluster, which is named after the Virgo-Cluster in its center.

The SMC measures $7^\circ \times 4^\circ$ on the sky and has an assumed depth extent of up to 20 kpc (Mathewson et al. 1988; Hatzidimitriou et al. 1993; Crowl et al. 2001; Lah et al. 2005). The main body of the SMC has a distance from the sun of 60 kpc¹ and is ~ 20 kpc away from the LMC. Both galaxies form the Magellanic Clouds (MCs), which are named after the Portuguese conqueror Ferdinand Magellan (1480-1521) who was the first European embossing the two Clouds during his circumnavigation. The LMC is classified as an irregular galaxy (Irr) and lies about 50 kpc away from the sun. The larger of the two Clouds has a luminosity of about $2 \times 10^9 L_\odot$ and is the fourth most luminous galaxy in the LG. The SMC has about 10% of the LMC luminosity ($3 \times 10^8 L_\odot$). In optical and in near-infrared wavelengths the LMC has a pronounced bar and some spiral structures why it is sometimes classified as a spiral galaxy. The SMC has no spiral structure, but has a moderately dense “bar”. Both Clouds contain large amounts of hydrogen gas that arranges in star forming disorganized patches, which are located all over the Clouds. This resembles more the morphology of a dIrr. dIrrs are defined as gas-rich irregular shaped galaxies with recent or on-going star formation. Therefore, they host stars of various ages.

The star formation histories of the MCs show significant differences. The SMC hosts only one old globular star cluster, NGC 121, which is 2-3 Gyr younger than the oldest globulars in the MW and LMC (see Chapter 3). Since ~ 7.5 Gyr ago, compact populous star clusters have formed fairly continuously until the present day (see Chapter 4). In the LMC, two epochs of cluster formation have been observed that are separated by an “age gap” of about 4-9 Gyr (Holtzman et al. 1999; Johnson et al. 1999; Harris & Zaritsky 2001). In the early epoch, star clusters were formed with comparable ages like the oldest globular clusters in the MW and in the Galactic dwarf spheroidal companions (Grebel & Gallagher 2004). In a second epoch, a large population of intermediate-age clusters with ages less than 3-4 Gyr have developed.

Stellar kinematics in the SMC shows only little or no rotation (e.g., Harris et al. 2006) while the HI gas in the SMC has a rotational kinematic with the maximum circular velocity of $\sim 60 \text{ km s}^{-1}$ (Stanimirović et al. 2004). This velocity corresponds to a total SMC mass of $1.6 - 2.4 \times 10^8 M_\odot$.

¹References of quantities are listed in Table 2.1.

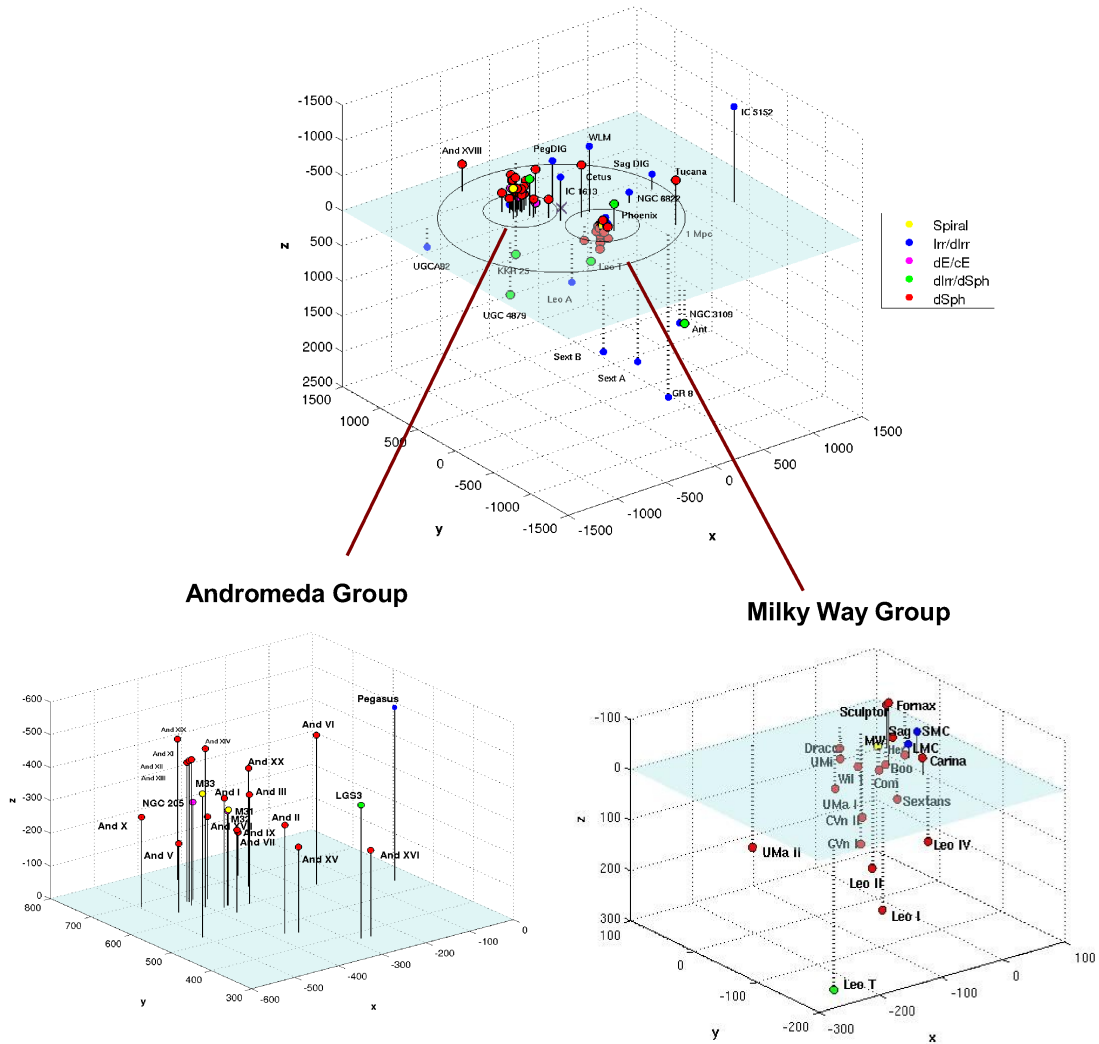


FIGURE 2.1. **The Local Group.** Shown is a 3-dimensional view of the Local Group and its surroundings, including the M31 group, the NGC 3109 group, and the five field galaxies IC 5152, UGCA 92, KKR 25, GR 8, and UGC 4879 (including galaxies published before August 11, 2008). The coordinates and distances were adopted from Grebel et al. (2003); Harbeck et al. (2005); McConnachie et al. (2008) and <http://seds.org/messier/more/local.html>. The light blue plane symbolizes the Galactic plane. The solid lines represent those galaxies lying above the plane, the dashed lines those lying below. The large black circle marks a radius of 1 Mpc around the LG barycenter (black cross). The two small circles enclose the two galaxy sub-groups of the Milky Way and M31.

Bekki & Stanimirović (2008) concluded that it might be possible that the central region of the SMC only consists of baryonic components (e.g. gas and stars) and its dark matter content is unusually low. Dwarf galaxies usually contain a large amount of dark matter and if their result gets verified, this would make the SMC a very special case and makes the riddle about its origin even more exciting.

The MCs are the only dIrrs within the close-by neighborhood of a large spiral galaxy, while most dIrrs are located at larger distances and in isolation (see Fig. 2.1). All other galaxies closely concentrated around the large spirals in the LG are dwarf ellipticals (dE), dwarf spheroidals (dSph), or transition types (dIrr/dSph). While dE are compact objects containing intermediate-age and old

TABLE 2.1. **Properties of the MCs**

PARAMETER	LMC	SMC	REFERENCE
Right Ascension (J2000.0)	05 ^h 23 ^m 34.6 ^s	00 ^h 52 ^m 38 ^s	Karachentsev et al. (2004)
Declination (J2000.0)	−69°45′22″	−72°48′01″	Karachentsev et al. (2004)
Galactic Longitude (J2000.0)	280.47	302.80	
Galactic Latitude (J2000.0)	−32.89	−44.33	
Distance Modulus [mag]	18.50 ± 0.02	18.88 ± 0.1	Alves (2004); Storm et al. (2004)
Distance [kpc]	50.1	59.7	
HI mass [M_{\odot}]	4.6 × 10 ⁸	4.2 × 10 ⁸	Brüns et al. (2005) Stanimirović et al. (1999)
Total Mass [M_{\odot}]	1.5 × 10 ¹⁰	2.4 × 10 ⁹	Schommer et al. (1992) Stanimirović et al. (2004)
Total Visual Magnitude [mag]	+0.50	+2.5	de Vaucouleurs et al. (1991)
Visual Luminosity [L_{\odot}]	2 × 10 ⁹	3 × 10 ⁸	de Vaucouleurs et al. (1991)
Radial Velocity [km/s]	275	160	Cole et al. (2005); Stanimirović et al. (2004)
Inclination	32°	40° ± 20°	Karachentsev et al. (2004) Stanimirović et al. (2004)
[Fe/H] [dex] (present day)	~ −0.40	~ −0.70	Keller & Wood (2006) (Hill 1999; Venn 1999)
Proper Motions (north) (mas yr ^{−1})	−2.03 ± 0.08	−1.16 ± 0.18	Kallivayalil et al. 2006a/b
Proper Motions (west) (mas yr ^{−1})	0.44 ± 0.05	−1.17 ± 0.18	Kallivayalil et al. 2006a/b
Galactic radial velocities (km s ^{−1})	89 ± 4	23 ± 7	Kallivayalil et al. 2006a/b

populations and some gas, dSph are almost devoid of gas, have a diffuse shape and belong to the least massive galaxies known. Like the dE, they are dominated by intermediate-age and old populations. But no two dwarf galaxies in the LG have the same star formation history (Grebel 1999).

1.1. The Formation and Evolution

The origin of the MCs is controversial and a variety of formation scenarios exist. Historically, the MCs are gravitationally bound to the MW and all three galaxies are in orbit around each other, which causes tidal interaction and distortions. The MW had a major influence on the development of the MCs, including their star formation history (Holtzman et al. 1997; Harris & Zaritsky 2001; Smecker-Hane et al. 2002), structural and chemical evolution (Mathewson et al. 1986; Bekki & Chiba 2005), and kinematics (Hatzidimitriou et al. 1993; Cole et al. 2005). Possible orbits of the SMC, LMC, and MW have been modelled by several authors (e.g., Kallivayalil et al. 2006a/b, Bekki & Chiba 2005; Besla et al. 2007).

Evidence for the strong interactions between this triple system offer two large HI-streams connecting the two Clouds and the MW. The *Magellanic Bridge* is a band of material that joins the two Clouds and consists of a few recently formed stars (e.g., Muller et al. 2003), and low-metallicity material (e.g., Dufton et al. 2008). It is widely considered to be the remnant of the last close encounter of the two Clouds ~200 Myr ago (Murai & Fujimoto 1980; Gardiner et al. 1994). The *Magellanic Stream* (Gardiner & Noguchi 1996; Sawa et al. 1999) is a 100° wide tail following behind the MCs and is moving up towards the galactic plane connecting the MCs with the MW. According to Gardiner & Noguchi (1996), the Magellanic Stream formed from stripped gas material from the SMC at its previous perigalactic approach ~1.5 Gyr ago, which fell together with the last close encounter with the

LMC. Model calculations by Besla et al. (2007) showed that it is very well possible that the MCs are on their first passage and that the last perigalactic passage of the SMC happened ~ 3 Gyr ago. Only in their "best-case-scenario" there will occur another passage within a Hubble time. With these new results, the tidal stripping formation scenario of the Magellanic Stream becomes very ineffective and it is doubtful that it was produced as suggested by Gardiner & Noguchi (1996). Today, the LMC has a distance from the SMC of ~ 20 kpc, but during their last perigalactic passage, they probably came as close as 10 kpc of each other. The *Leading Arm* is an HI feature extending $\sim 60^\circ$ in the direction of their motion ahead of the MCs. Figure 2.2 shows a simulation of the interacting galaxies and the tidally stripped HI-gas.

Recent proper motion measurements of the MCs based on HST data (Kallivayalil et al. 2006a/b, see also Piatek et al. 2008) combined with Monte Carlo simulations modelling the orbits of the Clouds and the MW have suggested that it is possible that the Clouds can have bound orbits (see also Besla et al. 2007). The simulations, however, also show that it is very difficult to keep the Clouds bound to each other for more than 1 Gyr in the past. It is therefore possible, that the Clouds are making their first passage close to the MW (see also e.g., Bekki & Chiba 2005) and have only interacted long enough to produce the Stream. This scenario might also give a plausible explanation for the "age-gap" in the LMC (see § 1.2). If the MCs are a bound system and star clusters are produced through strong tidal shock compressions (e.g., Whitmore 1999), there is no reason for the existence of an age-gap in the LMC and star clusters should have formed continuously from ~ 15 Gyr ago to the present day.

Bekki & Chiba (2005) explained the LMC age-gap with differences in birth locations and initial mass of the MCs. The LMC was born as a low-surface brightness galaxy ~ 150 kpc away from the MW. Therefore, the Galactic tidal field had no influence on the LMCs star cluster formation until the first encounter with the SMC, which was formed closer to the MW and less massive. The smaller distance to the MW caused a continuous cluster formation in the SMC. Therefore, they find a similar result as Kallivayalil et al. 2006a/b.

Bekki & Stanimirović (2008) found that there is no dark matter halo within the optical radius (~ 3 kpc) of the SMC and that the optical mass-to-light ratio is ~ 1 . They conclude that the SMC is purely baryon-dominated, at least within the analyzed radius of 3 kpc. Two scenarios are possible to explain their result: (1) most of the dark halo mass is located outside the optical radius and has lost a large fraction of its mass through strong tidal interactions with the MW and/or LMC. Ergo, the SMC of today is the stripped core of an initially much larger galaxy. (2) The SMC is a "tidal dwarf" that formed from tidal tails of merging/interacting galaxies (e.g., Duc et al. 2000) and never had a dark matter halo. The SMC hosts young and old stellar populations, while tidally stripped galaxies are dominated by young populations. Moreover, the tidal dwarf scenario does not explain the missing rotation of stars, but these galaxies are supposed to originate from rotating stellar gaseous disks. These are the main reasons for Bekki & Stanimirović (2008) to favorize the first scenario, in which tidal interactions with LMC and MW might have caused the loss of a large mass fraction. Further, the SMC with an originally larger mass could have had a stronger influence on the LMC (for the last ~ 3 Gyr). The orbital model of Bekki & Chiba (2005) was repeated assuming larger total SMC masses. They found that for an initial mass of $\sim 8 \times 10^{10} M_\odot$ the bound orbits of the MCs was hard to maintain for more than a few Gyr.

The SMC did not experience a smooth chemical enrichment. Recent studies have shown that field stars have a similar age-metallicity relation (AMR) as star clusters (Piatti et al. 2005a; Carrera et al. 2008, Kayser et al., in prep.). Furthermore, Carrera et al. (2008) find a weak metallicity gradient in the SMC, which is surprising because to this point there is almost no evidence for gas abundance radial gradients in dIrr systems. The gradient seems to be related to an age gradient, meaning that metal-richer young stars are concentrated in the central region of the SMC while the metal-poorer stars are located in the outer parts.

The stellar AMR shows a rapid chemical enrichment at a very early epoch, which was followed by a period of very slow metallicity evolution until ~ 3 Gyr ago. Most young stars are found in the innermost SMC fields where a second period of fairly rapid chemical enrichment was observed. The present-day abundance of the SMC is $[\text{Fe}/\text{H}] \approx -0.70$. Irr/dIrr are expected to be well-mixed due to the

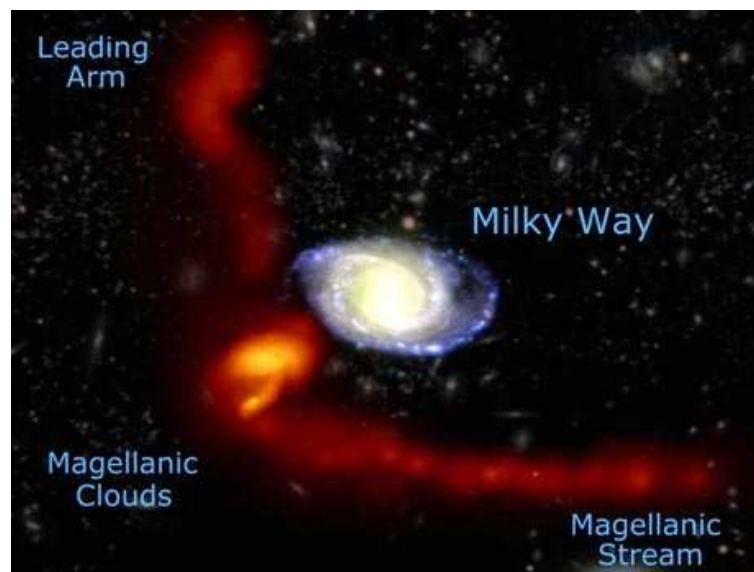


FIGURE 2.2. A simulation of the Magellanic Clouds and the MW including the streams of HI-gas caused by interaction between the triple-system. Illustration: [http : //www.atnf.csiro.au/news/press/images/magellanic_pics/](http://www.atnf.csiro.au/news/press/images/magellanic_pics/)

probable existence of galactic winds originated in supernova explosions, which mix the interstellar medium. The SMC, however, contains young populations (e.g. NGC 330, Grebel & Richtler 1992; Gonzalez & Wallerstein 1999) that are metal deficient in comparison to other SMC field populations.

Kayser et al., in prep. confirm that the spread in cluster metallicity at several Gyr is a real abundance dispersion and not due to uncertainties in earlier measurements. Star clusters with similar ages differ in metallicity by 0.64 dex. The reason for this scatter in metallicity is still not clear. An infall of unenriched gas is one option. Another possibility is that the chemical enrichment towards the periphery of the SMC proceeded more slowly, and the difference in cluster metallicity is a 'distance from the center' effect.

1.2. The Clouds' Star Clusters

Old globular clusters (GCs) are among the first objects that have formed in the early universe. Therefore, they represent a unique opportunity for tracing the galaxies' first star formation episodes. Typically, GCs contain $10^4 - 10^6$ gravitationally bound stars and are devoid of gas/dust and dark matter. A GC is defined as a star cluster older than 10 Gyr, containing RR Lyrae variables, or a star cluster capable to survive for a Hubble time. Their properties trace the physical conditions of the host galaxy at the time of their formation. The most massive elliptical and spiral galaxies contain many rich, old GCs (e.g., Larsen et al. 2001; Dirsch et al. 2003; Harris et al. 2006; Tamura et al. 2006), which are not present in the SMC. Numerous studies were performed to understand the formation processes of these objects leading to two important discoveries: (1) the GCs show a bimodal metallicity/color distribution (e.g., Gebhardt & Kissler-Patig 1999; Puzia et al. 1999; Kundu & Whitmore 2001) and (2) in merging Irr/dIrr and starburst galaxies a large population of young and intermediate-age massive star clusters are present (e.g., Whitmore & Schweizer 1995; Puzia et al. 2002; Goudfrooij et al. 2004; Georgiev et al. 2008). 'Old' star clusters are being defined older than 10 Gyr, 'intermediate-age' star clusters have ages between 1-10 Gyr and 'young' star clusters are younger than 1 Gyr.

In the MCs young and intermediate-aged populous, compact star clusters have been found, which are not present in the MW. There are three major theories explaining the formation of such massive objects. In the first scenario massive galaxies merge and accrete pre-galactic dwarf-sized gas fragments (Searle & Zinn 1978) and the old metal-poor star clusters form *in situ* while the younger population

originates from a second star-formation event (Forbes et al. 1997) from fragments of infalling gas. The second scenario describes two merging spirals (Schweizer 1987; Ashman & Zepf 1992) where the metal-poor GCs form during the major merging events. In the third and last scenario old, metal-poor clusters are formed during a first star-burst event (Pipino et al. 2007) and the younger massive clusters were accreted from smaller dwarf-sized galaxies. In case of bound orbits, the Clouds' cluster formation could have been triggered by strong tidal perturbations due to interactions (e.g., Whitmore 1999). In the MCs, a slightly enhanced number of star clusters have formed with ages around 1 Gyr, which might have been produced through a cloud-cloud collision after a pericenter passage. However, as seen in the previous section, there is more and more evidence that the MCs are on their first passage around the MW.

Even though the MCs seem to have a similar morphology, the two galaxies show strong differences in their cluster formation history. The LMC contains globular clusters with ages similar to the MW (e.g., Olszewski et al. 1991; Olsen et al. 1998; Johnson et al. 1999), but star clusters have formed during two main epochs of cluster formation (e.g., Bertelli et al. 1992) that are separated by a well-known "age gap" of about 4-9 Gyr, in which no star clusters have formed. Only one star cluster is known being within the age-gap, ESO 121-SC03, which has an age of 8.3-9.8 Gyr (Mackey et al. 2006). In the SMC, massive clusters formed continuously from ~ 8 Gyr ago to the present day and is therefore the only dwarf galaxy containing star clusters within the age range between ~ 4 and 7.5 Gyr. Furthermore, the SMC has a 'delayed' cluster formation history with NGC 121 being the oldest and only GC. It is, however, several Gyr younger than the oldest GCs in the LMC and MW. Moreover, NGC 121, is rather metal-rich with a metallicity of $[\text{Fe}/\text{H}] = -1.46 \pm 0.10$ (Da Costa & Hatzidimitriou 1998), while the oldest and metal-poorest globulars in the LMC and MW have metallicities of up to $[\text{Fe}/\text{H}] \approx -2.3$ dex (e.g. M 92, NGC 6426; Harris et al. 1996). It is not yet understood why populous star clusters older than 4 Gyr have not formed and survived continuously in the LMC, while in the SMC they did. Bekki & Chiba (2005) explained the different cluster formation histories of the Clouds as a difference in birth locations and initial mass of the host galaxies. Another scenario has been described above with the LMC being on its first passage around the MW. The first close encounter happened ~ 1 -3 Gyr ago causing the formation of populous star clusters.

A correlation between young star clusters in the LMC and putative close encounters with the SMC and MW has been found by e.g. Girardi et al. (1995), although the most recent proper motion measurements indicate that the MCs are currently on their first passage around the MW. The smaller number of SMC clusters might be the reason that for young SMC clusters a relation between close encounters and the cluster formation history is not as evident as for LMC clusters (Chiosi et al. 2006). The LMC contains about ~ 4200 star clusters, while in the SMC ~ 770 star clusters have formed (and survived).

2. THE COLOR-MAGNITUDE DIAGRAM

In a *color-magnitude diagram* (CMD) the absolute or relative magnitude of stars is plotted as a function of color. Originally, it was known as H-R diagram after Ejnar Hertzsprung and Henry Norris Russell who were the first to plot absolute magnitude vs spectral type (or temperature, since these quantities are closely related). The hottest stars are located on the left (blue), the coolest stars on the right side (red).

Star clusters formed from giant, unstable gaseous clouds at individual points in time with resulting equivalent properties of their member stars, as e.g. same age, chemical abundance, and distance to the observer. Member stars only differ in stellar mass and therefore today they reside at different stages of evolution. This becomes obvious when plotting CMDs of star clusters. In Figure 2.3 the CMD of the Galactic globular cluster M 3 is shown with the labelled individual evolutionary stages.

Main-sequence (MS): Most stars in a CMD are located on the MS. In this early stage of evolution, stars generate nuclear energy by burning hydrogen (H) in their core producing mainly helium (He).

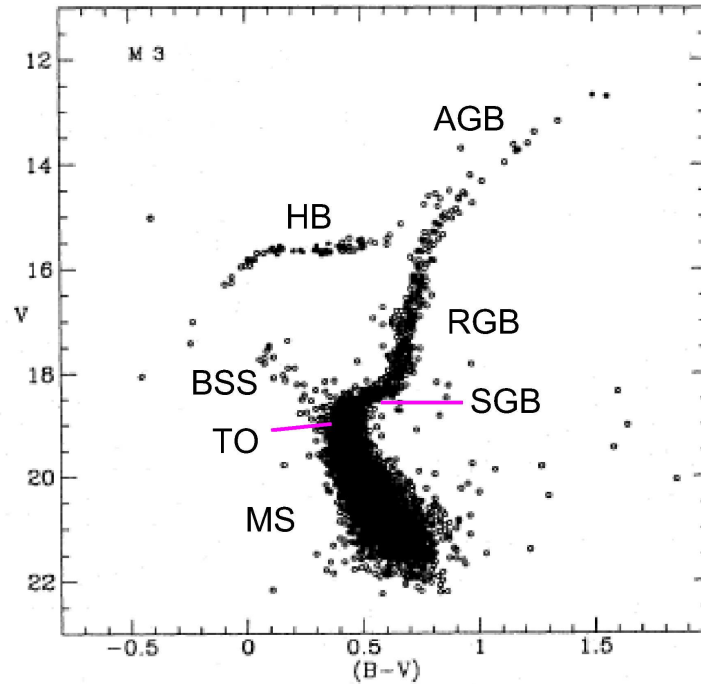


FIGURE 2.3. Color-magnitude diagram for the Galactic globular cluster M3 taken from Buonanno et al. (1994). All important features are labelled: AGB -asymptotic giant branch, BSS - blue straggler stars, MS - main-sequence, RGB - red-giant branch, SGB - subgiant branch, TO - turn-off point.

Energy is transported outwards by radiation and/or by convection. The core is in thermal equilibrium. The lowest-mass stars ($0.08 \lesssim M \lesssim 0.26 M_{\odot}$) that possess a core temperature high enough to ignite the H-core burning are fully convective due to the high surface opacities, which drive the surface convection zone deep into the stellar interior. Stars with masses between $0.26 \lesssim M \lesssim 1.2 M_{\odot}$ are dominated by the pp-chain at core temperatures of up to $\sim 5 \times 10^6$ K and therefore have radiative cores and convective envelopes. More massive stars ($M \gtrsim 1.2 M_{\odot}$) have convective cores due to the highly temperature-dependent CNO-cycle and radiative envelopes. The chemical composition within a convective zone is uniform due to permanent mixing. For a $5 M_{\odot}$ star, the central convection zone decreases somewhat in mass during core H-burning, leaving behind a slight composition gradient. As the star moves up the MS, the convective core retreats more rapidly with increasing stellar mass and disappears entirely before the H is exhausted for those stars with masses greater than $10 M_{\odot}$.

The effective temperature (T_{eff} of a star's surface) is determined only by its mass and chemical composition. Therefore, the MS is a mass sequence with star masses $M < 0.08 M_{\odot}$ at the faint end and increasing masses towards the bright end. The less massive a star, the longer it remains on the MS and the lower its surface temperature. Brown dwarfs populate the MS at even fainter magnitudes, but these objects never ignite hydrogen in their cores and therefore are barely detectable. The end of the MS lifetime is reached for an individual star when the H burning ceases and consequently the thermal equilibrium is destroyed. A $5 M_{\odot}$ star remains ~ 100 Myr on the MS, while a $1 M_{\odot}$ star stays there for ~ 10 Gyr. Throughout their evolution, stars suffer from permanent mass loss, but the rate of mass loss is variable over a wide range. On the lower MS, however, this effect is negligible, while it becomes more intense when going to more massive stars.

Turn-off point (TO): This evolutionary stage occurs when the star leaves the MS, which happens when the H-core burning ceases. The stellar core contracts due to reduced radiation pressure from the internal source. Due to the virial theorem, half of the energy is radiated away and half of the energy

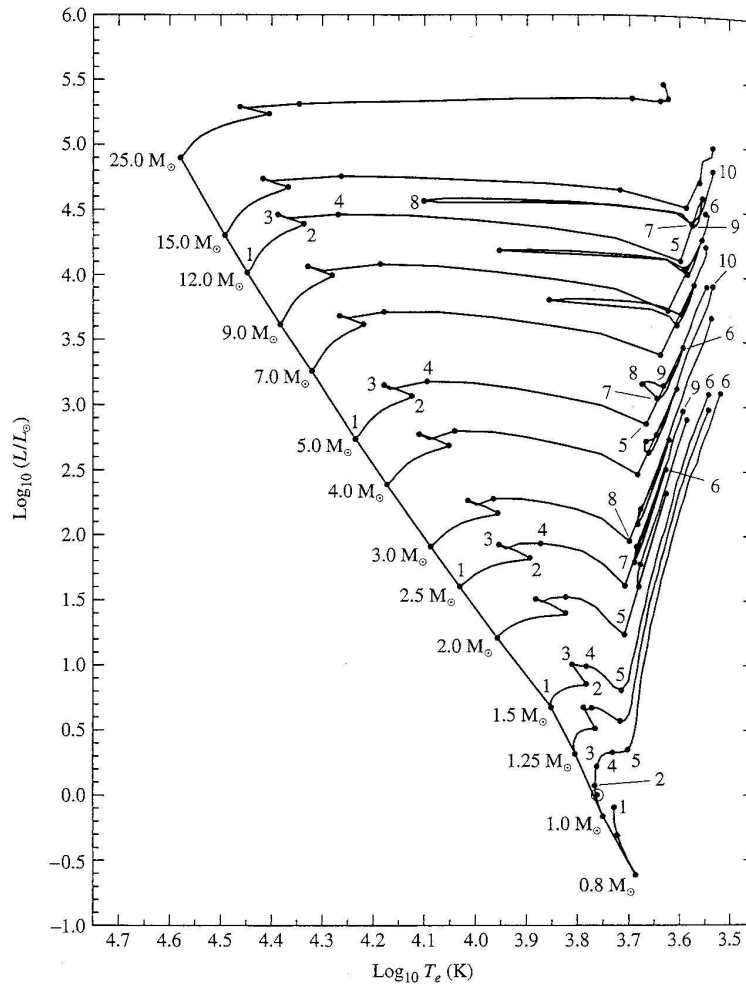


FIGURE 2.4. MS and post-MS evolutionary tracks for stars with different masses. The diagram is taken from Carroll & Ostlie (2006). The diagonal line connecting the TOs is the zero-age main sequence. The numbers along the tracks symbolize stages of stellar evolution and the elapsed times are listed in Table 2.2.

goes into increasing the thermal energy and hence the temperature of the gas. In Figure 2.4 this phase corresponds to point 3 for $1 M_{\odot}$ stars and point 2 for $5 M_{\odot}$ stars. The core of a $1 M_{\odot}$ star contracts while a thick H-burning shell forms rapidly around it and continues to consume H. The shell separates the core from the outer envelope. The temperature in the shell raises due to core contraction and the shell produces more energy than the core did on the MS. Consequently, the luminosity increases, while the envelope is slightly expanding.

For stars with masses higher than $\sim 1.25 M_{\odot}$, the tracks in Figure 2.4 show a hook-like feature (points 2-3), due to an **overall** contraction of the star on the Kelvin-Helmholtz-timescale. As for low-mass stars, the core contraction releases gravitational potential energy and the star expands and T_{eff} decreases (points 2 and 3), but the H-burning shell does not form immediately, but after the overall contraction.

The TO is a reliable tool for measuring the age of a star cluster. The older the cluster, the more bright stars have left the MS. The TO can therefore be used as a clock.

Subgiant branch (SGB): Low-mass stars burn H in their shell, while the He-core steadily increases, which does not provide any contribution to the energy production of the star. The mass of the He-core is below the Schönberg-Chandrasekhar-limit, which causes the electron gas in the core to degenerate. The electron degeneracy provides the pressure necessary to support the overlaying

INITIAL MASS (M_{\odot})	1	2	3	4	5
	6	7	8	9	10
25	0 6.51783	6.33044 7.04971	6.40774 7.0591	6.41337	6.43767
15	0 11.6135	11.4099 11.6991	11.5842 12.7554	11.5986	11.6118
12	0 16.1150	15.7149 16.4230	16.0176 16.7120	16.0337 17.5847	16.0555 17.6749
9	0 26.5019	25.9376 27.6446	23.3886 28.1330	26.4198 28.9618	26.4580 29.2294
7	0 43.4304	42.4607 45.3175	43.1880 46.1810	43.2291 47.9727	43.3388 48.3916
5	0 95.2108	92.9357 99.3835	94.4591 100.888	94.5735 107.208	94.9218 108.454
4	0 166.362	162.043 185.435	164.734 192.435	164.619 192.198	165.701 194.284
3	0 357.310	364.240 366.880	352.503 420.502	352.792 440.536	355.018
2.5	0 595.476	574.337 607.356	584.916 710.235	586.165 757.056	589.786
2	0 1148.10	1094.08 1160.96	1115.94 1379.94	1117.74 1411.25	1129.12
1.5	0 2910.76	2632.52	2690.39	2699.52	2756.73
1.25	0 5588.92	4703.20	4910.11	4933.83	5114.83
1	0 12269.8	7048.40	9844.57	11386.0	11635.8
0.8	0	18828.9	25027.9		

TABLE 2.2. The elapsed times since leaving the zero-age main sequence to reaching the indicated points in Fig. 2.4, measured in millions of years. The data are taken from Schaller et al. (1992). No track for stars with $M < 0.8 M_{\odot}$ are shown, because none has left the MS since the Big Bang ~ 15 Gyr ago.

envelope. When the core approaches central H-exhaustion the star has a radiative core. The produced energy causes an expansion with a resulting decrease of the effective temperature. H keeps on burning in a shell that becomes increasingly thinner as the star moves across the CMD (points 3-5). The photospheric opacity increases causing the development of a convection zone close to the stellar surface (point 5). During the SGB phase, the luminosity is almost constant and the convective stellar envelope reaches deeper into the star.

In a more massive star, an H consuming shell forms after the overall contraction, but the expanding envelope is able to absorb the gravitational energy from the core to cause a decrease of luminosity. The He-core mass is typically larger than the Schönberg-Chandrasekhar limit and contracts very slowly, while the envelope expands why the outer layers cool and the envelope opacity increases. During this phase, the star moves across the CMD from the blue to the red side until it reaches the Hayashi-track. The stellar envelope becomes convective for stars with $M > 5 M_{\odot}$ (point

5). For a $3 M_{\odot}$ star the SGB phase takes ~ 10 Myr and for a $1 M_{\odot}$ star ~ 1 Gyr. Because this phase for low and intermediate-mass stars is so short (Kepler-Helmholtz-timescale), stars in this stage are barely observed on CMDs, which is the reason for the presence of the so-called *Hertzsprung gap*.

Red-giant branch (RGB): Energy is transported more efficiently to the surface, which causes a rapid rise of the star's luminosity. While the star climbs the RGB along the Hayashi-track its effective temperature remains almost constant, only the luminosity increases. The He-core still contracts liberating gravitational potential energy causing an increase of the core temperature and expansion of the shell. The convective core reaches deeper into the stellar interior until the base encounters a region where the chemical composition has been modified by nuclear processes. These processes have produced heavier elements that are then being mixed with material above it through the convection zone. This process is called *first dredge-up* and leaves behind a chemical discontinuity.

For stars with $M > 2 M_{\odot}$ the H-burning shell moves steadily outwards until it crosses this chemical discontinuity. When this border is encountered by the H-burning shell the rate at which the star climbs the RGB drops and even reverses for a while due to a change in H-burning efficiency. The star becomes fainter. After the discontinuity is passed the surface luminosity grows again monotonically. During this phase the star crosses the same luminosity three times which is called the *red bump*. The luminosity of the red bump decreases as the border between shell and envelope, hence the discontinuity, moves deeper into the star.

For stars with masses smaller than $\sim 2 M_{\odot}$, the He-core becomes strongly electron-degenerate. It starts to react more like a liquid than a gas. The core temperature reaches $\sim 10^8$ K and the He ignites in an explosion at the RGB tip (point 6); the so-called *helium flash*. The luminosity of the star in this short phase (a few seconds) reaches $10^{11} L_{\odot}$, which is comparable to the luminosity of an entire galaxy. Most of the released energy is absorbed by the overlaying layers and goes into "lifting" the degeneracy. Afterwards, the energy is used to increase the thermal energy required to expand the core, which decreases its density and temperature.

For stars with masses greater than $\sim 2 M_{\odot}$, the He-burning phase is reached sooner and therefore the lifetime on the RGB is much shorter than for low mass stars. The He-core remains gaseous at the tip of the RGB the central density and temperature have finally become high enough to ignite the triple alpha process quietly. However, the H-burning shell remains the dominant energy source and the expansion of the core pushes the H-burning shell outward. It cools down a bit, which causes the energy output of the shell to decrease. The result is the decrease in the luminosity of the star, while the envelope contracts and the effective temperature starts to increase again.

Horizontal branch (HB): The electron-degeneracy of low-mass stars is removed about 1 Myr after the He flash. First, HB stars populate the *zero age horizontal branch (ZAHB)*. Its evolution depends on He content, He mass, metal abundance, and total mass of the star. Stars burn He in a chemically homogeneous convective core, and H in a surrounding shell. The larger the mass of the stellar envelope the more stars are located on the red HB. The star burns He in its steadily growing core to CO as it burned H before on the MS and moves blueward (points 7-8). The timescale, however, is much shorter (see Table 2.2). At point 8, the He core is exhausted, and the star moves back redward by contracting its CO core (point 9) burning He in a shell outside the CO core. Along with the contraction of the He-exhausted core, neutrino production increases to the point that the core cools a bit. A star with a mass $M \gtrsim 2 M_{\odot}$ performs a *blue loop* on the CMD, and its extent mainly depends on the envelope mass and the envelope He abundance. With decreasing mass, the blue loop extent decreases. The timescale of the blue loop phase is ~ 10 Myr for a $5 M_{\odot}$ star and ~ 2 Myr for a $10 M_{\odot}$ star. Stars with masses between $\sim 1-2 M_{\odot}$ (original mass on MS) form a *red clump* by staying cool and red. Stars of lower mass can develop instabilities during their passage along the HB, leading to periodic pulsations (RR Lyrae stars).

Asymptotic giant branch (AGB): The CO core contracts as the star expands while the effective temperature decreases. The AGB is the analog of the RGB except He is now burning in an inner and H in an outer shell. The He-burning shell is the dominant energy source in this stage while the H-burning shell is almost inactive at this point. As for the RGB, the star moves up the AGB and becomes a supergiant (point 10). A convective zone from the surface deepens again, mixing

heavy elements processed in the core with the outer material (*second dredge-up*). In the upper part of the AGB the H-burning shell eventually reignites and dominates again the energy production. The narrowing He-burning shell begins to turn on and off periodically.

Stars with $2 \gtrsim M_{\odot}$ experience a *third dredge-up* bringing carbon-rich material to the surface due to a convective zone that is established between He-burning and H-burning shell. This convective zones will merge and extend down into regions where carbon has been synthesized. What happens next is strongly dependent on the original mass of the star and the amount of mass loss experienced during its lifetime.

Stars with masses $M \lesssim 8 M_{\odot}$ end their lives as white dwarfs. Stars with $M \gtrsim 8 M_{\odot}$ continue to burn their CO core to neon and magnesium or even silicon until only an iron core remains. Iron won't ignite because for heavier elements energy is required for the nuclear fusion.

Stars with $M > 8 M_{\odot}$ explode in Supernovae Type II and their cores are left as neutron stars or if the original stellar mass is greater than $25 M_{\odot}$ it end its life as a black hole. Sometimes a neutron star being part of a binary system blows apart completely as Supernovae Type I.

For this section the following books have been used:

Binney & Tremaine (1987); Sparke & Gallagher (2000); Prialnik (2000); Salaris & Cassisi (2005); Carroll & Ostlie (2006)

3. AGE DETERMINATION METHODS

3.1. Isochrones

Isochrone (greek: iso = equal + chronos = time) is the name of a theoretical CMD of a single stellar population (SSP). A stellar population is assumed with same initial chemical composition and various initial masses. These artificial stars evolve with time and change their position in the CMD depending on their initial mass. An isochrone is a "snapshot" in the evolution of an SSP at a certain time with stars in different evolutionary stages.

Isochrones are the major tool to determine *absolute ages* of resolved stellar populations and star formation histories of nearby galaxies. Several stellar evolution models have been computed to this point, which vary in their prediction and reproduction of the properties of a SSP in a CMD. These variations depend on the parameter space and the input physics of each model, as e.g., mass and metallicity range, consideration of α -enhancement (α -elements: Ne, Mg, Si, S, Ar, Ca, and Ti), opacity, equation of state, nuclear reaction rates, mixing length, mass loss, and/or diffusion and overshooting effects. In Table 2.3 we compare the parameters and the input physics of the four stellar evolution models used in this thesis.

The MSs and RGBs of old isochrones are not affected by the age, but highly dependent on the metallicity. The chemical composition strongly affects the temperature of RGB stars resulting in the dependence of the colors on the metallicity. Due to the chemical evolution younger stars have higher metallicities than older stars and are therefore redder than metal-poor stars. But stars also become redder with increasing age, which complicates the metallicity determination on RGB colors. This effect is called *age-metallicity degeneracy* and is the main reason for the limited amount of information that can be retrieved from the RGB of old populations (Gallart et al. 2005). The TO is affected by both age and metallicity and its position in the CMD at a given chemical composition is determined by the stellar mass evolution at the stage of central H exhaustion. The absolute magnitude of the HB remains age-independent for clusters older than $t \gtrsim 10$ Gyr (e.g., Girardi & Salaris 2001; Salaris & Cassisi 2005), but is sensitive to metallicity. The He core mass at the He flash decreases with increasing metallicity and therefore metal-richer HB stars are fainter than metal-poor stars. In Figure 2.5 two sets of Dartmouth isochrones with different age, metallicity, and α -abundance are compared to each

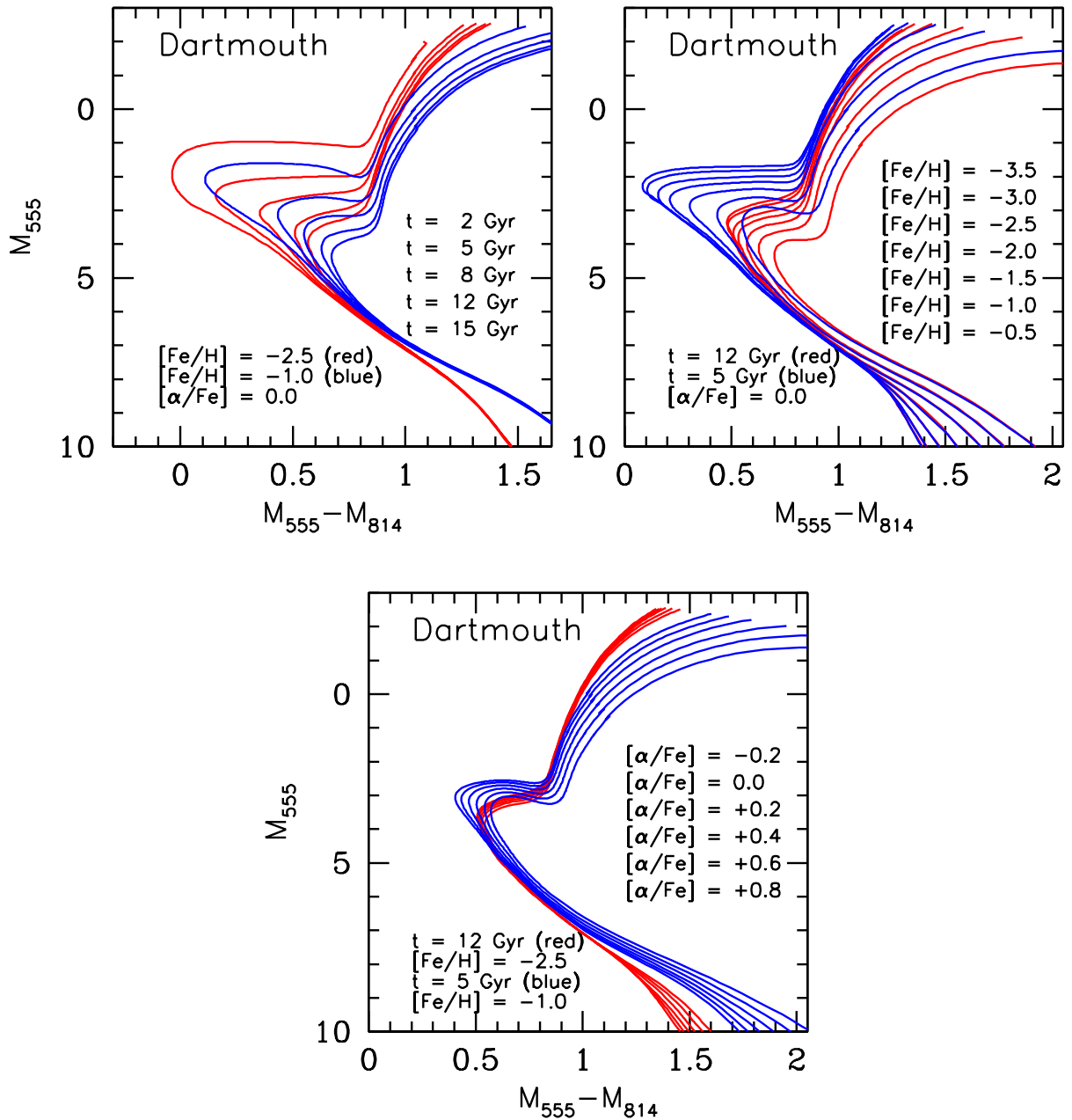


FIGURE 2.5. **Comparison of Dartmouth isochrones.** Panel 1: same metallicity ($[\text{Fe}/\text{H}] = -2.5$ (red) and -1.0 (blue)) and solar-scaled α -abundance but different age (2, 5, 8, 12, and 15 Gyr), Panel 2: same age (5 Gyr blue, 12 Gyr red) and solar-scaled α -abundance but different metallicity ($[\text{Fe}/\text{H}] = -3.5, -3.0, -2.5, -2.0, -1.5, -1.0, -0.5$), Panel 3: same age (5 Gyr blue, 12 Gyr red) and metallicity ($[\text{Fe}/\text{H}] = -2.5$ (red) and -1.0 (blue)) but different α -abundance ($[\alpha/\text{Fe}] = -0.2, 0.0, +0.2, +0.4, +0.6, +0.8$).

other. In the first panel, two solar-scaled isochrones of constant $[\text{Fe}/\text{H}]$ of different ages are shown. As expected, the isochrones have fainter TOs with decreasing ages. In the second panel, the age and α -abundance were kept constant, while the metallicities are varied. The brightest isochrones are the most metal-poor ones and they become fainter and redder with increasing Z ($[\text{Fe}/\text{H}] = \log(Z/Z_{\odot})$).

Models^a	DARTMOUTH	TERAMO	PADOVA	GENEVA
Mass range [M_{\odot}]	0.1-1.8	0.5-10	0.15-7	0.8-120
Z range	0.006-0.02	0.0001-0.04	0.0-0.07	0.0004-0.1
Age range	2-15 Gyr	30 Myr - 15 Gyr	100 Myr - 15 Gyr	10^3 yr - 16-20 Gyr
Z-mixture	SS+ α ($\pm 0.2, 0.4, 0.6, 0.8$)	SS	SS+ α (for $Z > 0.008$)	SS
Photometric Bands	JC-HST-SDSS IRAC-IR	JC-HST	JC-IR-SDSS HST-W-ESO	JC-IR-HST/WFPC2 G-W
Equation of state	I04	I04	K65+S88+M90	CG68
Nucl. Reactions	A02+Im04+K02	NACRE+K02	CF88+L90+WW93	CF88+C85+L90
Radiative Opacity	OPAL96+F05	OPAL96+AF94	OPAL92+AF94	OPAL92+K91
Conductive Opacity	HL69+C70	P99	HL69	HL69
Neutrino Losses	H94	H94+CS97	M85+IK83	I89
Z_{\odot}, Y_{\odot}	0.01885, 0.274	0.0198, 0.2735	0.01886, 0.273	0.0188, 0.282
α_{MLT}	1.938	1.25	1.68	1.63
Diffusion	yes	no	no	no

TABLE 2.3. **Parameters and physical inputs for four stellar evolution models** taken from Gallart et al. (2005) and the listed references. **A02**: Adelberger et al. (2002), **AK94**: Alexander & Ferguson (1994), **C70**: Canuto (1970), **C85**: Caughlan et al. (1985), **CG68**: Cox & Giuli (1968), **CF88**: Caughlan & Fowler (1988), **CS97**: Cassisi & Salaris (1997), **F05**: Ferguson et al. (2005), **H94**: Haft et al. (1994), **HL69**: Hubbard & Lampe (1969), **IK83**: Itoh & Kohyama (1983), **I89**: Itoh et al. (1989), **I04**: Irwin et al. (2004, in preparation), **Im04**: Imbriani et al. (2004), **L90**: Landre et al. (1990), **K65**: Kippenhahn et al. (1965), **K91**: Kurucz (1991), **K02**: Kunz et al. (2002), **NACRE**: Angulo et al. (1999), **M85**: Munakata et al. (1985), **M90**: Mihas et al. (1990), **OPAL92**: Rogers & Iglesias (1992), **OPAL96**: Iglesias & Rogers (1996), **P99**: Potekhin (1999), **S88**: Straniero (1988), **WW93**: Weaver & Woosley (1993)

^a **Dartmouth**: Dotter et al. (2007), **Teramo**: Pietrinferni et al. (2004), **Padova**: Girardi et al. (2000), **Geneva**: Lejeune & Schaerer (2001)

SS = Scaled-solar mixture,

Photometric systems: JC = Johnson-Cousins, HST = Hubble Space Telescope, SDSS = Sloan Digital Sky Survey, IRAC = Spitzer Telescope, IR = Infrared, W = Washington, ESO = ESO system, G = Geneva.

The SGBs also change their shapes and become shorter with increasing age. While for the most metal-poor isochrones the SGB has a color range of ~ 0.7 mag, the most metal-rich SGB has a range of ~ 0.35 mag for the age of 5 Gyr. Isochrones of different α -abundance but constant age and Z are shown in the third panel. At very low metallicity they are almost identical, but with increasing Z differences in both luminosity and temperature are present.

To determine ages of young and intermediate-age star clusters, isochrone models are almost the only method, because the HB is dependent on age (see § 3.2). The TO and the SGB of SSPs are almost depopulated, because of the much faster evolution. Therefore, the vertical and horizontal age determination methods cannot be used.

Star clusters usually are SSPs and all member stars have a uniform [Fe/H]-abundance. Therefore stellar evolution models provide an excellent opportunity to determine ages of these objects. Observed

CMDs are, however, influenced by photometric errors, blending effects, and unresolved binaries, which broaden the sequences. Therefore, one usually first determines an empirical 'ridgeline' or 'fiducial line' dividing the observed CMD in magnitude bins to determine the color distribution of the stars in each bin. On the almost horizontal SGB, color-bins are considered rather than magnitude bins. The obtained line can then be compared to the theoretical isochrones.

3.2. Relative Ages

The *vertical* age determination method is based on the fact that the absolute magnitude of the TO depends on the age of a star cluster (e.g., Alves & Sarajedini 1999), while the absolute magnitude of the HB remains approximately age-independent for clusters older than $t \gtrsim 10$ Gyr (e.g., Girardi & Salaris 2001). Therefore, 10 Gyr gives the limit for which this age dating method can be used. The difference $\Delta V = V_{TO} - V_{ZAHB}$ is calculated and together with the cluster's metallicity a relation between ΔV , age, and metallicity (e.g., Buonanno et al. 1989; Walker 1992) can be applied (see § 4.2.4). This method should only be used in the V band (or photometric bands at a similar wavelength) where the HB is horizontal.

This method has the advantage of being independent of reddening and photometric zero-points. However, the accurate determination of the TO luminosity can be a problem if one is dealing with data that does not reach deep enough to clearly outline the TO. In addition, the TO region is almost vertical (large V range at almost constant color), which makes the precise detection of the TO point difficult. For example Chaboyer et al. (1996a); Buonanno et al. (1998a) used a point shifted 0.05 mag in color to the red of the TO, either on the MS or the SGB, to avoid this problem. Sometimes not the ZAHB magnitude is used but the mean level $\langle V_{HB} \rangle$ of stars in the RR Lyrae instability strip for which also relations have been published (e.g., Sandage 1990). Another difficulty can occur, when the cluster is very old and the HB is populated only in the blue part or when the HB includes only a few stars. In these cases, one can use the so-called *horizontal* method.

The *horizontal* method (e.g., Sarajedini & Demarque 1990; Vandenberg et al. 1990) is based on the comparison of $\Delta(B - V) = (B - V)_{RGB} - (B - V)_{TO}$ (or equivalently in V-I colors) values, measured from theoretical and observed CMDs. $(B - V)_{TO}$ represents the color of the TO and $(B - V)_{RGB}$ the color at the base of the RGB. It is difficult to define the RGB base accurately. For example, one $(B - V)_{RGB}$ measures 2.5 mag above the TO magnitude (Salaris & Cassisi 2005). As for the vertical method, the RGB is not affected by age, while the color of the TO is age sensitive becoming redder with increasing age.

This method requires a high accuracy in both the observational determination and theoretical prediction of the values to keep the errors as small as possible. The derivative $\Delta(B - V)/\Delta t$ is ~ 0.010 - 0.015 mag Gyr $^{-1}$ around 12 Gyr (Salaris & Cassisi 2005). Because already color transformations cause an error of ~ 0.01 - 0.02 mag, this method is mostly used to determine age differences.

3.3. The Second Parameter Problem

The color of the HB mainly depends on the clusters metallicity and age. At higher metallicities the HB is redder at a fixed age due to larger evolving masses on the HB phase. After the He flash, stars are located at a lower T_{eff} (redder color) for increasing metallicity, because metal-richer RGB stars lose more mass during the RGB transition phase. This results in a higher luminosity of the RGB tip and a lower T_{eff} along the RGB. This effect, however, is reversed by the larger evolving mass in metal-richer RGB stars of a fixed age due to higher TO masses with increasing metallicities at a given age. The higher envelope opacity of metal-richer stars is the second effect why these stars are redder along the HB phase.

On the other hand, clusters of a fixed metallicity have bluer HBs with increasing age due to the smaller mass evolving along the HB. Therefore, the color distribution of HBs in principle depends on age and metallicity. At the beginning of CMD analysis, metallicity was thought to be the only

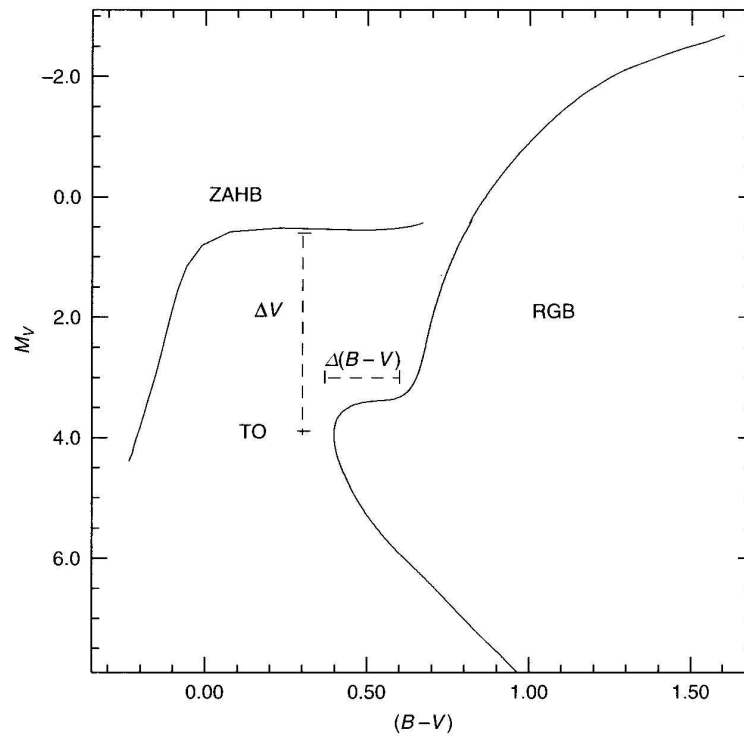


FIGURE 2.6. Graphical representation of the ΔV (vertical) and $\Delta(B - V)$ (horizontal) age indicators for old SSPs. Illustration taken from Salaris & Cassisi (2005).

parameter the HB color. There are well-known cluster pairs with similar metallicity (e.g. NGC 228 and NGC 362) but different HBs. This is the origin of the so-called second parameter problem. The applied horizontal and vertical methods provided a negligible age difference of the two clusters. Today it is known that the age difference between these two clusters is about 2 Gyr and age became the well-known second parameter. But apparently, there exists a "third" parameter which still has to be determined. Possible parameters are stellar rotation causing a different mass-loss law, dynamical interactions within the cluster, or different initial He abundances.

CHAPTER 3

NGC 121

“The most exciting phrase to hear in science, the one that heralds the most discoveries, is not ‘Eureka!’ (I found it!) but ‘That’s funny!’.”

Isaac Asimov

As first Paper of a series devoted to study the old stellar population in clusters and fields in the Small Magellanic Cloud, we present deep observations of NGC 121 in the F555W and F814W filters, obtained with the Advanced Camera for Surveys on the *Hubble Space Telescope*. The resulting color-magnitude diagram reaches ~ 3.5 mag below the main-sequence turn-off; deeper than any previous data. We derive the age of NGC 121 using both absolute and relative age-dating methods. Fitting isochrones in the ACS photometric system to the observed ridgeline of NGC 121, gives ages of 11.8 ± 0.5 Gyr (Teramo), 11.2 ± 0.5 Gyr (Padova) and 10.5 ± 0.5 Gyr (Dartmouth). The cluster ridgeline is best approximated by the α -enhanced Dartmouth isochrones. Placing our relative ages on an absolute age scale, we find ages of 10.9 ± 0.5 Gyr (from the magnitude difference between the main-sequence turn-off and the horizontal branch) and 11.5 ± 0.5 Gyr (from the absolute magnitude of the horizontal branch), respectively. These five different age determinations are all lower by 2–3 Gyr than the ages of the oldest Galactic globular clusters of comparable metallicity. Therefore we confirm the earlier finding that the oldest globular cluster in the Small Magellanic Cloud, NGC 121, is a few Gyr younger than its oldest counterparts in the Milky Way and in other nearby dwarf galaxies such as the Large Magellanic Cloud, Fornax, and Sagittarius. If it were accreted into the Galactic halo, NGC 121 would resemble the “young halo globulars”, although it is not as young as the youngest globular clusters associated with the Sagittarius dwarf. The young age of NGC 121 could result from delayed cluster formation in the Small Magellanic Cloud or result from the random survival of only one example of an initially small number star clusters.

This study was accomplished together with John S. Gallagher III., Eva K. Grebel, Antonella Nota, Elena Sabbi, Marco Sirianni, Gisella Clementini, Monica Tosi, Daniel Harbeck, Andreas Koch, and Misty Cracraft.

It has been published in The Astronomical Journal (2008, vol. 135, p. 1106).

1. INTRODUCTION

Characterizing old stellar populations provide important constraints on the early star formation histories of galaxies. Only the satellite galaxies of the Milky Way (MW) are sufficiently close to resolve individual stars well below the oldest main-sequence turn-offs, which is a pre-condition for accurate photometric age dating of old stellar populations. All Local Group galaxies, for which adequate data exist, appear to contain stars older than 10 Gyr (Grebel & Gallagher 2004). This result is based on main-sequence turn-off photometry of globular clusters and field populations in Galactic satellites and a few more distant Local Group galaxies (e.g., Brown et al. 2007; Cole et al. 2007), as well as the detection of horizontal branch stars (including RR Lyrae variables) in the Local Group and beyond (e.g., Held et al. 2001; Harbeck et al. 2001; Sarajedini et al. 2002; Clementini et al. 2003; Pritzl et al. 2004).

Globular clusters are preferred as the basis for old stellar population age tracers since they are usually single-age, single-metallicity objects facilitating comparative studies. Moreover, while globular cluster systems exhibit a range of ages (e.g., De Angeli et al. 2005), the oldest ones may belong to the most ancient surviving stellar systems to have completed their formation in the youthful Universe (e.g., Moore et al. 2006). In those nearby galaxies where relative age dating based on main-sequence photometry was carried out in comparison to the oldest globular clusters in the Milky Way, no age difference within the measurement accuracy was found (e.g., Grebel & Gallagher 2004; Brown et al. 2007; Cole et al. 2007, and references therein). The relative age dating of the oldest identifiable Population II objects thus indicates a common epoch of substantial early star formation in the Milky Way and its companions, although information about a putative, even older Population III remains to be uncovered in these objects.

A galaxy that may *not* share this common epoch of early star formation – at least not with respect to its globular clusters (e.g., Sarajedini et al. 1998) – is the Small Magellanic Cloud (SMC)¹. The SMC is one of the closest and therefore best studied dwarf galaxies orbiting our Galaxy.

While the SMC hosts a large number of intermediate-age and young star clusters, it only contains one "old" globular cluster, NGC 121, which is also the most massive star cluster. NGC 121 is located $\sim 2.4^\circ$ (~ 3 kpc) west of the SMC bar at $(\alpha_{J2000.0}, \delta_{J2000.0}) = (0^h 26^m 47.0^s, -71^\circ 32' 12.0'')$.

NGC 121 is the only cluster in the SMC that is sufficiently old to have developed an extended red horizontal branch (Stryker et al. 1985) and to contain RR Lyrae stars. Indeed, whether or not to call a star cluster a globular cluster is a matter of definition. In this case we refer to Salaris & Girardi (2002a) who consider Lindsay 1 as having a stumpy red clump and not a red horizontal branch. Three RR Lyrae stars were discovered in NGC 121 by Thackeray (1958). Graham (1975) found a fourth RR Lyrae variable in the cluster and an additional 75 in a 1×1.3 square degree field centered on NGC 121. Fiorentino et al. (2008) identified 50 candidate variables in NGC 121 of which 27 are located on the cluster horizontal branch and thus are very likely RR Lyrae stars. They also detected 20 Dwarf Cepheid (blue straggler star) candidates in the central region of NGC 121. Studies of various clusters in the LMC and in the MW showed that the presence of RR Lyrae variables indicates that the parent population is as old as or older than ~ 10 Gyr.

An important question is whether NGC 121 is as old as the typical old globular clusters in the Large Magellanic Cloud (LMC) and in the MW. Previous studies found ages ranging from 8 to 14 Gyr for NGC 121 (Stryker et al. 1985; Walker 1991; Mighell et al. 1998a; Udalski 1998b; Shara et al. 1998; Dolphin et al. 2001) using a variety of different techniques. Studies based on the deepest available color-magnitude diagrams from Hubble Space Telescope (HST) observations with the Wide Field and Planetary Camera 2 (WFPC2) indicate an age of 10 to 10.6 Gyr for NGC 121, suggesting that this globular cluster is several Gyr younger than the oldest globulars in other nearby galaxies and in the MW (Shara et al. 1998; Dolphin et al. 2001).

¹There may be additional exceptions in more distant dwarf irregular galaxies regarding the common epoch of earliest Population II star formation, although also these galaxies evidently contain old populations (e.g., Grebel 2001; Makarova et al. 2002)

The capabilities of the Advanced Camera for Surveys (ACS) provide an improvement in both sensitivity (depth) as well as angular resolution, which is essential for a reliable photometric age determination in this dense star cluster. Here we present deep photometry of NGC 121 obtained with ACS aboard the HST. We determine the age of NGC 121 utilizing both absolute and relative methods (e.g., Chaboyer et al. 1996b). The current study is the first in a series of papers based on HST studies of rich intermediate-age and old star clusters in the SMC.

In addition to NGC 121, six intermediate-age SMC star clusters have been observed as part of our program: Lindsay 1, Kron 3, NGC 339, NGC 416, Lindsay 38 and NGC 419. We will derive fiducial ridgelines and fit isochrones to obtain accurate ages for each cluster using the same reduction techniques and isochrone models as described here (see § 2-4), and will present our results in future papers. In Table 3.1 we list the cluster identification, date of observation, passband, exposure times and location of all clusters in our HST program (GO-10396; principal investigator: J. S. Gallagher).

In the next Section we describe the data reduction procedure. In § 3 we present the color-magnitude diagram (CMD) of NGC 121 and discuss its main features. In § 4 we describe our age derivation methods and present our results.

2. OBSERVATIONS AND REDUCTIONS

The SMC cluster NGC 121 was observed with HST's ACS on 2006 March 21 as part of our program focused on star clusters and field stellar populations in the SMC. The program aims at exploring the star formation history and properties of the SMC using both a number of carefully selected clusters and field regions. For NGC 121 we obtained imaging in the F555W and F814W filters, which resemble the Johnson V and I filters in their photometric properties (Sirianni et al. 2005). The images were obtained using the Wide Field Channel (WFC) of ACS and cover an area of $200'' \times 200''$ with a pixel scale of ~ 0.05 arcsec. One set of exposures was taken at the nominal position of the cluster center. Four long exposures were obtained in each filter for hot pixel removal and to fill the gap between the two halves of the 4096×4096 pixel detector. Each pointing has an exposure time of 496 s in the F555W, and 474 s in the F814W filter. Moreover, two short exposures were taken in each filter with an exposure time of 10 s in F555W and 20 s in F814W.

The data set was processed adopting the standard Space Telescope Science Institute ACS calibration pipeline (CALACS) to subtract the bias level and to apply the flat field correction. For each filter, the short and long exposures were co-added independently using the MULTIDRIZZLE package (Koekemoer et al. 2002). With this package the cosmic rays and hot pixels were removed and a correction for geometrical distortion was applied. The resulting NGC 121 data consist of one 40 s and one 1940 s exposure in F555W and one 20 s as well as one 1896 s exposure in F814W. The two short exposures allowed us to measure brighter stars that are saturated in the long exposures.

The photometric reductions were carried out using the DAOPHOT package in the IRAF environment². We discarded saturated foreground stars and background galaxies using the *Source Extractor* package (Bertin & Arnouts 1996).

Due to the different crowding and signal-to-noise ratio properties of the long and the short exposure images, photometry involving point spread function (PSF) fitting was only performed on the long exposures. For the short exposures we used aperture photometry, which turned out to yield smaller formal errors than PSF photometry. We ran DAOPHOT on our data and set the detection threshold at 1σ above the local background level in order to detect even the faintest sources. The list of stars detected in the F814W image was then used as coordinate input list to identify the stars in the F555W image and serve as our coordinate reference. 49,493 sources were found to be common to both long exposure frames. For these sources, we performed aperture photometry using an aperture radius of

²IRAF is distributed by the National Optical Astronomy Observatory, which is operated by the Association of Universities for Research in Astronomy, Inc. under cooperative agreement with the National Science Foundation.

CLUSTER	IMAGE NAME	DATE (YY/MM/DD)	FILTER	TOTAL EXPOSURE TIME s	R.A.	DEC.
NGC 121	J96106030	2006/03/21	F555W	40.0	$0^h26^m42.98^s$	$-71^\circ32'16.54''$
	J96106040			1984.0	$0^h26^m43.26^s$	$-71^\circ32'14.61''$
	J96106010		F814W	20.0	$0^h26^m42.98^s$	$-71^\circ32'16.54''$
	J96106020			1896.0	$0^h26^m43.26^s$	$-71^\circ32'14.61''$
Lindsay 1	J96105030	2005/08/21	F555W	40.0	$0^h03^m53.19^s$	$-73^\circ28'15.74''$
	J96105040			1984.0	$0^h03^m52.66^s$	$-73^\circ28'16.47''$
	J96105010		F814W	20.0	$0^h03^m53.19^s$	$-73^\circ28'15.74''$
	J96105020			1896.0	$0^h03^m52.66^s$	$-73^\circ28'16.47''$
Kron 3	J96107030	2006/01/17	F555W	40.0	$0^h24^m41.64^s$	$-72^\circ47'47.49''$
	J96107040			1984.0	$0^h24^m41.92^s$	$-72^\circ47'45.49''$
	J96107010		F814W	20.0	$0^h24^m41.64^s$	$-72^\circ47'47.49''$
	J96107020			1896.0	$0^h24^m41.92^s$	$-72^\circ47'45.49''$
NGC 339	J96104030	2005/11/28	F555W	40.0	$0^h57^m47.40^s$	$-74^\circ28'26.25''$
	J96104040			1984.0	$0^h57^m47.13^s$	$-74^\circ28'24.16''$
	J96104010		F814W	20.0	$0^h57^m47.40^s$	$-74^\circ28'26.25''$
	J96104020			1896.0	$0^h57^m47.13^s$	$-74^\circ28'24.16''$
NGC 416	J96121030	2006/03/08	F555W	40.0	$1^h07^m53.59^s$	$-72^\circ21'02.47''$
	J96121040			1984.0	$1^h07^m54.09^s$	$-72^\circ21'01.79''$
	J96121010		F814W	20.0	$1^h07^m53.59^s$	$-72^\circ21'02.47''$
	J96121020			1896.0	$1^h07^m54.09^s$	$-72^\circ21'01.79''$
Lindsay 38	J96102030	2005/08/18	F555W	40.0	$0^h48^m57.14^s$	$-69^\circ52'01.766''$
	J96102040			1940.0	$0^h48^m56.76^s$	$-69^\circ52'03.07''$
	J96102010		F814W	20.0	$0^h48^m57.14^s$	$-69^\circ52'01.76''$
	J96102020			1852.0	$0^h48^m56.76^s$	$-69^\circ52'03.07''$
NGC 419	J96103030	2006/01/05	F555W	40.0	$1^h08^m12.53^s$	$-72^\circ53'17.72''$
	J96103040			1984.0	$1^h08^m12.71^s$	$-72^\circ53'15.49''$
	J96103010		F814W	20.0	$1^h08^m12.53^s$	$-72^\circ53'17.72''$
	J96103020			1896.0	$1^h08^m12.71^s$	$-72^\circ53'15.49''$

TABLE 3.1. **Journal of Observation**

3 pixels. We then constructed a PSF by combining 150 bright and isolated stars that were distributed fairly uniformly across the image. Finally, PSF photometry was carried out.

The photometric calibration was accomplished by converting the magnitudes of the individual stars to the standard ACS magnitude system by using an aperture with a radius of $0.5''$ (or 10 pixels on the image), in combination with the aperture correction from the $0.5''$ aperture radius to infinity and the synthetic zero points for the ACS/WFC (Sirianni et al. 2005). The aperture correction was derived for each frame independently. The objects found in both images were cross-identified and merged with a software package written at the Bologna Observatory by P. Montegriffo (private communication). Altogether we were able to cover a luminosity range of ~ 10 magnitudes after combining the resultant photometry of the short and long exposures.

In Figure 3.1 we show the photometric errors assigned by DAOPHOT. For stars measured on the short exposures, the formal photometric errors remain negligible over a wide range of magnitudes. In the long exposures, all the brighter stars with $m_{555} < 19.3$ mag and $m_{814} < 19.5$ mag are saturated. At $m_{555,814} \sim 19.6$ mag, the short exposure (*blue dots*) and aperture photometry from the long exposure (*black dots*) samples were combined, and for stars fainter than $m_{555,814} \sim 22.2$ mag, long exposure

PSF photometry (*red dots*) was used. We chose where to cut between the aperture and PSF photometry catalogues based on the m_{555} data and adopted the same value for m_{814} so as to avoid a color slope associated with this division. For our study, we rejected all stars with a σ error larger than 0.2 mag and a DAOPHOT sharpness parameter $-0.2 \leq s \leq 0.2$ in both filters. To obtain a superior CMD, we discarded all stars within a radius of $35''$ from the cluster center, which excludes the very dense core of the cluster. With this selection, our final sample contains 17,464 stars common in both filters.

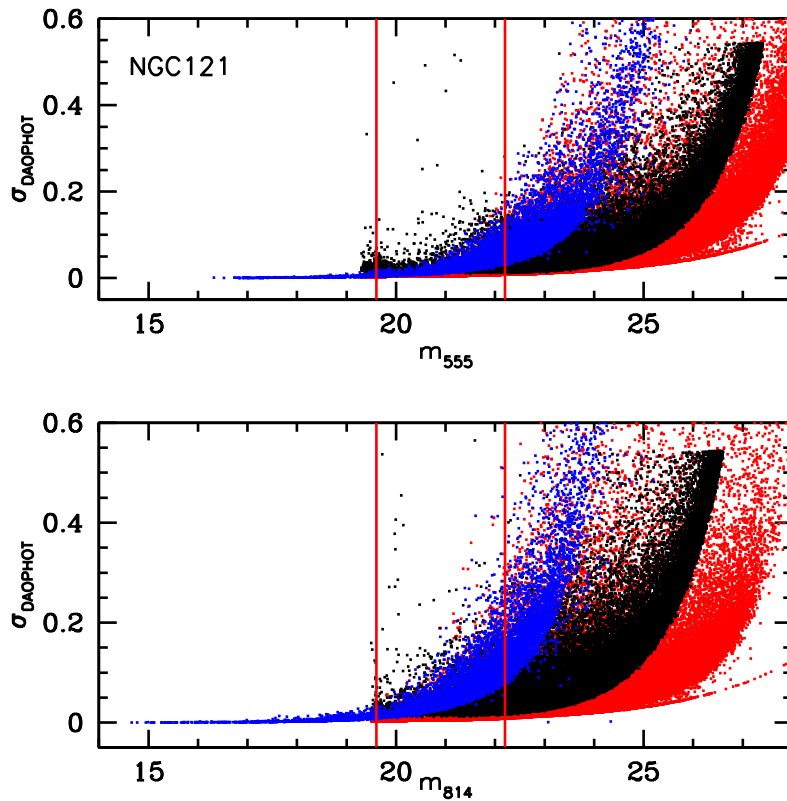


FIGURE 3.1. Photometric errors assigned by DAOPHOT to stars in the short exposures (blue dots), in the aperture photometry from the long (red dots), and on the PSF photometry from the long (black dots) exposures. Note the very small formal errors in the aperture photometry of the short exposures. Stars brighter than ~ 19.3 mag in the long F555W exposure and brighter than ~ 19.5 mag in the long F814W exposure are saturated and are therefore not shown. The lower envelope of the error distribution of the stars in the short and long F555W exposure (aperture photometry) cross over at $m_{555,814} = 19.6$ mag, and in the aperture and PSF photometry at $m_{555,814} = 22.2$ mag (also indicated by two thin vertical lines). Here the photometry of the short and long exposures was combined. For the F814W exposures we chose the same magnitude value in order to avoid introducing a color slope in the color-magnitude diagram of the resultant data set.

3. THE COLOR-MAGNITUDE DIAGRAM

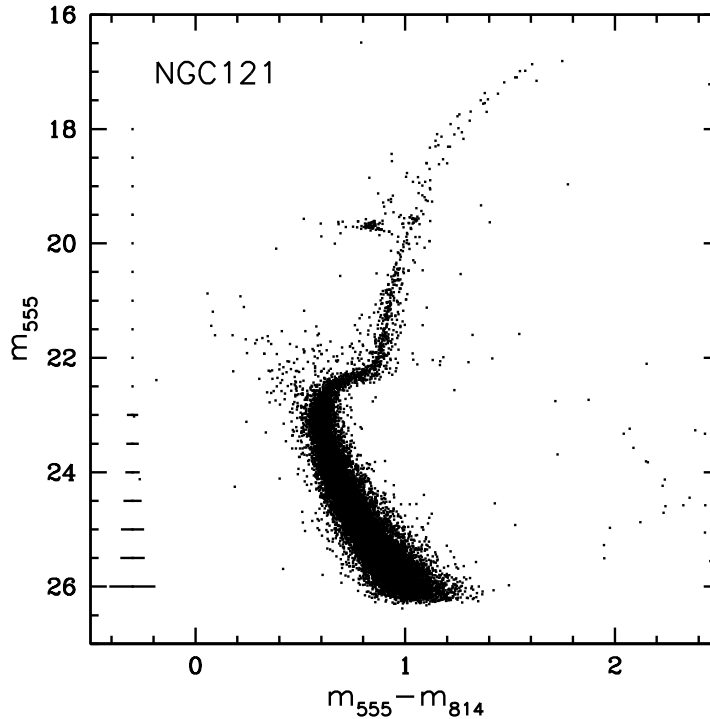


FIGURE 3.2. Color-magnitude diagram of NGC 121 and its surroundings. Stars within a radius of $35''$ from the cluster center have been discarded. All stars with "good" photometry ($\sigma \leq 0.2$ mag and $0.2 \geq \text{sharpness} \geq -0.2$) are shown; 17,464 stars in total. Representative errorbars (based on the errors assigned by DAOPHOT) are shown on the left for the $m_{555} - m_{814}$ color.

The resulting color-magnitude diagram (CMD) of NGC 121 and its surroundings is shown in Figure 3.2. Our CMD for NGC 121 reaches ~ 3.5 mag below the MSTO (~ 0.5 magnitudes deeper than the previous deepest available photometry), which allows us to carry out the most accurate age measurements obtained so far. The CMD shows a well-populated main sequence (MS), subgiant branch (SGB), red giant branch (RGB), horizontal branch (HB), and asymptotic giant branch (AGB). The gap on the RGB at $m_{555} \sim 20$ mag is an artificial feature due to small number statistics resulting from our exclusion of crowded stars in the cluster center. NGC 121 appears to be a single-age population object just as one would expect for a canonical star cluster. As expected, there is no obvious evidence for field star contamination by younger populations due to the location of NGC 121 in a low-density area in the outer parts of the SMC. Within the field of view of the ACS and at the high Galactic latitude of the SMC, Galactic foreground contamination is very low (e.g., Ratnatunga & Bahcall 1985).

Another possible contamination source is the massive and extended Galactic globular cluster 47 Tuc, which has a tidal radius of 42.86 arcmin (Harris 1996) and an angular distance from NGC 121 of ~ 32 arcmin.

We visually estimated the location of the center of NGC 121 on the image and selected all stars within an annulus of $35''$ and $45''$ to create a bona fide sample. This CMD is displayed in Figure 3.3. There is no evidence for a binary sequence in NGC 121, but we cannot exclude their presence, due to

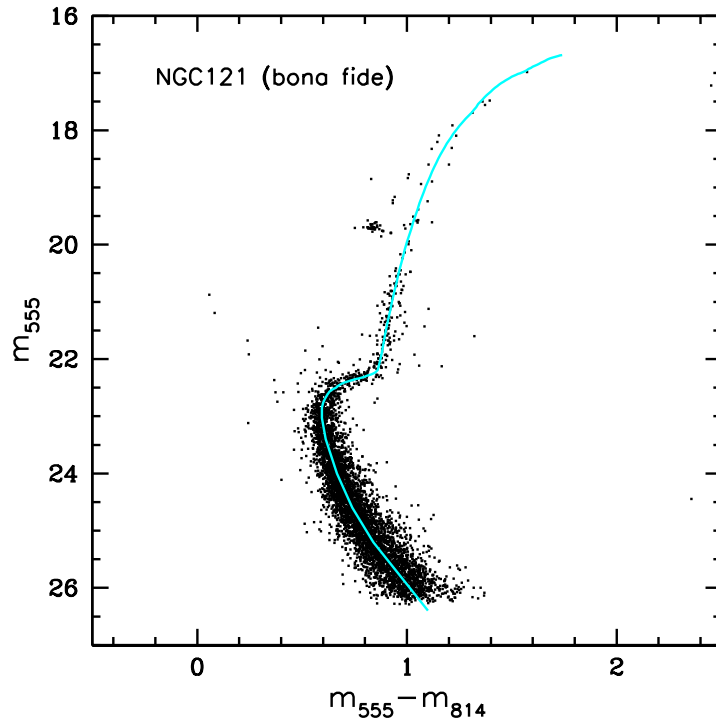


FIGURE 3.3. Color-magnitude diagram of all stars within an annulus between $35''$ and $45''$ of NGC 121. We used this CMD for the determination of a representative color-magnitude ridgeline of NGC 121 (cyan line). This CMD contains 5,112 stars. Only stars with good photometry ($\sigma \leq 0.2$ mag and $0.2 \geq \text{sharpness} \geq -0.2$) are shown.

the photometric error. The aforementioned traces of minor field contamination have mainly vanished. Due to crowding, incompleteness becomes significant at the faint end of the MS: This affects particularly faint stars in the cluster center. Hence in Figure 3.3 the MS becomes less densely populated at fainter magnitudes.

The red HB is well populated and extends into the RR Lyrae instability strip (Clementini et al., in preparation). The presence of a red HB provides a circumstantial suggestion that NGC 121 may be younger than old Galactic and LMC globular clusters, since the HBs of the oldest globular clusters tend to extend farther into the blue (e.g., Olszewski et al. 1996; Olsen et al. 1998; Mackey & Gilmore 2004). Red HBs, however, can also be due to a "second parameter" other than age affecting the HB morphology (e.g., Lee et al. 1994; Buonanno et al. 1997; Harbeck et al. 2001; Catelan et al. 2001a). Since a true HB is present, an age measurement for NGC 121 can be made using the ΔV_{TO}^{HB} age measurement, which we will do in § 4.2. This method requires the determination of the apparent mean magnitude of the HB. Our data yield $m_{555,HB} = 19.71 \pm 0.03$ mag for this observable, which is in agreement with the magnitudes determined by Shara et al. (1998), Alves & Sarajedini (1999) and Dolphin et al. (2001).

At $m_{555} = 19.58 \pm 0.03$ mag we find the NGC 121 RGB bump ($m_{555,Bump}$) which is 0.06 mag brighter than the magnitude found by Alves & Sarajedini (1999). The difference in luminosity is due to the exclusion of the center stars. If we determine the $m_{555,Bump}$ on the entire sample, we obtain $m_{555} = 19.52 \pm 0.04$ mag, which is in excellent agreement with the magnitude found by Alves & Sarajedini (1999). This feature is predicted by stellar evolution models, which also show that the luminosity of the RGB bump is dependent on the metallicity and age of the cluster. When the metallicity is known the difference between V_{HB} and V_{Bump} can be used as an age indicator.

Above the MS turn-off, Shara et al. (1998) found 42 candidate blue straggler stars (BSS). Evolved descendants of the BSSs are important as possible sources of stars lying above the traditional HB (e.g.,

Catelan 2005). In our ACS study we recovered the Shara et al. (1998) BSS sample and also found more stars in the BSS region of which some (about 20) turned out to be pulsating variables (dwarf Cepheids). These stars will be discussed in Clementini et al. (in preparation) where we will present the results of an HST study of variable stars in NGC 121.

4. AGE OF NGC 121

4.1. Age Based on Isochrone Fits

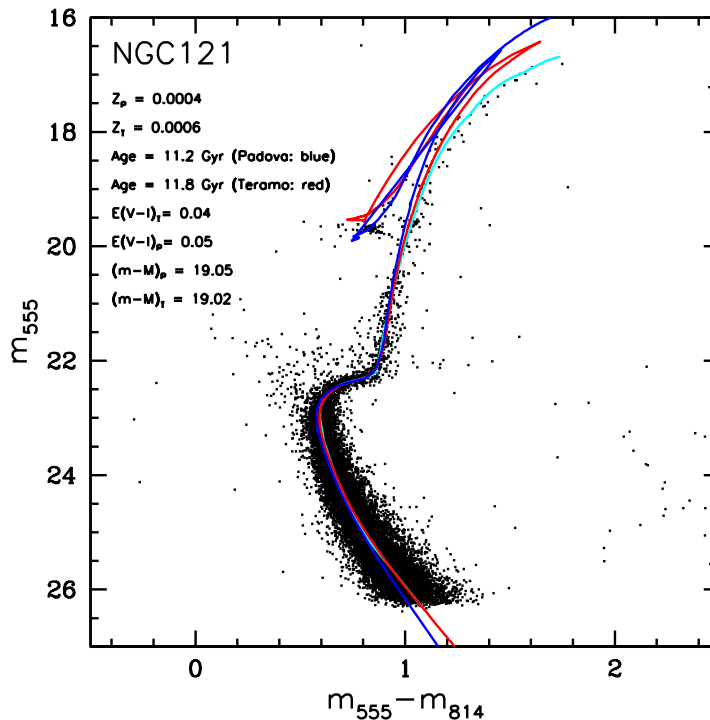


FIGURE 3.4. The CMD of NGC 121 with the best-fitting isochrones of two different models: The blue solid line shows the best-fitting Padova (Girardi et al. 2000, 2008) isochrone that is closest to the spectroscopically measured metallicity of the cluster. The red solid line is the best-fitting Teramo (Pietrinferni et al. 2004) isochrone approximating the known metallicity. Neither model is α -enhanced. The cyan solid line is our fiducial ridgeline. The fitting parameters are listed in the plot legend.

Age determinations of star clusters using isochrones depend crucially on the interstellar extinction, distance, and metallicity of the cluster, as well as on the chosen isochrone models. In fitting isochrones to the CMD of NGC 121 we adopted the spectroscopic metallicity measurement of $[\text{Fe}/\text{H}] = -1.46 \pm 0.10$ from Da Costa & Hatzidimitriou (1998, see also Johnson et al. 2004) on the metallicity scale introduced by Zinn & West (1984) (ZW84). The distance and the extinction were treated as free parameters. The SMC distance modulus is $(m - M)_0 = 18.88 \pm 0.1$ mag (60 kpc) (e.g., Storm et al. 2004), but due to the large depth extension of the SMC along the line of sight we adjusted the distance modulus $(m - M)_0$ to produce the best isochrone fits to our CMD data.

For easier comparison to the isochrones, we first derived a fiducial ridgeline (see Appendix A), which reproduces the mean location of the stellar distribution in the CMD (exempting the HB). In order to determine the ridgeline, we separated the cluster center CMD into three sections: the MS, the SGB and the RGB. On the MS we determined the mode of the color distribution in magnitude bins of

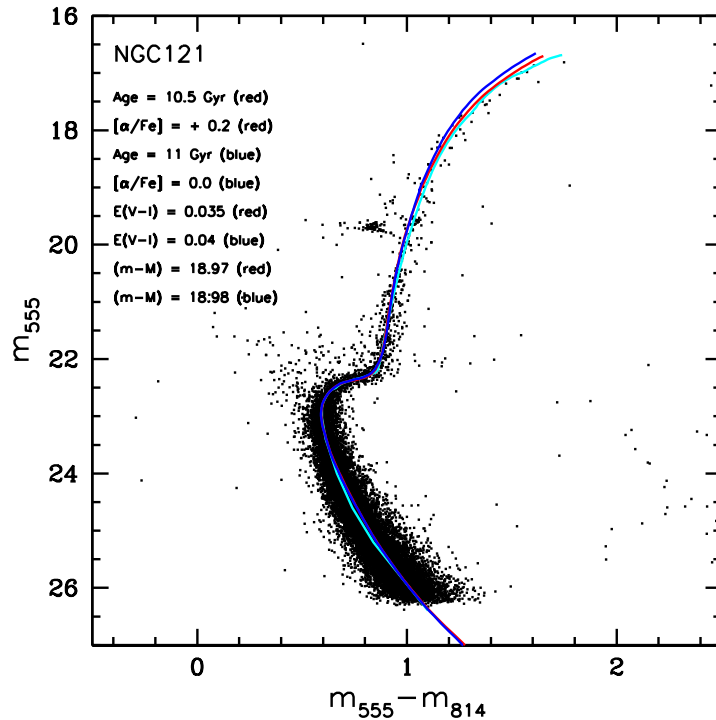


FIGURE 3.5. The NGC 121 CMD with the best-fitting Dartmouth (Dotter et al. 2007) isochrones overplotted in red. As before, the cyan line represents our fiducial for NGC 121. The fit parameters are listed in the plot. Note the excellent agreement of this α -enhanced isochrone with the observed CMD.

0.3 mag width. For the SGB, we performed a linear least squares fit of a polynomial of 5th order to a Hess diagram of this region in the CMD. Finally, the RGB was fit by a third-order polynomial of the mean color, again in magnitude bins with a size of 0.3 mag each. The resulting ridgeline is shown in Fig. 3.3 as a cyan line.

We fitted our m_{555} vs. $m_{555}-m_{814}$ CMD with three different isochrone models: Padova isochrones (Girardi et al. 2000, 2008)³, Teramo isochrones (Pietrinferni et al. 2004), both with scaled solar isochrones ($[\alpha/\text{Fe}] = 0.0$), and Dartmouth isochrones (Dotter et al. 2007) with both $[\alpha/\text{Fe}] = 0.0$ and $+0.2$. The Padova isochrone grid has an age resolution of $\log(t)=0.05$, the Teramo isochrone grid of 0.1 Myr and the Dartmouth isochrone grid of 0.5 Gyr. Our adopted spectroscopic metallicity of $[\text{Fe}/\text{H}] = -1.46$ corresponds most closely to $Z = 0.0004$ in the Padova models, to $Z = 0.0006$ in the Teramo models, and to $[\text{Fe}/\text{H}] = -1.49$ in the Dartmouth models. All three sets of isochrone models are available in the standard ACS color system.

We fitted a large number of isochrones using different combinations of reddening, age, and distance. For each set of models, we selected the isochrone that best matched the observed data (Fig. 3.4, Fig. 3.5).

First we discuss Figure 3.4. Our best-fit age using Padova isochrones is 11.2 Gyr with $(m-M)_0 = 19.05$ mag and $E_{V-I} = 0.05$. The best fitting Teramo isochrone yields an age of $t = 11.8$ Gyr, $(m-M)_0 = 19.02$ mag, and $E_{V-I} = 0.04$. On the MS, both the Teramo isochrone and the Padova isochrones trace the ridgeline almost perfectly. At the faint end of the MS, the Padova isochrone continues further to the blue than the Teramo isochrone and our derived ridgeline; however, this only becomes more apparent at magnitudes of $m_{555} \sim 25.5$ mag and below. Both isochrones also provide

³http://pleiadi.pd.astro.it/isoc_photsys.02/isoc_acs_wfc/index.html

an excellent approximation to the SGB and to the lower RGB up to about half a magnitude below the HB.

At brighter magnitudes, the two isochrones deviate increasingly to the blue of the observed upper RGB. Here the Padova isochrone shows the strongest difference, deviating by approximately 0.38 mag in color from the observed tip of the RGB. The isochrone shows a magnitude for the base of the red HB that is about 0.5 mag fainter than the observed one. Unlike Teramo and Dartmouth, the Padova isochrone also models the AGB and its tip, which is ~ 1 mag brighter than the tip of the RGB. The Teramo isochrone is too blue by about 0.23 mag at the magnitude of the tip of the RGB and indicates a magnitude for the base of the red HB that is 0.2 mag too bright.

If we had no prior knowledge of the metallicity of NGC 121 and were to use the upper RGB as a metallicity indicator, a better fit would be obtained by choosing isochrones of a different metallicity or α abundance. The problems of various isochrone models of given metallicities in reproducing the upper red giant branches of globular clusters with the same metallicities are a well-known problem (e.g., Grebel 1997, 1999). Our Figure 3.4 reflect the general failure of the chosen stellar evolutionary models to simultaneously reproduce the major features of CMDs (Gallart et al. 2005) in spite of the excellent fit to the lower RGB, SGB, and MS. Fortunately the latter are the most age-sensitive features of the CMD.

The isochrone model provided by Dotter et al. (2007) with $[\alpha/\text{Fe}] = +0.2$ yield the best fit to the CMD (Fig. 3.5). The best-fit isochrone has the parameters $t = 10.5$ Gyr, $(m - M)_0 = 18.96$ mag, and $E_{V-I} = 0.035$, using the α -enhanced isochrones of $[\alpha/\text{Fe}] = +0.2$. All the major features of the CMD are very well reproduced, including the upper RGB where the isochrone is offset slightly to the blue relative to the fiducial ridgeline. This offset is no more than 0.01 to 0.02 on average along the entire upper RGB; i.e., even the *slope* of the RGB is very well reproduced along its entire extent. Unfortunately the stellar evolution models used here terminate at the He flash, and therefore do not fit the HB or the AGB.

Is our use of α -enhanced models justified? For NGC 121 a value of $[\text{Ca}/\text{Fe}] = +0.24$ has been measured, which is similar to the outer LMC cluster Hodge 11 and to the old Galactic outer halo clusters with $[\text{Ca}/\text{Fe}] = +0.3$ (Johnson et al. 2004). Consequently, we assume that NGC 121 also is enhanced in α -elements. We note that in this respect NGC 121 differs from the general trend observed in red giant stars in the LMC and in dwarf spheroidal galaxies, where the $[\alpha/\text{Fe}]$ ratios at a given $[\text{Fe}/\text{H}]$ tend to be lower by up to a few tenths of a dex than in the Galactic halo (e.g., Hill et al. 2000; Shetrone et al. 2001; Fulbright 2002; Pritzl et al. 2005; Johnson et al. 2006; Koch et al. 2007).

When we adopt the values for distance and reddening, but fit the cluster with an isochrone scaled solar, NGC 121 gets a slightly older age of 11 Gyr. The isochrone model with $[\alpha/\text{Fe}] = 0.0$ still provides a better fit than the Teramo or Padova models, but has an offset of ~ 0.05 on average along the upper RGB. Past studies found that α -enhanced models imply a higher luminosity and temperature for the same mass than the solar scaled models and therefore an older age for the same magnitude (e.g., VandenBerg et al. 2000b). The Dartmouth models show exactly the opposite behavior. This is because in these models an increase in $[\alpha/\text{Fe}]$ is accompanied by a corresponding increase of the total metallicity Z , which makes the isochrones cooler at constant age and $[\text{Fe}/\text{H}]$.

Finally, we note that the derived reddenings agree with the extinction $A_V = 0.1 \pm 0.03$ from the Schlegel et al. (1998) maps. The reddening law of O'Donnell (1994) is assumed.

In the Figures 3.6 and 3.7 we show a range of isochrones for the three sets of stellar evolution models in order to illustrate the age uncertainty in a given model. The finally chosen, "best" isochrone is always displayed along with two younger and two older isochrones. For the cases of the Teramo and Padova models, the two isochrones that are one age step younger or older than the chosen, central isochrone provide an upper or lower envelope for the location of the high-density part of the SGB, the MS turn-off, and the base of the RGB. For the Dartmouth isochrones the outermost isochrones provide this envelope. Considering the high quality of the fit of the central isochrone in this CMD region in all models and the larger deviations of the adjacent isochrones, we estimate that the resultant age uncertainty is of the order of approximately ± 0.5 Gyr for the Teramo and Dartmouth isochrones

and ± 0.7 Gyr for the Padova isochrones.

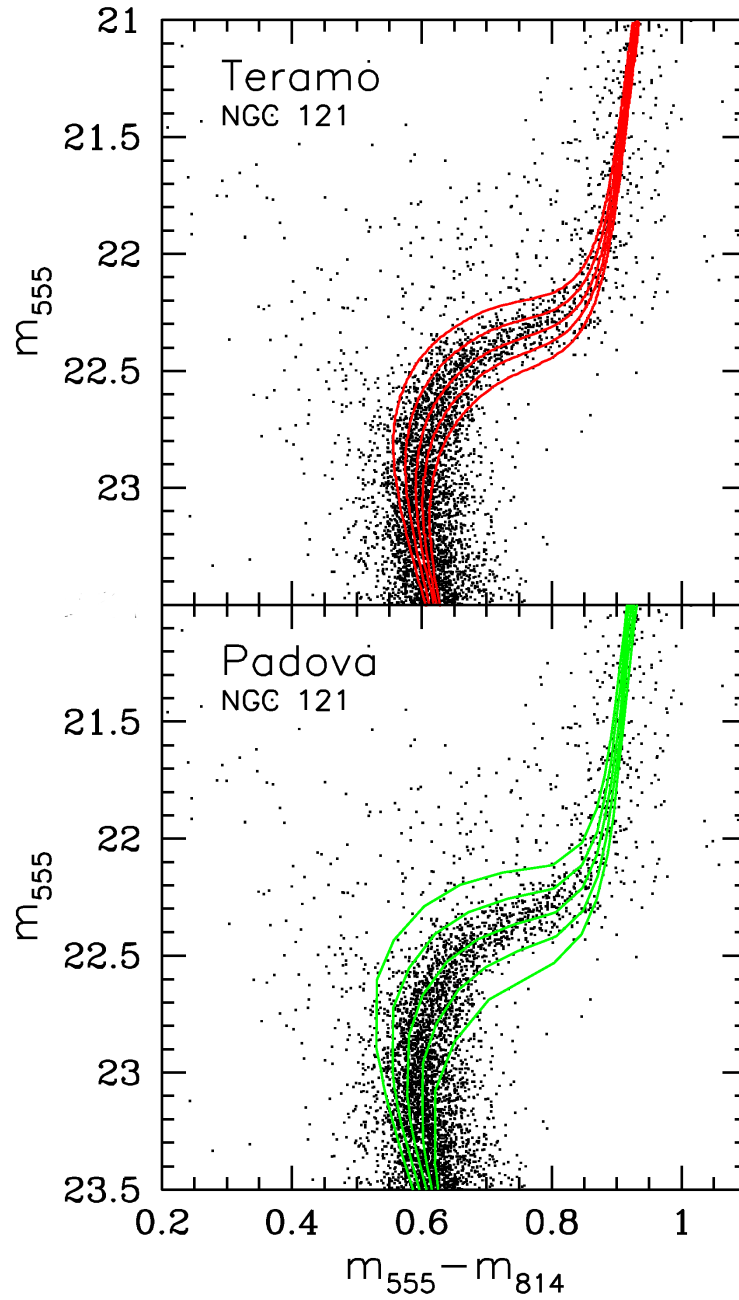


FIGURE 3.6. The color-magnitude diagram of NGC 121 after zooming in on the region of the main-sequence turn-off, subgiant branch, and lower red giant branch. In the upper panel, we show Teramo isochrones as solid lines, covering an age range of 10, 10.9, 11.8, 12.6, and 13.5 Gyr. These are the age steps in which these isochrones are provided (Pietrinferni et al. 2004). The central isochrone is our chosen best-fitting isochrone. In the lower panel we show the same plot for Padova isochrones (solid lines) in the Padova age steps of 8.9, 10, 11.2, 12.6, and 14 Gyr (Girardi et al. 2000, 2008). All other parameters are the same as in Figs. 3.4 and 3.5.

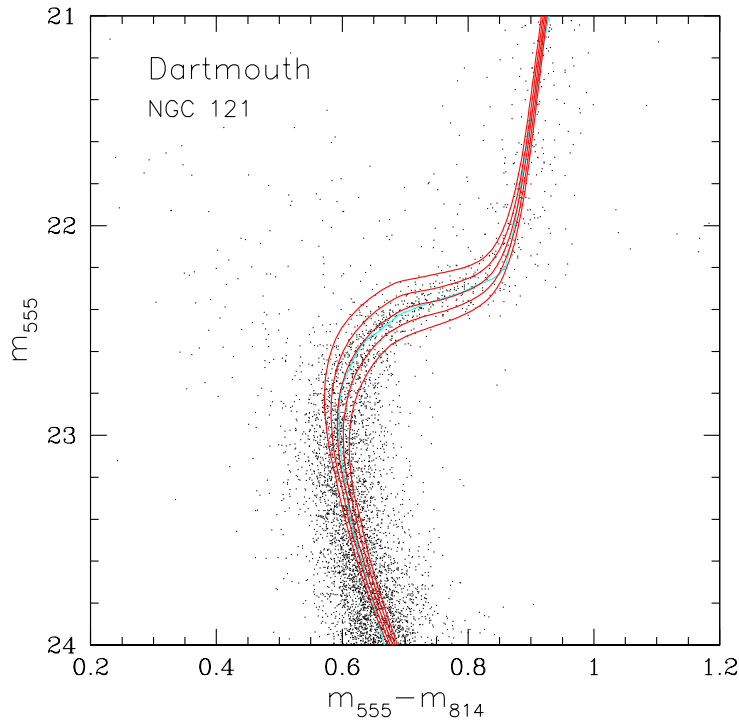


FIGURE 3.7. Same as Fig. 3.6, but for the α -enhanced Dartmouth isochrones covering an age range of 9.5, 10, 10.5, 11, and 11.5 Gyr (Dotter et al. 2007).

4.2. Empirical Age Estimates

4.2.1. Vertical Method

To check the reliability of the isochrone ages, we use a reddening-independent method to derive relative ages of NGC 121. This method is also independent of the photometric zeropoint of our data. This "vertical method" relies on the fact that the absolute magnitude of the MSTO depends on the age of the cluster (e.g., Alves & Sarajedini 1999), while the absolute magnitude of the HB remains approximately age-independent for clusters older than $t \gtrsim 10$ Gyr (e.g., Girardi & Salaris 2001). We measure the apparent magnitudes of the MSTO and HB, i.e., V_{TO} and V_{HB} , in order to obtain the magnitude difference ΔV_{TO}^{HB} . With increasing age, a cluster has generally larger values of this parameter since the MS moves to fainter magnitudes. Unfortunately, the determination of these two points comes with significant uncertainties. ΔV_{TO}^{HB} is hard to measure accurately both because of the width of the HB in luminosity and the MSTO's vertical extent in the turn-off region.

First, we calculate the magnitude difference $\Delta m_{TO,555}^{HB}$ between the HB and the MSTO, as originally described by Iben & Faulkner (1968). Because m_{555} is proportional to V and we are only interested in the magnitude difference, which we measure at constant color, there is no need to transform the magnitudes from the ACS system to V and I magnitudes (Sirianni et al. 2005). We follow the general definition of the MSTO as the bluest point along the MS; in our case represented by the bluest point on the ridgeline. We find the MSTO at $m_{TO,555} = 22.98 \pm 0.05$ mag, $(m_{555} - m_{814}) = 0.59 \pm 0.005$ mag. As described in Section 2, the mean HB magnitude is $m_{HB,555} = 19.71 \pm 0.03$ mag. This yields a $\Delta m_{TO,555}^{HB} = 3.27 \pm 0.06$ mag. Our result is only slightly lower than former values, e.g., $\Delta V_{TO}^{HB} = 3.32$ determined by Stryker et al. (1985), 3.33 by Shara et al. (1998) or 3.29 by Dolphin et al. (2001). Buonanno et al. (1989) published a mean value of $\Delta V_{TO}^{HB} = 3.55$ mag for old Galactic halo globular clusters (GC). The $\Delta m_{TO,555}^{HB}$ of NGC 121 is 0.28 mag smaller than this value, which indicates that NGC 121 is younger than most of the older *Galactic* GCs.

Walker (1992) (see also Buonanno et al. 1989) found a relation between age and ΔV_{TO}^{HB} based on a study of 41 Galactic globular clusters. Adopting again a metallicity of $[\text{Fe}/\text{H}] = -1.46 \pm 0.10$, we find with the formula $\log t = -0.045[\text{Fe}/\text{H}] + 0.37\Delta V_{TO}^{HB} - 0.24$ an age of 10.9 ± 0.5 Gyr for NGC 121.

4.2.2. Age Estimate using $M_V(\text{HB})$

In order to compare our data directly with Dolphin et al. (2001), we use the age calibration provided by Chaboyer et al. (1996c) as was done by these authors. For this purpose we must adopt the metallicity $[\text{Fe}/\text{H}] = -1.19 \pm 0.12$ of Da Costa & Hatzidimitriou (1998) on the metallicity scale introduced by Carretta & Gratton (1997) (CG97) to be consistent with Dolphin et al. (2001)'s calculation. Note that elsewhere in the paper we are using metallicities on the ZW84 scale which agrees reasonably well with the spectroscopically derived chemical abundances (Johnson et al. 2004). Using this method and the higher metallicity we determine an age of 9.7 ± 1.0 Gyr for NGC 121, which is similar to the age that Dolphin et al. (2001) found. We have to emphasize that this age is younger than the absolute ages determined in Section 4.1 due to the different metallicity scale. If we use our preferred ZW84 metallicity scale with this method we obtain an older age of 10.8 ± 1.0 Gyr.

While the measurement of V_{TO} is affected by significant observational errors (~ 0.05 mag), the color of the MSTO is well-defined. Chaboyer et al. (1996d) found that the usage of a point on the SBG brighter than the MSTO and 0.05 mag redder (V_{BTO}) provides more precise relative ages than V_{TO} . Chaboyer et al. (1996d) provide a conversion between $M_V(BTO)$ and V, I data for a grid of five metallicities. We choose the conversion for $[\text{Fe}/\text{H}] = -1.5$ because it is closest to the metallicity of NGC 121. In our data, we measured $m_{BTO,555} = 22.45 \pm 0.02$ at $(m_{555} - m_{814})_{BTO} = 0.64 \pm 0.005$ mag. To convert $m_{BTO,555}$ to the absolute magnitude $M_{BTO,555}$ we use the distance modulus derived above. This yields $M_{BTO,555} = 3.49 \pm 0.1$ mag. With the modified calibration by Johnson et al. (1999) we obtain an age of 11.50 ± 0.5 Gyr for NGC 121. We have summarized all our age results in Table 3.2.

4.2.3. Red Bump

Calculating $\Delta m_{555,Bump}^{HB} = m_{555,Bump} - m_{555,HB}$ we find -0.13 ± 0.05 mag. There is a general trend of increasing RGB bump brightness with decreasing age (Alves & Sarajedini 1999), assuming that a different "second parameter" is not affecting the position of the RGB bump. Alves & Sarajedini (1999) presented a V_{Bump}^{HB} vs. $[\text{Fe}/\text{H}]$ diagram (their Fig. 6), where the brightness difference between the RGB bump and the HB is plotted against the cluster metallicity. If we assume that the HB magnitude does not critically depend on age, then NGC 121 is slightly older than 10 Gyr based on this relation.

These comparative results are sensitive to the abundance of α -elements in NGC 121 as compared to Galactic globular clusters. Many nearby Galactic globular clusters are enhanced in α -elements relative to the solar value (Johnson et al. 2004). As mentioned earlier, spectroscopic results for NGC 121 indicate that this cluster is similarly enhanced in α elements, which means that the relative ages should not be affected as long as we confine ourselves to the comparison of globular clusters with similar α -element ratios. The fact that NGC 121 does not follow the trend of reduced $[\alpha/\text{Fe}]$ ratios observed in other nearby dwarf galaxies facilitates both our relative age determinations.

4.2.4. Relative Age of NGC 121

In Table 3.3 we compare the relative age of NGC 121 with those for a sample of Galactic globular clusters. While this comparison sample is located in the Galactic halo, some objects may have formed outside the Galaxy and might have been subsequently captured or accreted. We list the clusters by their identification in column (1). The $[\text{Fe}/\text{H}]$ values are given in column (2) in the scale by Zinn & West (1984). Column (3) shows the ΔV_{TO}^{HB} and column (4) the ages obtained by using the Walker (1992) calibration. Finally, column (5) gives the relative age difference of these clusters to NGC 121 $\delta(t)_W$. For ΔV_{TO}^{HB} we adopted the values from De Angeli et al. (2005), unless differently stated (see footnotes of Table 3.3).

AGE [GYR]	METHOD	REFERENCE FOR METHOD
10.9 ± 0.5	ΔV_{TO}^{HB}	Walker (1992) (ZW)
11.5 ± 0.5	$M_V(BTO)$	Chaboyer et al. (1996d)
10.8 ± 1.0	$M_V(HB)$	Chaboyer et al. (1996c)
11.8 ± 0.5	Isochrones	Pietrinferni et al. (2004)
11.2 ± 0.7	Isochrones	Girardi et al. (2008) Girardi et al. (2000)
10.5 ± 0.5	Isochrones	Dotter et al. (2007)

TABLE 3.2. **Ages for NGC 121 derived in this paper.** All derived ages are listed along with the method applied. In all cases, we adopted the ZW84 metallicity scale.

The clusters are listed in order of increasing ΔV_{TO}^{HB} and are divided into two groups. The first group shows nine "pure" GCs with similar metallicities as NGC 121. Among these nine clusters is NGC 2808 for which multiple MSTOs have been found (Piotto et al. 2007). Its ΔV_{TO}^{HB} value, derived prior to the study by (Piotto et al. 2007), is comparatively small. Even though those nine clusters have all similar metallicities, the spread in ΔV_{TO}^{HB} and therefore in age is quite large: NGC 1262 shows the lowest $\Delta V_{TO}^{HB} = 3.24$ and is similar in age to NGC 121, while NGC 6656 has $\Delta V_{TO}^{HB} = 3.55$, which makes it ~ 3 Gyr older than NGC 121.

The second group includes a subset of Galactic halo clusters that appear to be significantly younger than the average of the Galactic globular cluster population (e.g., Rosenberg et al. 1999; VandenBerg 2000a; Salaris & Weiss 2002b). Some members of this group are listed in the last part of Table 3.3. NGC 362 and NGC 288 are known to be a second parameter cluster pair of different ages, as reflected in their different ΔV_{TO}^{HB} (e.g., Fusi Pecci et al. 1996; Catelan et al. 2001b; Bellazzini et al. 2001). As NGC 362 has a similar ΔV_{TO}^{HB} and [Fe/H] as NGC 121, it should therefore be of a similarly young age. Other members of this group of young halo globulars are IC 4499 (Ferraro et al. 1995), Ruprecht 106 (assumed to be 3–5 Gyr younger than the bulk of the Galactic globulars with similar metallicities; Da Costa et al. 1992; Buonanno et al. 1993), Arp 2 (Buonanno et al. 1995a), Terzan 7 (Buonanno et al. 1995b), and Pal 14 (Sarajedini 1997).

Among the theories that try to explain the existence of these young objects is the model according to which they are intergalactic clusters captured by the MW (Buonanno et al. 1995b), or clusters formed during interactions between the MW and the Magellanic Clouds assuming that they are on bound orbits (Fusi Pecci et al. 1995). Zinn (1993) argued that the apparent young halo globular clusters formed in dwarf galaxies that later merged with the MW. Hence the Galactic globular clusters are assumed to be a mixture of objects that formed with the MW itself (old halo group) and others accreted from destroyed dwarf satellites (young halo clusters) (see also Mackey & Gilmore 2004). At least six globular clusters are believed to be associated with the Sagittarius dwarf galaxy (e.g., Carraro et al. 2007, and references therein), providing support for the accretion scenario. Note, however, that Sagittarius is contributing both old (M54, Ter 8, Arp 2) and "young" (Ter 7, Pal 12, Whiting 1) globular clusters to the MW. Similarly, the only other Galactic dSph galaxy known to contain globular clusters, Fornax, would contribute both kinds of globulars (Buonanno et al. 1998b, 1999) if it were to merge with our Galaxy. This also holds for the LMC (Olsen et al. 1998, see also discussion in Grebel, Gallagher, & Harbeck 2003).

If we take all the ages determined in this paper into account, we find that NGC 121 is consistently 2–3 Gyr younger than the oldest Galactic globular clusters (absolute age ~ 13 Gyr according to Krauss & Chaboyer 2003) and LMC globular clusters. The age offset remains when comparing NGC 121 to old Galactic globular clusters in the same metallicity range (see Tab. 3.3, upper panel). We also show that NGC 121 is not as young as the youngest Galactic and Sagittarius globular clusters, some of which are ~ 2 Gyr younger than NGC 121.

CLUSTER	$[Fe/H]_{ZW84}$	ΔV_{TO}^{HB}	AGE [GYR]	$\delta(t)_W$
NGC 121	-1.46	3.27	10.9	0
NGC 1261	-1.32	3.24	10.4	-0.5
NGC 5272	-1.66	3.24	10.8	0.1
NGC 2808	-1.36	3.25	10.6	-0.3
NGC 3201	-1.53	3.28	11.0	0.1
NGC 5904	-1.38	3.34	11.4	0.5
NGC 6254	-1.55	3.37	11.9	1.0
NGC 6218	-1.40	3.48	12.9	2.0
NGC 6752	-1.54	3.53	13.7	2.8
NGC 6656	-1.41	3.55	13.7	2.8
Pal 12	-0.94	3.17	9.45	-1.3
IG 4499	-1.75	3.25	11	0.1
NGC 362	-1.33	3.27	10.7	-0.2
Pal 14	-1.65	3.33	11.7	0.8
NGC 288	-1.40	3.45	12.6	1.7

TABLE 3.3. **Comparison of globular clusters ages (vertical method).** Ages were determined using the Walker (1992) calibration. The metallicity of NGC 121 was adopted from Da Costa & Hatzidimitriou (1998). The other results for NGC 121 were derived in this Paper. The data for NGC 6656 were taken from Rosenberg et al. (1999); for IGC 4499 from Ferraro et al. (1995); for Pal 12 from Rutledge et al. (1997) and for Pal 14 from Sarajedini (1997). All other values were taken from De Angeli et al. (2005).

5. SUMMARY AND DISCUSSION

We derived ages for the old SMC globular cluster NGC 121 based on our high dynamic range HST/ACS photometry that extends at least three magnitudes below its MSTO. In order to obtain absolute ages, we applied three different isochrone models. These isochrone models yielded ages of 11.2 ± 0.7 Gyr (Padova), 11.8 ± 0.5 Gyr (Teramo), and 10.5 ± 0.5 Gyr (Dartmouth). We find the α -enhanced Dartmouth isochrones provide the closest approximation to the MS, SGB, and RGB, whereas the other models cannot reproduce the slope of the upper RGB. High-resolution spectroscopy indicates that NGC 121 is indeed α -enhanced (Johnson et al. 2004), a property that it shares with many of the old outer Galactic halo globulars. Given the proximity of NGC 121 to the SMC on the sky and its distance, its physical association with the SMC seems well-established.

Our determinations of relative ages for NGC 121 are consistent with the results of our absolute age determination. Relative age estimates, when converted to an absolute age scale, are 10.9 ± 0.5 Gyr (ΔV_{TO}^{HB}), 10.8 ± 1.0 Gyr ($M_V(HB)$) and 11.5 ± 0.5 Gyr ($M_V(BTO)$). These numbers agree well with the absolute age derivations. Our results confirm that NGC 121 is 2–3 Gyr younger than the oldest MW and LMC clusters (as also found in earlier WFPC2 studies).

NGC 121 is similar in age to the youngest globular cluster in the Fornax dSph (Buonanno et al. 1999), and to several of the young Galactic halo clusters. On the other hand, NGC 121 is not as young as some of the Sgr dwarf galaxy’s globular clusters or the youngest Galactic globular clusters.

It is intriguing that the SMC – in contrast to other Galactic companion dwarf galaxies with globulars – does not contain any old classical globular clusters. But given the existence of only one cluster and the question of star cluster survival, this could be a result of the one survivor from the SMC’s epoch of globular cluster formation randomly sampling an initial distribution of star cluster ages. On the other hand, in low-mass galaxies without bulges, spiral density waves, and shear it is much

more difficult to destroy globular clusters through external effects. That this cluster is both younger than the Galactic mean and enhanced in α -elements may have interesting implications for the early development of the SMC.

It also is intriguing that the only globular cluster in the SMC is not very metal-poor. The SMC must have experienced substantial enrichment prior to the formation of NGC 121. In the LMC, where two main epochs of the formation of populous compact star clusters have been found (e.g., Bertelli et al. 1992), a few globular clusters are found that are old enough to exhibit blue HBs. Interestingly, these globular clusters, which are similarly old as the oldest Galactic globulars (Olsen et al. 1998), have a similar metallicity to NGC 121 (Johnson et al. 2004) (e.g., NGC 1898, NGC 2019), indicating very early chemical enrichment. The MW also contains old classical globular clusters (with blue HBs) that have similarly high metallicities as the somewhat younger NGC 121. Evidently, the conditions for and the efficiency of star formation varied in these three galaxies at early epochs.

After NGC 121 formed there was a hiatus in surviving stars clusters and thus possibly in cluster formation activity in the SMC: The second oldest SMC cluster is Lindsay 1 with an age of ~ 8 Gyr (Glatt et al. 2008b). Since then compact populous star clusters formed fairly continuously until the present day in the SMC (e.g., Da Costa 2002) – in contrast to both the LMC and the MW. In forthcoming papers on our ACS photometry of SMC clusters and field populations we will explore the evolutionary history of the SMC in more detail. Clearly, clues about the early star formation history of the SMC will have to come from its old field populations.

AGE DETERMINATION OF SIX INTERMEDIATE-AGE SMC STAR CLUSTERS WITH HST/ACS

“Imagination, not intelligence, made us human.”

Terry Pratchett

We present a photometric analysis of the star clusters Lindsay 1, Kron 3, NGC 339, NGC 416, Lindsay 38, and NGC 419 in the Small Magellanic Cloud (SMC), observed with the *Hubble Space Telescope* Advanced Camera for Surveys (ACS) in the F555W and F814W filters. Our color-magnitude diagrams (CMDs) extend ~ 3.5 mag deeper than the main-sequence turnoff points, deeper than any previous data. Cluster ages were derived using three different isochrone models: Padova, Teramo, and Dartmouth, which are all available in the ACS photometric system. Fitting observed ridgelines for each cluster, we provide a homogeneous and unique set of low-metallicity, single-age fiducial isochrones. The cluster CMDs are best approximated by the Dartmouth isochrones for all clusters, except for NGC 419 where the Padova isochrones provided the best fit. Using Dartmouth isochrones we derive ages of 7.5 ± 0.5 Gyr (Lindsay 1), 6.5 ± 0.5 Gyr (Kron 3), 6 ± 0.5 Gyr (NGC 339), 6 ± 0.5 Gyr (NGC 416), and 6.5 ± 0.5 Gyr (Lindsay 38). The CMD of NGC 419 shows several main-sequence turn-offs, which belong to the cluster and to the SMC field. We thus derive an age range of 1.2-1.6 Gyr for NGC 419. We confirm that the SMC contains several intermediate-age populous star clusters with ages unlike those of the Large Magellanic Cloud (LMC) and the Milky Way (MW). Interestingly, our intermediate-age star clusters have a metallicity spread of ~ 0.6 dex, which demonstrates that the SMC does not have a smooth, monotonic age-metallicity relation. We find an indication for centrally concentrated blue straggler star candidates in NGC 416, while for the other clusters these are not present. Using the red clump magnitudes, we find that the closest cluster, NGC 419 (~ 50 kpc), and the farthest cluster, Lindsay 38 (~ 67 kpc), have a relative distance of ~ 17 kpc, which confirms the large depth of the SMC. The three oldest SMC clusters (NGC 121, Lindsay 1, Kron 3) lie in the north-western part of the SMC, while the youngest (NGC 419) is located near the SMC main body.

This study was conducted together with Eva K. Grebel, John S. Gallagher III., Antonella Nota, Elena Sabbi, Marco Sirianni, Gisella Clementini, Monica Tosi, Daniel Harbeck, Andreas Koch, Andrea Kayser, and Gary Da Costa.

It has been published in The Astronomical Journal (2008, vol. 136, p. 1703).

1. INTRODUCTION

Star clusters are powerful tools for probing the star-formation history and the associated chemical evolution of a galaxy. As one of the closest star forming galaxies with star clusters covering a wide range of ages, the Small Magellanic Cloud (SMC) is a preferred location for detailed studies of this class of objects. The SMC is the only dwarf galaxy in the Local Group containing populous intermediate-age star clusters of all ages. The SMC appears to be part of a triple system together with the Large Magellanic Cloud (LMC) and the Milky Way (MW). Its star formation activity may be triggered by interactions with its companions (e.g. Yoshizawa & Noguchi 2003). The proximity of the SMC allows us to resolve individual stars in compact and massive star clusters of intermediate and old age, down to the sub-solar stellar mass regime.

The globular cluster (GC) system of the MW exhibits a range of ages between ~ 10.5 and 14 Gyr (e.g., De Angeli et al. 2005) with the oldest populations belonging to the most ancient surviving stellar systems. In the Galactic halo, a "young" group of star clusters is found with Pal 1 being the youngest with an age of 8 ± 2 Gyr (Rosenberg et al. 1998). Theories explaining the origin of these so-called young halo clusters, consider them to have been captured by the MW (Buonanno et al. 1995b), to have been formed during interactions between the MW and the Magellanic Clouds (Fusi Pecci et al. 1995), or to have been accreted from destroyed and/or merged dwarf satellites (e.g., Zinn 1993; Mackey & Gilmore 2004).

The star formation history of the LMC shows pronounced peaks that coincide with the times of possible past close encounters between the LMC, SMC and MW, indicative of interaction-triggered cluster formation (e.g., Girardi et al. 1995). In the LMC, two epochs of cluster formation have been observed that are separated by an "age gap" of about 4-9 Gyr (e.g., Holtzman et al. 1999; Johnson et al. 1999; Harris & Zaritsky 2001). In the early epoch a well-established population of metal-poor ($\langle [Fe/H] \rangle \sim -2$) star clusters with comparable properties to Galactic halo clusters (Suntzeff et al. 1992; Olsen et al. 1998; Dutra et al. 1999) was formed. These clusters are as old as the oldest globular clusters in the MW and in the Galactic dwarf spheroidal companions (Grebel & Gallagher 2004). In a second epoch, a large population of intermediate-age clusters with ages less than 3-4 Gyr have developed.

In contrast, the SMC contains only one old GC, NGC 121, which is 2-3 Gyr younger than the oldest GC in the LMC and MW (Glatt et al. 2008a) (Chapter 2). The second oldest SMC star cluster, Lindsay 1, has an age of 7.5 ± 0.5 Gyr, and since then compact populous star clusters have formed fairly continuously until the present day (e.g., Da Costa 2002). Furthermore, the intermediate-age clusters in the SMC might survive for a Hubble time, due to their high mass and the structure of the SMC (no bulge or disk to be passed) (Hunter et al. 2003; Lamers et al. 2005; Gieles et al. 2007).

The existing age determinations to this point have often been associated with large uncertainties. Stellar crowding, field star contamination and faintness of the main-sequence turnoffs made the measurement of precise ages difficult. These problems affect in particular ground-based data. Another difficulty is the large depth extent of the SMC which exacerbates the distance modulus-reddening degeneracy for each cluster. These uncertainties can affect the age determination considerably.

The capabilities of the Advanced Camera for Surveys (ACS) aboard the *Hubble Space Telescope* (HST) provide an improvement both in sensitivity (depth) as well as angular resolution, which is essential for reliable photometric age determinations in dense clusters. We present improved cluster ages and distance determinations for Lindsay 1, Kron 3, NGC 416, NGC 339, Lindsay 38, and NGC 419. This is part of a ground-based and space-based program to uncover the age-metallicity evolution of the SMC. Our space-based imaging data were obtained with HST/ACS and our ground-based spectroscopy was obtained with *Very Large Telescope* (VLT). We combine our photometric results with spectroscopic metallicity determinations to obtain a well-sampled age-metallicity relation.

The age-metallicity relation determined so far indicated that SMC clusters of similar age may differ by several tenths of dex in metallicity (Da Costa & Hatzidimitriou 1998). Previous studies provided ages and metallicities of SMC star clusters using a variety of techniques and telescopes (see

CLUSTER	DATE (YY/MM/DD)	FILTER	TOTAL EXPOSURE TIME s	R.A.	DEC.
Lindsay 1	2005/08/21	F555W	40.0	$0^h03^m53.19^s$	$-73^\circ28'15.74''$
			1984.0	$0^h03^m52.66^s$	$-73^\circ28'16.47''$
		F814W	20.0	$0^h03^m53.19^s$	$-73^\circ28'15.74''$
			1896.0	$0^h03^m52.66^s$	$-73^\circ28'16.47''$
Kron 3	2006/01/17	F555W	40.0	$0^h24^m41.64^s$	$-72^\circ47'47.49''$
			1984.0	$0^h24^m41.92^s$	$-72^\circ47'45.49''$
		F814W	20.0	$0^h24^m41.64^s$	$-72^\circ47'47.49''$
			1896.0	$0^h24^m41.92^s$	$-72^\circ47'45.49''$
NGC 339	2005/11/28	F555W	40.0	$0^h57^m47.40^s$	$-74^\circ28'26.25''$
			1984.0	$0^h57^m47.13^s$	$-74^\circ28'24.16''$
		F814W	20.0	$0^h57^m47.40^s$	$-74^\circ28'26.25''$
			1896.0	$0^h57^m47.13^s$	$-74^\circ28'24.16''$
NGC 416 (WFC)	2006/03/08	F555W	40.0	$1^h07^m53.59^s$	$-72^\circ21'02.47''$
			1984.0	$1^h07^m54.09^s$	$-72^\circ21'01.79''$
		F814W	20.0	$1^h07^m53.59^s$	$-72^\circ21'02.47''$
			1896.0	$1^h07^m54.09^s$	$-72^\circ21'01.79''$
NGC 416 (HRC)	2006/08/12	F555W	70.0	$1^h07^m58.76^s$	$-72^\circ21'19.70''$
			1200.0	$1^h07^m58.96^s$	$-72^\circ21'19.30''$
		F814W	40.0	$1^h07^m58.76^s$	$-72^\circ21'19.70''$
			1036.0	$1^h07^m58.96^s$	$-72^\circ21'19.30''$
Lindsay 38	2005/08/18	F555W	40.0	$0^h48^m57.14^s$	$-69^\circ52'01.77''$
			1940.0	$0^h48^m56.76^s$	$-69^\circ52'03.07''$
		F814W	20.0	$0^h48^m57.14^s$	$-69^\circ52'01.76''$
			1852.0	$0^h48^m56.76^s$	$-69^\circ52'03.07''$
NGC 419 (WFC)	2006/01/05	F555W	40.0	$1^h08^m12.53^s$	$-72^\circ53'17.72''$
			1984.0	$1^h08^m12.71^s$	$-72^\circ53'15.49''$
		F814W	20.0	$1^h08^m12.53^s$	$-72^\circ53'17.72''$
			1896.0	$1^h08^m12.71^s$	$-72^\circ53'15.49''$
NGC 419 (HRC)	2006/04/26	F555W	70.0	$1^h08^m17.93^s$	$-72^\circ53'03.60''$
			1200.0	$1^h08^m17.78^s$	$-72^\circ53'02.80''$
		F814W	40.0	$1^h08^m17.93^s$	$-72^\circ53'03.60''$
			1036.0	$1^h08^m17.78^s$	$-72^\circ53'08.80''$

TABLE 4.1. **Journal of Observation**

§ 7). Combining all published cluster ages for e.g. Kron 3 (5-10 Gyr) (Gascoigne 1966; Alcaino et al. 1996; Mighell et al. 1998a; Udalski 1998b; Rich et al. 2000), we find a wide range of ages for some key star clusters depending on the method used for the determination.

Here we present the deepest available photometry with HST/ACS, which allows us to carry out the most accurate age measurements obtained so far. We determine the ages of these clusters utilizing three different isochrone models, which also yields distances. In the next Section we describe the data reduction procedure. In § 3 we present the color-magnitude diagrams (CMD) of the clusters and discuss their main features. In § 5 we describe our age derivation method and present our results. We give an estimate of the distances of our clusters long the line-of-sight in § 6 and present a discussion and a summary in Sections § 7 and § 8, respectively.

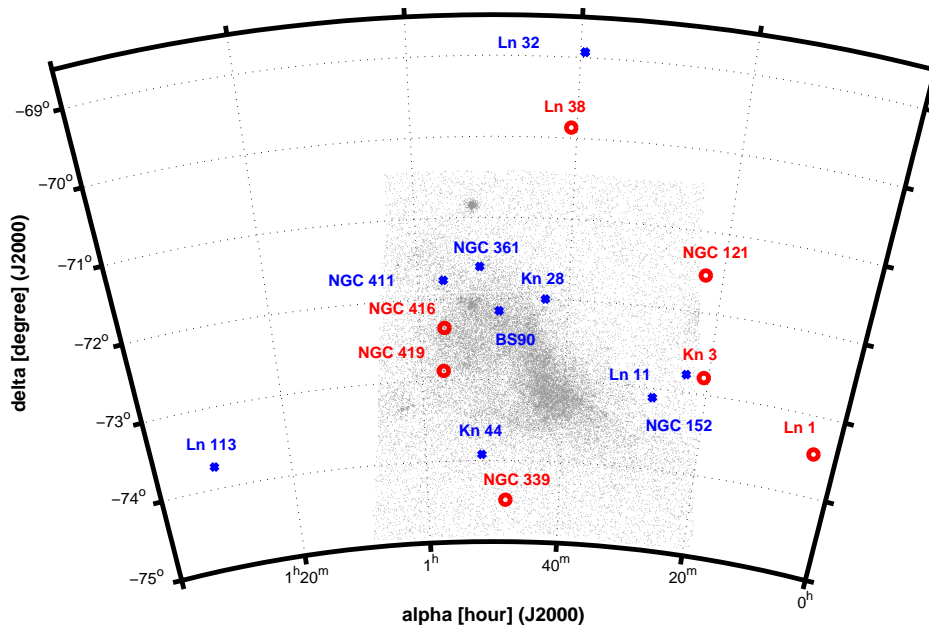


FIGURE 4.1. Spatial Distribution in 2D of our cluster sample (red circles). The location of eight additional SMC clusters, for which reliable ages from the literature are available, is shown (blue crosses). We obtain a complete sample of all intermediate-age and old SMC star clusters (see § 5), which we will discuss in § 6 and 7. One of the clusters, Lindsay 116, lies outside the coordinate boundaries of the Figure. The cluster locations are shown superimposed on a star map of the SMC generated using the point source catalog of the Small Magellanic Cloud Photometric Survey (Zaritsky et al. 2002) for stars with $V < 16.5$ mag.

2. Observations and Reductions

The SMC clusters Lindsay 1, Kron 3, NGC 339, NGC 416, Lindsay 38, and NGC 419 were observed with the HST/ACS between 2005 August and 2006 March (Table 4.1). The observations are part of a project (GO-10396; principal investigator: J. S. Gallagher, III) that is focused on cluster and field populations and the star formation history of the SMC.

The images were taken with the F555W and F814W filters, which closely resemble the Johnson V and I filters in their photometric properties (Sirriani et al. 2005). For Lindsay 1, Kron 3, NGC 416, NGC 339, and Lindsay 38 we discuss photometry from the *Wide Field Camera* (WFC), while for NGC 419 and for the center region of NGC 416 photometry from the *High Resolution Camera* (HRC) was used. The WFC images cover an area of $200'' \times 200''$ at each pointing with a pixel scale of ~ 0.05 arcsec. The HRC images cover an area of $29'' \times 26''$ at each pointing with a pixel scale of ~ 0.025 arcsec.

The data sets were processed adopting the standard Space Telescope Science Institute ACS calibration pipeline (CALACS) to subtract the bias level and to apply the flat field correction. For each filter, the short and long exposures were co-added independently using the MULTIDRIZZLE package (Koekemoer et al. 2002). Cosmic rays and hot pixels were removed with this package and a correction for geometrical distortion was provided. Because these mainly affect the faint stars we did not

perform CTE corrections. The resulting data consist of one 40 s and one 1984 s exposure (1940 s for Lindsay 38) in F555W and one 20 s as well as one 1896 s exposure (1852 s for Lindsay 38) in F814W (Tab. 4.1). The HRC data of NGC 419 consist of 70 s and 1200 s exposure in F555W and 40 s and 1036 s exposure in F814W each.

The photometric reductions were carried out using the DAOPHOT package in the IRAF¹ environment on DRIZZLED images.

WFC: Saturated foreground stars and background galaxies were discarded by using the Source Extractor (Bertin & Arnouts 1996). Due to the different crowding and signal-to-noise ratio properties of the long and the short exposure, photometry involving point spread function (PSF) fitting was only performed on the long exposures. For the short exposures, we used aperture photometry, which turned out to yield smaller formal errors than PSF photometry (see also Chapter 2). The detection thresholds were set at 3σ above the local background level for Lindsay 1, 1σ for Kron 3 and 4σ for NGC 339, NGC 416, and Lindsay 38 in order to detect even the faintest sources. The threshold levels were set based on the different crowding effects of the single clusters. The data reduction and photometry for the WFC images followed exactly the procedures outlined in Chapter 2, and for a detailed description we refer the reader to this paper.

HRC (NGC 416, NGC 419): The photometry was carried out independently in F555W and F814W. The detection threshold was set at 4σ for both NGC 416 and NGC 419 above the local background level.

For those stars common in both filters, we first performed aperture photometry using an aperture radius of 2 pixels to avoid the diffraction ring. Due to the fact that the PSF does not vary on the HRC images, a PSF then was constructed by combining 10 bright and isolated stars that were uniformly distributed over the entire image. The PSF photometry was then carried out. The objects found in both images were cross-identified and merged with a software package written by P. Montegriffo (private communication).

A spatial projection of the clusters' location towards the SMC (*red circles*) is shown in Figure 4.1 superimposed on a star map of the SMC generated using the point source catalog of the Small Magellanic Cloud Photometric Survey (Zaritsky et al. 2002) for stars $V < 16.5$ mag. Additionally, we show the location of the eight intermediate-age star clusters (*blue crosses*), which we will discuss in § 7.

We show the photometric errors assigned by DAOPHOT for Kron 3 in Figure 4.2 as these are representative of our WFC data. The formal photometric errors remain negligible over a wide range of magnitudes for stars measured on the short exposures. Photometry obtained with aperture photometry on the long exposure yields smaller errors for stars brighter than $m_{555,814} \sim 22$ mag than with PSF photometry. In Kron 3, all brighter stars in the long exposures down to $m_{555} < 18.5$ mag and $m_{814} < 18.7$ mag are saturated. For stars brighter than $m_{555,814} = 20$ mag, the short exposure sample (*blue dots*), in the interval between $21.8 < m_{555,814} < 20$ mag the long exposure aperture photometry sample (*red dots*) and for stars fainter than $m_{555,814} = 21.8$ mag the long exposure PSF photometry sample (*black dots*) was used. We determined the cuts between the samples based on the m_{555} data and adopted the same value for m_{814} so as to avoid a color slope associated with this division.

For our study, we rejected all stars with a σ error larger than 0.2 mag and a DAOPHOT sharpness parameter $-0.2 \leq s \leq 0.2$ in both WFC and HRC filters. The resulting color-magnitude diagrams (CMD) of Lindsay 1, Kron 3, NGC 339, NGC 416, Lindsay 38, and NGC 419 are shown and discussed in the following Section.

3. The Color-Magnitude Diagrams

All the CMDs of our six clusters show a well-populated main-sequence (MS), and clearly defined sub-giant and red-giant branches (SGB and RGB, respectively). The asymptotic giant branch (AGB) is less tightly defined, but clearly present in all cases, and especially evident in NGC 416 (Fig. 4.9).

¹IRAF is distributed by the National Optical Astronomy Observatory, which is operated by the Association of Universities for Research in Astronomy, Inc. under cooperative agreement with the National Science Foundation.

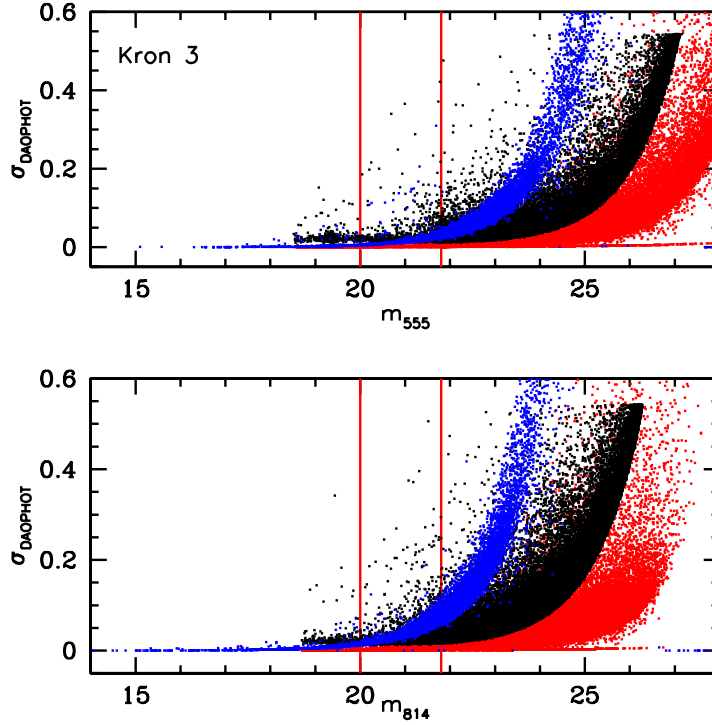


FIGURE 4.2. Photometric errors assigned by DAOPHOT to stars on the short (blue dots), and on the long (aperture photometry: red dots, PSF photometry: black dots) exposures for the cluster Kron 3. Stars brighter than ~ 18.5 mag in the long F555W exposure and brighter than ~ 18.7 mag in the long F814W exposure are saturated and are therefore not shown. The samples of the short, and the long exposures measured with aperture photometry and PSF photometry are combined at 21.8 mag and $m_{555} = 20$ mag (indicated by the thin vertical lines). For the F814W exposures we chose the same magnitude value in order to avoid introducing a color slope in the color-magnitude diagram of the resultant data set.

We define the main-sequence turnoff-point (MSTO) to represent the bluest point on the observed ridgeline. The data allow us to carry out the most accurate age measurement obtained so far (see Section 5), while also deriving improved distances. Lindsay 1, Kron 3, NGC 339, NGC 416, and Lindsay 38 appear to be single-age, simple stellar population objects, while the WFC data of NGC 419 shows multiple turnoff-points. For this reason we will discuss this cluster in greater detail in a separate paper (Sabbi et al., in preparation).

The CMDs show no obvious evidence for Galactic foreground contamination due to the high Galactic latitude of the SMC (e.g., Ratnatunga & Bahcall 1985). However, we find significant SMC field star contamination in the CMDs of Kron 3, NGC 339, NGC 416, and also in the HRC CMD of NGC 419. Field stars naturally are more problematic in CMDs of clusters near the SMC main body. For all clusters we give the magnitude of the MSTO, the red clump, and the red bump in Table 4.2. For the red clump and the red bump the mean magnitude was calculated by averaging the magnitudes of all clump and bump stars respectively and finding the maximum of each luminosity function.

For Kron 3 and Lindsay 38 no red bump was found. The red bump is a feature predicted by stellar evolution models, which imply that the luminosity of the RGB bump is dependent on the metallicity and age of the cluster. The failure to identify a red bump in the CMD of Lindsay 38 is due to its sparseness. The CMD of Kron 3, however, is well-populated, but despite sufficient statistics a red bump is not present, for which we have no physical explanation. In the CMDs of Lindsay 1, Kron 3, and NGC 339 a gap on the RGB at ~ 20 mag is visible. For Lindsay 1 and Kron 3 this feature is

artificial due to the cuts in photometric errors and sharpness we applied. However, for NGC 339 the gap appears to be real (see § 3.3).

3.1. Lindsay 1

The populous cluster Lindsay 1 (Lindsay 1958) is the westernmost known cluster in the SMC and lies around 3.5° west of the bar. Lindsay 1 is the second oldest star cluster in the SMC after NGC 121 (e.g., Chapter 2). The color-magnitude diagram (CMD) of Lindsay 1 is presented in Figure 4.3. The CMD reaches ~ 3 mag deeper than the previous deepest available photometry (Mighell et al. 1998a; Alcaino et al. 2003). Lindsay 1 is located in a low-density area outside the main body of the SMC (see Fig. 4.1). Therefore we find only little field star contamination by younger populations near Lindsay 1.

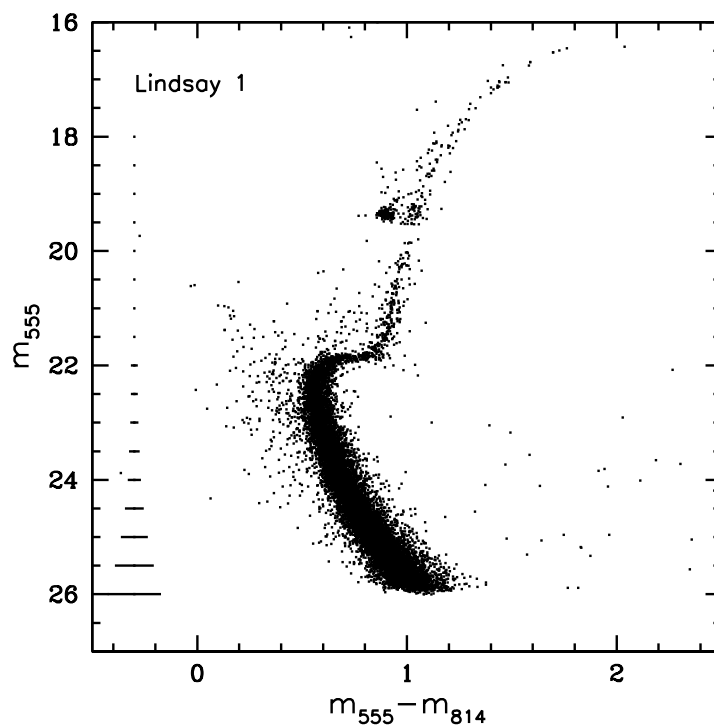


FIGURE 4.3. CMD of Lindsay 1 and its surroundings. Only stars with good photometry ($\sigma \leq 0.2$ mag and $-0.2 \leq \text{sharpness} \leq 0.2$) are shown; 15,321 stars in total. Representative errorbars (based on errors assigned by DAOPHOT) are shown on the left for the $m_{555}-m_{814}$ color.

In Figure 4.4 we display the CMD for the stars in the center region of Lindsay 1. The location of the cluster center was visually estimated. All stars within a radius of $45''$ were selected to create the center sample. Most of the field contamination has vanished. Given the width of our MS, we cannot infer any information on the presence and percentage of unresolved binary systems.

We find a well-populated red clump at a mean magnitude of $m_{555} = 19.36 \pm 0.04$ mag. Our value is in excellent agreement with the horizontal branch magnitude found by Sarajedini et al. (1995); Alves & Sarajedini (1999); Rich et al. (2000); Crowl et al. (2001, and Alcaino et al.(2003)). Obviously, Lindsay 1 is not old enough to have developed an extended red horizontal branch, which in itself is already a strong indication that Lindsay 1 is younger than NGC 121. We refer to Salaris & Girardi (2002a) who study the behavior of the red clump as a function of age.

The red clump of Lindsay 1 is ~ 0.35 mag brighter in F555W than that of NGC 121. The luminosity difference may imply that Lindsay 1 is closer than NGC 121 along the line-of-sight, which actually

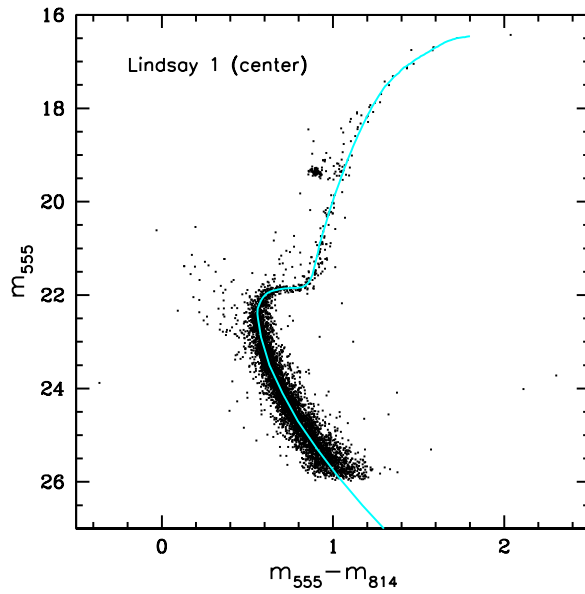


FIGURE 4.4. CMD of the central region of Lindsay 1. All stars within a radius of $45''$ were selected. We used this CMD for the determination of a representative color-magnitude ridgeline (cyan line) of Lindsay 1. This CMD contains 5,561 stars.

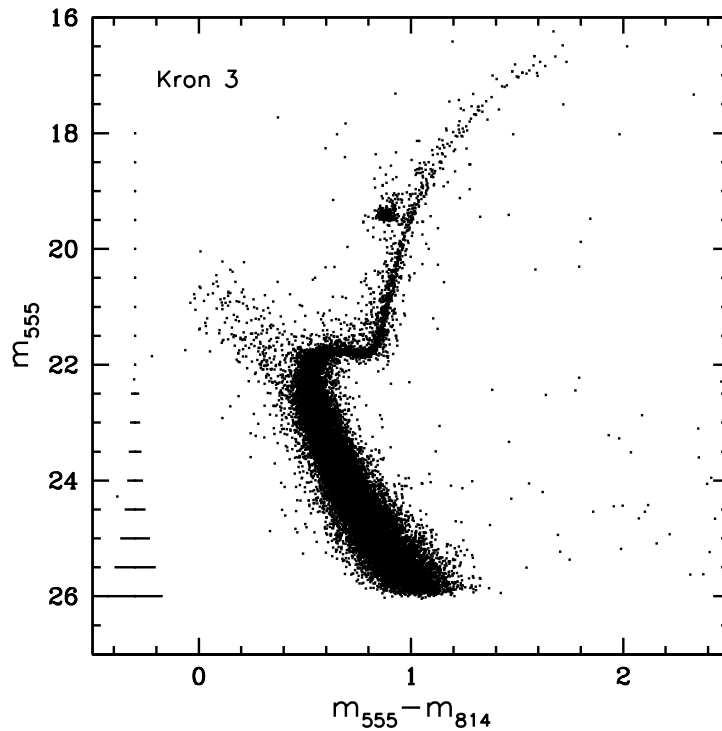


FIGURE 4.5. CMD of Kron 3 and its surroundings. Only stars with good photometry ($\sigma \leq 0.2$ mag and $-0.2 \leq \text{sharpness} \leq 0.2$) are shown; 30,264 stars in total. Representative errorbars (based on errors assigned by DAOPHOT) are shown on the left for the $m_{555} - m_{814}$ color.

seems to be the case (see § 6). Adopting the absolute red clump magnitudes given by Girardi & Salaris (2001), and the reddening values from the Schlegel maps (Schlegel et al. 1998) of $E_{B-V} = 0.03$ mag,

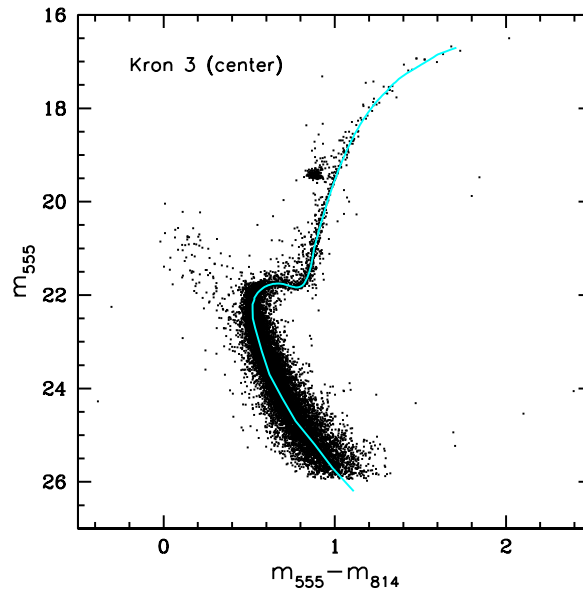


FIGURE 4.6. CMD of the central region of Kron 3. All stars within a radius of $40''$ were selected. We used this CMD for the determination of a representative color-magnitude ridgeline (cyan line) of Kron 3. This CMD contains 13,584 stars.

we find an absolute red clump magnitude difference between NGC 121 and Lindsay 1 of $\Delta M_{m555}^{RC} \sim 0.28$ mag. Therefore, the feature seen in Lindsay 1, should be considered a red clump and not a red horizontal branch.

The gap on the RGB at $m_{555} \sim 19.8$ mag is an artificial feature due to small number statistics resulting from our photometric selection (only photometry with $\sigma < 0.2$ mag and $-0.2 \leq s \leq 0.2$ is shown).

3.2. Kron 3

Kron 3 lies well outside the main SMC body, about 2° west of the bar. The cluster was first cataloged by Shapley & Wilson (1925), and it is number 3 in Kron's (1956) catalog of SMC star clusters. The highly populated CMD of Kron 3 is presented in Figure 4.5. The CMD reaches ~ 2 mag deeper than the previous deepest available photometry (Rich et al. 2000).

Field star contamination is visible along an extension of the main-sequence, towards brighter and bluer objects than at the cluster's MSTO. However, the cluster center is not affected by crowding, even though the center region is very dense.

In Figure 4.6 we display the CMD for the stars within $40''$ of the center of Kron 3. From the width of the MS, we cannot draw any conclusions about the presence of unresolved binary systems. The aforementioned traces of field contamination are still visible.

3.3. NGC 339

NGC 339 is located outside the SMC main body, around 1° south of the bar. The resulting CMD is shown in Figure 4.7, which reaches ~ 2 mag deeper than the previous deepest available photometry, published by Rich et al. (2000).

The SMC field is present along the luminous extension of the main-sequence. The cluster center is fully resolved and not affected by crowding since this is a very low density cluster. All features in our CMD are well defined. We cannot infer any information on unresolved binary systems due to the width of our MS. Unlike for the other clusters in our sample, the gap on the RGB at $m_{555} \sim 20$ mag

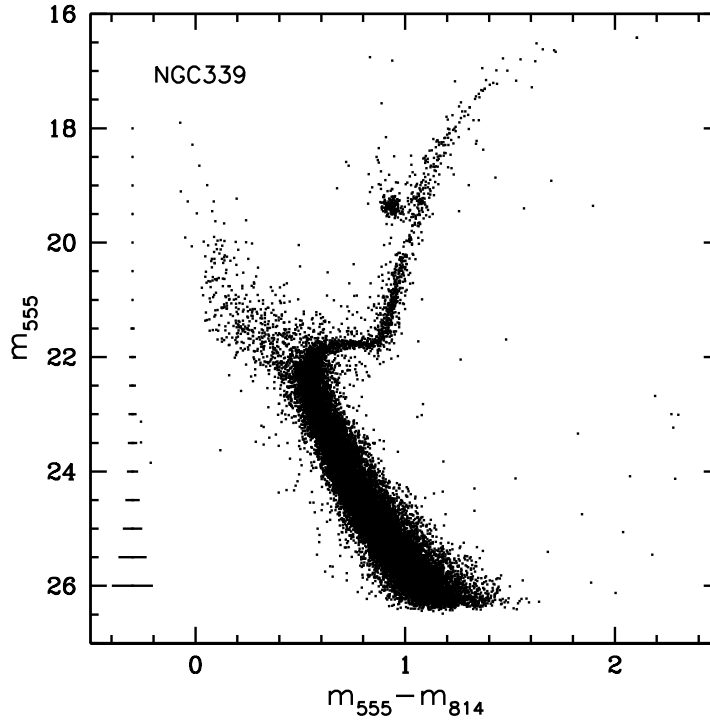


FIGURE 4.7. CMD of NGC 339 and its surroundings. Only stars with good photometry ($\sigma \leq 0.2$ mag and $-0.2 \leq \text{sharpness} \leq 0.2$) are shown; 29,304 stars in total. Representative errorbars (based on errors assigned by DAOPHOT) are shown on the left for the $m_{555}-m_{814}$ color.

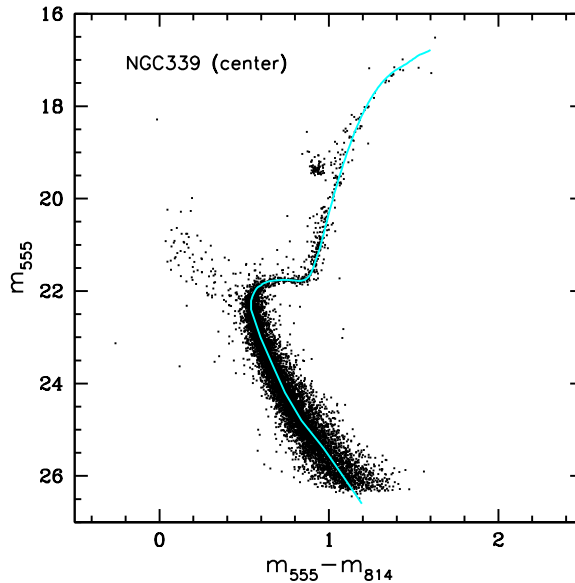


FIGURE 4.8. CMD of the central region of NGC 339. All stars within a radius of $35''$ were selected. We used this CMD for the determination of a representative color-magnitude ridgeline (cyan line) of NGC 339. This CMD contains 8,555 stars.

is not an artificial feature. It is visible in both the single short and long exposures and has also been found in other SMC clusters, e.g. NGC 288 (Bellazzini et al. 2002).

To create the center sample, all stars within a radius of $35''$ around a visually estimated center were selected and displayed in Figure 4.8. The SMC field is still clearly visible, which was expected due to the location of the cluster close to the SMC main body.

3.4. NGC 416

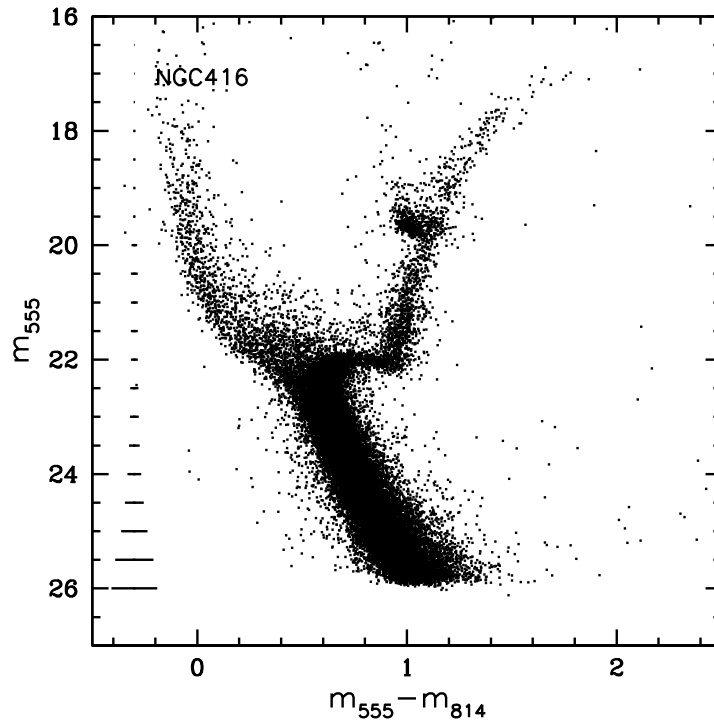


FIGURE 4.9. CMD of NGC 416 and its surroundings. Only stars with good photometry ($\sigma \leq 0.2$ mag and $-0.15 \leq \text{sharpness} \leq 0.15$) are shown; 18,764 stars in total. Additionally, we discarded all stars located within a radius of $15''$ around the cluster center, due to the high density of the cluster center and the resulting insufficient photometry. Representative errorbars (based on errors assigned by DAOPHOT) are shown on the left for the $m_{555}-m_{814}$ color.

The cluster NGC 416 is located in the wing of the SMC. This part of the SMC is characterized by an increased stellar density that may represent a tidal extension towards the LMC. Due to the location of NGC 416 in the wing of the SMC, we expect a very rich CMD with strong SMC field star features. Our resulting CMD (Fig. 4.9) indeed presents a densely populated MS, SGB, RGB, AGB and red clump as well as more luminous blue MS and blue loop stars that belong to younger SMC field populations. The RGB is also broadened by SMC field stars and is not as narrow as in the other clusters in our sample. About 0.1 mag offset to the blue of the RGB, we find a very well-populated AGB.

To obtain the final CMD we combine the HRC and the WFC photometry and discard the overlapping center region from the WFC catalog. For the WFC catalog, we only use PSF photometry of the long exposures and aperture photometry of the short exposures, because aperture photometry could not resolve single stars in the dense center region. The high density of the cluster center made it very difficult to find bright and isolated stars for the PSF sample in the cluster center. For the HRC data the long exposure images provided the better photometric quality. Therefore we do not include the short exposures in our final HRC catalog.

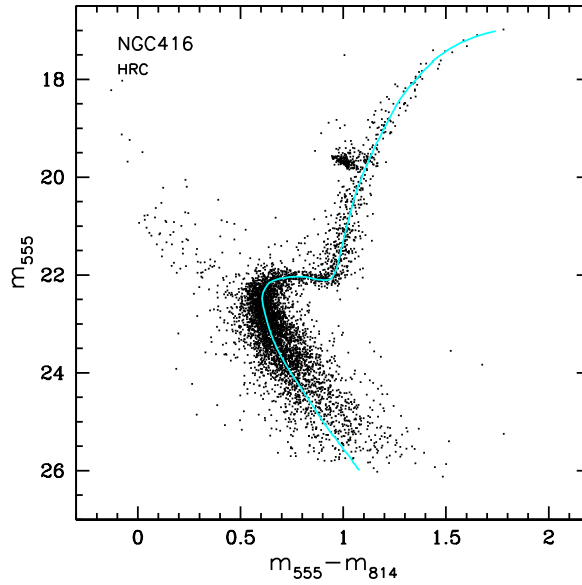


FIGURE 4.10. CMD of the HRC data of the center region of NGC 416. We used this CMD for the determination of a representative color-magnitude ridgeline (cyan line) of NGC 416. This CMD contains 4,992 stars.

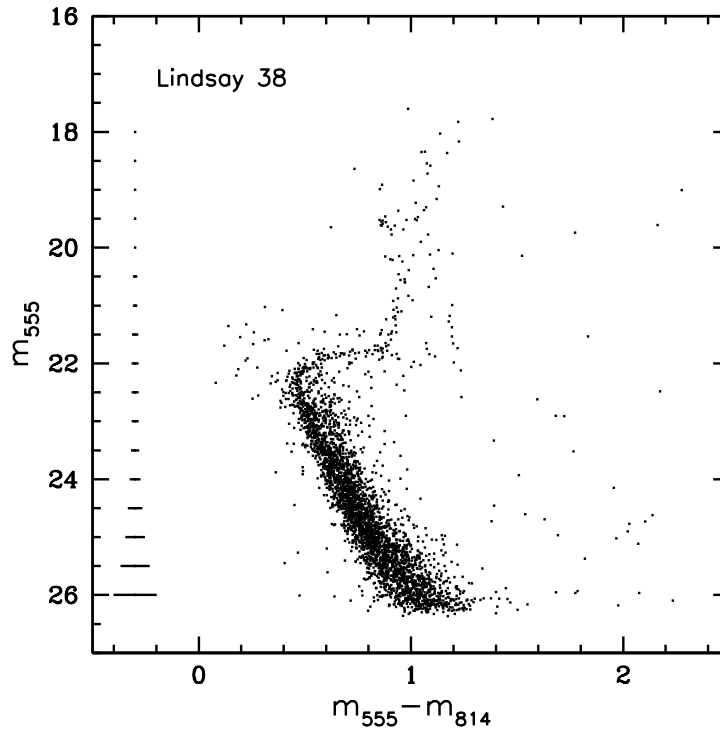


FIGURE 4.11. CMD of Lindsay 38 and its surroundings. Only stars with good photometry ($\sigma \leq 0.2$ mag and $-0.2 \leq \text{sharpness} \leq 0.2$) are shown; 3,716 stars in total. Representative errorbars (based on errors assigned by DAOPHOT) are shown on the left for the $m_{555} - m_{814}$ color.

In Figure 4.10 we display only the HRC data of the center region of NGC 416, which was used for the ridgeline fit. The CMD is still densely populated and all cluster features are clearly outlined.

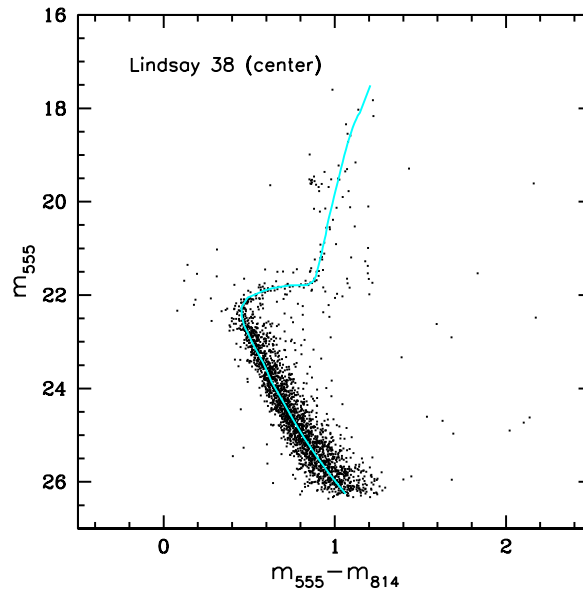


FIGURE 4.12. CMD of the central region of Lindsay 38. All stars within a radius of $70''$ were selected. We used this CMD for the determination of a representative color-magnitude ridgeline (cyan line) of Lindsay 38. This CMD contains 1,151 stars.

Interestingly, the RGB of NGC 416 is still broadened by contaminating field stars. The main-sequence is well defined until ~ 24 mag and fades out for fainter magnitudes. A number of younger stars of the SMC field are still visible above the MSTO.

3.5. Lindsay 38

Lindsay 38 is located about 3.3° north of the bar and is among the outermost SMC clusters. Piatti et al. (2001) published the first and as yet only CMD of Lindsay 38. Our resulting CMD of the cluster and its surroundings is shown in Figure 4.11. Our CMD reaches ~ 3 mag deeper than the CMD presented by Piatti et al. (2001), which was obtained from ground-based photometry. The cluster is very sparse and we identify only 3,716 candidate member stars.

In Figure 4.12 we show the CMD for the center sample. We selected stars within a radius of $70''$ around a visually estimated center location. The radius is almost twice as large as for the other clusters, due to the sparseness of the cluster.

The MS and the SGB are nevertheless well defined. Only a few stars populate the upper RGB, but the red clump is clearly visible.

3.6. NGC 419

Like NGC 416, the cluster NGC 419 is located in the wing of the SMC. For this cluster, we show in this paper only the HRC data, and will discuss and analyze the full CMD in a separate paper due to its complexity. The CMD reaches ~ 2 mag deeper than the previous deepest available photometry, published by Rich et al. (2000).

Figure 4.13 displays our CMD of NGC 419, the youngest cluster in our sample. Only long exposure PSF photometry was used. The upper MS is rather broad and densely populated. The CMD reaches ~ 4.5 mag below the MSTO, but due to shorter exposure times and crowding, the MS becomes less densely populated at fainter magnitudes. The tip of the extended turn-off region lies at $m_{555} \sim 20$ mag, and more than one MSTO appear to be visible. For stellar populations in the corresponding age range (~ 1 - 1.6 Gyr), the hydrogen-shell burning phase lasts only for a short time (~ 70 Myr), which explains the sparse SGB (Schaller et al. 1992).

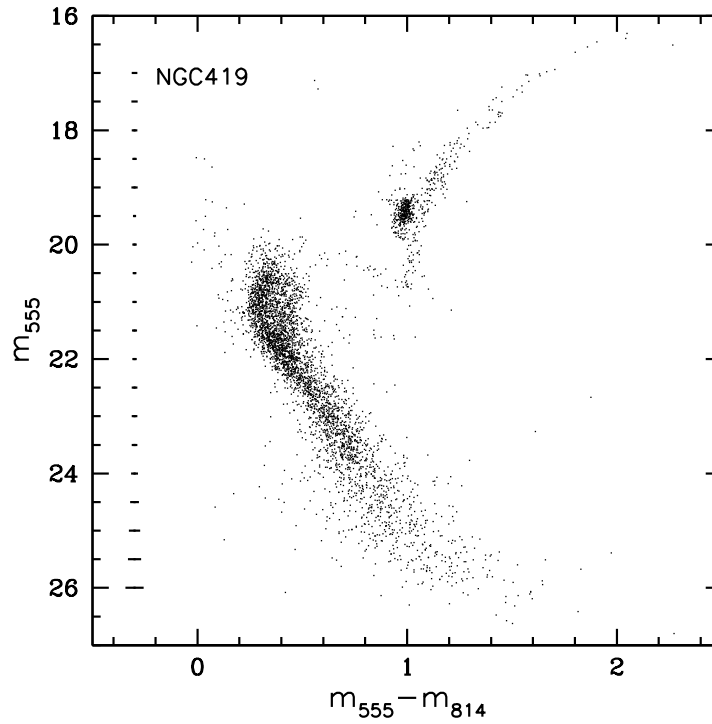


FIGURE 4.13. CMD of NGC 419 from the HRC images. Only stars with good photometry ($\sigma \leq 0.2$ mag) are shown; 4,543 stars in total. Representative errorbars (based on errors assigned by DAOPHOT) are shown on the left for the $m_{555}-m_{814}$ color.

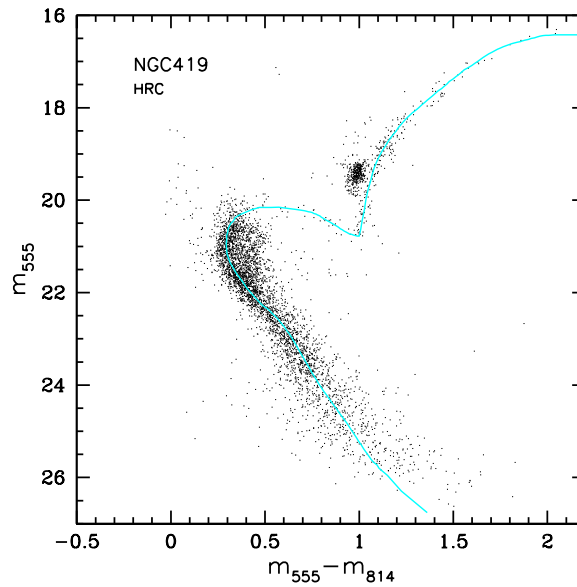


FIGURE 4.14. CMD of the central region of NGC 419. The derived fiducial ridgeline is shown as the cyan line.

At $m_{555} \sim 21.5$ mag and $m_{555} - m_{814} \sim 0.5 - 0.9$ mag in the CMD we find ~ 30 SMC field stars, which may belong to an older MSTO. Mackey et al. (2008) (see also Mackey & Broby Nielsen 2007) discovered the only two star clusters in the LMC known to have a double MS, NGC 1846 and

CLUSTER	$m_{555,TO}$ MAG	$m_{555,Bump}$ MAG	$m_{555,RC}$ MAG
NGC 121	22.98 ± 0.05	19.52 ± 0.04	19.71 ± 0.03
Lindsay 1	22.36 ± 0.05	19.25 ± 0.05	19.36 ± 0.04
Kron 3	22.40 ± 0.05	-	19.46 ± 0.03
NGC 339	22.30 ± 0.05	19.27 ± 0.04	19.38 ± 0.08
NGC 416	22.44 ± 0.05	19.65 ± 0.06	19.70 ± 0.07
Lindsay 38	22.36 ± 0.05	-	19.60 ± 0.05
NGC 419	21.40 ± 0.10	18.86 ± 0.12	19.41 ± 0.12

TABLE 4.2. **Observational data**

NGC 1806, which both have similar metallicities of about $Z = 0.0075$. The CMDs look very similar to NGC 419. Padova isochrones were used to determine the ages of NGC 1846 and NGC 1806 and yielded ages of 1.6 and 1.9 Gyr for both NGC 1846 and NGC 1806.

In Figure 4.14 we show the CMD with the derived ridgeline. At 19.41 ± 0.12 mag we find the vertically extended red clump. Below the red clump, ~ 0.2 mag fainter and ~ 0.1 mag in color to the blue, we find parts of a second red clump population at 19.53 ± 0.17 mag. For the old globular cluster NGC 121, we found the red clump at 19.71 ± 0.03 mag. Therefore we speculate that these fainter stars belong to a red clump of the old SMC field star population. If the luminosity difference (0.12 mag) between the two putative red clump populations were primarily due to distance (not age), then the distance d between the two populations can be calculated. We obtain $\delta d = 4$ pc.

The MSTO is located at 21.4 ± 0.1 mag and 0.41 ± 0.05 mag. We have to be cautious with the reliability of the determined MSTO, because as we will see in § 5.6 the isochrone models describe a hook-like feature past the MSTO, which is not visible in our CMD. This phase is traversed quite rapid (~ 27 Myr) for stars with ages between 1 and 1.6 Gyr (Schaller et al. 1992). This short phase lifetime is likely the reason why the hook is not visible.

4. BSS candidates

The stars blueward of and above the cluster MSTO are blue straggler star (BSS) candidates. In the same region often stars of the surrounding younger field population of the host galaxy are located. Knowledge of the BSS population of clusters is of interest with respect to constraining the binary fraction in these objects and with regard to understanding the formation mechanism of the BSS themselves (e.g., Bailyn 1995). BSS have been detected in a wide range of cluster types including very young, populous Magellanic Cloud clusters (e.g., Grebel et al. 1996), and old globular clusters (e.g., Ferraro et al. 2003). Carraro et al. (2008) showed for three open Galactic clusters that BSS are centrally concentrated when comparing the CMDs of the clusters and the surrounding field as one would expect for populations associated with a cluster. These authors re-emphasized the problem of field star contamination when trying to photometrically identify BSS.

Our ACS data do not cover fields adjacent to the clusters. Therefore, we calculated the projected distance from the cluster center for each BSS candidate. We then constructed a cumulative distribution of the number of blue stragglers as a function of projected radius. We have selected the BSS candidates by defining a region above the cluster main-sequence turnoff in the CMDs. We show the sample selection in the CMD of Kron 3 in Figure 4.15 as a representative example.

The cumulative radial distributions of the selected stars for all clusters can be seen in Figures 4.16, and 4.17. The dashed lines show the cumulative distributions for our BSS candidate samples, and the solid lines show the cumulative distributions of the cluster sample for comparison, including the SGB, the lower RGB, and the red clump.

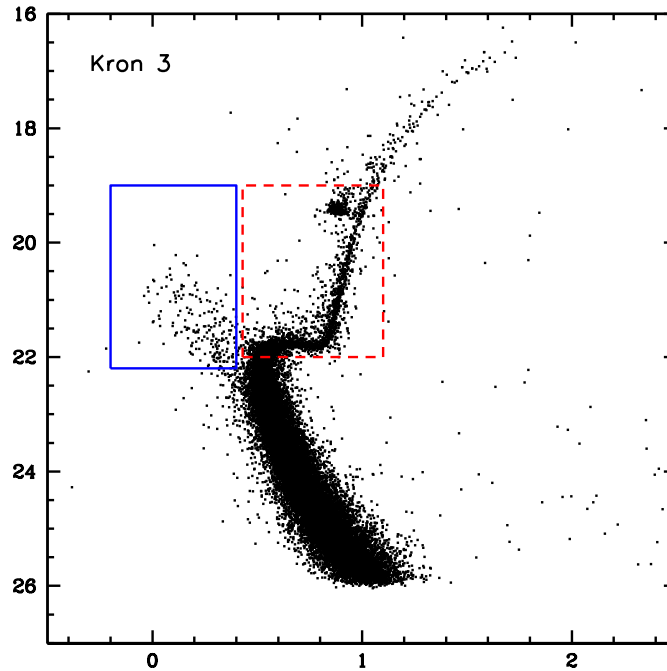


FIGURE 4.15. CMD of Kron 3 with displayed sample selection for the BSS sample (solid lines) and the cluster sample (dashed lines) including SGB, lower RGB, and red clump.

Each BSS candidate was examined by eye on the image and stars with hints of being affected by blends were eliminated from the catalog (see Table 4.3). The cumulative distributions of the remaining stars are normalized to our BSS candidate sample. The first panel of Figure 4.16 shows the cumulative distributions of NGC 121, of which we know that it contains BSSs (Shara et al. 1998, Clementini et al. in preparation). The BSS candidates are evidently more centrally concentrated than the stars from the cluster sample.

In Lindsay 1, Kron 3, NGC 339, Lindsay 38, and NGC 419 the blue stars lying above the cluster MSTOs do not show any obvious concentration toward the cluster centers and are fairly evenly distributed across our images. This supports the interpretation that they are not BSS candidates belonging to these clusters, but instead part of the younger MS of the SMC field star population. We have used the Kolmogorov-Smirnov (KS) test to search for statistical differences between the cumulative projected radial distributions. The KS probabilities that BSS candidates and cluster sample stars are extracted from the same parent population are 17% (Lindsay 1), 0% (Kron 3), 0% (NGC 339), 4% (Lindsay 38), and 25% (NGC 419). For NGC 416 and NGC 419, the radial distributions are only shown for the HRC data. Because BSSs are assumed to be located in the cluster center, and the field stars are already overdense in the BSS candidate region on the HRC CMD, the analysis of the HRC data instead of the entire sample is justified. Even though we know that NGC 121 contains BSSs and the radial distribution shows a concentration of the BSS candidates towards the cluster center, the KS-Test gives a probability of 16% that the two samples are from the same distribution.

Clementini et al. (in preparation) detected 20 pulsating variables in the region of the NGC 121 BSS stars that are all on the Planetary Camera (PC) camera of the Wide Field and Planetary Camera 2 (WFPC2) observations, hence are centrally concentrated within 20 arcsec from the cluster center. However, according to their pulsation periods these BSS stars are a mixture of 1) SX Phoenicis stars having a typical short period (P less than 0.1 days) and being old and metal-poor Population II variables generally observed in GCs; and 2) δ Scuti stars, which are Population I variables with typical

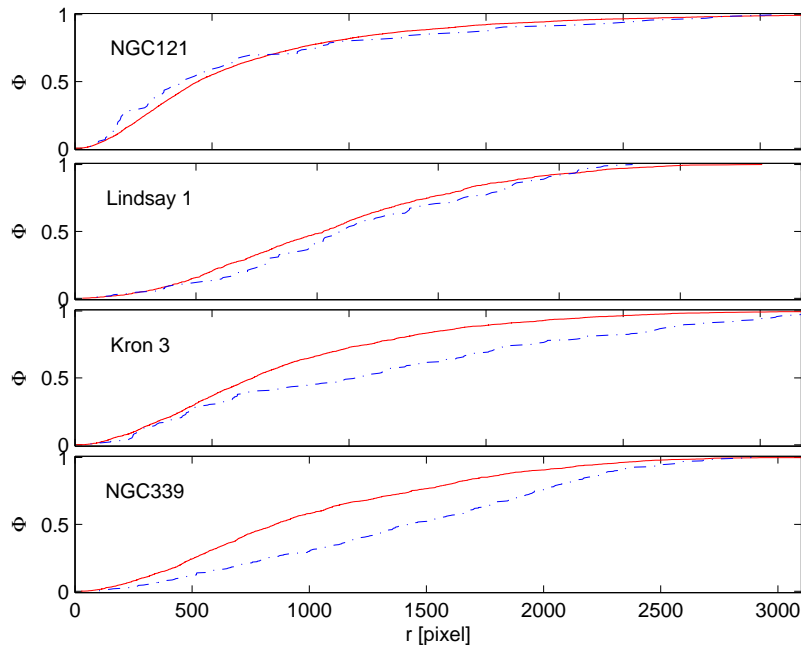


FIGURE 4.16. Cumulative radial distributions of blue straggler candidates as a function of projected radius for the clusters NGC 121, Lindsay 1, Kron 3, and NGC 339. The solid line represents the 'cluster sample' including the SGB, RGB, and red clump. The dashed line represents the stars found in the BSS region. The uppermost panel shows the distributions of NGC 121 for comparison, because we know it contains blue straggler stars (Shara et al. 1998, Clementini et al., in preparation). It is clearly visible that the BSS candidates are associated with the cluster rather than the field population. For Lindsay 1, Kron 3, and NGC 339, the BSS candidates are not as clearly concentrated in the cluster center and are rather younger main-sequence objects of the SMC field.

periods around $0.1 < P < 0.22$ days being generally young and metal-rich and typically found in the field of the Milky Way. Thus of the variables found in the BSS region of the NGC 121 CMD a fraction could be bona fide cluster variables (likely the SX Phe stars) and part could belong to the SMC field (likely the δ Scuti stars). It is surprising though that also the δ Scuti stars are found only on the PC (i.e. within 20 arcsec from the cluster center), while no short period variable was found in the three Wide Field Cameras of the WFPC2, as one would expect if the δ Scuti stars belong to the SMC field. Thus it is not obvious whether the short period variables of NGC 121 belong to the cluster or to the SMC field. Clementini et al. (in preparation) recovered all 34 BSS candidates of Shara et al. (1998) in their study of the NGC 121 variables, however only $\sim 50\%$ of the 20 short period variables coincide with the sample of Shara et al. (1998).

Within the center region of NGC 416 covered by the HRC data, we find an indication for centrally concentrated BSS candidates. The dashed line (BSS candidate sample) almost lies on top of the solid line (cluster sample). The cluster location is close to the SMC main body, hence some of the BSS candidates are likely field MS stars of the SMC. We will discuss the SMC field stellar population in greater detail in a separate paper. The KS probability for NGC 416 is 85%.

5. Cluster Ages

Age determinations of star clusters using isochrones depend crucially on the interstellar extinction, distance and metallicity of the cluster, as well as on the chosen isochrone models. We used

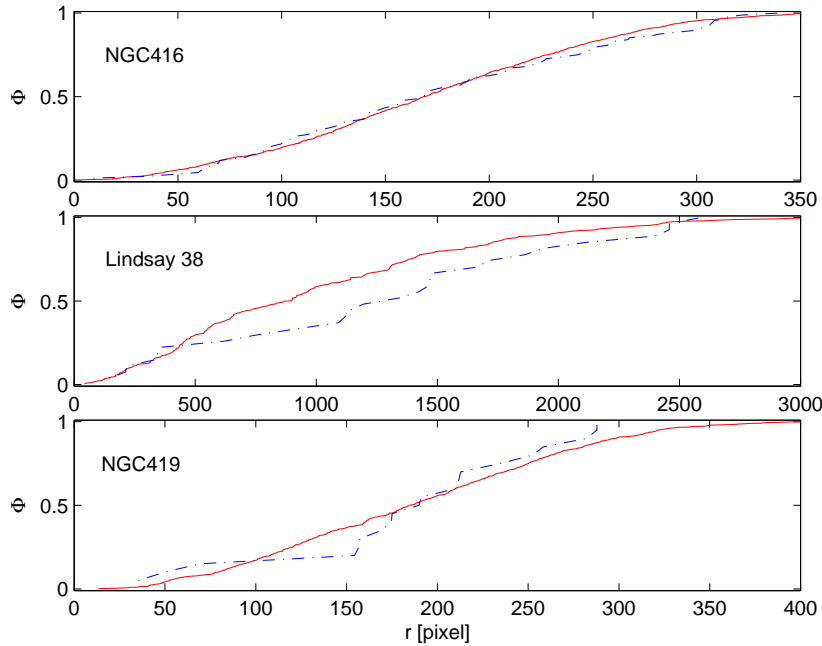


FIGURE 4.17. Cumulative radial distributions of blue straggler candidates with projected radius for the clusters NGC 416, Lindsay 38, and NGC 419. The solid line represents the 'cluster sample' including the SGB, RGB, and red clump. The dashed line represents the stars found in the BSS region. In Lindsay 38 and NGC 419, the BSS candidates are not significantly concentrated in the cluster center and are likely regular main-sequence stars. The distributions of NGC 416 and NGC 419 are obtained using the HRC sample. In NGC 416 there is indication for centrally concentrated BSS candidates.

CLUSTER	NUMBER OF BSS CANDIDATES ^a
Lindsay 1	110
Kron 3	229
NGC 339	616
NGC 416	91
Lindsay 38	23
NGC 419	8

TABLE 4.3. **BSS candidates.**

^a Number of BSS candidates after removal of stars possibly affected by blends

spectroscopic metallicities (Da Costa & Hatzidimitriou 1998; Kayser et al. 2006, 2007, Kayser et al., in preparation) in order to eliminate metallicity as a free parameter when fitting isochrone models. The distance and the extinction were treated as free parameters. The mean SMC distance modulus is assumed to be $(m - M)_0 = 18.88 \pm 0.1$ mag (60 kpc) (e.g., Storm et al. 2004). Due to the large depth extension of the SMC and thus an expected wide spread in the cluster distances we adjusted the distance modulus for each star cluster to produce the best isochrone fits to our CMD data.

As mentioned before, we visually estimated the location of the cluster center on the image and selected all stars within an individually defined radius on the WFC data, except for NGC 416 and

NGC 419 for which we used the HRC data. The center samples were used to fit the fiducial ridgelines for easier comparison to the isochrones.

In order to fit ridgelines, we separated the cluster sample CMDs into three sections: the MS, the SGB and the RGB. On the MS we determined the mode of the color distribution in magnitude bins of 0.3 mag width. For the SGB, we performed a linear least squares fit of a polynomial of 5th order to a Hess diagram of this region in the CMD. Finally, the RGB was fit by a third-order polynomial of the mean color, again in magnitude bins with a size of 0.3 mag each. The resulting ridgelines are shown as cyan lines in our CMDs. The full ridgeline Tables can be found in Appendix A.

We fitted our m_{555} vs $m_{555}-m_{814}$ CMDs with three different isochrone models: Padova isochrones (Girardi et al. 2000, 2008)², Teramo isochrones (Pietrinferni et al. 2004) and Dartmouth isochrones (Dotter et al. 2007), all with scaled solar abundances ($[\alpha/\text{Fe}]=0.0$). The Padova isochrone grid has an age resolution of $\log(t)=0.01$, the Teramo isochrone grid of 0.1 Myr and the Dartmouth isochrone grid of 0.5 Gyr. The Padova isochrones model the AGB and its tip, which is ~ 1 mag brighter than the tip of the RGB. The Teramo isochrones include the RGB, HB and the lower AGB. The Dartmouth isochrones terminate at the He flash, because they do not have the HB and the AGB sequence calculated. All sets of isochrones are available in the standard ACS color system.

We fitted a large number of isochrones using different combinations of reddening, age and distance. For each set of models, we selected by trial and error the isochrone that best matched the observed data.

5.1. Age of Lindsay 1

We adopted the metallicity of $[\text{Fe}/\text{H}] = -1.14 \pm 0.10$ from Da Costa & Hatzidimitriou (1998) in the scale of Zinn & West (1984) (ZW84). This metallicity corresponds most closely to $Z = 0.001$ in both the Padova and the Teramo models. Our best-fit age using Padova isochrones is 7.76 Gyr with $(m - M)_0 = 18.69$ mag and $E_{V-I} = 0.06$. The best fitting Teramo isochrone yields an age of $t = 8.3$ Gyr, $(m - M)_0 = 18.75$ mag, and $E_{V-I} = 0.04$ (see Fig. 4.18).

On the MS, the Padova isochrone is slightly offset to the red by about ~ 0.1 mag in color, while the Teramo isochrone is slightly offset by about ~ 0.02 mag in color. Between $22 \lesssim m_{555} \lesssim 23$ mag, both the Padova isochrone and the Teramo isochrone are shifted by ~ 0.05 mag to the blue with respect to the main ridgeline. Both isochrones provide an excellent approximation to the SGB and to the lower RGB up to about 1 mag below the red clump. At brighter magnitudes, the two isochrones deviate increasingly to the blue of the observed upper RGB. Here the Padova isochrones show the strongest difference, deviating by approximately 0.24 mag in color from the observed tip of the RGB. The Teramo isochrone is too blue by about 0.13 mag at the magnitude of the tip of the RGB.

The best fit using the Dartmouth isochrones is obtained with 7.5 Gyr, $(m - M)_0 = 18.73$ mag and $E_{V-I} = 0.02$ for an isochrone corresponding to a metallicity $[\text{Fe}/\text{H}] = -1.00$ (Fig. 4.19). As for the Padova and the Teramo isochrones, on the MS the isochrone is ~ 0.02 mag offset to the red. The SGB is fitted to a very well and the deviation on the RGB is much smaller than for the other two isochrone models. On the upper RGB, the isochrone is increasingly offset to the red relative to the fiducial ridgeline. The derived reddening by the Dartmouth isochrones agrees best with the extinction $A_V = 0.1$ from the Schlegel et al. (1998) maps ($E_{V-I} = 0.024$ mag). The reddening law of Dean et al. (1978) is assumed.

In the Figures 4.20 and 4.21 we show a range of isochrones for the three sets of stellar evolution models in order to illustrate the age uncertainty in a given model. The best fit isochrone is always displayed along with two younger and two older isochrones. Due to the high quality of the fit of the central isochrone in the region of the upper MS, SGB, and lower RGB in all models and the larger deviations of the adjacent isochrones, we estimate that the resultant age uncertainty is of the order of approximately ± 0.7 Gyr for the Teramo and Padova isochrones and ± 0.5 Gyr for the Dartmouth isochrones.

²http://pleiadi.pd.astro.it/isoc_photsys.02/isoc_acs.wfc/index.html

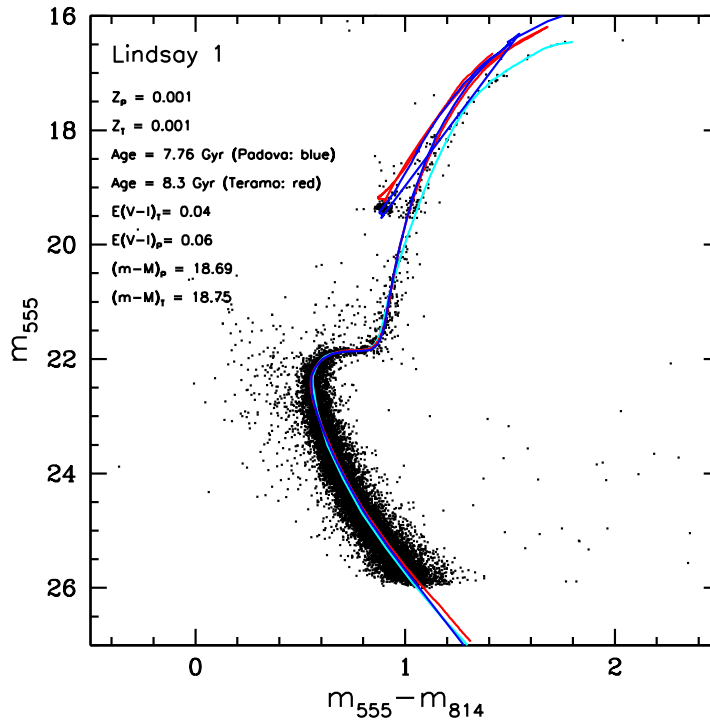


FIGURE 4.18. The CMD of Lindsay 1 with the best-fitting isochrones of two different models: The blue solid line shows the best-fitting Padova (Girardi et al. 2000, 2008) isochrone that is closest to the spectroscopically measured metallicity of the cluster. The red solid line is the best-fitting Teramo (Pietrinferni et al. 2004) isochrone approximating the known metallicity. The cyan solid line is our fiducial ridgeline. The fitting parameters are listed in the plot legend.

5.2. Age of Kron 3

We adopted the spectroscopic metallicity derived by Da Costa & Hatzidimitriou (1998) of $[\text{Fe}/\text{H}] = -1.08 \pm 0.12$. This metallicity corresponds most closely to $Z=0.001$ in the Padova models, $Z=0.002$ in the Teramo models and $[\text{Fe}/\text{H}] = -1.00$ in the Dartmouth models. The best-fit age using the Padova isochrones was found to be 7.1 Gyr, $(m - M)_0 = 18.80$ mag and $E_{V-I} = 0.033$. The best fit for the Teramo isochrones is obtained with $t = 7.2$ Gyr, $(m - M)_0 = 18.80$ mag and $E_{V-I} = -0.013$ (Fig. 4.22). No reasonable fit with a zero or positive reddening value was obtained.

On the MS, both isochrones are slightly offset to the red by about ~ 0.02 (Teramo) and ~ 0.01 (Padova) in color. The Teramo isochrone traces the SGB and the lower RGB to a high accuracy. Only at the faint end of the SGB the isochrone is about ~ 0.02 mag brighter than our fiducial ridgeline. The isochrone deviates increasingly to the blue of the observed upper RGB, but fits the color of the RGB tip very well with a small deviation of about 0.02 mag. The base of the red clump, however, is ~ 0.4 mag too bright. The Padova isochrone lies ~ 0.1 mag below our observed SGB and is ~ 0.02 mag offset in color on the lower RGB. The isochrone continues further to the blue on the upper RGB as seen for the Teramo isochrone. The Padova isochrone shows the strongest difference at the RGB tip, deviating by approximately 0.22 mag in color from the observed tip of the RGB. The base of the red clump is fitted very well.

The Dartmouth isochrone model provided by Dotter et al. (2007) yields the best fit to the CMD (Fig. 4.23). The best-fit isochrone has the parameters $t = 6.5$ Gyr, $(m - M)_0 = 18.83$ and $E_{V-I} = 0.008$. All the major features of the CMD are very well reproduced, including the upper RGB where the isochrone is offset slightly to the blue relative to the fiducial ridgeline. This offset is no more than

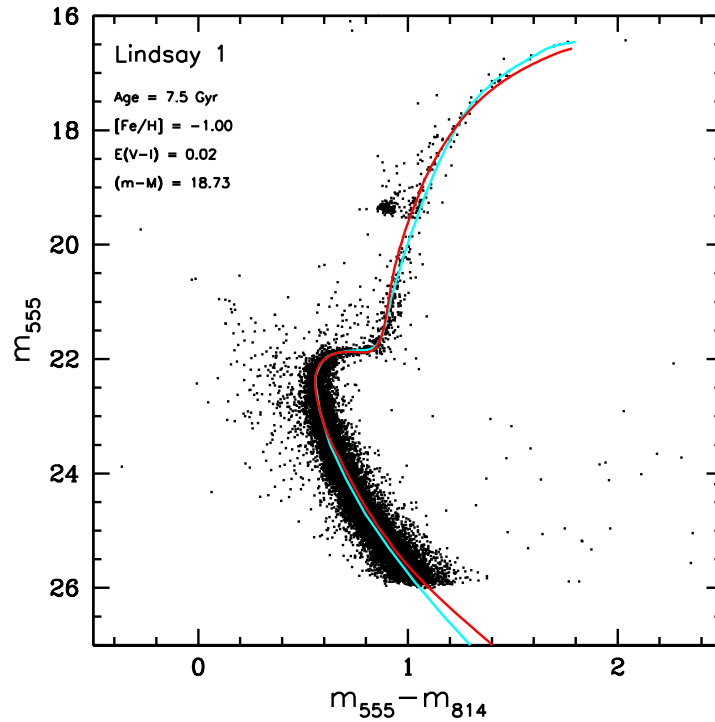


FIGURE 4.19. The Lindsay 1 CMD with the best-fitting Dartmouth (Dotter et al. 2007) isochrones overplotted in red. As before, the cyan line represents our fiducial for Lindsay 1. The fit parameters are listed in the plot.

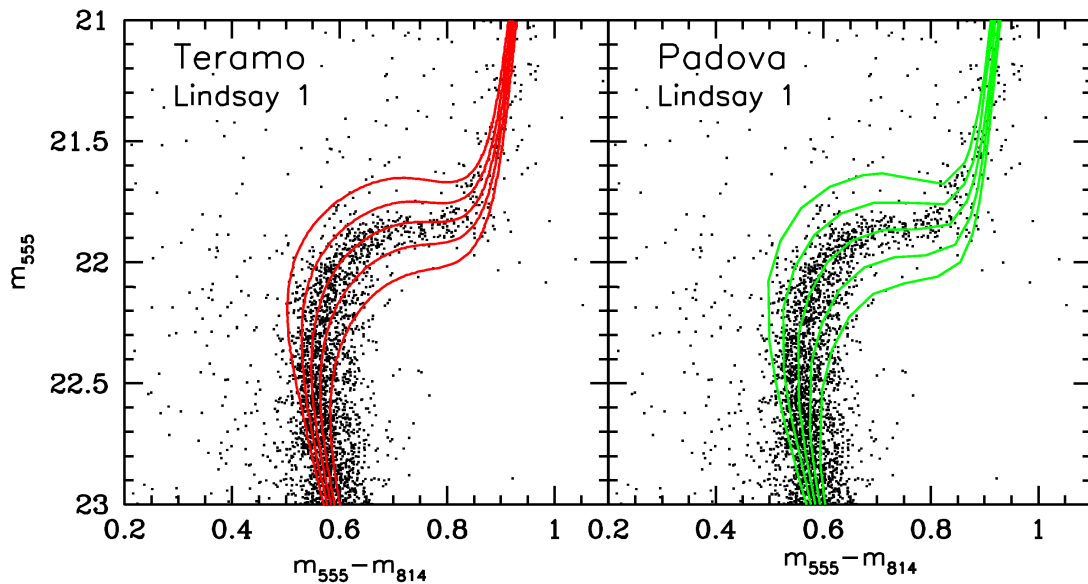


FIGURE 4.20. The CMD of Lindsay 1 after zooming in on the region of the main-sequence turnoff, subgiant branch, and lower red giant branch. In the upper panel, we show Teramo isochrones as solid lines, covering an age range of 6.8, 7.5, 8.2, 9 and 10 Gyr. In the lower panel we show the same plot for Padova isochrones in the available age steps of 6.16, 6.92, 7.76, 8.7, and 9.77 Gyr. All other parameters are the same as in Figs. 4.18 and 4.19.

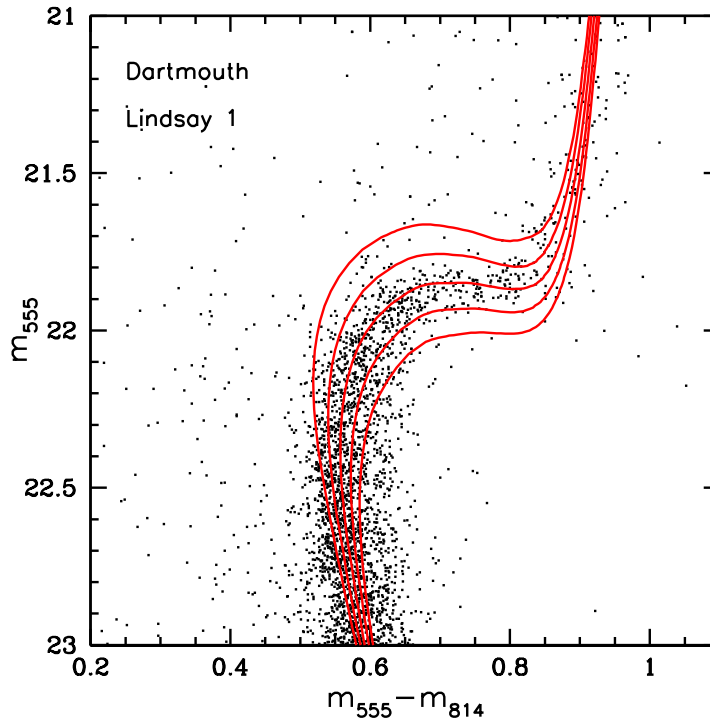


FIGURE 4.21. Same as Fig. 4.20, but for the Dartmouth isochrones with ages of 6.5, 7, 7.5, 8 and 8.5 Gyr.

0.02 mag on average along the entire upper RGB. Even the slope of the RGB is very well reproduced along its entire extent. The derived reddening for Padova isochrones agrees best with the extinction $A_V = 0.09$ from the Schlegel et al. (1998) maps ($E_{V-I} = 0.024$ mag).

In Figures 4.24 and 4.25 we display our "best" isochrone along with two older and two younger ones for each model. Here the deviations of these isochrone models from the observed upper MS and SGB are very clearly visible. We estimate the resultant age uncertainty in order of approximately ± 0.5 Gyr for the Teramo and Dartmouth isochrones and ± 0.7 Gyr for the Padova isochrones.

5.3. Age of NGC 339

We adopted a spectroscopic metallicity of $[\text{Fe}/\text{H}] = -1.12 \pm 0.10$ from Da Costa & Hatzidimitriou (1998), which made us use isochrones with $Z = 0.001$ for both the Teramo and the Padova models. The best age fit using the Teramo isochrone is found with the parameters $t = 6.6$ Gyr, $(m - M)_0 = 18.75$ mag and $E_{V-I} = 0.08$. Our best fitting Padova isochrone yields an age of $t = 6.3$ Gyr with $(m - M)_0 = 18.75$ mag and $E_{V-I} = 0.08$.

Both isochrones provide an excellent approximation to all features of the CMD (Fig. 4.26), the MS, the SGB and even the upper RGB, where the isochrones are only slightly offset to the blue relative to the fiducial ridgeline. These offsets are no more than 0.01 mag (Teramo) and 0.03 mag (Padova) in color on average along the entire upper RGB. Also the slope of the RGB is very well reproduced along its entire extent. At the RGB tip, the Padova isochrone deviates by approximately 0.15 mag in color to the red from the observed RGB tip, while the Teramo isochrone match the observed color and luminosity of the tip better, deviating ~ 0.10 mag in color to the red. The Teramo isochrone shows a magnitude for the base of the red clump that is about 0.2 brighter than the observed one. The Padova isochrone indicates a magnitude for the base of the red clump that is 0.2 mag too faint.

Figure 4.27 shows the best-fit isochrone for the Dartmouth model. The best fit is obtained with an age of $t = 6$ Gyr and the parameters $(m - M)_0 = 18.75$ mag and $E_{V-I} = 0.06$. The Dartmouth

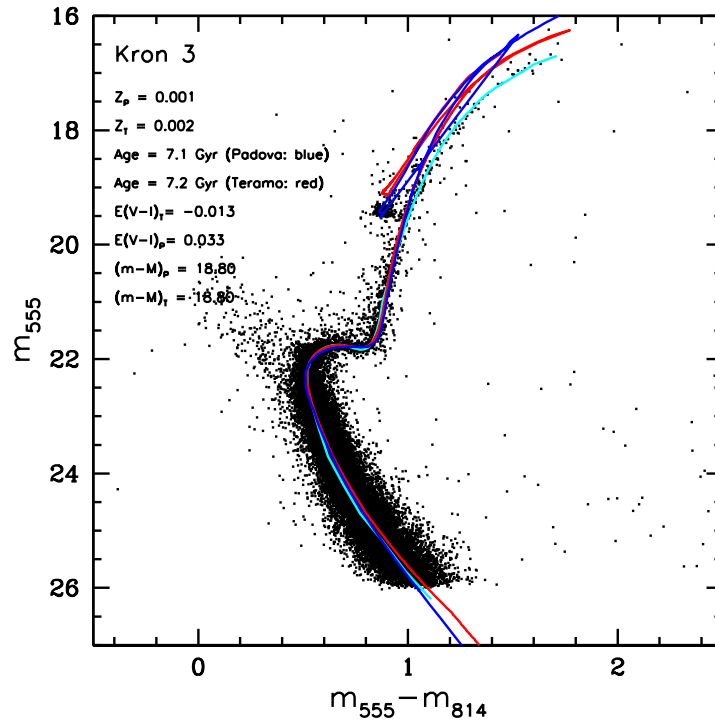


FIGURE 4.22. The CMD of Kron 3 with the best-fitting isochrones of two different models: The blue solid line shows the best-fitting Padova isochrone that is closest to the spectroscopically measured metallicity of the cluster. The red solid line is the best-fitting Teramo isochrone approximating the known metallicity. The cyan solid line is our fiducial ridgeline. The fit parameters are listed in the plot legend.

isochrone traces the ridgeline on the MS, the SGB and the lower RGB to a very well. On the lower RGB, the isochrone is offset to the blue by ~ 0.03 mag, while on the upper RGB it is ~ 0.05 mag too red. The derived reddening for Dartmouth isochrones agrees best with the extinction $A_V = 0.15$ from the Schlegel et al. (1998) maps ($E_{V-I} = 0.04$ mag).

In Figures 4.28 and 4.29 we show a range of isochrones for each model to illustrate the age uncertainty. We always display our "best" fit isochrone along with two older and two younger ones. Considering the excellent fit of all age-sensitive features of the CMD by all three stellar evolution models, we estimate the resultant age uncertainty to be approximately ± 0.5 Gyr for all three models.

5.4. Age of NGC 416

The latest spectroscopic metallicity measurement was performed by Kayser et al. (in preparation) and yields a metallicity $[Fe/H]_{CG97} = -0.87 \pm 0.06$ in the scale of Carretta & Gratton (1997) (CG97). We transform this metallicity to the ZW84 scale using the transformation given by Carretta & Gratton (1997), and obtain a metallicity of $[Fe/H]_{ZW84} = -1.00$. This metallicity corresponds most closely to $Z = 0.002$ for both the Teramo and the Padova models. In Figure 4.30, the CMD with the overplotted Teramo and Padova isochrones is shown. The best fit for the Teramo isochrones is obtained with $t = 6.0$ Gyr, $(m - M)_0 = 18.88$ mag and $E_{V-I} = 0.105$, while the Padova isochrones provide $t = 6.6$ Gyr, $(m - M)_0 = 18.76$ mag and $E_{V-I} = 0.10$. The relatively high reddening value is due to the location of the cluster close to the SMC main body (see Fig. 4.1).

On the MS, both the Teramo isochrone and the Padova isochrone are offset to the blue by about ~ 0.01 mag. While the Teramo isochrone fits the MSTO rather nicely, the Padova isochrone is ~ 0.05 mag too blue. At the blue end of the SGB, both isochrones are slightly too faint. The Teramo

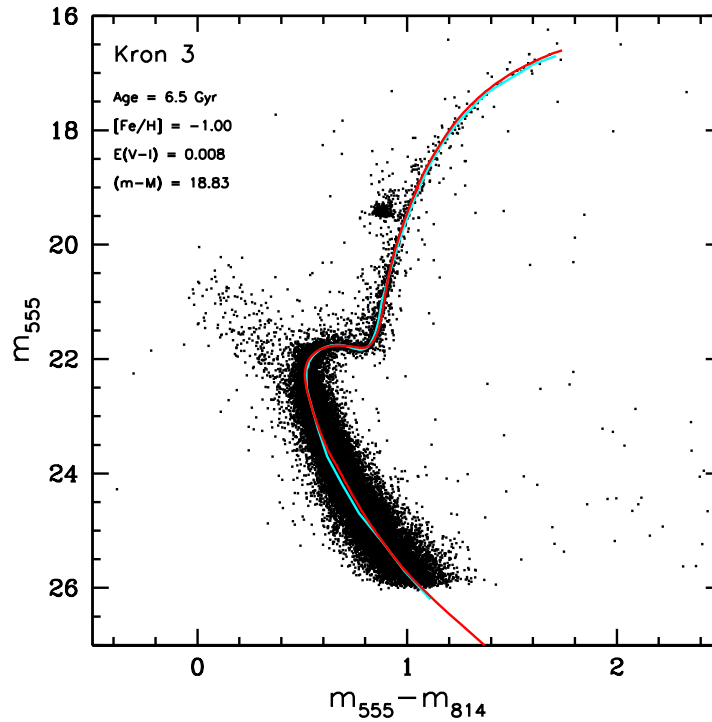


FIGURE 4.23. The Kron 3 CMD with the best-fitting Dartmouth isochrones overplotted in red. As before, the cyan line represents our fiducial for Kron 3. The fit parameters are listed in the plot.

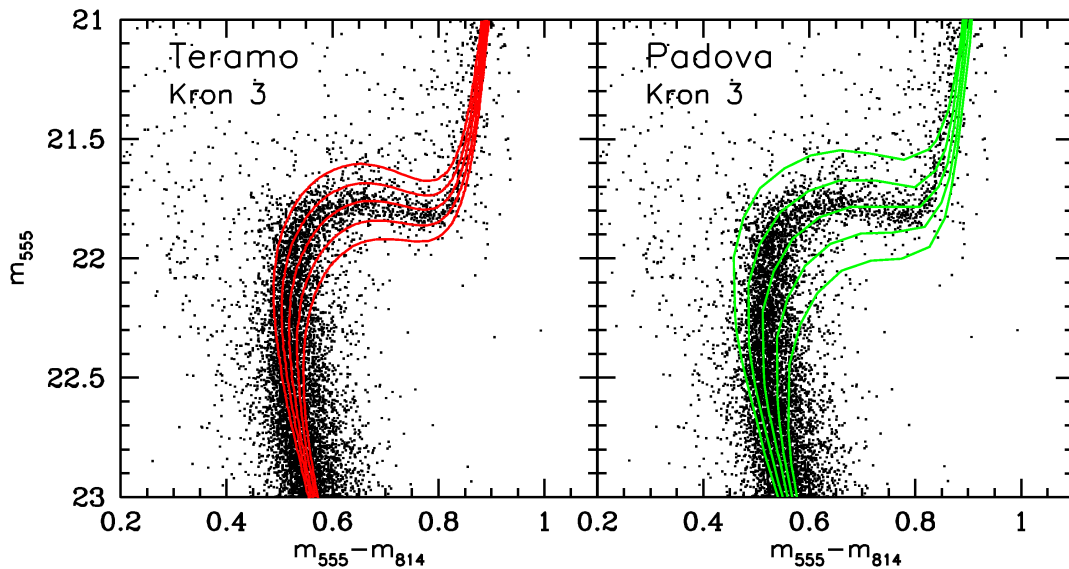


FIGURE 4.24. The CMD of Kron 3 after zooming in on the region of the main-sequence turnoff, subgiant branch, and lower red giant branch. In the upper panel, we show Teramo isochrones as solid lines, covering an age range of 5.2, 6.1, 7, 7.8, and 8.4 Gyr. In the lower panel we show the same plot for Padova isochrones in the available age steps of 5.6, 6.3, 7.1, 7.9, and 8.9 Gyr. All other parameters are the same as in Figs. 4.22 and 4.23.

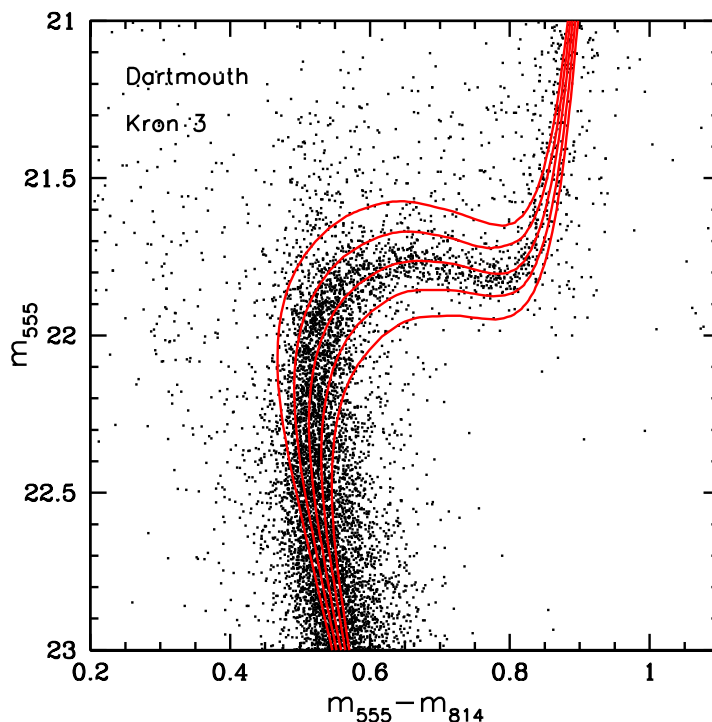


FIGURE 4.25. Same as Fig. 4.24, but for the Dartmouth isochrones with ages of 5.5, 6, 6.5, 7, and 7.5 Gyr.

isochrone fits the red part of the SGB and the entire RGB almost perfectly up to about 0.5 magnitudes below the RGB tip (see Fig. 4.30). The Padova isochrone fits the red end of the SGB almost perfectly, but deviates increasingly to the blue on the RGB with respect to our fiducial ridgeline. The isochrone shows a magnitude for the base of the red clump that is about 0.1 mag brighter than the observed one. The Teramo isochrone indicates a magnitude for the base of the red clump that is 0.25 mag too bright.

In Figure 4.31 the best fitting isochrone for the Dartmouth models (Dotter et al. 2007) is displayed with $t = 6$ Gyr, $(m - M)_0 = 18.83$ mag and $E_{V-I} = 0.12$. We adopted the isochrone set with a metallicity of $[Fe/H] = -1.0$. All age-sensitive features of the CMD are well reproduced. On the upper RGB, the isochrone is increasingly offset to the blue relative to the fiducial ridgeline with 0.03 mag in color being the strongest difference. Our derived reddenings agree with the extinction $A_V = 0.32$ from the Schlegel et al. (1998) maps ($E_{V-I} = 0.1$ mag).

In Figures 4.32 and 4.33 a range of five isochrones is displayed for each isochrone model. Even though the approximation of all features that are important for the age determination important features is close, we estimate the age uncertainty to be ~ 0.8 Gyr. It is possible that the broad width of the RGB suggests a spread in metallicity and therefore in age, which we have to take into account. The main reason for the broadening of the RGB, however, are SMC field stars.

5.5. Age of Lindsay 38

The latest measured spectroscopic metallicity provided by Kayser et al. (2006, 2007, 2009 in prep.) is $[Fe/H]_{CG97} = -1.35 \pm 0.10$, which we transformed to $[Fe/H]_{ZW84} = -1.59$ (Carretta & Gratton 1997). This metallicity is in excellent agreement with the photometric metallicity found by Piatti et al. (2001). We used isochrones of $Z = 0.0004$ in the Padova models, $Z = 0.0006$ in the Teramo models and $[Fe/H] = -1.49$ in the Dartmouth models. The best-fit age using the Teramo isochrone is $t = 6.3$ Gyr with $(m - M)_0 = 19.02$ mag and $E_{V-I} = 0.06$. The best fitting Padova isochrone yields an age of $t = 6.3$ Gyr, $(m - M)_0 = 19.00$ and $E_{V-I} = 0.075$ (Fig. 4.34). Surprisingly, Lindsay 38 is the

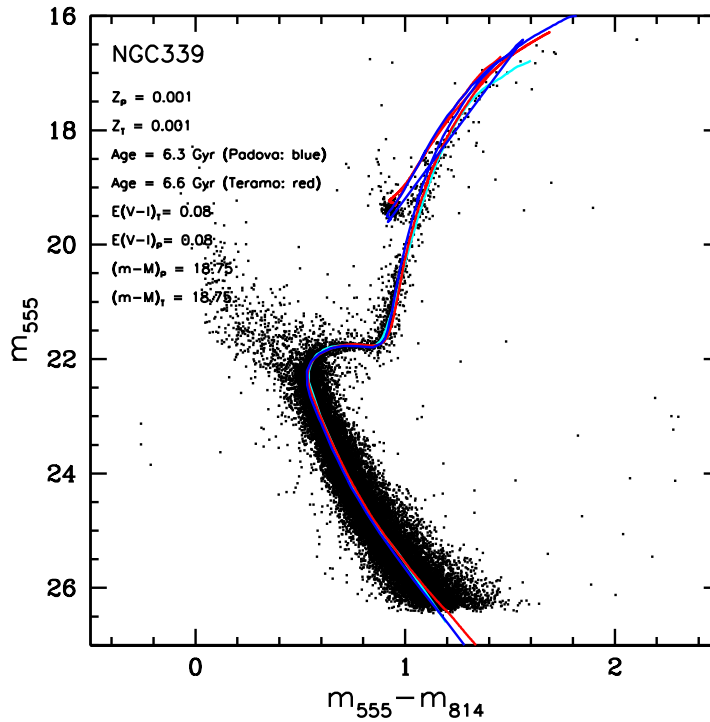


FIGURE 4.26. The CMD of NGC 339 with the best-fitting isochrones of two different models: The blue solid line shows the best-fitting Padova isochrone that is closest to the spectroscopically measured metallicity of the cluster. The red solid line is the best-fitting Teramo isochrone approximating the known metallicity. The cyan solid line is our fiducial ridgeline. The fit parameters are listed in the plot legend.

only cluster for which we found a high quality fit using α -enhanced Dartmouth isochrones ($[\alpha/\text{Fe}] = +0.20$), which yield an age of 6 Gyr using the same fitting parameters.

All features of the CMD are traced very well by both the Teramo and the Padova isochrones. At the faint end of the MS, the Teramo isochrone continues further to the red than the Padova isochrone and our derived ridgeline; however, this only becomes more apparent at magnitudes of $m_{555} = 25.5$ mag and below. The MS, the SGB and the lower RGB are very well reproduced. The upper part of the RGB is too sparse for the fit of a ridgeline. Therefore, a statement about the quality of the theoretical fiducials cannot be made. The base of the red clump for the Padova isochrone is about 0.2 mag too faint, while for the Teramo isochrone it is about 0.4 mag too bright.

In Figure 4.35 the best-fit age provided by the Dartmouth isochrone (Dotter et al. 2007) is shown with $t = 6.5$ Gyr, $(m - M)_0 = 18.94$ mag and $E_{V-I} = 0.05$ (red line in Fig. 4.35). The MS and the SGB are very well reproduced. The lower RGB is slightly offset by about 0.02 on average along the entire RGB. The isochrone deviates increasingly to the red starting at 1.5 mag above the red clump. The reddening value found using isochrones is too high compared with the extinction taken from the Schlegel et al. (1998) maps ($A_V = 0.05$, $E_{V-I} = 0.016$ mag).

In Figures 4.36 and 4.37 we show a selection of isochrones to estimate the age uncertainty. For each isochrone model two older and two younger isochrones are shown along with the "best" one. We estimate the age uncertainty to be ± 0.5 Gyr for all of the three isochrone models.

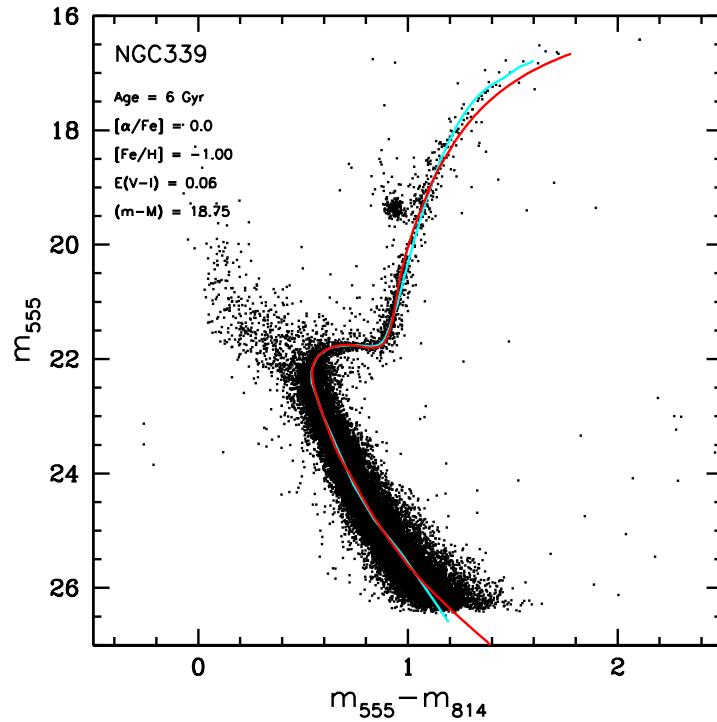


FIGURE 4.27. The NGC 339 CMD with the best-fitting Dartmouth isochrones overplotted in red. As before, the cyan line represents our fiducial for NGC 339. The fit parameters are listed in the plot.

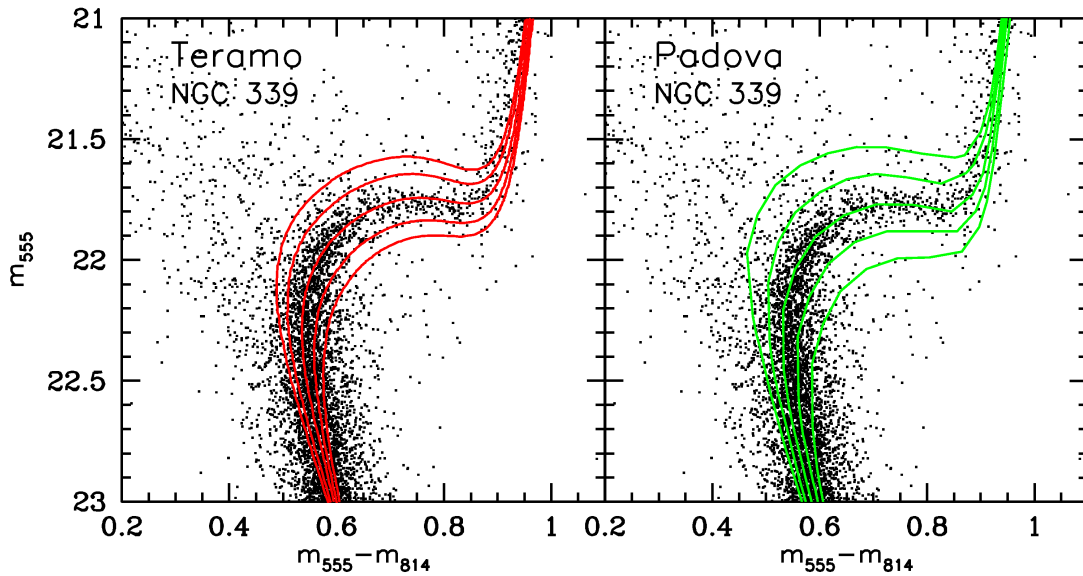


FIGURE 4.28. The CMD of NGC 339 after zooming in on the region of the main-sequence turnoff, subgiant branch, and lower red giant branch. In the upper panel, we show Teramo isochrones as solid lines, covering an age range of 5.6, 6, 6.6, 7.2, and 7.7 Gyr. In the lower panel we show the same plot for Padova isochrones in the available age steps of 5, 5.6, 6.3, 7, and 7.9 Gyr. All other parameters are the same as in Figs. 4.26 and 4.27.

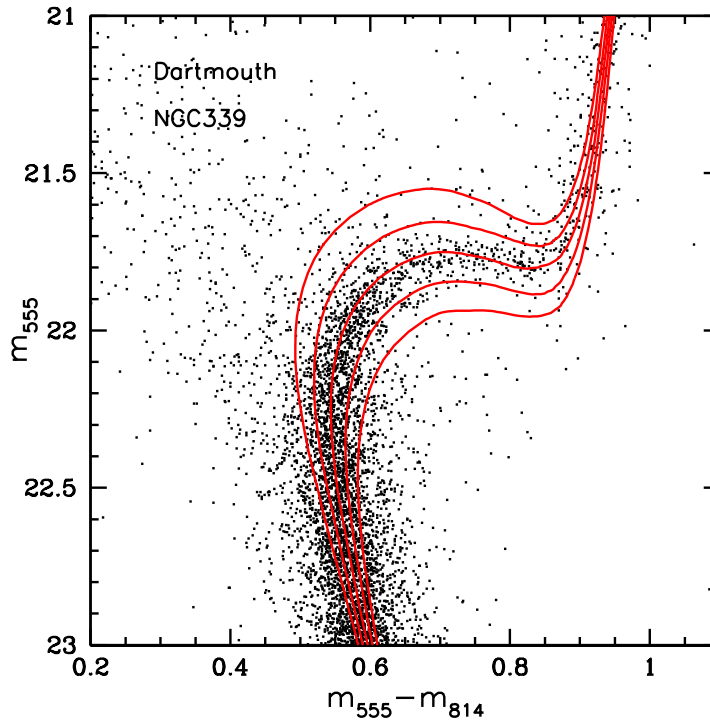


FIGURE 4.29. Same as Fig. 4.28, but for the Dartmouth isochrones with ages of 5, 5.5, 6, 6.5, and 7 Gyr.

5.6. Age of NGC 419

The latest spectroscopic metallicity measurement was performed by Kayser et al. (in preparation) and yields a metallicity $[Fe/H]_{CG97} = -0.71 \pm 0.12$ in the CG97 scale. We transform this metallicity to the ZW84 scale using the transformation given by Carretta & Gratton (1997), and obtain a metallicity of $[Fe/H]_{ZW84} = -0.67$. This metallicity corresponds most closely to $Z = 0.004$ (Padova and Teramo) and $[Fe/H] = -0.5$ (Dartmouth). The best fit for the Padova isochrones provides $t = 1.25$ Gyr with $(m - M)_0 = 18.75$ mag and $E_{V-I} = 0.12$ (see Fig. 4.38). The best-fit age using the Dartmouth isochrones is $t = 1.5$ Gyr with $(m - M)_0 = 18.60$ mag and $E_{V-I} = 0.07$. The Teramo model has problems with fitting all cluster features simultaneously (see Fig. 4.39). The best-fitting age is $t = 1$ Gyr with $(m - M)_0 = 18.94$ mag and $E_{V-I} = 0.11$. Note that it is not obvious where the exact location of NGC419's MSTO is.

As for NGC 416, we find a relatively high reddening parameter due to the cluster location close to the SMC main body, where also a lot of crowding is expected. The Padova isochrone fits the MS and the SGB very well, while the lower RGB is offset by ~ 0.05 mag in color, and its slope is not fitted at all. The isochrone does not fit the red clump, lies ~ 0.02 mag to the red and is ~ 0.6 mag too faint.

In Figure 4.41 we show Padova isochrones superimposed on the NGC 419 region. These are isochrones of 1.25, 1.4, and 1.6 Gyr. Because the exact location of the MSTO of the cluster is uncertain, we do not give a single age for NGC 419. Instead, we determine an age range of 1.2-1.6 Gyr.

In Figure 4.39 we can clearly see the inability of the Teramo isochrones to fit all cluster features simultaneously. The best-fitting Teramo isochrone (1 Gyr) deviates increasingly to the blue along the MS. At the MSTO the isochrone is about 0.15 mag offset to the blue. The RGB turn-off is ~ 0.2 mag too faint and the isochrone deviates again increasingly to the blue on the RGB.

The two youngest available Dartmouth isochrones have an age of 1 and 1.5 Gyr (Fig. 4.40). The age of NGC 419 lies between these two isochrones. This might be the reason why the best-fitting

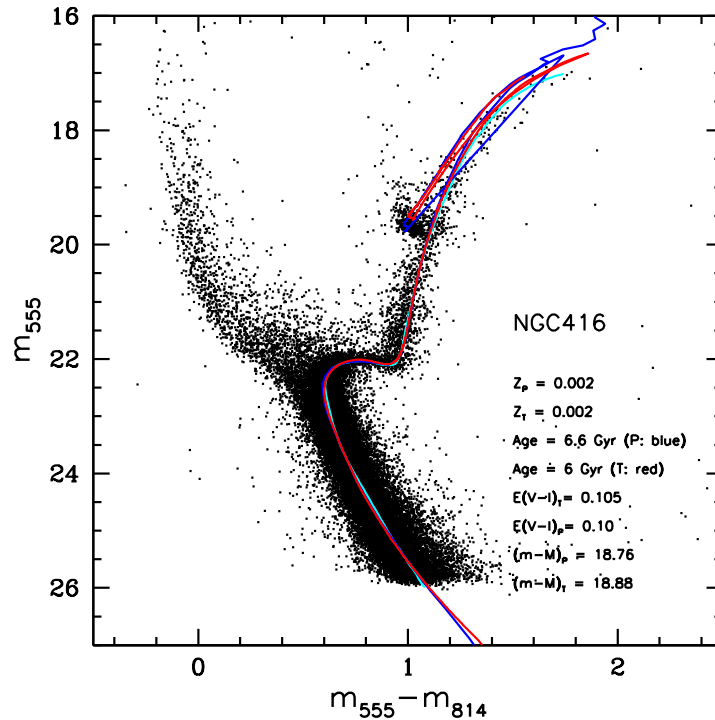


FIGURE 4.30. The CMD of NGC 416 with the best-fitting isochrones of two different models: The blue solid line shows the best-fitting Padova isochrone that is closest to the spectroscopically measured metallicity of the cluster. The red solid line is the best-fitting Teramo (Pietrinferni et al. 2004) isochrone approximating the known metallicity. The cyan solid line is our fiducial ridgeline. The fit parameters are listed in the plot legend.

Dartmouth isochrone does not provide a very good fit. The isochrone fits the RGB slope very well, but is ~ 0.04 mag offset to the blue at the RGB turn-off. The isochrone is ~ 0.25 mag too bright at the blue end of the SGB, and on the MS, the isochrone is slightly offset by about ~ 0.02 mag to the red. In Figure 4.42 we show the isochrones of 1 and 2 Gyr for comparison, which are obviously either too old or too young for NGC 419. As for the Padova isochrones, we cannot give a single age for NGC 419 and confirm the age range of 1.2-1.6 Gyr using the Dartmouth isochrones. Our derived reddening using the Dartmouth isochrone agrees with the extinction $A_V = 0.31$ from the Schlegel et al. (1998) maps ($E_{V-I} = 0.08$ mag), while the reddening values found using the Padova and the Teramo isochrones are too high.

Because of the complexity of NGC 419, we will discuss its CMD in more detail in a separate paper.

6. Distances

There are no direct determinations of the cluster distances along the line-of-sight, but it is assumed that the SMC has a depth extent of up to 20 kpc (Mathewson et al. 1988; Hatzidimitriou et al. 1993; Crowl et al. 2001; Lah et al. 2005). We assume that the main body of the SMC has a distance modulus of $(m - M)_0 = 18.88 \pm 0.1$ mag (e.g., Storm et al. 2004).

In addition to the distance estimates that result from our isochrone fits, we can use the apparent magnitudes of the red clump measured in this paper to provide a distance estimate for our clusters.

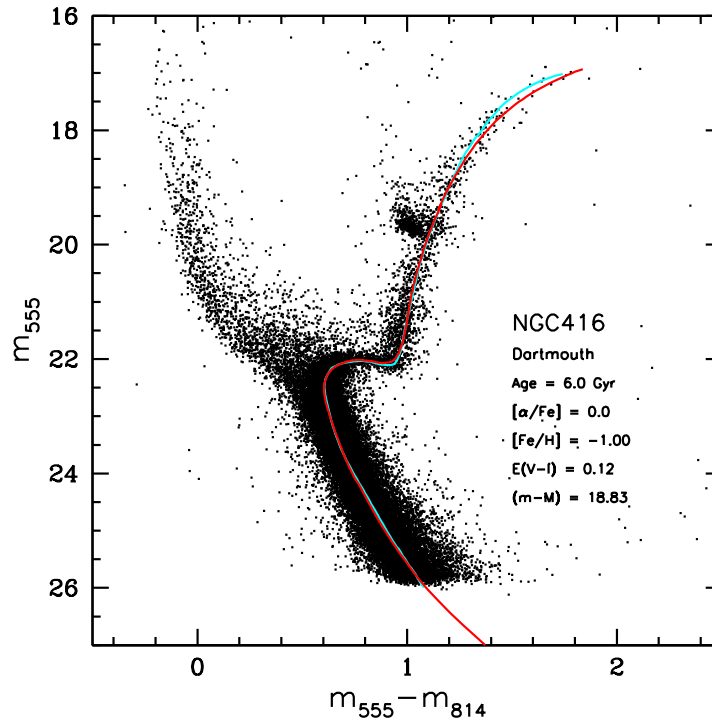


FIGURE 4.31. The NGC 416 CMD with the best-fitting Dartmouth (Dotter et al. 2007) isochrones overplotted in red. As before, the cyan line represents our fiducial for NGC 416. The fit parameters are listed in the plot.

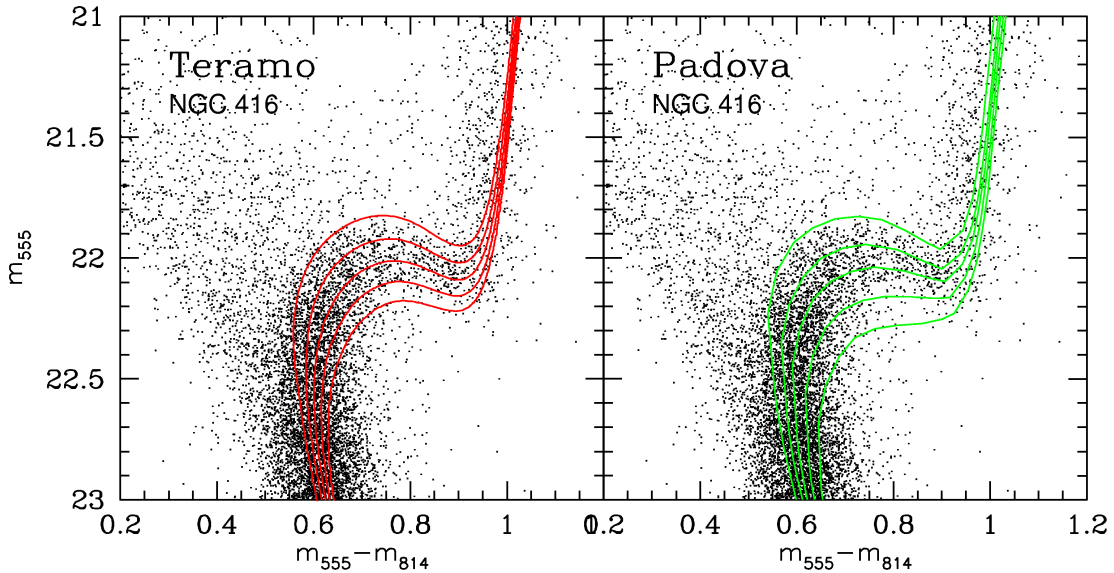


FIGURE 4.32. The CMD of NGC 416 after zooming in on the region of the main-sequence turnoff, subgiant branch, and lower red giant branch. In the upper panel, we show Teramo isochrones as solid lines, covering an age range of 5, 5.5, 6, 6.5, and 7 Gyr. In the lower panel we show the same plot for Padova isochrones in the available age steps of 5.4, 6.0, 6.6, 7.4, and 8.3 Gyr. All other parameters are the same as in Figs. 4.30 and 4.31.

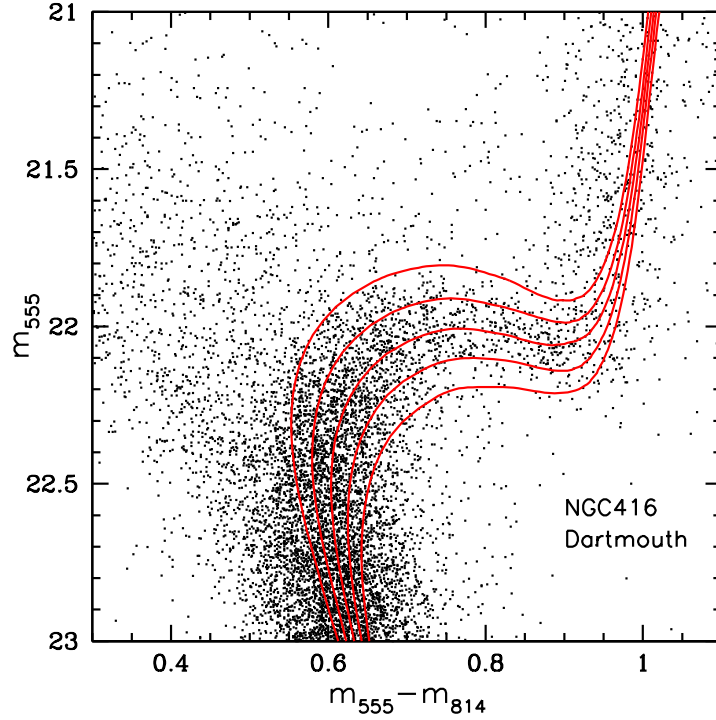


FIGURE 4.33. Same as Fig. 4.32, but for the Dartmouth isochrones with ages of 5, 5.5, 6, 6.5, and 7 Gyr.

CLUSTER	$V_{HB,RC}$ MAG	$\langle M_V \rangle$ MAG	$E_{V-I,S,M}$ MAG	$(m - M)$ MAG	DISTANCE KPC
NGC 121	19.71 ± 0.03	0.574	0.024	19.06 ± 0.03	64.9 ± 1.2
Lindsay 1	19.36 ± 0.04	0.509	0.024	18.78 ± 0.04	56.9 ± 1.0
Kron 3	19.46 ± 0.03	0.474	0.024	18.91 ± 0.04	60.6 ± 1.1
NGC 339	19.38 ± 0.08	0.455	0.040	18.80 ± 0.08	57.6 ± 4.1
NGC 416	19.70 ± 0.07	0.474	0.104	18.90 ± 0.07	60.4 ± 1.9
Lindsay 38	19.60 ± 0.05	0.430	0.016	19.12 ± 0.05	66.7 ± 1.6
NGC 419	19.41 ± 0.12	-	0.080	18.50 ± 0.12	50.2 ± 2.6

TABLE 4.4. **Distance Estimate.** The values for $V_{HB,RC}$ are taken from this paper and Chapter 2. The values for $\langle M_V \rangle$ were adopted from Girardi & Salaris (2001). For NGC 121 and Lindsay 38, we chose the model of $Z=0.004$, for Lindsay 1, Kron 3, NGC 339, and NGC 416 the model of $Z=0.001$, and for NGC 419 the model of $Z=0.004$. The reddenings E_{B-V} are taken from the Schlegel maps (Schlegel et al. 1998) and transformed into E_{V-I} by adopting $E_{V-I}/E_{B-V} = 1.25$ from Dean et al. (1978). For NGC 419 not the luminosity of the red clump but the distance modulus found with the Padova isochrones ($(m - M) = 18.75$) was used to determine the distance due to the age and metallicity dependence of the absolute red clump magnitude.

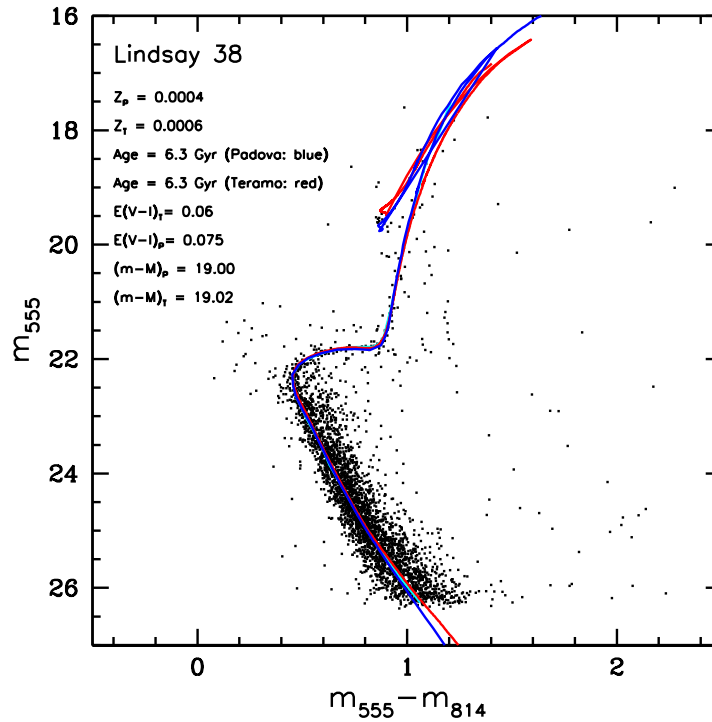


FIGURE 4.34. The CMD of Lindsay 38 with the best-fitting isochrones of two different models: The blue solid line shows the best-fitting Padova isochrone that is closest to the spectroscopically measured metallicity of the cluster. The red solid line is the best-fitting Teramo isochrone approximating the known metallicity. The cyan solid line is our fiducial ridgeline. The fit parameters are listed in the plot legend.

We use the absolute red clump magnitudes $\langle M_V \rangle$ given in Girardi & Salaris (2001), as a function of age and metallicity. These authors provide mean properties of the red clump for metallicities from $Z=0.0004$ to 0.03, and ages from 0.5 to 12 Gyr, based on the theoretical horizontal branch models of Girardi et al. (2000, see also Girardi & Salaris 2001). We corrected our distance modulus for the interstellar extinction by consulting the Schlegel maps (Schlegel et al. 1998). The adopted parameters and the resulting distances are listed in Table 4.4. Due to the fact that NGC 419 may be a multiple population object and therefore its age and the metallicity are uncertain, we do not use its absolute red clump magnitude for the distance estimate. Instead we apply the distance modulus found using the Padova isochrones $(m-M) = 18.75$ mag and correct for the extinction.

We find that Lindsay 38 is the most distant cluster of our sample with a distance modulus $(m-M) = 19.12$ mag (~ 67 kpc), while NGC 419 is the closest cluster with a distance modulus of $(m-M) = 18.50$ mag (~ 50 kpc). NGC 419 thus has a similar distance from us as the LMC, whose distance modulus is 18.50 ± 0.02 mag (e.g., Alves 2004). Taking NGC 419 into account, the closest and farthest cluster in our sample have a distance from each other of ~ 17 kpc. Excluding NGC 419, the depth extension of the SMC as derived from our cluster sample is ~ 10 kpc. We have to emphasize that the distance of NGC 419 is the most uncertain of our sample due to its complexity.

Crowl et al. (2001) used the same approach and derived distances for 12 clusters, six of which overlap with our sample. Their determined distance values are generally lower than the values we obtained, due to fainter absolute red clump magnitudes, which they adopted from Sarajedini (1999). Crowl et al. (2001) do not have NGC 419 in their sample, but NGC 411, NGC 152, Lindsay 113, NGC 361, Kron 28, and Kron 44. The closest cluster using the reddening values from the Schlegel maps is Kron 28 (45.2 ± 1.7 kpc), and the farthest cluster is NGC 121 (65.4 ± 1.9 kpc). Therefore

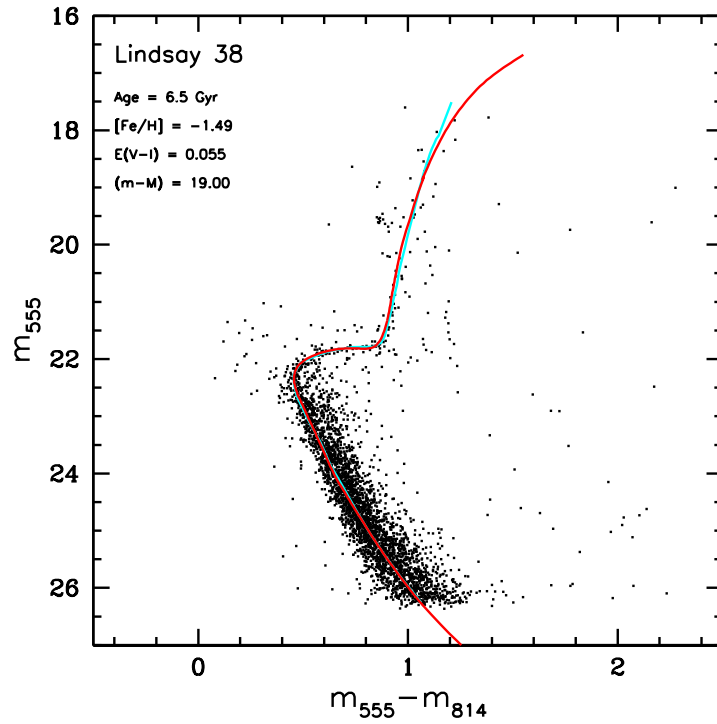


FIGURE 4.35. The Lindsay 38 CMD with the best-fitting Dartmouth isochrones overplotted in red. As before, the cyan line represents our fiducial for Lindsay 38. The fit parameters are listed in the plot.

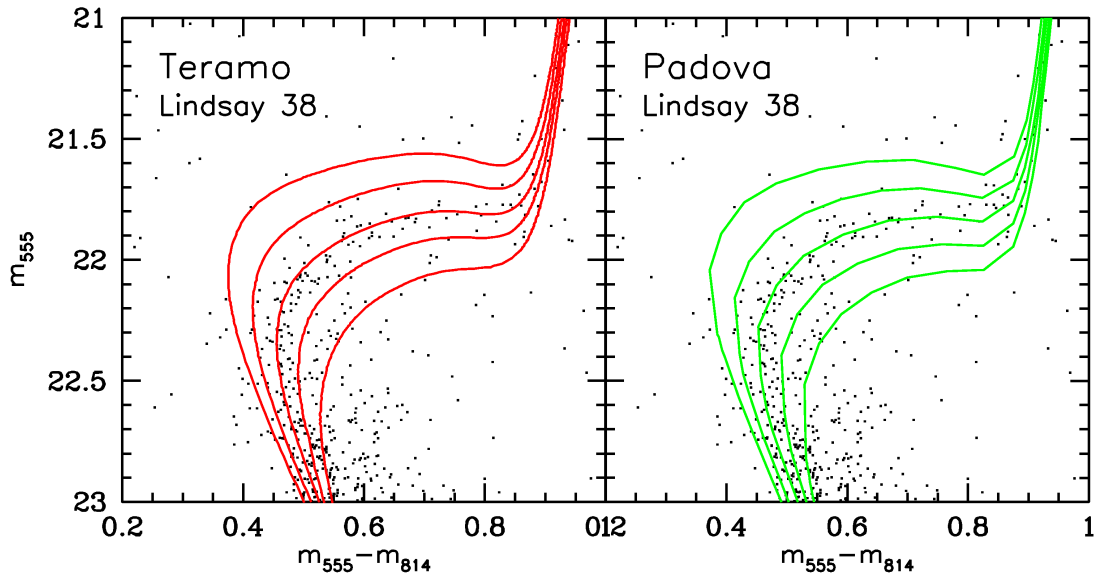


FIGURE 4.36. The CMD of Lindsay 38 after zooming in on the region of the main-sequence turnoff, subgiant branch, and lower red giant branch. In the upper panel, we show Teramo isochrones as solid lines, covering an age range of 5, 5.6, 6.3, 7, and 8 Gyr. In the lower panel we show the same plot for Padova isochrones in the available age steps of 5, 5.6, 6.3, 7.1, and 7.9 Gyr. All other parameters are the same as in Figs. 4.34 and 4.35.

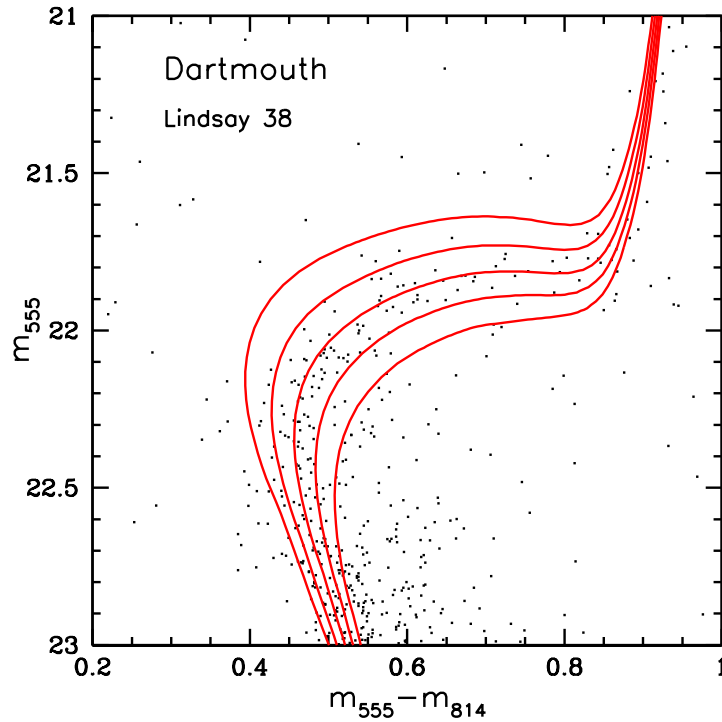


FIGURE 4.37. Same as Fig. 4.36, but for the Dartmouth isochrones with ages of 5.5, 6, 6.5, 7, and 7.5 Gyr.

Kron 28 is ~ 3 kpc closer than NGC 419. In Crowl et al.'s sample, the clusters have a maximum distance of 20.2 kpc from one another, which is a higher value than what we have found with our smaller cluster sample.

7. Discussion

7.1. Comparison of our age determination with previous studies

Previous studies done by several different authors provided ages and metallicities of SMC star clusters using a variety of techniques and telescopes. Therefore, if we combine all published cluster ages, we find a wide range of ages and metallicities for a given cluster, depending on the method used for the determination: Lindsay 1 has an age range from 7.3-10 Gyr (Gascoigne 1966, 1980; Olszewski et al. 1987; Sarajedini et al. 1995; Mighell et al. 1998a; Udalski 1998b; Alcaino et al. 2003), Kron 3 from 5-10 Gyr (Gascoigne 1966; Rich et al. 1984; Alcaino et al. 1996; Mighell et al. 1998a; Udalski 1998b; Rich et al. 2000), and NGC 339 from 5-7.9 Gyr (Mighell et al. 1998a; Udalski 1998b; Rich et al. 2000).

No other cluster has such a wide range of different age determinations as NGC 416, reaching from 2.5-11.2 Gyr (Durand et al. 1984; Elson & Fall 1985; Bica et al. 1986; Mighell et al. 1998a; Udalski 1998b; Rich et al. 2000). The cluster is located close to the SMC main body where a large interstellar extinction is expected. The separation of field stars from the real cluster members was a major problem in the age determination process, among uncertain values for metallicity, reddening and distance. Using photometry obtained with the WFPC2 aboard HST, Mighell et al. (1998a) found an absolute age of 6.6 ± 0.5 Gyr for NGC 416, while Rich et al. (2000) derived an age of 7.1 to 11.2 Gyr using the same data set.

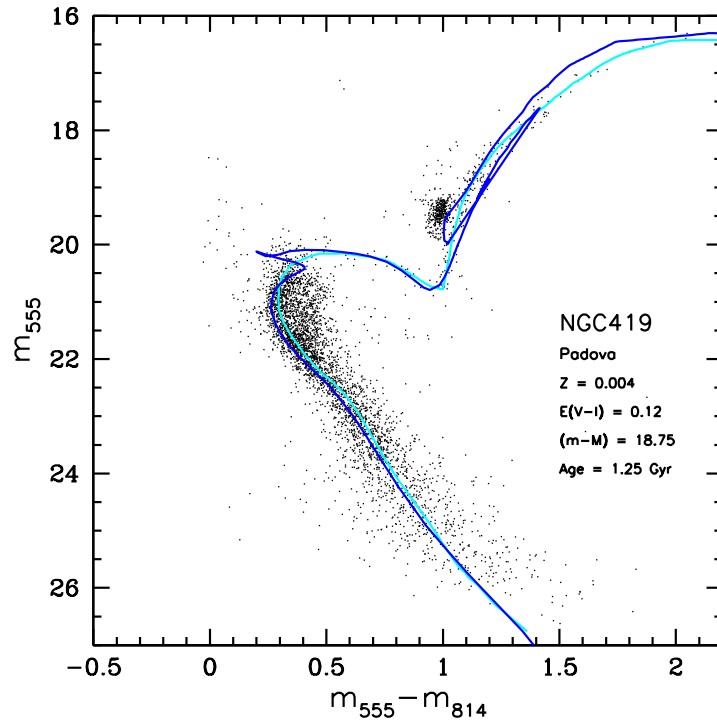


FIGURE 4.38. The CMD of NGC 419 with the best-fitting isochrone of the Padova model: the blue solid line shows the best-fitting Padova isochrone that is closest to the spectroscopically measured metallicity of the cluster. The distinction of the cluster from the field population is difficult due to the multiple turnoffs and the sparse SGB.

REF.SOURCE	LINDSAY 1 GYR	KRON 3 GYR	NGC 339 GYR	NGC 416 GYR	LINDSAY 38 GYR	NGC 419 GYR
This paper	7.5 ± 0.5	6.5 ± 0.5	6 ± 0.5	6 ± 0.5	6.5 ± 0.5	1.2 – 1.6
Rich et al. (2000)	-	5.6 – 7.9	5.0 – 7.9	4.0 – 7.1	-	1.0 – 1.8
Mighell et al. (1998a)	7.7 ± 0.4	4.7 ± 0.7	5.0 ± 0.6	5.6 ± 0.6	-	-
Udalski (1998b)	9.0	7.5	4.0	6.6	-	3.3
Sarajedini et al. (1995)	7.3 ± 0.6	-	-	-	-	-
Alcaino et al. (1996, 2003)	9 – 10	8	-	-	-	-
Piatti et al. (2001)	-	-	-	-	6.0 ± 0.6	-

TABLE 4.5. **Age Comparison.** Comparison of our ages derived with the Dartmouth isochrones. For NGC 419 Padova isochrones provided the best fit.

The only available CMD of Lindsay 38 is provided by Piatti et al. (2001). The observation was carried out with the Cerro Tololo Inter-American Observatory (CTIO) 0.9 m telescope using the Tektronix 2K # 3 CCD. They presented the first age determination of Lindsay 38 with 6 ± 0.6 Gyr. For NGC 419, the latest CMD was published by Rich et al. (2000) based on WFPC2 data. Udalski (1998b) published an age of 3.3 Gyr and Rich et al. (2000) give an age range of 1.0 – 1.8 Gyr.

For Lindsay 1, Kron 3, NGC 339, NGC 416, and NGC 419, the latest and deepest available CMD was provided with WFPC2 (Mighell et al. 1998a; Rich et al. 2000), while for Lindsay 38 only ground-based data existed.

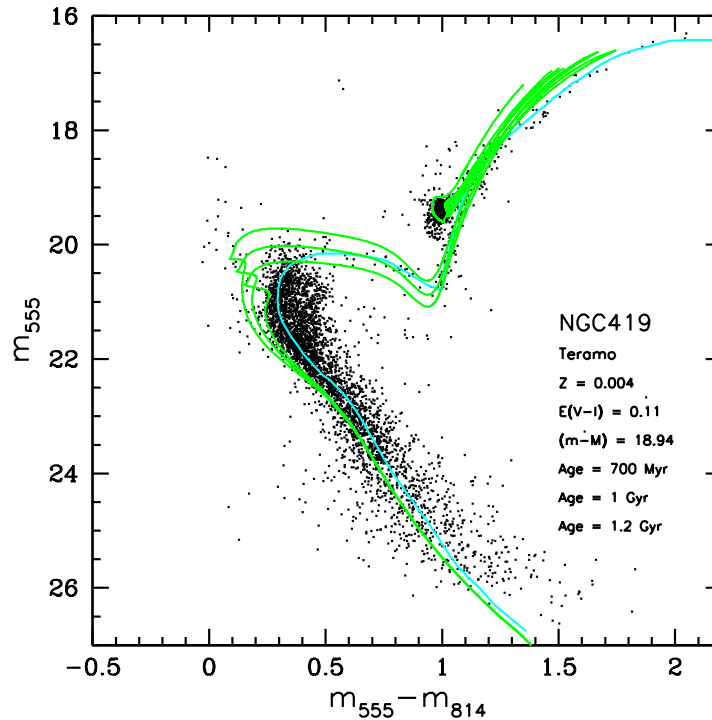


FIGURE 4.39. The CMD of NGC 419 with the Teramo isochrones overplotted in green. As before, the cyan line represents our fiducial for NGC 419. We show isochrones in the age range of 0.8, 1, 1.2 Gyr. The fit parameters are listed in the plot.

In Table 4.5 we compare our ages using the best-fitting Dartmouth isochrones (except NGC 419, for which the Padova isochrones provided the best fit) with results published in the most recent studies based on HST/WFPC2 photometry. The data reach ~ 2 mag below the turnoff points, while our ACS data have a depth of 3.5 mag below turnoffs. We can see that Mighell et al. (1998a) derived a similar age for Lindsay 1, while for the remaining clusters in the overlapping sample they found younger ages than the ones derived here. Rich et al. (2000), who used the same WFPC2 "snapshots" as Mighell et al. (1998a), gave age ranges for certain metallicities for the clusters in their sample, which cover the ages determined in this paper.

The ages published by Udalski (1998b) using OGLE (Optical Gravitational Lensing Experiment) data, do not exhibit a general trend to older or younger ages as compared to our results, and the age difference varies for each cluster. The OGLE survey is a shallow ground-based survey with a limiting magnitude of ~ 21 mag. Sarajedini et al. (1995) used the B-V color difference between the HB and the RGB for star clusters with red HB morphologies for their age determination. The CMDs were obtained using data from the 2048 RCA prime-focus CCD on the CTIO 4 m telescope (Olszewski et al. 1987) and the photometry reaches $V \sim 23$ mag. The age found for Lindsay 1 is in excellent agreement with our result.

Alcaino et al. (1996, 2003) used photometry for Lindsay 1 obtained with the 1.3 m Warsaw telescope, Las Campanas Observatory and reaches $V \sim 22$ mag. The age was determined by using the so-called vertical method, based on the difference between the luminosity of the MSTO and the HB level. For Kron 3, the photometry was taken with the EFOSC-2 CCD camera at the 2.2 m Max-Planck-Institute telescope of ESO, La Silla, and reaches $V \sim 23$ mag (Alcaino et al. 1996). The age was determined using isochrones. In both studies, the resulting ages are higher than our values. Piatti et al. (2001) were the first to publish an age for Lindsay 38, which is in excellent agreement with the age derived in this paper.

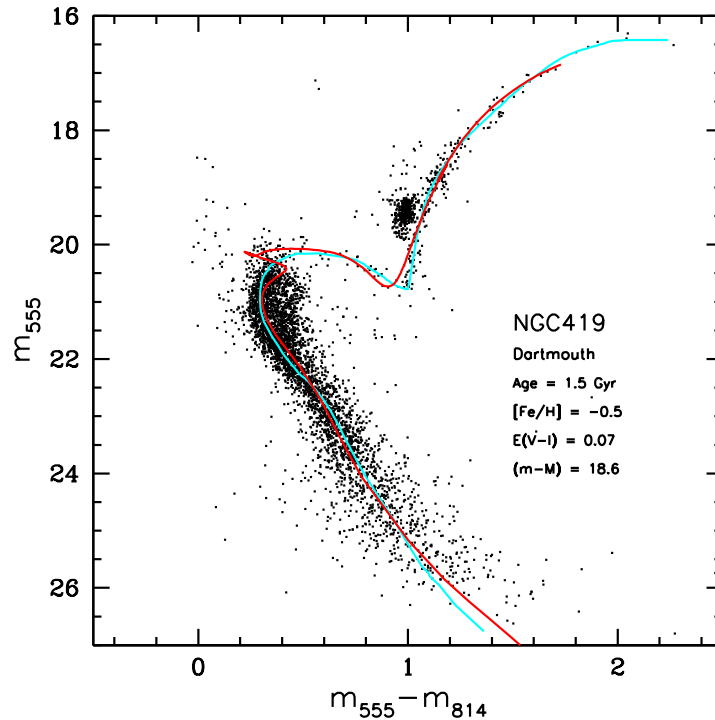


FIGURE 4.40. The CMD of NGC 419 with the best-fitting Dartmouth isochrone overplotted in red. As before, the cyan line represents our fiducial for NGC 419. The fit parameters are listed in the plot.

Most CMDs published in previous studies do not go deep enough to show a clearly outlined MSTO, which is an essential feature for most age determination techniques. Mighell et al. (1998a) determined their cluster ages relative to the age of Lindsay 1, measuring the difference between the RC and the RGB and found similar ages as in this paper. Kron 3 is an exception for which the authors derived a younger age due to large error associated with the MS photometry. Rich et al. (2000) fitted isochrones to the red clump and also calculated the difference between the MSTO and the RC (ΔV_{TO}^{RC}) in combination with the calibration of Walker (1992). The cluster ages found in this paper are within the age ranges given by Rich et al. (2000). CMDs using ground-based photometry reach $\sim V=20$ mag, which is not deep enough to show the SGBs or the MSTOs, which can lead to large age differences.

7.2. Age range and spatial distribution

The intermediate-age SMC star clusters Lindsay 1, Kron 3, NGC 339, NGC 416, and Lindsay 38 form a continuous age sequence from 6 to 7.5 Gyr. The SMC is the only dwarf galaxy of the Local Group known to contain populous star clusters in this age range. The only "true" globular cluster in the SMC, NGC 121, has an age of 10.5-11.5 Gyr (Chapter 2), but is still 2-3 Gyr younger than the oldest LMC and MW globular clusters (e.g., Olszewski et al. 1996; Olsen et al. 1998; Johnson et al. 1999; Mackey & Gilmore 2004). Between NGC 121, and the second oldest cluster, Lindsay 1, there is a small age-gap (~ 3 Gyr), in which no surviving star cluster has been formed.

In our sample, we have four clusters with ages between 6-6.5 Gyr, and one that is significantly younger (1.2-1.6 Gyr). Good quality ages are available from ground-based and space-based observations for ten additional intermediate-age SMC star clusters. Combining them with our star clusters, we obtain a complete sample of all intermediate-age and old SMC star clusters: Kron 28, Kron 44,

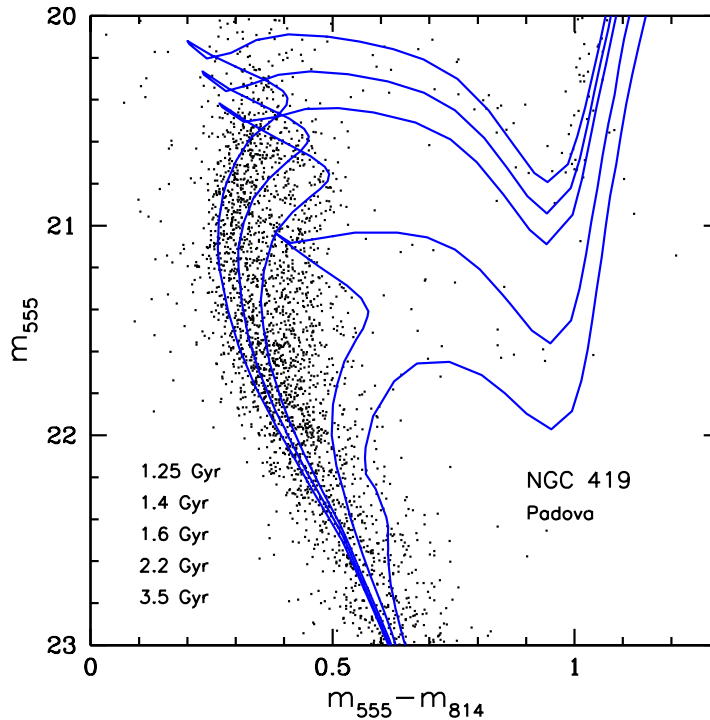


FIGURE 4.41. The CMD of NGC 419 after zooming in to the region of the MSTO, SGB, and lower RGB. We show Padova isochrones as solid lines to estimate the age of the cluster and field population visible in the CMD. The isochrones cover an age range of 1.25, 1.4, 1.6, 2, and 3.5 Gyr. All other parameters are the same as in Fig. 4.38.

Lindsay 116, Lindsay 32, Lindsay 11, NGC 152, NGC 361, NGC 411, Lindsay 113, and BS90 (Table 4.6).

For none of these clusters deep HST photometry is available, thus their ages should be considered with some caution. For NGC 152, NGC 361, NGC 411, Lindsay 113, and BS90 "snapshots" are available taken with WFPC2 (reaching $V \sim 23$ mag), and ACS (BS90, reaching $V \sim 26$ mag).

Looking at Figure 4.1, we clearly see that the youngest clusters are located near the SMC main body, while the clusters with ages higher than ~ 4 Gyr lie in the outer parts. NGC 361 seems to be an exception, but the cluster age is still uncertain, and the literature age of 8.1 Gyr probably is too high. Crowl et al. (2001) determined a distance of 51.7 ± 1.8 kpc for NGC 361 whereby the cluster lies ~ 7.5 kpc ahead of the SMC center. Another exception is BS90 that lies near the SMC main body, even though the cluster has an age of ~ 4.3 Gyr. The three oldest SMC clusters (NGC 121, Lindsay 1, Kron 3) are located in the north-western part of the SMC. We note that Lindsay 116 cannot be seen in Figure 4.1, because it is located $6^\circ.1$ south-east of the bar and lies therefore outside the displayed area.

The closest cluster in our sample, NGC 419, and the farthest cluster, Lindsay 38, have a relative radial distance of 17 kpc from each other. We can therefore confirm that the SMC has a large extension along the line-of-sight, as was also found by Crowl et al. (2001) based on its star clusters.

In Figure 4.43 we show the distribution of age vs the distance to the sun of the clusters in our sample. The locations are shown relative to our adopted SMC distance and indicate that the clusters generally are distributed within $\pm 6-7$ kpc of the SMC centroid. Interesting exceptions are the younger clusters Kron 28, NGC 411, and NGC 419 that in projection appear near the center of the SMC. In fact, they could be located considerably closer to us (see also Fig. 4.44). Further measurements of the distance of younger clusters thus would be worthwhile. Moreover, we included five clusters for

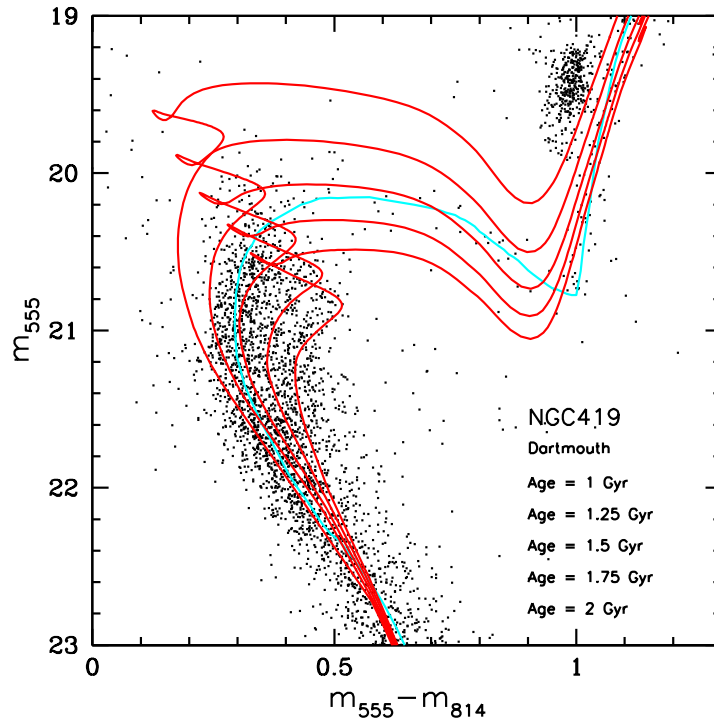


FIGURE 4.42. Same as Fig. 4.41, but for the Dartmouth isochrones with ages of 1, 1.25, 1.5, 1.75, and 2 Gyr.

CLUSTER	AGE GYR	DATA	METHOD	REF.SOURCE
Kron 28	2.1 ± 0.5	CTIO 0.9 m telescope / Tektronix 2K # 3 CCD	$\Delta V_{MSTO}^{RC,HB}$	Piatti et al. (2001)
Kron 44	3.1 ± 0.8	CTIO 0.9 m telescope / Tektronix 2K # 3 CCD	$\Delta V_{MSTO}^{RC,HB}$	Piatti et al. (2001)
Lindsay 116	2.8 ± 1.0	CTIO 0.9 m telescope / Tektronix 2K # 3 CCD	$\Delta V_{MSTO}^{RC,HB}$	Piatti et al. (2001)
Lindsay 32	4.8 ± 0.5	CTIO 0.9 m telescope / Tektronix 2K # 3 CCD	$\Delta V_{MSTO}^{RC,HB}$	Piatti et al. (2001)
Lindsay 11	3.5 ± 1.0	CTIO 4.0 m telescope / RCA CCD	Isochrones	Mould et al. (1992)
NGC 152	1.4 ± 0.2	HST/WFPC2	Isochrones	Crowl et al. (2001)
NGC 361	8.1 ± 1.2	HST/WFPC2	Isochrones	Mighell et al. (1998a)
NGC 411	1.2 ± 0.2	HST/WFPC2	Isochrones	Alves & Sarajedini (1999)
Lindsay 113	4.0 ± 0.7	HST/WFPC2	d_{B-V}^b	Mighell et al. (1998a)
BS90	4.3 ± 0.1	HST/ACS	Isochrones	Sabbi et al. (2007)

TABLE 4.6. **Literature cluster ages.** Ages for nine additional intermediate-age clusters from the literature.

The method used by Mighell et al. (1998a) is defined by the (B-V) color difference between the mean color of the red clump and the RGB at the level of the RGB. This value then was compared with Lindsay 1, NGC 416, and Lindsay 113.

which we found reliable ages, distances, and metallicities in the literature. We divided the cluster metallicities into four groups and use different symbols for each group in the plot. Even though our plot contains only 11 clusters, we can see trends in the distributions of their properties. Age and distance from the sun appear to be correlated. The closest cluster, NGC 419, is also the youngest and

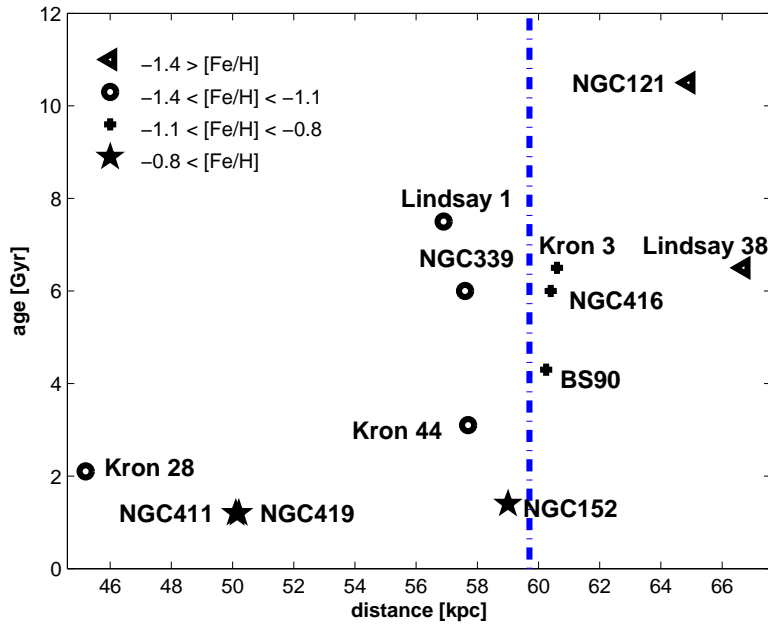


FIGURE 4.43. Age vs distance to the sun (projected distance) including different symbols for different metallicity ranges. For five clusters we found reliable distances Crowl et al. (2001), ages (Alves & Sarajedini 1999; Piatti et al. 2001; Crowl et al. 2001), and metallicities (Kayser et al., in preparation). All values for BS90 were adopted from Sabbi et al. (2007). The dashed line represents the SMC distance modulus of $(m - M)_0 = 18.88 \pm 0.1$ mag (Storm et al. 2004).

most metal rich cluster, while the most distant cluster, Lindsay 38, is also the most metal poor, in spite of not being the oldest cluster.

One could speculate that in regions at the outskirts of the double LMC-SMC system the star formation activity has been lower/slower than elsewhere, possibly with more unenriched gas, thus allowing for a more moderate enrichment. The oldest object, NGC 121, is not the most metal poor cluster, but the second metal poorest and the second farthest one. Its low metallicity could be the result of both a "natural" age-metallicity relation and a "distance from the system" effect.

Figure 4.44 illustrates the distribution of SMC star clusters with high quality distances derived from isochrone fits to CMDs derived from HST observations. This is a highly biased sample; star clusters seen in the direction of the SMC 'bar' are not preferred for these projects because of their large levels of field star contamination. The exception in this case is the cluster BS90 that was accidentally included in observations of NGC 346 (see Sabbi et al. 2007). The present limited data for clusters in this project show that the SMC is quite extended along the line of sight, consistent with other studies of individual stars and star clusters (see discussion in § 6). This three dimensional distribution of the clusters also demonstrates the lack of trends in cluster age or metallicity with radial distance from the center of the SMC.

7.3. Age distribution and cluster formation history

By combining the ages of our sample with 9 literature ages for intermediate-age SMC star clusters listed in Table 4.6, we obtain a well-observed sample of intermediate-age and old star clusters in the

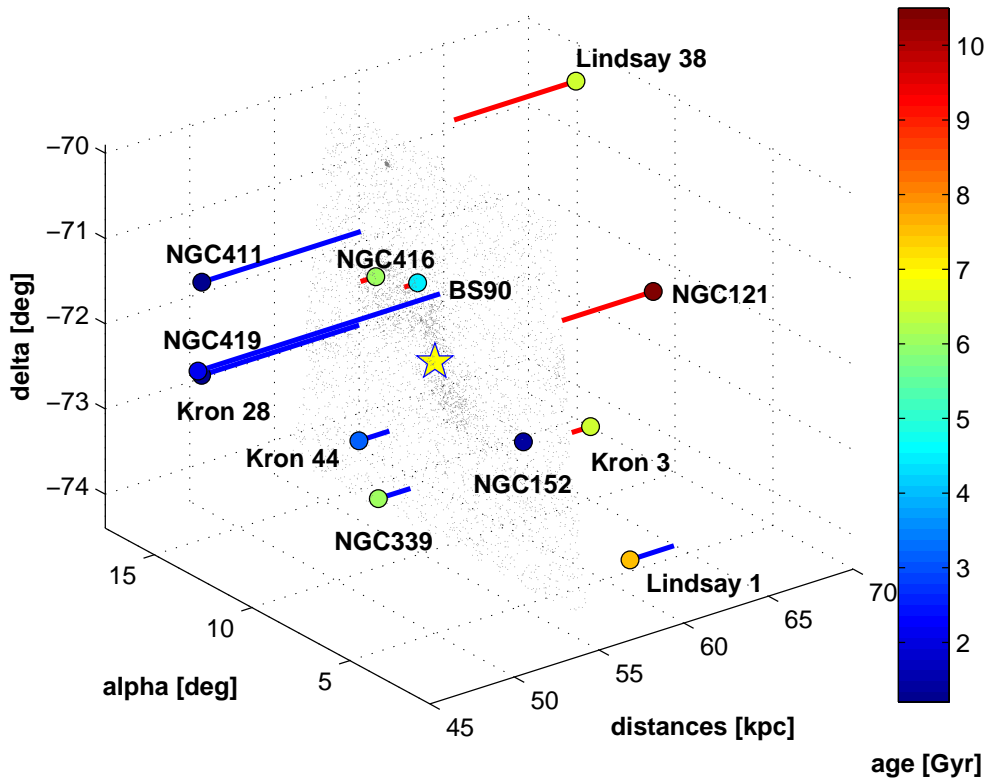


FIGURE 4.44. Three dimensional distribution is shown for SMC star clusters with ages and distances derived from isochrone fits to CMDs derived from HST observations. Note that the intermediate age clusters are distributed throughout much of the extended body of the SMC. As discussed in the text, the selection of clusters is biased in that our observations generally avoided clusters in locations with high field star densities. However, this incomplete sample suggests that age and radial distance from the center of the SMC are not correlated; e.g. the younger cluster Kron 28, NGC 411, and NGC 419 are at large radial distances and cover a range in metallicity. The yellow star symbolizes the SMC center.

SMC. The cluster NGC 361 was excluded from the sample, because the cluster is almost certainly younger than the assumed ~ 8 Gyr (Mighell et al. 1998a).

The age distribution is shown in Figure 4.46. In each panel we show our resulting age distribution using ages of different isochrone models (black histograms) and the combined sample (white histograms). Since the cluster ages from the literature were derived using different data and methods, their distribution does not change.

In all three plots of Figure 4.46, the small age gap between ~ 8 and 10 Gyr can clearly be seen. In the first panel we used ages derived with the Dartmouth isochrones. Rich et al. (2000) based on HST/WFPC2 found two brief cluster formation intervals with the oldest set 8 ± 2 Gyr ago and the second 2 ± 0.5 Gyr ago, and argued that there were gaps in between. During the older burst the clusters NGC 339, NGC 361, NGC 416, and Kron 3, and during the younger burst the clusters NGC 411, NGC 152, and NGC 419 have formed according to Rich et al. (2000).

Even though they used the same HST/WFPC2 data as Rich et al. (2000), Mighell et al. (1998a) found no evidence for such cluster formation bursts. We also find no evidence for two significant bursts of star cluster formation in our SMC age distribution, but we do see a slightly enhanced cluster formation activity around 6 Gyr (see also Fig. 4.45). In the second and the third panel we used our

CLUSTER	PROJECTED DIST.	DIST. TO SMC CENTER
	KPC	KPC
NGC 121	64.9 ± 1.2	8.76 ± 1.1
Lindsay 1	56.9 ± 1.0	13.28 ± 1.0
Kron 3	60.6 ± 1.1	7.19 ± 1.1
NGC 339	57.6 ± 4.1	0.73 ± 2.0
NGC 416	60.4 ± 1.9	3.94 ± 1.4
Lindsay 38	66.7 ± 1.6	6.27 ± 1.3
NGC 419	50.2 ± 2.6	10.83 ± 1.6
NGC 411	50.1 ± 1.7	11.1 ± 1.3
NGC 152	59.0 ± 1.8	5.58 ± 1.3
Kron 28	45.2 ± 1.7	14.78 ± 1.3
Kron 44	57.7 ± 1.8	4.37 ± 1.3
BS90	60.3	1.23

TABLE 4.7. **Distances.** The projected distances were calculated in this paper and adopted from Crowl et al. (2001); Sabbi et al. (2007). Using these values and the cluster coordinates, we determined the cluster distances to the SMC center ($\alpha = 0^h52^m44.8^s$, $\delta = -72^\circ49'43''$).

derived Teramo and Padova ages, respectively. The cluster formation at 6 Gyr is even more obvious for both isochrone models than in the upper panel.

Apparently, between ~ 5 and 6 Gyr no star cluster with sufficient mass to survive has formed, but if Lindsay 113 is older than the assumed 4 Gyr adopted from the literature, the cluster lies within the gap. We suggest that the SMC has formed its clusters during its entire lifetime with some epochs of more intense cluster formation activity. More detailed information about the age distribution requires additional deep observations of all remaining intermediate-age SMC star clusters.

As shown in Figure 4.44 there appears to be no simple relationship between cluster position and metallicity in any age range. This perhaps is to be expected given that tidal interactions may have perturbed the orbits of star clusters after they formed or provided opportunities for clusters to form at large radii, as in the present-day SMC wing. We have to emphasize that the cluster sample shown in Figure 4.44 is not complete. Only for 12 clusters reliable distances have been measured this far (see § 6), and these are shown in the Figure. The question of the metallicity distribution of the clusters and how this relates to age and position is more complex and beyond the scope of this paper.

7.4. Age-Metallicity Relation

The oldest SMC star cluster, NGC 121, is not only 2-3 Gyr younger than the oldest clusters in LMC and MW, but also has a fairly high metallicity of $[Fe/H]_{ZW84} = -1.46 \pm 0.10$ or $[Fe/H]_{CG97} = -1.19 \pm 0.12$ (Da Costa & Hatzidimitriou 1998). For comparison, the oldest globular clusters in the LMC and the MW have metallicities up to $[Fe/H]_{ZW84} \approx -2.32$ dex (e.g. M 92, NGC 6416; Harris et al. 1996). Therefore, the SMC must have experienced a relative rapid increase in abundances in its early history, but because the SMC does not host any clusters older than ~ 10 Gyr, conclusions on how uniformly this early enrichment took place cannot be drawn. In Figure 4.45 the age-metallicity relation (AMR) is presented showing metallicities in the CG97 scale that were all measured spectroscopically (except BS196). All adopted metallicities were published in the CG97 scale and therefore no transformation into the ZW84 scale was necessary, which is problematic for metallicities $[Fe/H]_{ZW84} > -0.60$.

After its first early enrichment, the mean metallicity $[\text{Fe}/\text{H}]$ of the SMC star clusters remained fairly constant at about -1 dex for several Gyr. Interestingly, around 6 Gyr, we find clusters of similar ages that show a wide spread in metallicity. The largest scatter is found for the clusters Lindsay 38 and NGC 416, which both have an age of ~ 6 -6.5 Gyr but differ in metallicity by 0.64 dex (Kayser et al., in preparation). The metallicities of the clusters NGC 339 and Lindsay 110, which also have ages around 6 Gyr, lie between Lindsay 38 and NGC 416. Metallicity and age are clearly not correlated at that time and it is obvious that the SMC was not well mixed. Bica et al. (2008b) observed the SMC star cluster BS196 using the 4.1-m SOAR telescope. BS196 is similarly sparse as Lindsay 38 and appears to be ~ 0.1 dex metal-poorer than Lindsay 38 with a metallicity $[\text{Fe}/\text{H}] = -1.45 \pm 0.10$ and an age of 5.0 ± 0.5 Gyr. The metallicity and the age of this cluster were determined by visually choosing Padova isochrones fitting best the CMD.

Looking at the younger clusters (age < 4 Gyr), the mean metallicity increases but still the SMC is not very well mixed. The latest measurements based on Ca II triplet spectroscopy by Parisi et al. (2008) clearly show that clusters with ages between ~ 0.9 and 2 Gyr have a spread in metallicity of 0.53 dex (HW 86: age 1.6 Gyr, $[\text{Fe}/\text{H}] = -0.61$; Lindsay 27: age 2.1 Gyr, $[\text{Fe}/\text{H}] = -1.14$). The youngest clusters in their sample, Lindsay 106 and Lindsay 108, both have ages around 0.9 Gyr, and metallicities of $[\text{Fe}/\text{H}] = -0.88$ and -1.05 , respectively. Around 3 Gyr ago, a sudden increase in $[\text{Fe}/\text{H}]$ was observed which can be explained with the most recent close encounter with the LMC and/or the MW described by e.g., Besla et al. 2007. Strong shock compressions could have triggered cluster formation at the recent past, which also leads to a strong metallicity increase (Pagel & Tautvaišienė 1998). The present day metallicity of the SMC is $[\text{Fe}/\text{H}] = -0.5$ dex (Rolleston et al. 2003), which was determined on high resolution spectroscopy of a B-type main sequence star. Earlier studies based on supergiant spectroscopy (5 A-type and 1 B-type star) in the young population NGC 330 (age ~ 20 -25 Myrs) rendered a metallicity of $[\text{Fe}/\text{H}] = -0.69 \pm 0.11$ dex (Hill 1999). Venn (1999) analyzed 10 A-type supergiants in the SMC and derived a metallicity of $[\text{Fe}/\text{H}] = -0.70 \pm 0.07$ dex.

Dwarf galaxies in general are expected to be well mixed (Roy & Kunth 1995) what makes the SMC an exciting exception. The variation in $[\text{Fe}/\text{H}]$ could have been caused by an inhomogeneous episodic gas accretion. At the present day, HI gas forms large supershells (Stanimirović et al. 2004) in which the youngest star clusters are located, while the older clusters lie farther out. Similar shells could also have existed when the SMC was younger. Self-enrichment by supernova type II-explosions (see e.g., Lanfranchi & Matteucci 2003) is an unrealistic possibility due to the large number needed (Kayser et al., in preparation).

The latest results from Ca II triplet measurements of SMC star clusters improved the understanding of the SMC's chemical evolution history enormously. Da Costa & Hatzidimitriou (1998) considered the SMC to be a self-contained system with no infall or outflow of gas, which can be described with a simple closed-box model. Pagel & Tautvaišienė (1998) presented a more sophisticated model combining a simple continuous model and a bursting model of star formation. The SMC was assumed to have been build up by gradual infall of unprocessed material. For the continuous model a constant star formation rate (SFR) was assumed, while the bursting model includes three intervals of constant but different SFRs. None of these two models can reproduce the AMR perfectly, but it is better fitted by the model of Pagel & Tautvaišienė (1998) with abruptly changing SFRs. This model is in agreement with the observed mean metallicity of the star clusters in the interval between 1.3 - 10 Gyr (Kayser et al., in preparation), but cannot reproduce the large scatter in metallicity.

7.5. Evolutionary history of the SMC as a whole

Looking at the metallicities of our star clusters (Tab. 4.9), we see that the SMC did not experience a smooth age-metallicity relation, even though the SMC is believed to be well-mixed at the present day (but see Grebel & Richtler 1992; Gonzalez & Wallerstein 1999; Parisi et al. 2008). The oldest SMC star cluster, NGC 121, has a metallicity of $[\text{Fe}/\text{H}] = -1.46 \pm 0.10$ and an age of 10.5-11.5 Gyr,

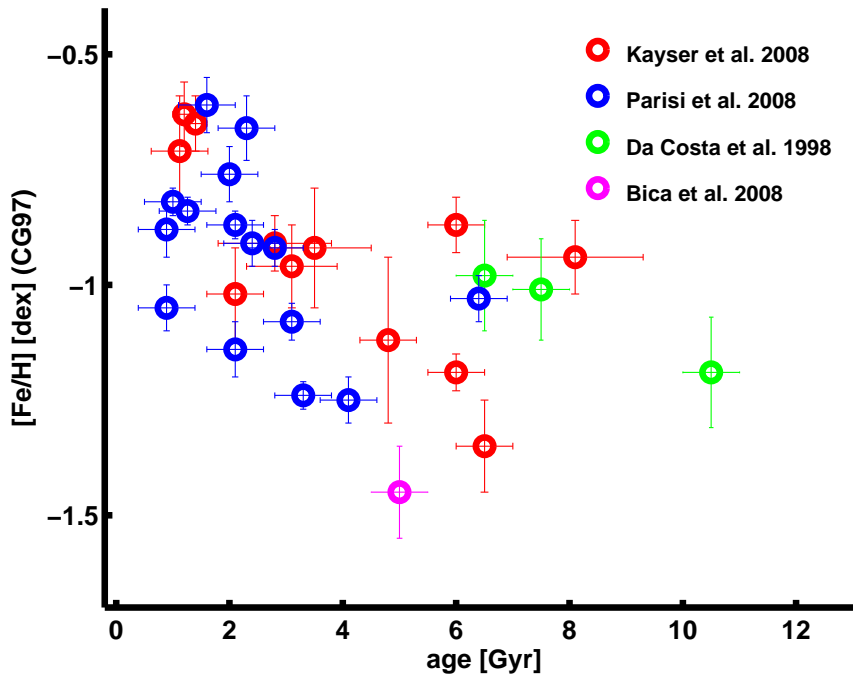


FIGURE 4.45. Age-metallicity relation of the SMC derived from star clusters. The metallicities are given in the CG97 scale. Indicated in red are clusters of this project, in blue are clusters from Da Costa & Hatzidimitriou (1998), and in turquoise are clusters from Parisi et al. (2008). The values are listed in Table 4.8. It is clearly visible that the SMC did not experience a smooth age-metallicity relation. The most recent results from Parisi et al. (2008) provide evidence that even at the present day the SMC is not as well-mixed as generally thought.

while Lindsay 38 is more metal-poor with $[Fe/H] = -1.59 \pm 0.10$ but has an age of 6.5 ± 0.5 Gyr. SMC star clusters of similar age may differ by several tenths of dex in metallicity (see also Da Costa et al. 1998, Kayser et al., in preparation). The probably most reasonable explanation involves the infall of unenriched, or less enriched gas. The Magellanic Clouds are surrounded by an extensive HI halo (e.g., Dickey 1996), therefore this possibility may be plausible. Another speculative explanation for the existence of those metal-poor clusters is that the SMC acquired these clusters in a past interaction with another dwarf galaxy, similar to the clusters from the Sagittarius dwarf galaxy being acquired by the Milky Way (e.g., Carraro et al. 2007).

The SMC, LMC, and MW form an interacting triple system, which affects each other's star formation history (SFH). However, recent studies have suggested that the Magellanic Clouds only entered the vicinity of the MW fairly recently (e.g., Kallivayalil et al. 2006a/b). It is intriguing that the LMC has a significant age gap between ~ 4 -9 Gyr, while the SMC formed its clusters continuously during the same time period. Moreover, the SMC appears to have a "delayed" globular cluster formation history and formed its first and only globular cluster, NGC 121, 2-3 Gyr later than the LMC or the MW.

Possible orbits of the SMC, LMC, and MW have been modelled by several authors (e.g., Kallivayalil et al. 2006a/b; Bekki & Chiba 2005). Strong tidal perturbations due to interactions could have triggered the cluster formation (e.g., Whitmore 1999) in the SMC. In the LMC, we find that star clusters have formed in evident bursts. The LMC has two main epochs of cluster formation (e.g., Bertelli et al. 1992) and a well-known age-gap of several billion years, in which no star clusters have formed. A few globular clusters are found with coeval ages like the Galactic globular clusters (e.g.,

CLUSTER	$[Fe/H]_{CG97}$ DEX	AGE GYR	REFERENCE <i>Age</i>
Metallicities from <i>Da Costa et al. 1998</i>			
NGC 121	-1.19 ± 0.12	10.5 ± 0.5	this work
Lindsay 1	-1.01 ± 0.11	7.5 ± 0.5	this work
Kron 3	-0.98 ± 0.11	6.5 ± 0.5	this work
Metallicities from <i>Kayser et al. 2009</i>			
NGC 339	-1.19 ± 0.04	6 ± 0.5	this work
NGC 416	-0.87 ± 0.06	6 ± 0.8	this work
Lindsay 38	-1.35 ± 0.10	6.5 ± 0.5	this work
NGC 419	-0.71 ± 0.12	1.2-1.6	this work
Kron 28	-1.02 ± 0.10	2.1 ± 0.5	1
Kron 44	-0.96 ± 0.09	3.1 ± 0.8	1
Lindsay 11	-0.92 ± 0.13	3.5 ± 1.0	2
Lindsay 116	-0.91 ± 0.06	2.8 ± 1.0	1
Lindsay 32	-1.12 ± 0.18	4.8 ± 0.5	1
NGC 152	-0.65 ± 0.06	1.4 ± 0.2	3
NGC 361	-0.94 ± 0.08	8.1 ± 1.2	4
NGC 411	-0.63 ± 0.07	1.2 ± 0.2	5
Metallicities from <i>Parisi et al. 2008</i>			
BS 121	-0.66 ± 0.07	2.3 ± 0.5	6
HW 47	-0.92 ± 0.04	2.8 ± 0.5	6
HW 84	-0.91 ± 0.05	2.4 ± 0.5	6
HW 86	-0.61 ± 0.06	1.6 ± 0.5	6
Lindsay 4	-1.08 ± 0.04	3.1 ± 0.5	6
Lindsay 5	-1.25 ± 0.05	4.1 ± 0.5	6
Lindsay 6	-1.24 ± 0.03	3.3 ± 0.5	6
Lindsay 7	-0.76 ± 0.06	2.0 ± 0.5	6
Lindsay 17	-0.84 ± 0.03	1.26 ± 0.5	7
Lindsay 19	-0.87 ± 0.03	2.1 ± 0.5	6
Lindsay 27	-1.14 ± 0.06	2.1 ± 0.5	6
Lindsay 106	-0.88 ± 0.06	0.89 ± 0.5	8
Lindsay 108	-1.05 ± 0.05	0.89 ± 0.5	8
Lindsay 110	-1.03 ± 0.05	6.4 ± 0.5	9
Lindsay 111	-0.82 ± 0.03	1.0 ± 0.5	10
Metallicities from <i>Bica et al. 2008a</i>			
BS196	-1.45 ± 0.10	5.0 ± 0.5	11

TABLE 4.8. **Age-Metallicity Relation.** Ages and Metallicities are taken from the listed references: 1. Piatti et al. (2001), 2. Mould et al. (1992), 3. Crowl et al. (2001), 4. Mighell et al. (1998a), 5. Alves & Sarajedini (1999), 6. Piatti et al. (2005a), 7. Rafelski & Zaritsky (2005), 8. Piatti et al. (2007a), 9. Piatti et al. (2007b), 10. Piatti et al. (2007c). 11. Bica et al. (2008b)

Olszewski et al. 1991; Olsen et al. 1998; Johnson et al. 1999). We know only of one star cluster, ESO 121-SC03, that lies within the age-gap, which has an age of 8.3-9.8 Gyr (Mackey et al. 2006). A correlation between young star clusters in the LMC and putative close encounters with the SMC and MW

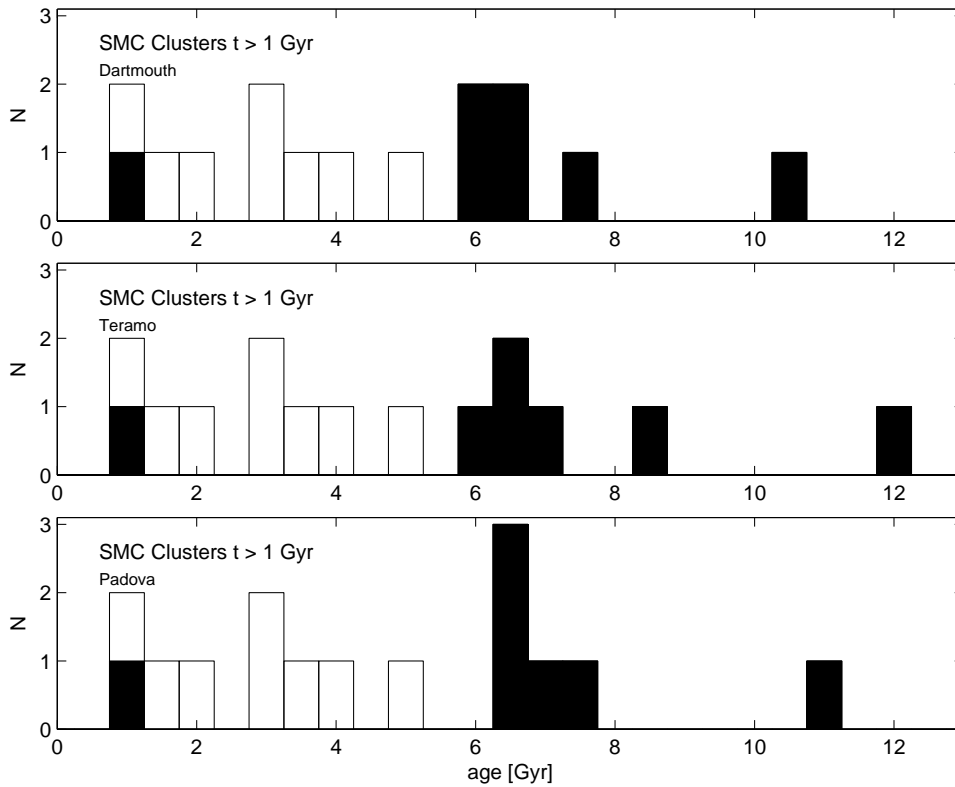


FIGURE 4.46. The age distribution of 15 intermediate-age and old SMC clusters (excluding NGC 361) with ages derived in this paper, in Chapter 2 (plotted as black histograms), and adopted from (Mighell et al. 1998a/b, Mould et al. 1992; Alves & Sarajedini 1999; Rich et al. 2000; Piatti et al. 2001; Crowl et al. 2001) (plotted as white histograms). Since the cluster ages from the literature were derived using different data and methods, their distribution does not change. In the first panel we used the ages found using the Dartmouth models, in the second we use the Padova ages, and in the last panel the Teramo ages were used. The literature ages of NGC 152, NGC 411, and Lindsay 113, are based on HST/WFPC2 data (Mighell et al. 1998a/b, Alves & Sarajedini 1999; Rich et al. 2000), while the adopted ages of Kron 28, Kron 44, Lindsay 11, Lindsay 32, and Lindsay 116 are derived from ground-based photometry (Mould et al. 1992; Crowl et al. 2001; Piatti et al. 2001). NGC 361 is not considered due to its uncertain age. The age distribution illustrates the continuous cluster formation with the small age gap between ~ 8 and 10 Gyr.

have been found by e.g. Girardi et al. (1995), although the most recent proper motion measurements indicate that the Magellanic Clouds are currently on their first passage around the MW.

For young SMC clusters a relation between close encounters and the cluster formation history is not as obvious as for LMC clusters probably due to a smaller number of clusters (Chiosi et al. 2006). The age distribution in Figure 4.46 shows that a slightly enhanced number of star clusters with ages around 1 Gyr is located in the SMC, which might have been produced through a cloud-cloud collision after a pericenter passage ~ 0.5 Gyr ago (Bekki & Chiba 2005). But evidently massive star clusters older than 1 Gyr have formed continuously until ~ 7.5 Gyr ago (Lindsay 1). It is not yet understood why populous star clusters older than 4 Gyr have not formed and survived continuously in the LMC, while in the SMC they did. Bekki & Chiba (2005) explained the different cluster formation histories of the Clouds as a difference in birth locations and initial mass of the host galaxies.

CLUSTER	$[Fe/H]_{ZW84}$	Age_{Teramo} GYR	Age_{Padova} GYR	$Age_{Dartmouth}$ GYR
NGC 121	-1.46 ± 0.10	11.8 ± 0.7	11.2 ± 0.7	10.5 ± 0.5
Lindsay 1	-1.14 ± 0.10	8.3 ± 0.7	7.7 ± 0.7	7.5 ± 0.5
Kron 3	-1.08 ± 0.12	7.2 ± 0.5	7.1 ± 0.7	6.5 ± 0.5
NGC 339	-1.12 ± 0.10	6.6 ± 0.5	6.3 ± 0.5	6 ± 0.5
NGC 416	-1.00 ± 0.13	6 ± 0.8	6.6 ± 0.8	6 ± 0.8
Lindsay 38	-1.59 ± 0.10	6.3 ± 0.5	6.3 ± 0.5	6.5 ± 0.5
NGC 419	-0.67 ± 0.12		1.2-1.6	1.2-1.6

TABLE 4.9. **Parameters.** All derived ages are listed. The metallicities for the clusters NGC 121, Lindsay 1, Kron 3 and NGC 339 are taken from Da Costa & Hatzidimitriou (1998), where we adopted the ZW84 metallicity scale. The metallicities for NGC 416, Lindsay 38, and NGC 419, were taken from Kayser et al. (in prep.) in the CG97 scale, and which we transformed to ZW84 scale by using the transformation by Carretta & Gratton (1997).

Kallivayalil et al. (2006a/b, see also Piatek et al. 2008) measured proper motions for the SMC and the LMC and used Monte Carlo simulations to model the orbits of the Clouds and the MW. While they found bound orbits for the Clouds, they also found that it was difficult to keep the Clouds bound to each other for more than 1 Gyr in the past. It is possible that the Clouds are not a bound system (see also e.g., Bekki & Chiba 2005), and that they are making their first passage close to the Milky Way.

8. Summary

In this paper, we have presented ages for the six intermediate-age SMC star clusters Lindsay 1, Kron 3, NGC 339, NGC 416, Lindsay 38, and NGC 419 based on HST/ACS stellar photometry in the F555W and F814W passbands. The resulting CMDs represent the deepest published photometry so far and extend at least three magnitudes below the respective MSTOs. In order to obtain absolute ages, we applied three different isochrone models. The resulting ages are summarized in Table 4.9. We list the clusters by their identification in column (1). The $[Fe/H]$ values are given in column (2) in the scale by Zinn & West (1984). Column (3) shows the magnitude of the MSTO $m_{555,TO}$, column (4) the magnitude of the red bump and column (5) the magnitude of the red clump $m_{555,RC}$. The columns (6), (7) and (8) show the absolute ages determined using the isochrone models of Teramo, Padova and Dartmouth.

We find that the Dartmouth isochrones provide the closest approximation to the MS, SGB, and RGB, whereas the other models mostly cannot reproduce the slope of the upper RGB when using the spectroscopically determined metallicity and requiring that the isochrones fit the MSTO and SGB. The Dartmouth isochrone models yield ages of 7.5 ± 0.5 Gyr for Lindsay 1, 6.5 ± 0.5 Gyr for Kron 3, 6 ± 0.5 Gyr for NGC 339, 6 ± 0.8 Gyr for NGC 416, and 6.5 ± 0.5 Gyr for Lindsay 38. In general the isochrones provide good fits to the MSTO and SGBs that determine ages.

For the youngest cluster, NGC 419, only the Padova isochrones fitted the CMD, while the Teramo isochrones had major problems with fitting the SGB and RGB, and the Dartmouth isochrones are not available for such young ages.

The difficulties of various isochrone models of given metallicities in reproducing the upper red giant branches of clusters with the same metallicities are a well-known problem (e.g., Grebel 1997,

1999). Figures 4.18, 4.22, and 4.30 reflect the general failure of the chosen stellar evolutionary models to simultaneously reproduce all of the major features of CMDs (e.g., Gallart et al. 2005) in spite of the excellent fit to the lower RGB, SGB, and MS. For each cluster we fitted a fiducial ridgeline that provides a unique set of low-metallicity fiducial isochrones, which are invaluable for detailed comparisons with stellar evolution models.

In each of our cluster CMDs stars blueward of and above the MSTOs are visible, which could be BSS. The radial cumulative distribution of BSS candidates in Lindsay 1, Kron 3, NGC 339, Lindsay 38, and NGC 419 showed that the stars found in the BSS regions are not concentrated toward the cluster centers and are therefore most probably part of the younger MS of the SMC field star population. For NGC 416, we find an indication for centrally concentrated BSS candidates.

Looking at the spatial distribution, we find that the three oldest SMC clusters (NGC 121, Lindsay 1, Kron 3) lie in the north-western part of the SMC, while the youngest clusters are located near the SMC main body. Star clusters with ages higher than ~ 4 Gyr are located in the outer parts.

From the observed red clump magnitude we give a distance estimate for our clusters. We find that Lindsay 38 is the most distant cluster in our sample with $d \sim 68$ kpc, while NGC 419 is the closest cluster with $d \sim 53$ kpc. Therefore, the closest and farthest cluster in our sample have a distance from each other of ~ 17 kpc, which agrees with the assumed large depth extent of the SMC.

Further, we conclude that the SMC experienced massive cluster formation, remnants of which have survived from over much of its lifetime, unlike the LMC or MW. The oldest and only globular cluster, NGC 121, has formed ~ 11 Gyr ago, while the next oldest set of surviving massive clusters, e.g. Lindsay 1 or NGC 361, date from approximately 3 Gyr later. After this time the largest age gaps are ~ 1 Gyr suggesting that massive star clusters occurred without any substantial multi-Gyr hiatus. The SMC apparently formed massive star clusters that have survived from most of its lifetime.

STRUCTURAL PARAMETERS OF SEVEN SMC INTERMEDIATE-AGE AND OLD STAR CLUSTERS

“Du wirst nicht danach beurteilt, was du sagst, sondern was du tust.”

Rosa Luxemburg

We present structural parameters for the seven intermediate-age and old star clusters NGC 121, Lindsay 1, Kron 3, NGC 339, NGC 416, Lindsay 38, and NGC 419 in the Small Magellanic Cloud. We fit King profiles and Elson, Fall, and Freeman (EFF) profiles to both surface-brightness and star count data taken with the Advanced Camera for Surveys aboard the Hubble Space Telescope. Clusters older than ~ 1 Gyr show a spread in cluster core radii that increases with age, while the youngest clusters have relatively compact cores. No evidence for post core collapse clusters was found. We find no correlation between core radius and distance from the SMC center, although consistent with other studies of dwarf galaxies, some relatively old and massive clusters have low densities. Clusters younger than 5 Gyr have larger ellipticities than older clusters, but the oldest SMC star cluster, the only globular NGC121, is the most elliptical in our study. No correlation is seen between ellipticity and distance from the SMC center. The structures of these massive intermediate-age (1-8 Gyr) SMC star clusters thus appear to primarily result from internal evolutionary processes.

This study was undertaken together with Eva K. Grebel, John S. Gallagher III., Antonella Nota, Elena Sabbi, Marco Sirianni, Gisella Clementini, Gary Da Costa, Monica Tosi, Daniel Harbeck, Andreas Koch, and Andrea Kayser.

It has been submitted to The Astronomical Journal.

1. INTRODUCTION

The Small Magellanic Cloud (SMC) contains populous star clusters similar to those found in the Large Magellanic Cloud (LMC), although the two galaxies experienced a very different cluster formation history and age-metallicity relation (e.g., Da Costa 2002). The smaller and less massive SMC contains many fewer clusters than the LMC. It formed its clusters continuously to the present day over the last ~ 7.5 Gyr (age of Lindsay 1, Glatt et al. 2008b). The oldest and only SMC globular star cluster, NGC 121, is 2-3 Gyr younger than the oldest Milky Way (MW) and LMC globular clusters (Glatt et al. 2008a).

Galactic globular clusters (GCs) can be described as an isothermal central region and a tidally truncated outer region (e.g., Binney & Merrifield 1998), but both regions evolve with time. Once formed, star clusters are affected by internal and external processes, which influence the spatial distribution of member stars. The evolution of star clusters is affected by mass loss caused by, e.g., expulsion of gas, large-scale mass segregation, stellar mass loss, and low-mass star evaporation (e.g., Gnedin & Ostriker 1997; Koch et al. 2004; Lamers et al. 2005; Goodwin & Bastian 2006). The galactic environment causes external perturbations such as tidal shocking that occurs as star clusters cross the disk or pass near the bulge (e.g., Gnedin & Ostriker 1997). These processes tend to decrease the cluster mass and might lead to core collapse, which has been observed in the oldest MW and LMC clusters (Djorgovski & Meylan 1994; Mackey & Gilmore 2003a). The investigation of the present-day structure of individual star clusters is an important instrument to probe cluster dynamical evolution.

In the SMC and the LMC, some of the older objects have apparently experienced a significant change in core radius, while for other old objects the core radii apparently have remained almost unchanged (Mackey & Gilmore 2003a,b). This trend seems most likely to be the result of real physical cluster evolution, but the processes causing this core expansion for some clusters are not yet understood. A spread in core radii beginning at a few 100 Myr is visible with a few clusters showing large core radii while others remain small and compact. The five Fornax and four confirmed Sagittarius clusters show the same spread: two of the Sagittarius and two of the Fornax clusters have large core radii, while the others have compact cores (Mackey & Gilmore 2003c). Galactic GCs show a spread in core radius size amounting to about two orders of magnitude (Trager et al. 1995) containing a large number of so called core-collapse clusters. However, many of the oldest GCs modified their original structure during their lifetime and have developed small cores (e.g., Trager et al. 1995; Bonatto & Bica 2008).

The ellipticity of the SMC clusters was noted to be larger than that of the MW and LMC clusters (Kontizas et al. 1990; Han & Ryden 1994; Goodwin 1997). Old Galactic GCs have a very spherical shape, while the oldest LMC globulars are flatter. The oldest SMC clusters are even flatter than those in the LMC (Kontizas et al. 1990).

If one assumes that star clusters had originally small core regions and elliptical shapes then why was this original structure of many of the Magellanic Cloud (MS) GCs modified during their lifetime and why did some of the oldest clusters hosted by LMC and SMC remain unchanged? Goodwin (1997) proposes that the strength of the tidal field of the parent galaxy is the dominant factor. If the tidal field is strong, the velocity anisotropies in a rapidly rotating elliptical globular cluster are destroyed, while a weak field is unable to remove these anisotropies and the cluster remains unchanged. In the MW, however, one has to distinguish between halo-, bulge-, and disk GCs. Disk GCs move in circular orbits around the MW center and experience only little variation of the Galactic gravitational field. Halo clusters pass the Galactic disk or bulge (Hunter et al. 2003; Lamers et al. 2005; Gieles et al. 2007), which has a strong influence on their dynamical evolution and hence structure. The GC system of the MW also contains a number of clusters acquired via merger processes (e.g., Bica et al. 2006).

We determine the structural parameters of the seven rich SMC star clusters NGC 121, Lindsay 1, Kron 3, NGC 339, NGC 416, Lindsay 38, and NGC 419 fitting *both* King and EFF profiles to projected number-density and surface-brightness profiles. The observations were obtained with the Advanced

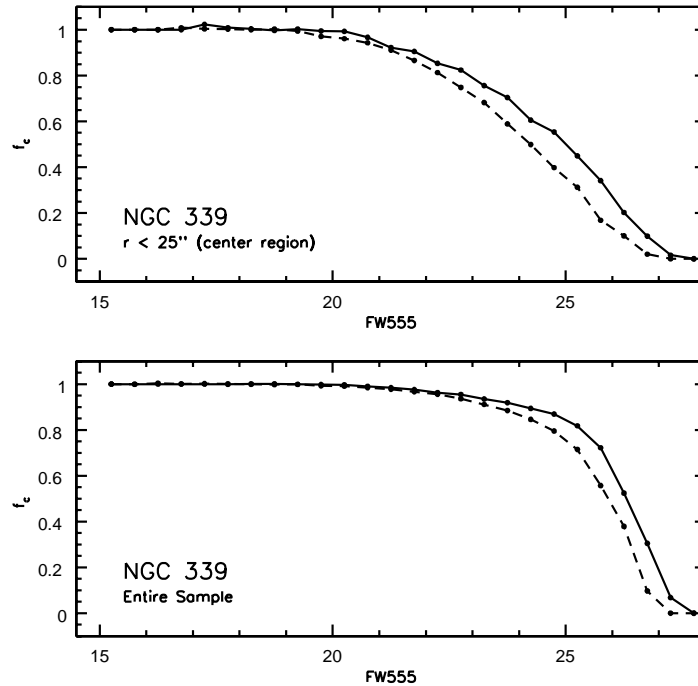


FIGURE 5.1. Completeness curves for the F555W (solid line) and F814W (dashed line) photometry of NGC 339 as a function of magnitude. The upper plot shows the completeness curves for the centre region ($r < 25''$) of the cluster and the lower plot shows the completeness curves for the entire sample. Only stars for which the completeness in the center region is better than 50% in the central regions of each cluster were used.

Camera for Surveys (ACS) aboard the Hubble Space Telescope (HST). The important characteristic radii of star clusters that we determine are the core radius (r_c), the projected half light radius (r_h), and the tidal radius (r_t). The core radius is defined as the radius at which the surface brightness has fallen to half its central value. The scale radius in the King (1962) analytic profile, r_0 , however exceeds the core radius such that it is larger for lower central concentrations. The difference between r_c and r_0 is greatest at low concentrations. The half light radius contains half the light of the cluster. The mean SMC distance modulus is assumed to be $(m - M)_0 = 18.88 \pm 0.1$ mag (60 kpc) (e.g., Storm et al. 2004), but our photometry also provides us with individual cluster distances (see Chapter 4).

Generally, beyond the tidal radius the external gravitational fields of the galaxy dominate the dynamics, and stars are no longer bound to the cluster (e.g., Elson et al. 1987; Gnedin & Ostriker 1997). In the MCs it is not obvious that the tidal field has set the observed tidal radii of star clusters. For example Elson et al. (1987) found that ten LMC star clusters with ages up to 8×10^8 yrs do not appear to be tidally truncated. This could result, for example, from interactions with other star clusters (Carvalho et al. 2008). Therefore, we use 'limiting radius' for the King model parameter r_t because it may well be that the limiting radii are not tidally generated.

In § 2 we give an overview of the data and the reduction process, which has been described in detail in Chapters 3 and 4. The methods used in the present Chapter are described in § 3 and the results are discussed in § 4.

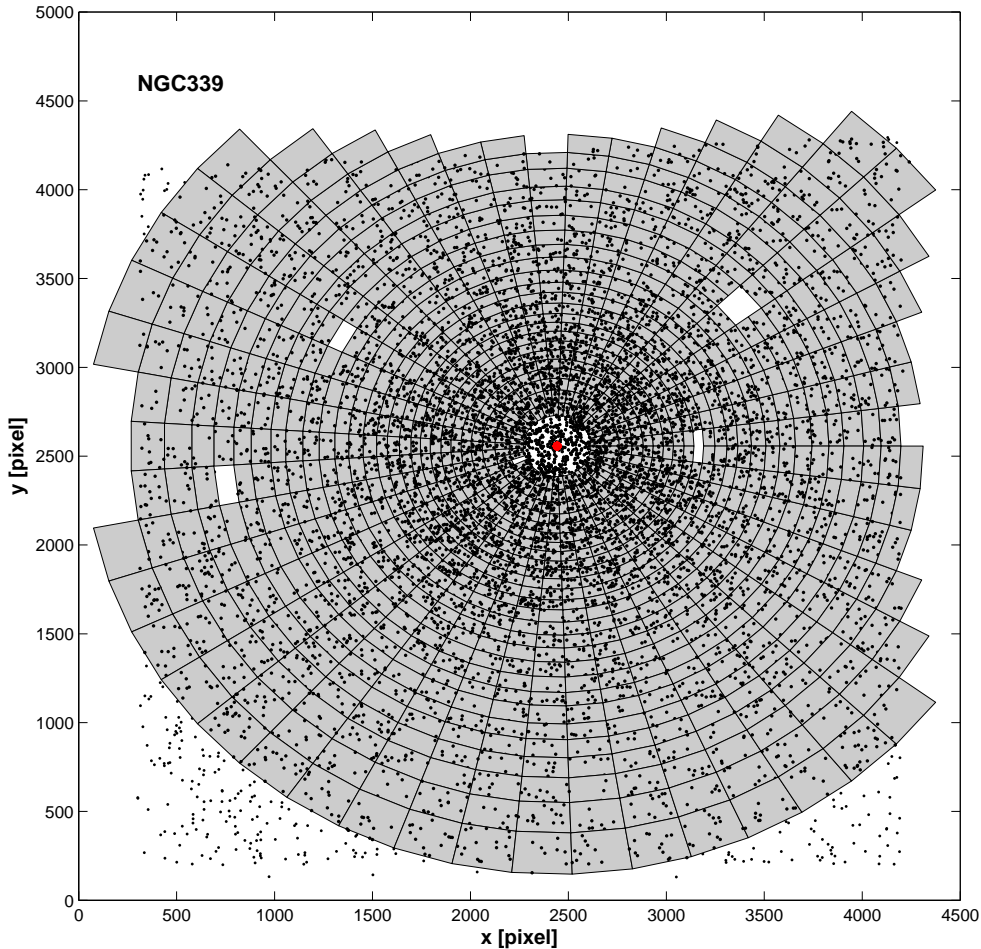


FIGURE 5.2. Star selection to calculate the number density profiles for NGC 339 as this is representative for all clusters. Those stars lying within the gray area were counted while the grey areas represent the parts of the annuli in which these stars are found. The red dot indicates the location of the center of gravity.

2. OBSERVATION

The SMC star clusters NGC 121, Lindsay 1, Kron 3, NGC 339, NGC 416, Lindsay 38, and NGC 419 were observed with the HST/ACS between 2005 August and 2006 March (Table 1 in Chapter 4). The images were taken in the F555W and F814W filters, which closely resemble the Johnson V and I filters in their photometric properties (Sirianni et al. 2005). All clusters were observed with the Wide Field Channel (WFC), while for the dense central regions of NGC 121, NGC 416, and NGC 419 images from the High Resolution Camera (HRC) are available. Each WFC image covers an area of $200'' \times 200''$ at each pointing with a pixel scale of ~ 0.05 arcsec. The HRC images cover an area of $29'' \times 26''$ with a pixel scale of ~ 0.025 arcsec.

The data sets were processed adopting the standard Space Telescope Science Institute ACS calibration pipeline (CALACS) to subtract the bias level and to apply the flat field correction. For each filter, the short and long exposures were co-added independently using the MULTIDRIZZLE package (Koekemoer et al. 2002). Cosmic rays and hot pixels were removed with this package and a correction for geometrical distortion was provided. The resulting data consist of one 40 s and one 1984 s

<i>Cluster</i>	α	δ	$[Fe/H]_{ZW84}$	AGE Gyr	DISTANCE KPC
NGC 121	$0^h26^m47^s.80$	$-71^\circ32'11''.40$	-1.46 ± 0.10	10.5 ± 0.5	64.9 ± 1.2
Lindsay 1	$0^h03^m53^s.22$	$-73^\circ28'16''.66$	-1.14 ± 0.10	7.5 ± 0.5	56.9 ± 1.0
Kron 3	$0^h24^m46^s.28$	$-72^\circ47'35''.76$	-1.08 ± 0.12	6.5 ± 0.5	60.6 ± 1.1
NGC 339	$0^h57^m46^s.38$	$-74^\circ28'14''.24$	-1.12 ± 0.10	6 ± 0.5	57.6 ± 4.1
NGC 416	$1^h07^m58^s.64$	$-72^\circ21'19''.75$	-1.00 ± 0.13	6 ± 0.8	60.4 ± 1.9
Lindsay 38	$0^h48^m50^s.03$	$-69^\circ52'07''.63$	-1.59 ± 0.10	6.5 ± 0.5	66.7 ± 1.6
NGC 419	$1^h08^m17^s.31$	$-72^\circ53'02''.49$	-0.67 ± 0.12	1.2-1.6	50.2 ± 2.6

TABLE 5.1. **Position of the photo-center.** The values for the metallicities [Fe/H] are adopted from Da Costa & Hatzidimitriou (1998) and Kayser et al. 2008, in prep. The ages are taken from Chapters 3 and 4 (best-fitting Dartmouth isochrones (Dotter et al. 2007) for all clusters except NGC 419, for which the Padova isochrones (Girardi et al. 2000, 2008) provided the best fit.)

exposure (1940 s for Lindsay 38) in F555W and one 20 s as well as one 1896 s exposure (1852 s for Lindsay 38) in F814W. The HRC data of NGC 419 consist of a 70 s and 1200 s exposure in F555W and a 40 s and 1036 s exposure in F814W.

Saturated foreground stars and background galaxies were discarded from the WFC images by using the Source Extractor (Bertin & Arnouts 1996). The detection thresholds were set at 3σ above the local background level for Lindsay 1, 1σ for Kron 3 and 4σ for NGC 339, NGC 416, and Lindsay 38 in order to detect even the faintest sources. The threshold levels were chosen based on the different crowding effects of the individual clusters. The photometric reductions were carried out using the DAOPHOT package in the IRAF¹ environment on DRIZZLED images. The exposure times, the selection cuts, and the photometry are described in the Chapters 3 and 4 and we refer to these two Chapters for detailed information.

3. STRUCTURAL PARAMETERS

3.1. Centers

To study the structural parameters of the clusters we first determined the photo-center (C_{phot}) of the stellar populations; for a symmetric system this will be close to the center of gravity. An accurate determination of the cluster center is necessary in order to avoid artificial distortions of the radial profiles. As a first approximation we estimated the location of the cluster center on the image by eye. A more precise center was then determined by calculating the average of the x and y coordinates within the cluster center region. First, the mean x and y coordinates were determined within a radius of 2000 pixels around the apparent center. In the following iterations, the radii were divided by two and using the center coordinates found in the previous iterations as their origin. We iterated until the radius was smaller than 10 pixels. The error is $\sim 0.5''$ for both α and δ , which corresponds to 10 pixels in the HST/ACS images. For NGC 121, NGC 416, and NGC 419 C_{phot} was determined on the HRC data using the same algorithm due to crowding of the WFC data. The resulting positions are summarized in Table 5.1.

¹IRAF is distributed by the National Optical Astronomy Observatory, which is operated by the Association of Universities for Research in Astronomy, Inc. under cooperative agreement with the National Science Foundation.

<i>Cluster</i>	r_0 <i>arcsec</i>	r_0^1 <i>pc</i>	r_t <i>arcsec</i>	r_t^1 <i>pc</i>	c	r_h <i>arcsec</i>	r_h <i>pc</i>	ϕ
<i>To number-density profiles</i>								
NGC 121	15.26 ± 0.42	4.80 ± 0.56	165.01 ± 23.28	51.92 ± 7.32	1.034 ± 0.12	27.01 ± 2.21	8.50 ± 0.70	10 ⁻³
Lindsay 1	61.67 ± 3.80	17.01 ± 1.55	230.77 ± 37.26	63.66 ± 10.28	0.573 ± 0.10	62.45 ± 5.84	17.23 ± 1.61	10 ⁻⁵
Kron 3	34.86 ± 1.07	10.24 ± 0.87	130.96 ± 6.70	38.47 ± 1.97	0.575 ± 0.02	35.38 ± 1.50	10.39 ± 0.44	10 ⁻²
NGC 339	32.84 ± 0.64	9.17 ± 0.75	186.73 ± 16.51	52.14 ± 5.10	0.755 ± 0.06	41.85 ± 2.37	11.69 ± 0.66	10 ⁻²
NGC 416	11.76 ± 0.95	3.44 ± 0.44	84.59 ± 19.65	24.77 ± 5.75	0.859 ± 0.16	16.96 ± 2.63	4.97 ± 0.77	10 ⁻²
Lindsay 38	31.24 ± 0.85	10.10 ± 0.84	173.82 ± 12.39	56.21 ± 4.00	0.745 ± 0.04	39.40 ± 1.65	12.74 ± 0.53	10 ⁻²
NGC 419	15.22 ± 1.78	3.70 ± 0.51	174.15 ± 18.57	42.38 ± 4.52	1.059 ± 0.08	27.69 ± 2.47	6.74 ± 0.60	10 ⁻²
<i>To surface-brightness profiles</i>								
NGC 121	11.56 ± 0.98	3.64 ± 0.31	175.52 ± 33.19	55.22 ± 10.44	1.246 ± 0.16	24.15 ± 3.20	7.60 ± 1.00	10 ⁻⁵
Lindsay 1	61.41 ± 4.95	16.94 ± 1.37	216.54 ± 41.92	59.73 ± 11.57	0.349 ± 0.08	60.08 ± 8.62	16.57 ± 2.37	10 ⁻⁵
Kron 3	25.53 ± 2.41	7.50 ± 0.71	180.25 ± 37.56	52.96 ± 11.03	0.848 ± 0.15	36.50 ± 3.50	10.72 ± 1.03	10 ⁻⁵
NGC 339	35.29 ± 2.86	9.86 ± 0.80	260.72 ± 39.79	72.80 ± 11.11	0.869 ± 0.14	51.58 ± 5.89	14.40 ± 1.65	10 ⁻⁵
NGC 416	10.22 ± 1.51	2.99 ± 0.44	107.95 ± 22.54	31.61 ± 6.60	1.023 ± 0.15	17.88 ± 3.18	5.24 ± 0.93	10 ⁻²
Lindsay 38	31.47 ± 3.68	10.18 ± 1.19	179.65 ± 34.08	58.09 ± 11.02	0.711 ± 0.05	40.32 ± 6.13	13.04 ± 1.98	10 ⁻⁵
NGC 419	12.98 ± 1.47	3.16 ± 0.36	207.19 ± 30.11	50.42 ± 7.33	1.203 ± 0.15	27.73 ± 3.58	6.75 ± 0.87	10 ⁻⁵
<i>To surface-brightness profiles for stars below the MSTOs</i>								
NGC 121	26.24 ± 1.11	8.26 ± 0.35	156.25 ± 28.88	49.16 ± 9.09	0.775 ± 0.11	34.31 ± 3.91	10.80 ± 1.23	10 ⁻²
Lindsay 1	78.21 ± 4.48	21.57 ± 1.24	269.84 ± 50.11	74.44 ± 13.82	0.538 ± 0.07	75.58 ± 9.83	20.85 ± 2.71	10 ⁻⁵
Kron 3	30.50 ± 1.48	8.96 ± 0.44	157.86 ± 30.84	46.38 ± 9.06	0.714 ± 0.08	37.01 ± 4.60	10.87 ± 1.35	10 ⁻²
NGC 339	32.54 ± 2.05	9.09 ± 0.57	271.17 ± 52.07	75.72 ± 14.55	0.921 ± 0.12	50.59 ± 5.92	14.13 ± 1.65	10 ⁻²
NGC 416	15.10 ± 0.89	4.42 ± 0.26	76.01 ± 18.66	22.26 ± 5.46	0.702 ± 0.12	18.05 ± 2.81	5.29 ± 0.82	10 ⁻⁵
Lindsay 38	29.01 ± 1.84	9.38 ± 0.60	192.65 ± 38.72	62.30 ± 12.52	0.822 ± 0.06	40.16 ± 5.29	12.99 ± 1.71	10 ⁻²
NGC 419	15.60 ± 1.66	3.80 ± 0.40	275.91 ± 53.94	67.15 ± 13.13	1.247 ± 0.12	35.03 ± 5.18	8.53 ± 1.26	10 ⁻²

TABLE 5.2. **Structural Parameters from the King profile fit.**

¹The MSTOs and the conversion of r_0 is based on the distances found in Chapter 4. The upper section of this table corresponds to the Figures 5.3, and 5.4 (solid lines), the middle section to Figures 5.5 and 5.6 (dashed lines) for which only stars brighter than the magnitude for which the completeness is 50% in the central region of each cluster were used. The lower section corresponds to the Figures 5.8 and 5.9 (dashed lines) for which only stars brighter than the magnitude for which the completeness is 50% in the central region of each cluster and stars fainter than the MSTOs were used. The half-light radii were computed by estimating L_{tot} from the King profiles.

3.2. King profile

The number surface density profiles of old GCs are usually described by the empirical King models (King 1962):

$$n(r) = k \cdot \left\{ \frac{1}{[1+(\frac{r}{r_c})^2]^{\frac{1}{2}}} - \left(\frac{1}{[1+(\frac{r_t}{r_c})^2]^{\frac{1}{2}}} \right) \right\}^2 + \phi$$

where $n(r)$ is the number of stars per unit area, r_0 is the King radius, and r_t is the limiting radius of the cluster. The parameter ϕ was added for the background contamination. No adjacent field was observed to measure the background. The field-of-view of ACS is too small for a reliable measurement of the background on the image. Hence, we treat it as a fitting parameter. The background density is assumed to be constant. As a result we cannot necessarily distinguish an extended halo around a cluster from the true stellar background. Although our background estimates are formally quite good, our values of ϕ can be considered as being greater than or equal to that of the actual background. Both for the number density and surface-brightness distributions King profiles were fitted, which are summarized in Table 5.2 (upper and middle sections).

<i>Cluster</i>	$(m - M)_0$ <i>mag</i>	E_{V-I} <i>mag</i>	M_V^{King} <i>mag</i>	M_V^{EFF} <i>mag</i>
NGC 121	19.06 ± 0.03	0.024	-8.51 ± 0.15	-8.37 ± 0.14
Lindsay 1	18.78 ± 0.04	0.024	-7.39 ± 0.09	-7.38 ± 0.09
Kron 3	18.91 ± 0.04	0.024	-7.75 ± 0.15	-8.10 ± 0.12
NGC 339	18.80 ± 0.08	0.040	-7.42 ± 0.14	-7.76 ± 0.11
NGC 416	18.90 ± 0.07	0.104	-8.03 ± 0.11	–
Lindsay 38	19.12 ± 0.05	0.016	-5.08 ± 0.19	-5.49 ± 0.21
NGC 419	18.50 ± 0.12	0.080	-8.85 ± 0.18	–

TABLE 5.3. **Estimate of the Absolute Magnitudes.** The distance moduli and the reddenings E_{V-I} are taken from Chapter 4.

Only clusters in the nearest galaxies are sufficiently well resolved with HST to provide number-density profiles. Due to field-of-view of the WFC the limiting radii of our clusters lie outside the ACS image. Therefore, the limiting radius r_t and as a consequence also the half-light radius r_h cannot be directly measured. We give an estimate of the projected half-light radius r_h by calculating the total luminosity from the King profiles. The values r_0 and r_t can be used to calculate the concentration parameter $c = \log(r_t/r_0)$. From r_h we can give an estimate of the absolute magnitude M_V of the star clusters by multiplying the flux within r_h by 2. Using the distance moduli and the extinctions from Chapter 4, M_V could be calculated. The result is summarized in Table 5.3.

Concentric annuli containing the same number of stars were constructed around C_{phot} . The radii and the enclosed number of stars depend on the richness of the clusters and on photometric incompleteness caused by crowding. The completeness corrections on the WFC images were determined for each cluster separately and applied to the number density calculation. The completeness factors were determined using the subroutine *addstar* in DAOPHOT to simulate 1,000,000 artificial stars (in steps of ≈ 2500 stars) in each long exposure frame. For a detailed description of the procedure we refer the reader to Sabbi et al. (2007). Figure 5.1 shows the completeness factor of NGC 339 in each filter, defined as the percentage of the artificial stars successfully recovered compared with the total number of stars added to the data. Only stars brighter than the magnitude for which the completeness is 50% in the central regions of each cluster were used.

Then the area of the annuli was calculated. We had to apply a geometrical area correction for those annuli that were not fully imaged due to the cluster centering in the upper right part of the MULTIDRIZZLED image. Therefore, only those parts of the annuli were considered that lie fully on the image while the others were excluded. Figure 5.2 displays the selected areas and stars of NGC 339 as this is representative for all clusters. The black dots lying within the grey area represent the stars considered in the number density profile, while the filled grey areas show the annuli parts in which these stars were found. The errors were propagated from the Poisson statistics of the number and area counts. For NGC 121, NGC 416, and NGC 419 the profiles were obtained on the WFC and HRC data independently and then combined. The WFC data were only considered outside the HRC field, hence avoiding overlaps.

The star density was obtained by dividing the number of stars by their area. Both the King and the EFF profiles were fitted to each of our clusters via χ^2 minimization.

In Figure 5.3 and 5.4 we show the stellar density distribution of our clusters with the best-fitting King profiles (solid line) and the best-fitting EFF profiles (dashed line) plus background. The filled circles represent the star density taken from the WFC data, the open circles the star density taken from the HRC data. The resulting structural parameters r_0 , r_t , r_h , and c from the King profiles are summarized in Table 5.2. The parameters r_c , r_t , γ , and ϕ from the EFF profiles are shown in Table 5.4. The listed errors are given by the χ^2 minimization fitting process.

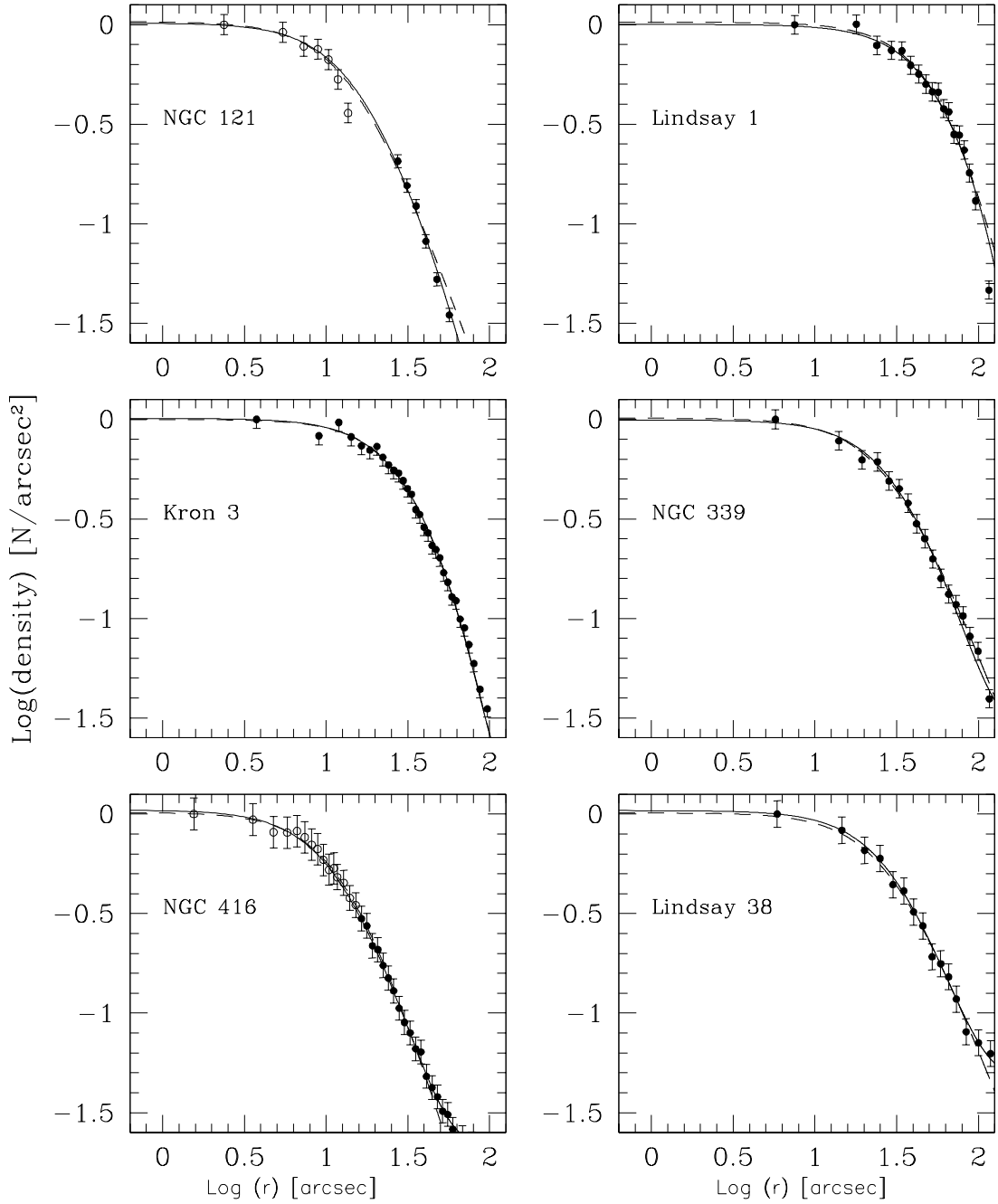


FIGURE 5.3. Number density profiles of the seven SMC clusters in our sample. The filled circles represent the WFC data, the open circles the HRC data. The solid line indicates the best-fitting King model of the radial density distribution of the clusters. The radial plots of NGC 416 and NGC 419 (Fig. 5.4) are truncated.

3.3. EFF profile

The EFF profile (Elson et al. 1987) is given by

$$n(r) = \mu_0 \cdot \left(1 + \left(\frac{r^2}{a^2}\right)^{-\gamma/2} + \phi,\right.$$

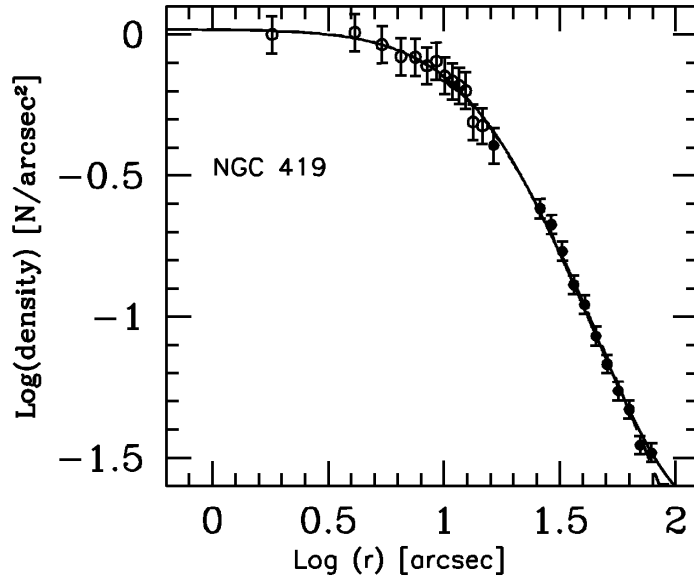


FIGURE 5.4. As for Fig. 5.3 but for NGC 419.

where n_0 is the central projected stellar density, a is a measure of the core radius and γ is the power-law slope. The parameter ϕ was added for the background contamination. The parameter a in the EFF profiles is related to the core radius of a centrally concentrated cluster by $r_c = a \cdot (2^{2/\gamma} - 1)^{1/2}$. To determine the parameters of the clusters we fitted the surface brightness profiles with $I(r) = I_0 \cdot [(1 + r^2/a^2)^{-\gamma/2}] + \phi$. No limiting radii can be derived from EFF profiles. We give an estimate of the projected half-light radius r_h by calculating the total luminosity from the EFF profiles. This method works well until a $\gamma \approx 2$ is reached, because then the total luminosity formally becomes infinite.

The EFF profiles were used in this study, because all recent studies (Kontizas et al. 1982; Kontizas & Kontizas 1983; Kontizas et al. 1986, 1990; Mackey & Gilmore 2003b; Hill & Zaritsky 2006; Carvalho et al. 2008) of structure parameters of SMC star clusters used EFF profiles. This choice facilitates the comparison of our results with the earlier studies. For the same reason we chose to work in the commonly used F555W ($\sim V$) band.

In order to measure the surface-brightness profiles, concentric annuli of coextensive areas were created around C_{phot} . The surface brightness μ_i of the i th annulus in a set was found by summing over the flux of all stars that fall into the annulus. For NGC 416, the profile was fitted only using the inner points ($\log(r) < 1.5$ arcsec), because the SMC field contribution is not negligible for this cluster. The same area and completeness corrections as for the number density profiles were applied. Saturated foreground stars were removed from the images. Only stars brighter than the magnitude for which the completeness is 50% in the central region of each cluster were used.

For Lindsay 1, Kron 3, NGC 339, and Lindsay 38 only WFC photometry is available, which resolves the clusters entirely. The surface brightness measured in four sets of concentric annuli with the same area are plotted for each cluster on the same axes in Figure 5.5. The first set was done with 76 arcsec^2 (pentagons, black), the second with 250 arcsec^2 (triangles, magenta), the third with 374 arcsec^2 (crosses, blue), and the fourth with 500 arcsec^2 (squares, red).

For the three densest clusters, NGC 121, NGC 416, and NGC 419, the central regions were observed with HST/HRC. The surface brightness profiles of the center region were determined using the HRC data, while the profiles of the outer regions were calculated using the WFC data. Three HRC sets measured in concentric annuli of the same area are displayed with different symbols (green): 37.5 arcsec^2 (triangles), 25 arcsec^2 (asterisks), and 50 arcsec^2 (circles). For the WFC data, the same

<i>Cluster</i>	$\mu_{555}(0)$ <i>mag/arcsec²</i>	<i>a</i> <i>arcsec</i>	r_c <i>arcsec</i>	r_c^1 <i>pc</i>	γ	r_h <i>arcsec</i>	r_h <i>pc</i>	ϕ
<i>To number-density profiles</i>								
NGC 121	18.87 ± 0.03	14.63 ± 2.85	13.42 ± 2.62	4.22 ± 00.82	2.27	–	–	10 ⁻⁵
Lindsay 1	21.25 ± 0.04	74.84 ± 32.40	48.53 ± 19.00	13.39 ± 5.24	3.95	76.18 ± 32.98	21.01 ± 9.10	10 ⁻⁵
Kron 3	20.56 ± 0.03	45.31 ± 7.89	28.66 ± 4.99	8.42 ± 1.47	4.12	43.54 ± 7.58	12.79 ± 2.23	10 ⁻⁵
NGC 339	20.03 ± 0.03	29.07 ± 5.49	27.58 ± 5.21	7.70 ± 1.46	2.16	–	–	10 ⁻⁵
NGC 416	18.21 ± 0.06	13.73 ± 2.92	11.27 ± 2.40	3.30 ± 0.70	2.69	34.98 ± 7.42	10.22 ± 2.17	10 ⁻²
Lindsay 38	22.90 ± 0.04	29.07 ± 9.51	27.58 ± 5.02	8.92 ± 1.62	2.16	–	–	10 ⁻⁵
NGC 419	18.18 ± 0.03	14.68 ± 2.67	14.20 ± 2.52	3.46 ± 0.61	1.05	–	–	10 ⁻⁵
<i>To surface-brightness profiles</i>								
NGC 121	18.60 ± 0.08	16.52 ± 0.76	11.91 ± 0.57	3.75 ± 0.39	3.36	22.66 ± 0.99	7.13 ± 0.31	10 ⁻⁵
Lindsay 1	21.94 ± 0.09	101.15 ± 4.52	50.05 ± 1.96	13.81 ± 0.60	6.33	62.14 ± 1.76	17.14 ± 0.48	10 ⁻⁵
Kron 3	20.13 ± 0.09	30.11 ± 1.35	22.79 ± 0.78	6.70 ± 0.26	3.06	49.47 ± 1.41	14.53 ± 0.33	10 ⁻⁵
NGC 339	21.31 ± 0.10	38.71 ± 1.52	29.02 ± 1.19	8.10 ± 0.11	3.11	61.06 ± 2.10	17.05 ± 0.45	10 ⁻⁵
NGC 416	18.31 ± 0.04	9.20 ± 0.50	9.04 ± 0.35	2.65 ± 0.07	2.05	–	–	1.8 × 10 ⁻²
Lindsay 38	23.21 ± 0.06	37.83 ± 1.47	28.76 ± 1.17	9.30 ± 0.48	3.04	64.71 ± 1.84	20.93 ± 0.55	10 ⁻⁵
NGC 419	17.70 ± 0.06	12.33 ± 0.56	11.73 ± 0.47	2.85 ± 0.09	2.15	–	–	10 ⁻²
<i>To surface-brightness profiles for stars below the MSTOs</i>								
NGC 121	21.90 ± 0.07	35.59 ± 0.86	23.46 ± 0.59	7.38 ± 0.21	3.99	35.72 ± 0.86	11.24 ± 0.27	10 ⁻⁵
Lindsay 1	21.89 ± 0.10	111.84 ± 3.61	64.48 ± 2.29	17.79 ± 0.63	5.11	83.83 ± 2.70	23.13 ± 0.74	10 ⁻⁵
Kron 3	21.79 ± 0.08	34.17 ± 0.17	25.31 ± 0.48	7.44 ± 0.12	3.20	50.40 ± 0.95	14.81 ± 0.28	10 ⁻⁵
NGC 339	22.37 ± 0.11	29.90 ± 0.18	28.32 ± 1.35	7.91 ± 0.38	2.19	–	–	10 ⁻⁵
NGC 416	20.91 ± 0.06	18.91 ± 0.56	17.08 ± 0.51	5.00 ± 0.16	2.42	96.70 ± 2.86	28.32 ± 0.83	1.8 × 10 ⁻²
Lindsay 38	24.67 ± 0.09	25.80 ± 1.88	25.20 ± 1.71	8.15 ± 0.59	2.07	–	–	10 ⁻⁵
NGC 419	11.62 ± 0.56	14.37 ± 0.49	17.65 ± 0.58	3.50 ± 0.10	1.56	–	–	10 ⁻²

TABLE 5.4. **Structural Parameters from the EFF profile fit.**

¹The conversion of r_c is based on the distances found in Chapter 4.

The upper section of this table corresponds to the Figures 5.5 and 5.6 (solid lines), the middle section to the Figures 5.3 and 5.4 (dashed lines) for which only stars brighter than the magnitude for which the completeness is 50% in the central region of each cluster were used. The third section of this table corresponds to the Figures 5.8 and 5.9 (solid lines) for which only stars brighter than the magnitude for which the completeness is 50% in the central region of each cluster and stars fainter than the MSTOs were used. The half-light radii were computed by estimating L_{tot} from the EFF profiles. For the clusters with a γ close to two a formally infinite model luminosity was derived and no half-light radius could be calculated.

areas as above have been used, but only those annuli are shown that lie outside the regions covered by the HRC data. The surface-brightness profiles were fitted via χ^2 minimization.

Two sets of EFF profiles were fitted. For the first set, all stars brighter than the magnitude for which the completeness is 50% in the central region of each cluster were used. The resulting parameters could be compared with literature values. The best-fitting EFF profiles are shown in Figures 5.5 and 5.6 (solid lines). The results are summarized in Table 5.4 (upper and middle section).

The surface brightness comes mostly from the brighter stars around the main-sequence turnoff (MSTO) and brighter, while the surface density distribution comes principally from the numerous stars below the MSTO. Due to the long 2-body relaxation times, we do not expect much mass segregation and therefore the surface brightness and surface density profiles should be the same. To check this assumption, we fitted a second set of EFF profiles using only stars fainter than the MSTO and brighter than the magnitude for which the completeness is 50% in the cluster central regions. The MSTOs were adopted from Chapters 3 and 4. The best-fitting EFF profiles are shown in Figures 5.8 and 5.9 (solid lines). The results are summarized in Table 5.4 (lower section). The profiles are much

less scattered and smoother toward the outer region than in the first set of profiles. The reason for the smoother profiles are probably the number of stars contributing to the surface brightness is larger, and hence statistical fluctuations are smaller.

Cluster core 2-body relaxation times range from 1-2 Gyr on upwards, and thus mass segregation from this process is only expected to be a factor in the densest and oldest clusters in the sample. Only in NGC 121 differences are seen at a possibly significant level in the expected sense of larger core radii for the low mass stars by more than 3 times the combined errors. Thus we find no compelling evidence for mass segregation in the seven intermediate mass clusters in our sample, although we emphasize that deeper observations are needed for a definitive test.

Both for the number density and surface-brightness distributions King profiles were fitted, which are summarized in the upper and middle sections of Table 5.2 for the sample containing all stars above the 50% completeness levels and in the lower section for all stars between the 50% completeness levels and the MSTOs.

3.4. Angular distribution and ellipticity

To calculate the projected angular distribution we chose all stars around C_{phot} that lie entirely inside a circle on the image (see Table 5.5). Because the clusters are centered in the upper chip of the camera and the tidal radii lie outside the ACS images, this restriction was necessary to avoid artificial fluctuations. Our cluster samples were subdivided into 12 degree sectors and plotted against the azimuthal angle θ . We used a maximum-likelihood approach (McLaughlin et al. 1994, 1995) to obtain a solution for the ellipticity ϵ . The observed number density for an intrinsically elliptical distribution of points sampled in *circular* annuli is given by

$$(1) \quad \sigma(R, \theta) = kR^{-\alpha} [\cos^2(\theta - \theta_p) + (1 - \epsilon)^{-2} \sin^2(\theta - \theta_p)]^{-\alpha/2} + \sigma_b$$

where θ_p is the position angle of the major axis and σ_b the background density. To get a constraint on σ_b we use the distribution of stars in the color-magnitude diagrams (CMDs) of the clusters. Because the SMC is not crowded and is located at high Galactic latitude (e.g., Ratnatunga & Bahcall 1985), we do not expect a high field star contamination. We select the objects in the cluster CMDs lying to the red and the blue of the clusters main features. The number of these objects we then use to predict how many background objects are lying on the images. The normalized background contaminations σ_b are then used to determine the ellipticities. The function was fitted to each of our clusters via χ^2 minimization. Because we cannot measure the ellipticities at the tidal radii, the values presented here refer to the light distribution near r_h . The angular distributions are shown in Figure 5.10 and the results are summarized in Table 5.5.

4. DISCUSSION

4.1. Comparison of the core radii with previous studies

The only study of structural parameters of SMC star clusters based on space-based observations (HST/WFPC2) was presented by Mackey & Gilmore (2003b). They used imaging data of 10 populous star clusters. Four of these clusters are also included in the present sample. The most recent ground-based study of structural parameters was published by Carvalho et al. (2008) and is based on data taken with the ESO, Danish 1.54 m telescope, in La Silla. These authors studied surface photometry of 25 SMC star clusters, of which four overlap with our sample. Hill & Zaritsky (2006) used data from the Magellanic Clouds Photometric Survey (MCPS) (Zaritsky et al. 2002). Structure parameters were derived from fitting both King and EFF profiles for 204 star clusters. McLaughlin & van der Marel (2005) fitted both King and EFF models to star-count data for clusters in the SMC of which four overlap with the present sample. The observed profiles come from combining the data from Mackey & Gilmore (2003b) with data from Kontizas et al. (1982) and Kontizas & Kontizas (1983).

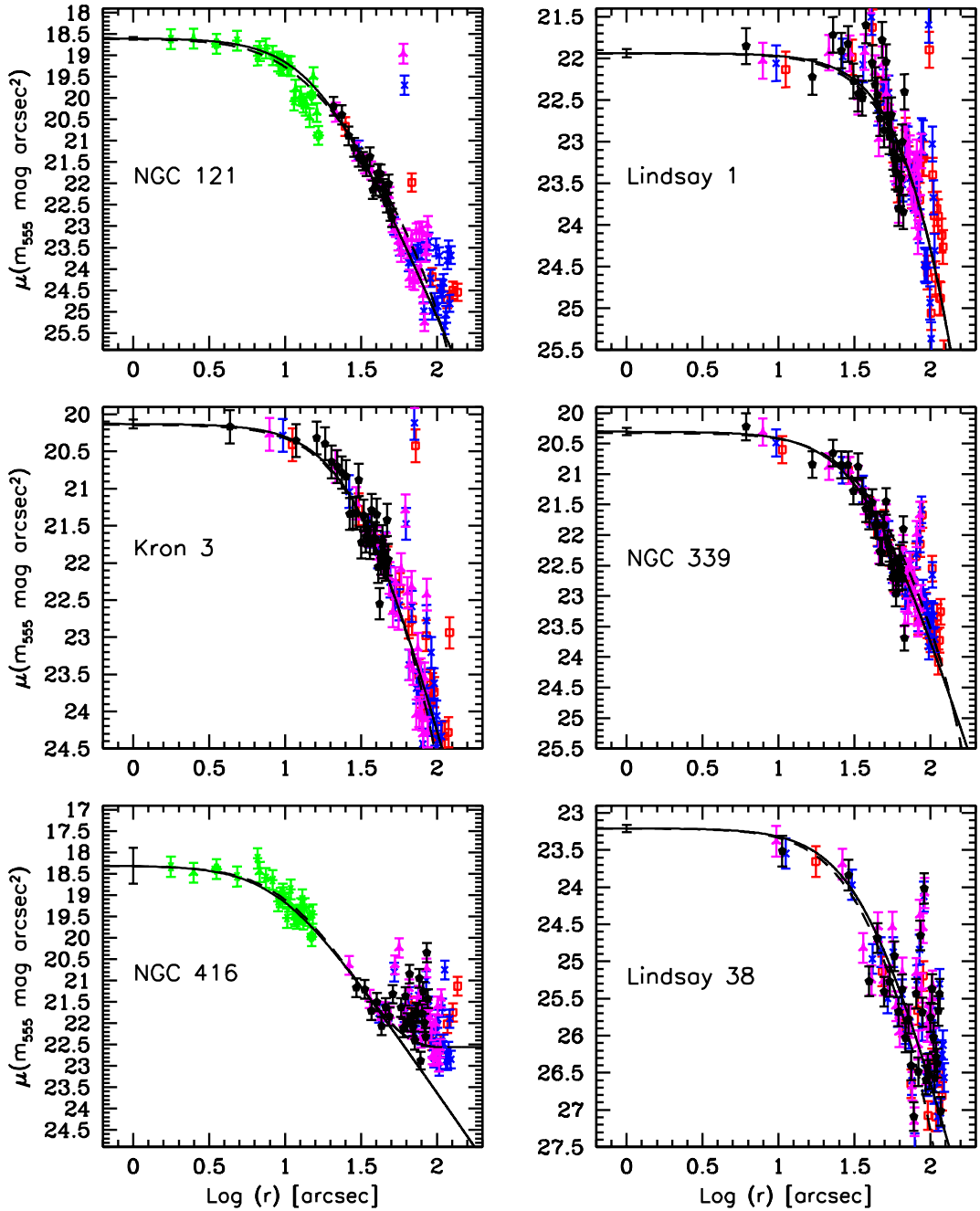


FIGURE 5.5. Surface-brightness profiles for each of the seven clusters in the present sample in the F555W-band. Only cluster stars brighter than the magnitude for which the completeness is 50% in the central region of each cluster were used. The surface-brightness was measured in four different areas which we display using different symbols (and different colors). For Lindsay 1, Kron 3, NGC 339, and Lindsay 38 only WFC images were used, while for NGC 121, NGC 416, and NGC 419 (Fig. 5.6) the dense center regions are covered with HRC data. The observations are not background subtracted.

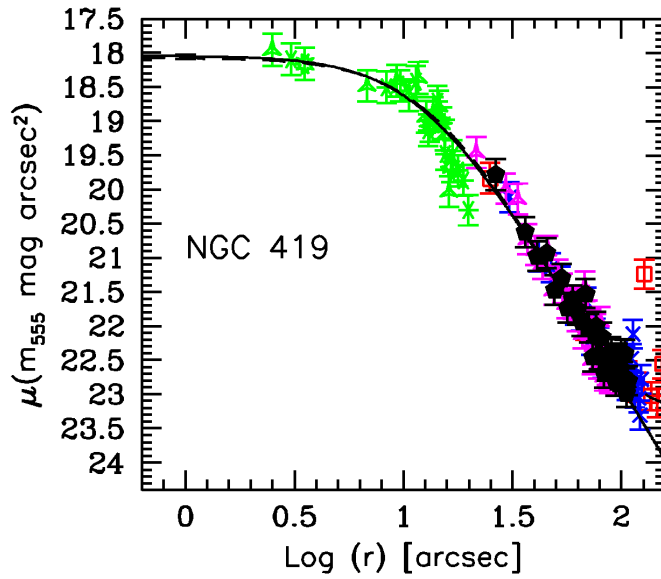
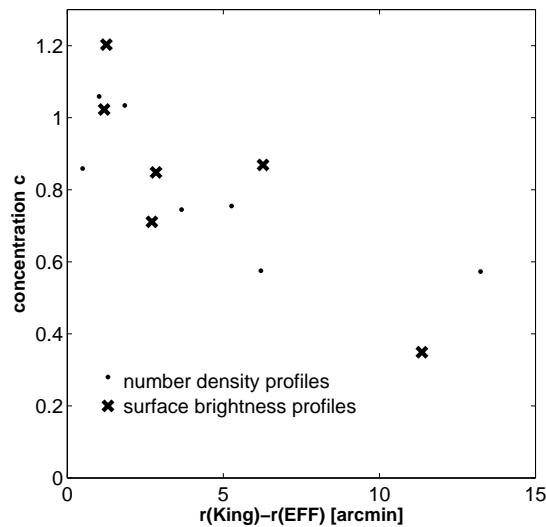


FIGURE 5.6. As for Fig. 5.5 but for NGC 419.

FIGURE 5.7. Difference between core radii from King and EFF profiles as a function of the concentration parameter c .

Earlier studies using number-density profiles were published by Kontizas et al. (1990) and are based on photographic plates obtained with the 1.2 m U.K. Schmidt Telescope in Australia. Five clusters of the present sample were also studied by Kontizas et al. (1990), but owing to the different resolution and depth of the shallower photographic plates we do not discuss these results here. As noted above, although often called the 'core radius', the King profile scale radius r_0 is larger than the true core radius r_c , with the difference being large for lower central concentrations. This effect is illustrated in Fig. 5.7 where we plot the difference between r_0 and r_c (derived from the EFF profile fits) against central concentration. We must therefore be careful to compare 'like with like', and we have thus compared our core radii from the EFF profile fits with literature data that also used EFF profile fits.

In Table 5.6 we compare the core radii from EFF profiles from surface-brightness profiles with the above mentioned previous studies. The EFF core radius of NGC 121 found in our study is ~ 1.4 pc

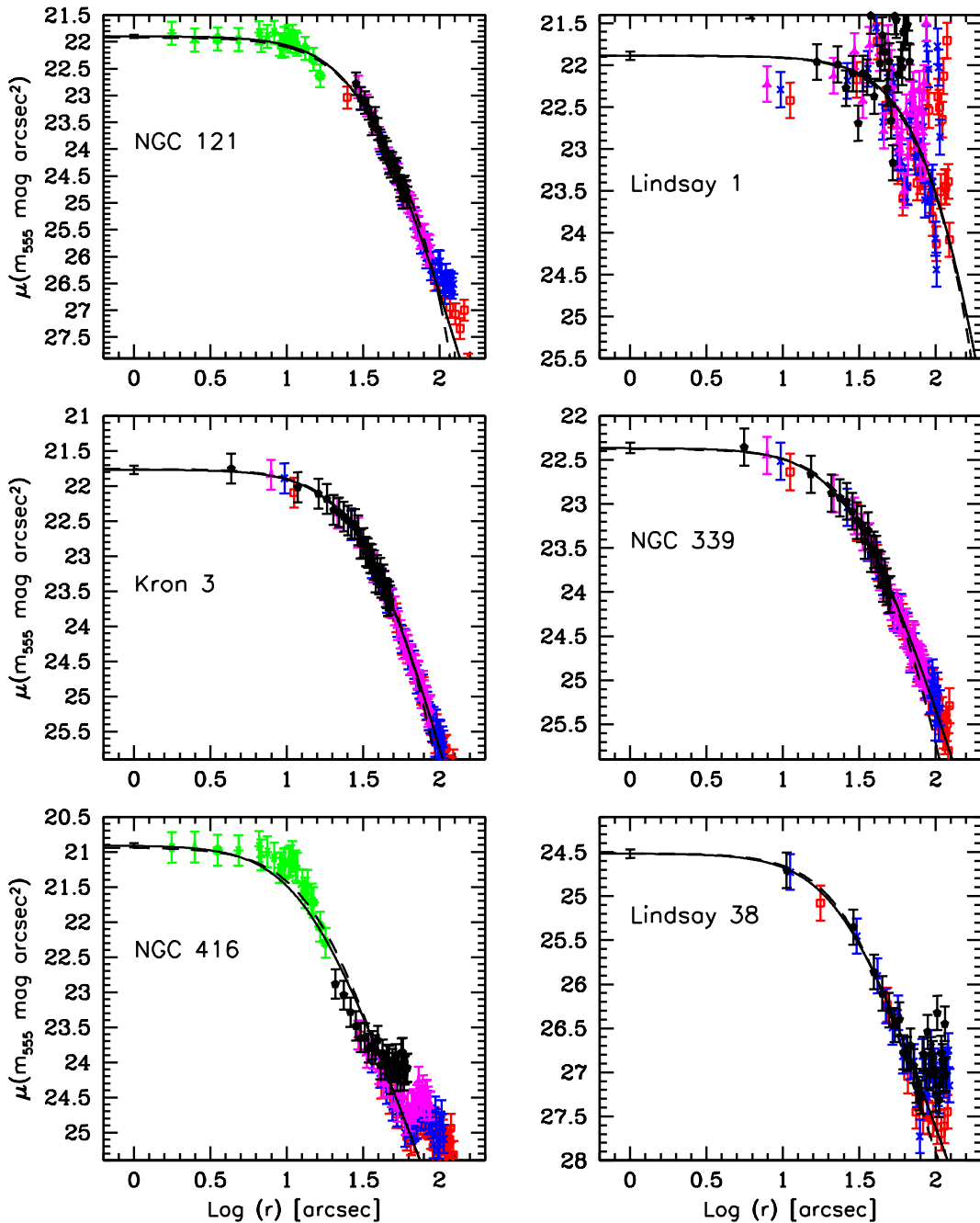


FIGURE 5.8. For this set of profiles all cluster stars brighter than the magnitude for which the completeness is 50% in the cluster central region and fainter than the MSTO were used. The applied method is the same as for the first set of EFF profiles shown in Fig. 5.5 and 5.6.

larger than the corresponding one published by Carvalho et al. (2008) and is ~ 0.75 pc larger than the one found by Mackey & Gilmore (2003b) and McLaughlin & van der Marel (2005). The core radius of NGC 339 is ~ 0.9 pc ($\sim 11\%$) larger than the radius published by Carvalho et al. (2008) ($1 \text{ pc} = 3.4''$), while the core radii of NGC 416 and Kron 3 are in good agreement. The core radii of Kron 3 and NGC 339 are ~ 0.6 pc ($\sim 10\%$) larger than the ones found by Mackey & Gilmore (2003b) while the core radius of NGC 416 agrees well with our value. The core radii of Kron 3 and NGC 339 are

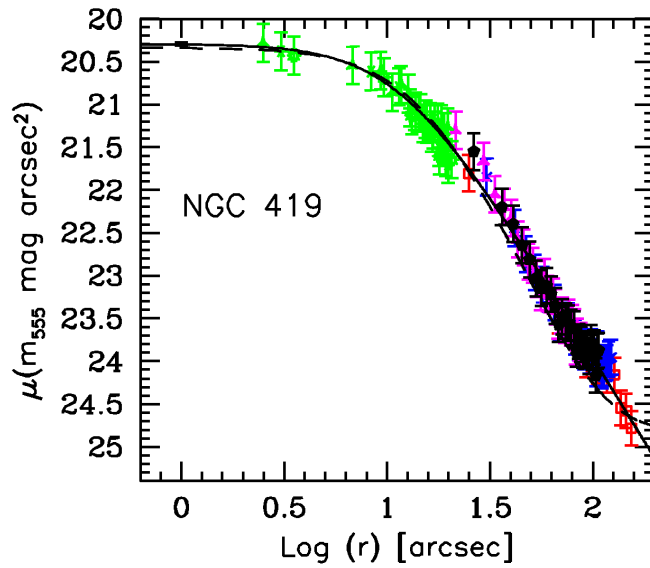


FIGURE 5.9. As for Fig. 5.8 but for NGC 419.

<i>Cluster</i>	<i>Distance from SMC center [kpc]</i>	<i>age Gyr</i>	<i>R arcmin</i>	ϵ	$\theta_p \pm 180$ <i>degree</i>	α	σ_b <i>arcmin²</i>
NGC 121	8.76 ± 1.1	10.5 ± 0.5	1.17	0.27 ± 0.06	83	1.77	22.48
Lindsay 1	13.28 ± 1.0	7.5 ± 0.5	1.52	0.16 ± 0.05	83	0.96	23.85
Kron 3	7.19 ± 1.1	6.5 ± 0.5	1.22	0.14 ± 0.05	88	0.96	28.80
NGC 339	0.73 ± 2.0	6 ± 0.5	1.46	0.17 ± 0.05	76	0.90	62.55
NGC 416	3.94 ± 1.4	6 ± 0.8	1.04	0.17 ± 0.06	109	0.90	264.33
Lindsay 38	6.27 ± 1.3	6.5 ± 0.5	1.18	0.21 ± 0.06	109	0.88	17.82
NGC 419	10.83 ± 1.6	1.2 – 1.6	1.14	0.14 ± 0.05	86	1.10	90.45
<i>Literature Sample</i>							
NGC 411	11.1 ± 1.3	1.2 ± 0.2	-	0.08	-	-	-
NGC 152	5.58 ± 1.3	1.4 ± 0.2	-	0.23	-	-	-
Kron 28	14.78 ± 1.3	2.1 ± 0.5	-	0.30	-	-	-
Kron 44	4.37 ± 1.3	3.1 ± 0.8	-	0.26	-	-	-
BS90	1.23	4.3 ± 0.1	-	0.05	-	-	-

TABLE 5.5. **Ellipticities.** The cluster 3d-distances from the SMC center were calculated in Chapter 4. R lists the radii within which all stars for the angular distribution calculation were considered. The ellipticities come from this Chapter and the literature values were adopted from Hill & Zaritsky (2006). The ages are taken from Chapters 3, 4 and Alves & Sarajedini (1999); Crowl et al. (2001); Piatti et al. (2001); Sabbi et al. (2007).

in very good agreement with McLaughlin & van der Marel (2005), but the core radius of NGC 416 is ~ 0.5 pc ($\sim 18\%$) smaller. Comparing our result with Hill & Zaritsky (2006) we find that their core radii for NGC 339, NGC 416, and NGC 419 are all larger than the values of this study about 0.5 pc, 0.4 pc, and 1.5 pc, respectively.

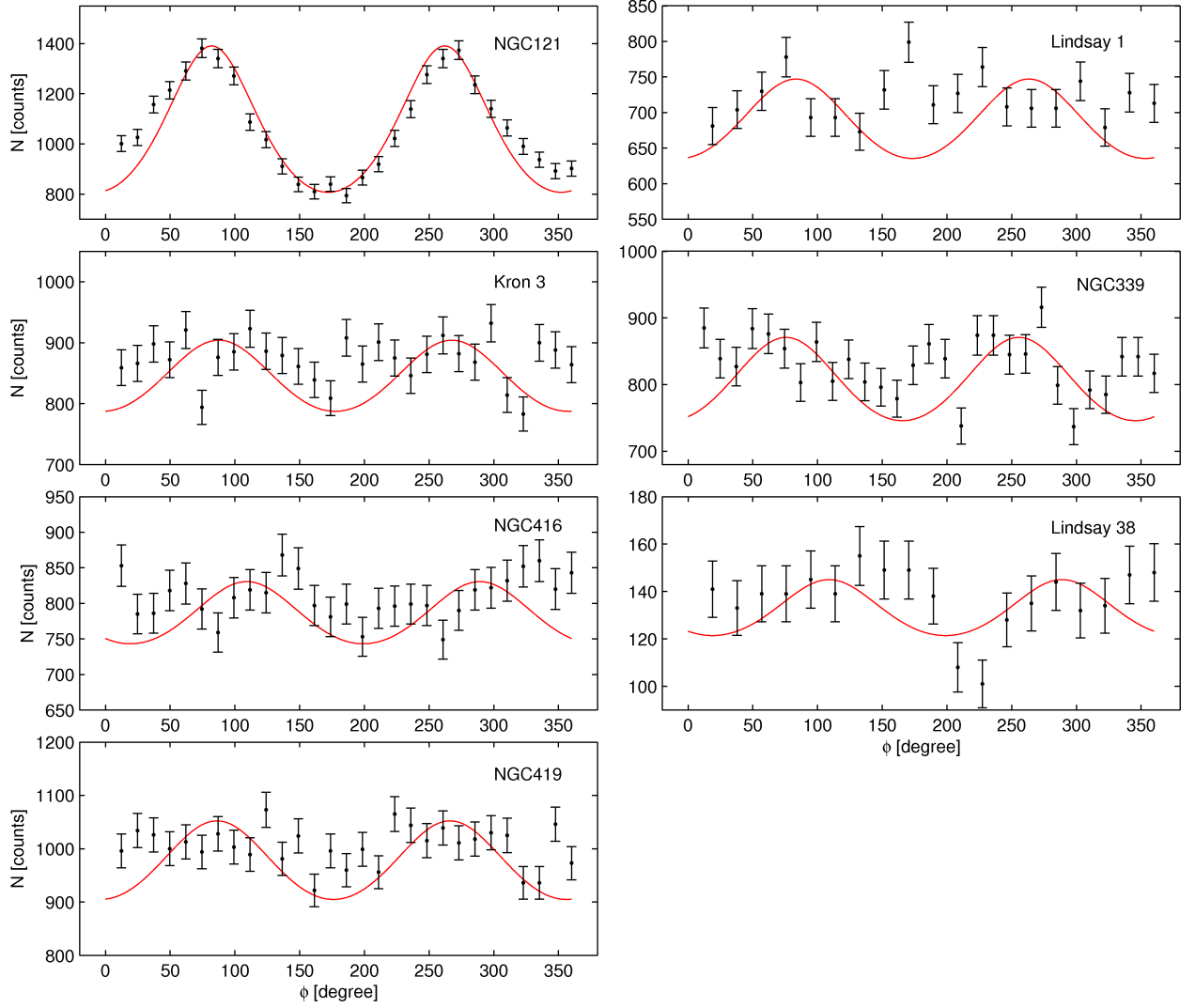


FIGURE 5.10. The angular distribution of member stars that lie entirely on the ACS images around the determined center of gravity. The solid red curves are the best fits of Eq.(3) of the text, indicating the ellipticity of the clusters.

Reference	NGC 121	Lindsay 1	Kron 3	NGC 339	NGC 416	Lindsay 38	NGC 419
This Chapter	3.75 ± 0.39	13.81 ± 0.60	6.70 ± 0.26	8.10 ± 0.11	2.65 ± 0.07	9.30 ± 0.48	2.85 ± 0.09
Carvalho et al. (2008)	2.39 ± 0.01	-	-	7.23 ± 0.71	2.30 ± 0.01	-	2.93 ± 0.01
Hill & Zaritsky (2006)	-	-	-	8.62	3.05	-	4.04
McLaughlin & van der Marel (2005)	3.05 ± 0.10	-	6.92 ± 0.26	7.98 ± 0.45	3.13 ± 0.10	-	-
Mackey & Gilmore (2003b)	3.02 ± 0.10	-	6.07 ± 0.18	7.05 ± 0.30	2.84 ± 0.10	-	-

TABLE 5.6. **Comparison of r_c [pc] from EFF model fits to literature data.** The core radii of Mackey & Gilmore (2003b); McLaughlin & van der Marel (2005); Hill & Zaritsky (2006) have been converted to the distances found in Chapter 4.

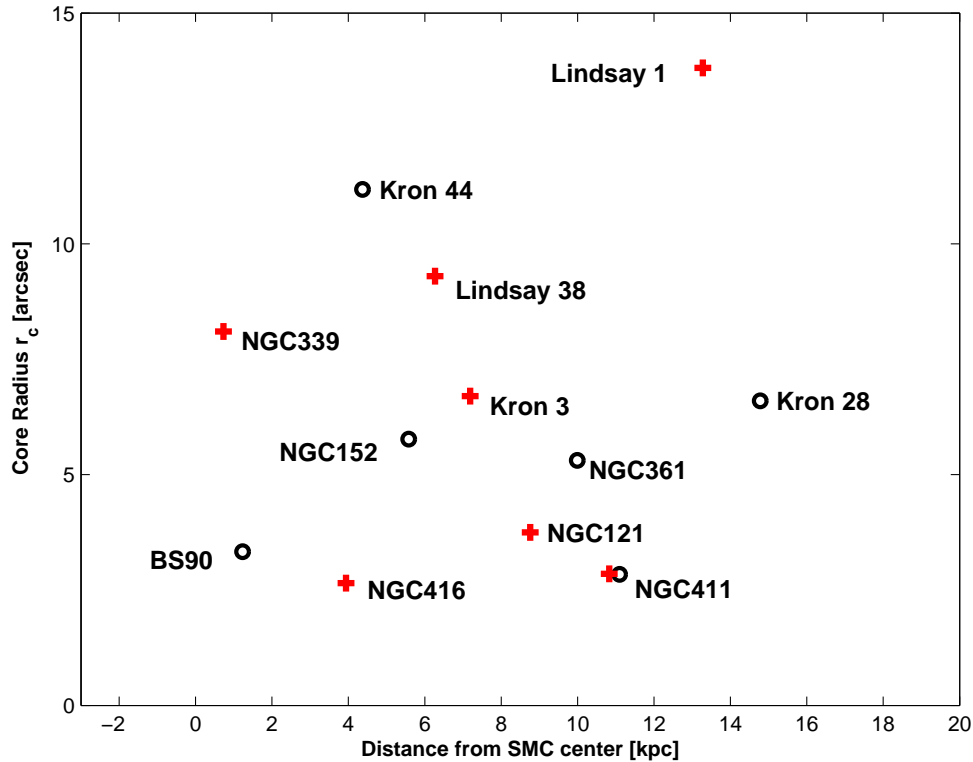


FIGURE 5.11. Core radii vs distance from the SMC center for the clusters in our sample (plus) and clusters for which reliable distances were found in the literature (circles). The distances were adopted from Chapter 4 and Crowl et al. (2001). The core radii for NGC 152, NGC 361, and NGC 411 are taken from Mackey & Gilmore (2003b), while for Kron 28 and Kron 44 the values are taken from Hill & Zaritsky (2006).

Comparing the half-light radii for NGC 121, Kron 3, and NGC 339 found estimating L_{tot} using surface-brightness data to those radii published by McLaughlin & van der Marel (2005), we find that their half-light radii of NGC 121, Kron 3, and NGC 339 are $\sim 16\%$ (5.96 pc), $\sim 27\%$ (10.54 pc), and $\sim 26\%$ (12.65 pc) smaller than those found in this study. The remaining clusters of the present sample do either not overlap or the half-light radii could not be calculated.

In the LMC, Mackey & Gilmore (2003a) found evidence for double or post-core-collapse (PCC) clusters in the surface brightness profiles among the oldest clusters, as well as in one globular cluster in the Fornax dwarf spheroidal galaxy (Mackey & Gilmore 2003c). A PCC cluster is characterized by an apparent power-law profile in its innermost region, which is different from a constant-density core as found in the EFF and King profiles. No evidence of this kind of clusters was found for SMC clusters (Mackey & Gilmore 2003b).

One additional uncertainty in the inter-comparisons of physical cluster core and tidal radii is the distance modulus. In previous studies a single distance modulus was assumed and applied to the calculations. However, the SMC may have a depth extent of up to 20 kpc (Mathewson et al. 1988; Hatzidimitriou et al. 1993; Crowl et al. 2001; Lah et al. 2005). With the exception of NGC 419, for which we used isochrone fitting, we determined the distance modulus for each cluster using the red clump magnitude (Glatt et al. 2008a). However, no correlation between core radius and distance from the SMC center was found (Fig. 5.11).

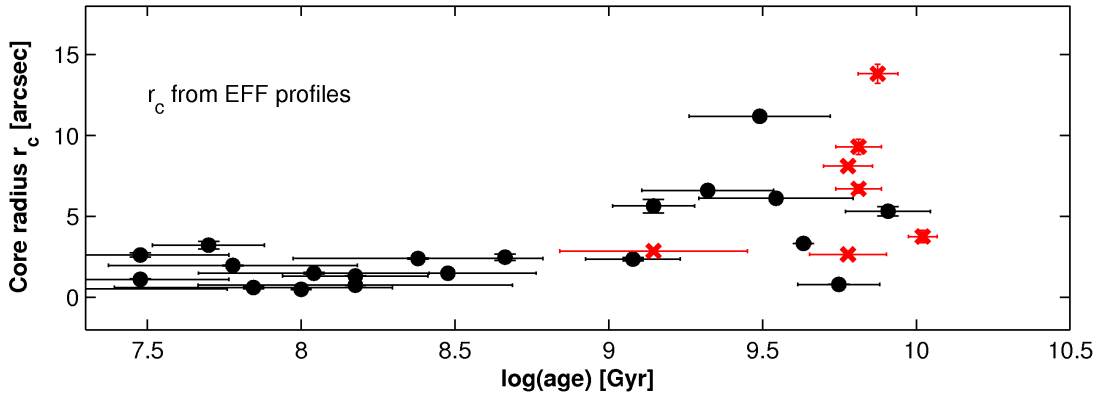


FIGURE 5.12. Age vs core radius r_c of our cluster sample (crosses) and additional sample found in the literature (circles). The adopted core radii and ages are listed in Table 5.7. Because the errors of the EFF core radii in both our and in the literature sample are very small, the errorbars are barely visible in the upper plot.

4.2. Age-radius relation

In the LMC, a trend for larger core radii with increasing age has been found (Mackey & Gilmore 2003a) and evidence for the same trend appears to be present in the SMC (Mackey & Gilmore 2003b). In their study, core radii of 10 SMC star clusters and 53 LMC clusters were determined using EFF profiles and compared to each other. The SMC clusters may have slightly larger core radii on average than the LMC clusters, but the authors claimed that this could be the result of uncertainties in both the SMC distance modulus (for all clusters a distance modulus of 18.9 was used) and the large depth extension of the SMC. The youngest SMC and LMC clusters all had compact cores, whereas older clusters showed a bifurcation with most clusters following a lower sequence and some clusters exhibiting increased core radii.

Combining our results and literature values (Tab. 5.7), we confirm the proposed relationship between cluster age and spread in core size in the SMC. In Figure 5.12 core radii from EFF profiles are shown. The trend of older clusters having a larger spread in core radii than the younger population is clearly visible. The oldest star cluster, NGC 121, has a small core radius of 3.75 ± 0.39 pc, while for the second oldest cluster, Lindsay 1, the core radius is rather large with 13.81 ± 0.60 pc. One of our intermediate-age clusters has a radius larger than 10 pc (Lindsay 1). The intermediate-age cluster Kron 44 has the largest core radius of the literature sample ($r_c = 11.18$ pc; Hill et al. 2006). Its age is 3.1 ± 0.8 Gyr (Piatto et al. 2001). Star clusters younger than 1 Gyr have core radii smaller than 4 pc. Nevertheless, only Lindsay 1 and Kron 44 have significantly larger core radii than the rest of the clusters considered here. The clusters NGC 361, NGC 152, Kron 28, Lindsay 11, Kron 3, NGC 339, and Lindsay 38 have radii between 5 and 8.5 pc, which is slightly larger on average than the core radii of the remaining 21 clusters, whose core radii are smaller than 5 pc. Figure 5.12 suggests that among the older clusters some objects seem to have experienced a significant change in r_c , while for others r_c remained almost unaltered.

For GCs, the concentration parameter c traditionally is around or even larger than 1, implying a compact isothermal central region and an extended tidally truncated outer region, while open clusters have $c < 1$, which is an indication that open clusters are more diffuse objects (e.g., Harris 1996; Binney & Merrifield 1998; Bonatto & Bica 2008). The oldest and only globular SMC cluster, NGC 121, has a concentration of $c = 1.034 \pm 0.12$. For comparison, the Galactic globular clusters 47 Tuc, NGC 288, and NGC 6909, all non-PCCs, have $c = 2.04$, $c = 0.98$, and $c = 0.76$ (Harris 1996). The youngest cluster in the present sample, NGC 419, with an age of 1.2-1.6 Gyr, has a globular cluster-like concentration parameter of $c = 1.059 \pm 0.08$. This is the case for all three profiles. In its CMD we see indications of a double or multiple main sequence turnoffs (see Chapter 4), a feature seen

<i>Cluster</i>	<i>age</i> <i>Gyr</i>	<i>r_{c,EFF}</i> <i>pc</i>	<i>References</i>
NGC 176	0.46 ± 0.01	2.48 ± 0.19	1, 14
Kron 17	0.30 ± 0.10	1.49 ± 0.01	2, 15
NGC 241 + 242	0.07 ± 0.04	0.60 ± 0.07	3, 15
NGC 290	0.03 ± 0.01	1.11 ± 0.03	4, 15
Lindsay 48	0.15 ± 0.04	1.32 ± 0.02	1, 15
Kron 34	0.24 ± 0.12	2.39 ± 0.04	3, 15
NGC 330	0.03 ± 0.01	2.61 ± 0.12	5, 14
Lindsay 56	0.006 ± 0.01	0.51 ± 0.01	4, 15
NGC 346	~ 0.003	2.01 ± 0.03	6, 6
IC 1611	0.11 ± 0.05	1.49 ± 0.06	3, 15
IC 1612	~ 0.10	0.49 ± 0.01	7, 15
Lindsay 66	0.15 ± 0.10	0.74 ± 0.01	8, 15
NGC 361	8.10 ± 1.20	5.31 ± 0.28	9, 14
Kron 47	~ 0.007	1.74 ± 0.15	7, 15
IC 1624	0.06 ± 0.03	1.97 ± 0.03	3, 15
NGC 411	1.20 ± 0.20	2.84 ± 0.11	10, 14
NGC 458	0.05 ± 0.01	3.22 ± 0.24	1, 14
Lindsay 114	5.60 ± 0.50	0.80 ± 0.02	4, 4
NGC 152	1.4 ± 0.20	5.77 ± 0.42	11, 14
Kron 28	2.1 ± 0.50	6.60	12, 15
Kron 44	3.1 ± 0.80	11.18	12, 15
Lindsay 11	3.5 ± 1	6.11	13, 15
BS90	4.3 ± 0.10	3.33	6, 15

TABLE 5.7. **Literature Sample.** The cluster ages we adopted from: (1) Hodge (1983), (2) Hodge & Flower (1987), (3) Elson & Fall (1985), (4) Ahumada et al. (2002), (5) Da Costa & Hatzidimitriou (1998), (6) Sabbi et al. (2007), (7) Chiosi et al. (2006), (8) Piatti et al. (2005b), (9) Mighell et al. (1998a), (10) Alves & Sarajedini (1999), (11) Crowl et al. (2001), (12) Piatti et al. (2001), (13) Mould et al. (1992), and the EFF core radii from: (14) Mackey & Gilmore (2003b) and (15) Carvalho et al. (2008).

also in the two LMC star clusters, NGC 1846 and NGC 1806, known to have a double main-sequence turn-off (Mackey et al. 2008, see also Mackey & Broby Nielson 2007).

Plotting mass versus core radius did not show any correlation for LMC and SMC star clusters (Mackey & Gilmore 2003a,b), and no significant difference between masses of young and old clusters was found. If only massive star clusters had large core radii one could argue that the younger low-mass clusters dispersed after a few Gyr, but at least in the LMC and SMC this does not seem to be the case. Since the age-radius correlation has been observed in the combined sample of SMC, LMC, Fornax, and Sagittarius star clusters, Mackey & Gilmore (2003c) emphasized the possibility of a universal physical process as the origin of this trend. While our results are consistent with this possibility, additional observations and theoretical studies are needed to establish if an internal process is at work.

4.3. Cluster evolution

It is intriguing that LMC and SMC clusters seem to have experienced a similar structural evolution, even though the two galaxies show strong differences in various other aspects. The SMC

contains only one old GC, NGC 121, which is 2-3 Gyr younger than the oldest GC in the LMC and MW (Chapter 3). The second oldest SMC star cluster, Lindsay 1, has an age of 7.5 ± 0.5 Gyr, and since then compact populous star clusters have formed fairly continuously until the present day (e.g., Da Costa 2002; Glatt et al. 2008a). Furthermore, the intermediate-age clusters in the SMC appear to be capable of surviving for a Hubble time, due to their high mass and the structure of the SMC (no bulge or disk to be passed; Hunter et al. 2003; Lamers et al. 2005; Gieles et al. 2007). However, the SMC has a moderately dense "bar" and we do not know how its clusters orbit in the SMC.

In contrast to the SMC, the LMC had two main epochs of cluster formation (e.g., Bertelli et al. 1992) and a well-known "age-gap" between ~ 4 -9 Gyr (e.g., Holtzman et al. 1999; Johnson et al. 1999; Harris & Zaritsky 2001), in which few (surviving) star clusters have formed. Several GCs are found with coeval ages like the Galactic GCs and GCs in other dwarf galaxies (e.g., Olszewski et al. 1991; Olsen et al. 1998; Johnson et al. 1999; Grebel & Gallagher 2004). We know only of one LMC star cluster, ESO 121-SC03, that has an age of 8.3-9.8 Gyr (Mackey et al. 2006), which defines the lower limit of the old LMC star cluster age distribution.

In the SMC, Hill & Zaritsky (2006) found the distribution of cluster core size to be broader than in the MW, which they argue is due to a prevalence of surviving low-concentration clusters in the SMC. In her analysis of the LMC star clusters, Elson (1991) noted that for clusters of a given age, there appears to exist an upper limit for its core size. Moreover, this limit was found to increase with age, which was later confirmed by the analysis of Mackey & Gilmore (2003a). Young clusters are observed to have very compact cores of e.g. ~ 2.13 pc (NGC 1711) and ~ 1.33 pc (NGC 1805), whereas the cores of older clusters can reach extents of up to 13 pc.

N-body simulations of Goodwin & Bastian (2006) illustrate how the structural parameters of star clusters change with time. A major driver of these changes is the expulsion of gas, which was not converted into stars via star formation. The minimum local star formation efficiency to leave a bound massive star cluster is $\sim 25\%$, and higher efficiencies are possible (e.g., Parmentier & Fritze 2008). But even in efficient cases, a significant amount of unused gas remains. Kroupa & Boily (2002) suggested that populous star clusters expel their unused gas explosively due to the presence of numerous O stars during their early evolutionary stages. Goodwin & Bastian (2006) also suggested a rapid gas removal caused by stellar winds and supernovae during the first 20 Myr. As a consequence the young clusters may find themselves out of virial equilibrium; the stars have too large a velocity dispersion for the new, reduced gravitational potential. In order to re-stabilize, the cluster expands on a few crossing times scales of < 10 Myr (see e.g., Sabbi et al. 2007). The most extreme core radii can be explained by external processes (e.g., for clusters that are not isolated), or by radically different stellar populations (mergers of clusters and effects from variable tidal fields, Mackey & Gilmore 2003a).

Various estimates of characteristic cluster disruption time-scales in different star cluster environments have been calculated (e.g., Gieles & Bastian 2008; Parmentier & de Grijs 2008). Many studies were based on a constant cluster formation rate (CFR) as a function of time. The poorly understood time-variable CFR of the LMC and SMC complicates such an analysis. Parmentier & de Grijs (2008) analyzed the cluster disruption time-scale in the LMC using Monte Carlo simulations. For younger clusters (age < 5 Gyr), the general behavior of the CFR is recovered. It has been increasing steadily from about 0.3 clusters Myr^{-1} 5 Gyr ago to a present rate of ~ 25 clusters Myr^{-1} . For older clusters (age > 5 Gyr), the CFR is very uncertain. It is possible that the CFR has increased steadily over a Hubble-time from ~ 1 cluster Gyr^{-1} 13 Gyr ago to its present value. For the SMC such studies have not been published, but the lack of very old SMC star clusters shows that the CFR of the LMC and SMC either varies significantly or that the CFR was rather constant but most clusters dissolved before reaching intermediate ages.

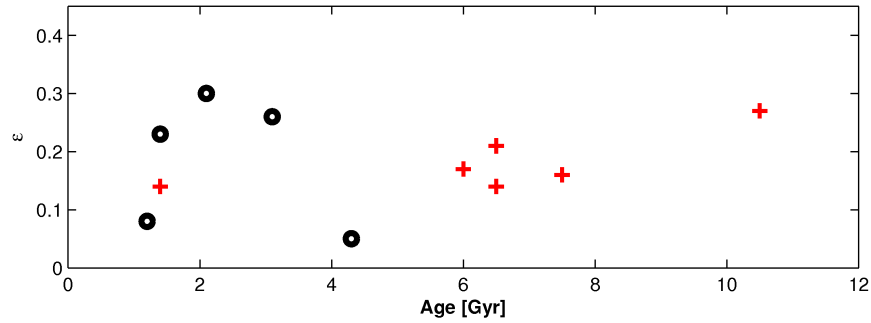


FIGURE 5.13. Age vs ellipticity showing the clusters from our sample (crosses) and five clusters from the literature (circles). The ellipticities for NGC 152, NGC 411, Kron 28, Kron 44, and BS90 are taken from Hill & Zaritsky (2006) and the ages from Alves & Sarajedini (1999); Crowl et al. (2001); Piatti et al. (2001); Sabbi et al. (2007). It seems that the younger clusters tend to be flatter than the older clusters, although NGC 121 is the oldest and the flattest cluster.

<i>Reference</i>	<i>NGC 121</i>	<i>Lindsay 1</i>	<i>Kron 3</i>	<i>NGC 339</i>	<i>NGC 416</i>	<i>Lindsay 38</i>	<i>NGC 419</i>
This Chapter	0.27 ± 0.06	0.16 ± 0.05	0.14 ± 0.05	0.17 ± 0.05	0.17 ± 0.06	0.21 ± 0.06	0.14 ± 0.05
Hill & Zaritsky (2006)				0.17	0.11		0.09
Kontizas et al. (1990)	0.28	0.10	0.10	0.23	0.13		0.23
Geyer et al. (1983)	0.30						

TABLE 5.8. **Comparison of the ellipticities.** The ellipticities by Kontizas et al. (1990) were measured at the inner-most parts.

4.4. Ellipticities

4.4.1. Comparison with previous studies

None of the clusters in our sample exhibits a significant flattening except NGC 121 and Lindsay 38, the sparsest cluster in the present sample. Because the tidal radii of our clusters lie outside the ACS images, we have to assume that the ellipticities in the clusters' interiors are the same as at the tidal radii. For Lindsay 38, no ellipticity determination was found in the literature.

Measuring ellipticities is strongly dependent on the correct determination of the cluster center. Background and foreground determination, as well as stochastic effects influence the determination of isophotes. However, as much of the SMC is not crowded and at high Galactic latitude (e.g., Ratnatunga & Bahcall 1985), the effects of field star contamination should not be severe. Another explanation for the large SMC cluster ellipticities might be the influence of the local SMC field star background, the different measuring methods as well as the differing radii at which the ellipticities were measured. Some galactic globular clusters have been found showing increasing ellipticities at larger distances from the cluster core (White & Shawl 1987). These might be the reasons for the differences between the values presented here and those found by Kontizas et al. (1990) and Hill & Zaritsky (2006). We have to emphasize that the determination of the ellipticity is quite uncertain, especially when it is fairly small as it is for most of the present clusters. The results between the different studies are in good agreement (Table 5.8).

4.4.2. Astrophysical Implications

The flattening distribution of star clusters in the SMC, LMC and the MW are known to be very different (e.g., Kontizas et al. 1989; Han & Ryden 1994; Goodwin 1997). SMC star clusters in their outer regions are typically much more flattened than those of the MW and even flatter than those in the LMC (Kontizas et al. 1990). In Figure 5.13 we show the relation of ellipticity versus age. No evident correlation can be seen. Unfortunately, not enough reliable distances have been measured to make an accurate statement about possible dependence on galactocentric radius in the LMC and the SMC for a large sample of clusters. We extend our sample by adding five populous star clusters for which reliable distances, ages, and ellipticities have been determined elsewhere in the literature (see Table 5.5 for References). The younger clusters (age $\lesssim 5$ Gyr) seem to be flatter (larger ϵ) than the older objects. In the MW, the flatter GCs are located close to the Galactic center, while for SMC such a correlation is not visible. Clusters lying behind the SMC center seem to be flatter than the ones lying in front. But we have to emphasize that the shown sample is very small and highly incomplete.

Like the SMC, the LMC does not show a relation between age and ellipticity, while clusters of all ages are significantly more elliptical than the Galactic GCs (Goodwin 1997). The Galactic GCs appear to modify their original structure and become less flattened at higher age. Han & Ryden (1994) argue that the difference between GC ellipticities in the LMC and the Milky Way are caused by the morphologies of the parent galaxies. They further showed that the GCs also vary in their shapes: LMC and SMC clusters are well-represented by triaxial spheroids, while Galactic GCs are oblate spheroids. Young LMC clusters appear to be highly flattened. Did the original structure of the older Galactic population get modified during their lifetime, and if yes, why did the old LMC and SMC cluster population remained unchanged? This may be explained with the different dynamical influence and therefore the varying strength of the tidal field of the parent galaxy (van den Bergh 2008). A strong tidal field will make the Galactic GCs more spherical during their orbits around the galaxy. The LMC and SMC have a totally different structure and no bulge or disk has to be passed (Hunter et al. 2003; Lamers et al. 2005; Gieles et al. 2007). The tidal field of the LMC and the SMC might not be strong enough to modify the shape of their clusters significantly, which might be the reason for their flat shapes. This point merits further exploration, e.g. via massive star cluster shape studies in nearby starburst and normal galaxies.

5. Summary

We derive structural parameters for seven SMC star clusters NGC 121, Lindsay 1, Kron 3, NGC 339, NGC 416, Lindsay 38, and NGC 419 based on stellar number density and surface brightness profiles and HST/ACS stellar photometry. We used King and EFF models to determine core radii, half-light radii, tidal radii, concentration parameters, and ellipticities of the star clusters. Half-light radii could only be estimated because the tidal radii lie outside the field of view of the ACS images.

Although our sample of SMC clusters is highly incomplete even after adding literature values, we confirm the result of Mackey & Gilmore (2003b) who found an increased scatter in core radii for older clusters (age > 1 Gyr) in dwarf galaxies. In the LMC this trend is more apparent (Mackey & Gilmore 2003a), perhaps a result of the LMC containing a much larger number of star clusters than the SMC.

We find intermediate age star clusters in the SMC to have larger half light radii and smaller concentration parameters than typical Galactic globular star clusters of similar mass (e.g., Djorgovski & Meylan 1994). Indeed some of the clusters in this study could be classified as “faint fuzzies” based on their sizes and luminosities (Sharina et al. 2005). Thus these SMC clusters add to the trend for low density galaxies to contain older survivor star clusters with relatively high masses with a wide range of central densities extending from the dense globular cluster regime to quite low values. We also note a potential bias in that low central density star clusters also may be easier to find and study in less dense galaxies.

The cluster formation history of the LMC also appears to be quite different from that of the SMC. The similar cluster structural patterns in the two galaxies is therefore intriguing. In the MW, many of the oldest clusters experienced modifications of their original structure during their lifetimes, and many of the oldest halo clusters have developed cores, probably due to internal processes. One possible additional reason for the differences in the evolution of cluster structures between MW and SMC might be the morphology of the host galaxies. Low central concentration clusters can more easily survive in the SMC and LMC, while in the MW clusters have to pass the Galactic disk or bulge while orbiting the Galaxy. The lack of correlation between core radius and distance from the SMC center and the low density of the SMC both suggests that the cluster structures are little disturbed by external effects and primarily are driven by internal dynamical evolution (e.g., McLaughlin & van der Marel 2005).

Our data also show that the inner regions of intermediate-age clusters in this sample have rather spherical shapes, while in their outer zones and the oldest cluster, NGC 121, have higher ellipticities. Previous studies found higher ellipticities for the intermediate-age clusters at larger radii. We find no correlation between outer ellipticity and age, or outer ellipticity and distance from the SMC center, where we can take advantage of the 3-D information on the SMC cluster distribution from Chapter 4. Consistent with our conclusion regarding structures, the shapes of SMC clusters could remain elliptical if they experience little externally driven dynamical modification during their lifetimes.

This study indicates that the properties of the rich SMC star clusters are largely determined by internal processes. These objects thus can provide powerful tests for models of the intrinsic dynamical evolution of star clusters, while also serving as evolutionary markers for the SMC. Combinations of data from the MW and its satellites will continue to illuminate the actions of the internal and external astrophysical processes which shape star clusters.

CHAPTER 6

AGES OF YOUNG SMC STAR CLUSTERS

“In order to make an apple pie from scratch, you must first create the universe.”

Carl Sagan

Ages of 324 populous star clusters in the Small Magellanic Cloud have been determined fitting isochrone models of Padova and Geneva. The clusters cover an age range between 10 Myr and 1 Gyr. A constant distance modulus of $(m-M) = 18.90$, a metallicity of $Z = 0.004$, and a variable color excess were used to derive the cluster ages. Two peaks of enhanced cluster formation were found around 160 Myr and 630 Myr of which the first one might have been triggered by a close encounter between the SMC and the LMC. The youngest clusters reside in the super giant shells, giant shells, and the inter-shell region, and toward regions with a high $H\alpha$ content, suggesting that their formation is related to expansion and shell-shell interaction. No evidence for cluster dissolution was found. Computed V band luminosities show a trend for fainter magnitudes with increasing age as well as a trend for brighter magnitudes with increasing radii.

*This study was conducted together with Eva K. Grebel and Andreas Koch.
It will be submitted to Astronomy & Astrophysics, 2009*

1. INTRODUCTION

Due to its proximity the Small Magellanic Cloud (SMC) offers an excellent opportunity to study spatially resolved star formation (SF) histories of galaxies. SF can be triggered by several mechanisms such as e.g. the self-induced gravitational collapse of a molecular cloud, tidal shocking, a turbulent interstellar medium, or cloud-cloud collisions (e.g., McKee & Ostriker 2007). The SMC has been part of a triple system together with the Large Magellanic Cloud (LMC) and the Milky Way (MW) since at least 1 Gyr (e.g., Bekki & Chiba 2005, Kallivayalil et al. 2006a/b). The formation of star clusters younger than $\lesssim 1$ Gyr in the Magellanic Clouds (MCs) were probably triggered by interactions of the galaxies with each other and the MW (e.g., Yoshizawa & Noguchi 2003). Star clusters may be produced through strong shock compressions induced by close encounters of their host galaxies, which causes enhanced star formation. In these models, the star formation rate increases, if a neighboring galaxy's orbit leads to a close encounter with the LMC. Conversely, the star formation rate decreases again once the galaxy recedes from the LMC's proximity, thereby leading to episodic cluster formation. In the MCs, a correlation between young star clusters and putative close encounters with each other and MW have been found by e.g. Girardi et al. (1995, G95), Pietrzynski & Udalski (2000, PU99), Chiosi et al. (2006, C06). Possible orbits of the SMC, LMC, and MW have been modeled by several authors (e.g., Bekki & Chiba 2005, Kallivayalil et al. 2006a,b). They found that it was difficult to keep the Clouds bound to each other for more than 1 Gyr in the past. It is possible that the Clouds are not a bound system and that they are making their first passage close to the MW. Strong tidal perturbations could also have triggered the formation of clusters (e.g., Whitmore 1999) in the SMC.

However, the cluster formation histories of the LMC and SMC show large differences. In the LMC, two main epochs of cluster formation (e.g., Bertelli et al. 1992) have been observed that are separated by an "age gap" of about ~ 4 -9 Gyr (e.g., Holtzman et al. 1999; Johnson et al. 1999; Harris & Zaritsky 2001), in which no star clusters have formed. In the LMC a few globular clusters are found that are similarly old as the oldest Galactic globulars (Olsen et al. 1998). Since the gap, star clusters formed continuously until the present day. The star clusters in the SMC cover a wide range of ages and were formed continuously over at least the last ~ 10.5 Gyr (e.g., Glatt et al. 2008a,b; Parisi et al. 2008) to the present day. Interestingly, the SMC appears to have a "delayed" cluster formation history and formed its first and only globular cluster, NGC 121, 2-3 Gyr later than the LMC or the MW (Glatt et al. 2008a, and references therein). In the SMC about ~ 770 star clusters have formed (and survived) and probably more will be detected considering the small and faint clusters that were not observable to this point. Ongoing and prospective space-based observations will certainly increase the number of known star clusters.

The most recent catalog cross-correlating all known objects from the SMC, LMC, and the Magellanic Bridge region was published by Bica et al. (2008a) (B08). However, the cluster sample still is highly incomplete as pointed out by the authors. Only for a few clusters in B08's catalog, ages have been determined. For young SMC clusters, Pietrzynski & Udalski (1999) (PU99) used isochrone fitting on data from the Optical Gravitational Lensing Experiment (OGLE II; Udalski et al. 1998a) to determine ages for 93 clusters and Rafelski & Zaritsky (2005) (RZ05) made use of integrated colors and derived ages for 200 clusters. C06 determined ages of 164 associations and 311 star clusters based on data from the OGLE using isochrone fitting. Their sample is the largest available catalog containing SMC cluster ages.

Luminosities have been published for 204 SMC star clusters by RZ05 measuring integrated colors from the Magellanic Clouds Photometric Survey (MCPS).

In the present study we increase the number of age-dated young SMC star clusters and calculate V-band luminosities. We aim at improving the understanding of the cluster age distribution of this irregular galaxy and present a spatial distribution map of its star clusters. To achieve this goal, we make use of ground-based data of the Magellanic Clouds Photometric Survey (MCPSs) (Zaritsky et al. 2002). In the next Section the observations and data reduction are described. In § 3 the distances, reddenings, and metallicities of both the SMC and the LMC are given. In § 4 the clusters'

age distribution, spatial distribution, and dissolution effects are discussed and in § 5 the correlation between the cluster luminosities and age/radius is derived.

2. LITERATURE DATA

We made use of two catalogs to obtain color-magnitude diagrams (CMDs) of young SMC star clusters (age <1 Gyr). The first catalog was published by B08 (see also Bica & Schmitt 1995; Bica & Dutra 2000) and includes cluster positions, angular sizes, and object classes of 17,815 objects in the LMC, SMC, and Magellanic Bridge. This catalog combines and cross-identifies objects measured on the ESO/SERC R and J Sky Survey Schmidt films and other catalogs (e.g., Pietrzynski & Udalski 1999).

The second catalog is the MCPS presented by Zaritsky et al. (2002) containing U, B, V, and I photometry of the central 18 deg² area of the SMC (5,156,057 stars). The data was obtained using the Las Campanas Swope telescope (1 m) in Chile. The V frame was used as reference because most stars are expected in this band, and only stars that have a match in the B frame were retained for the final catalog. The limiting magnitude of the photometry is V~24 mag. The photometry is highly incomplete below U = 21.5 mag, B = 23.5 mag, V = 23 mag, and I = 22 mag. This means it is difficult to derive ages of star clusters older than ~1 Gyr due to the limited photometric depth of the MCPS, which does not resolve main-sequence turnoff-points (MSTOs) of older clusters.

Each object in B08's catalog is categorized by an object class. Obvious star clusters are indicated by a 'C' and emissionless associations by an 'A'. 'CA' and 'AC' indicate intermediate classes for which a classification was not clear. 'NC' refers to small HII regions with embedded star clusters, while 'CN' are clusters that show traces of emission. 'DCN' refers to clusters that are decoupled from nebulae. For our study, only objects including a 'C'-classifications were used (in total 765 objects), because these objects are not too extended so that cluster stars could be separated from the surrounding field. Supernovae remnants ('N'), HII regions with embedded associations ('NA'), and associations with traces of emissions ('AN') were discarded, because the SMC field was too dominant in the CMDs and the cluster member stars could not be reliably separated. For the same reason, star clusters having very small radii or are very sparse could not be age-dated (see § 4.1). Our resulting catalog contains ages of star clusters between ~10 Myr and 1 Gyr. Clusters whose appearance in the CMDs indicated an age older than 1 Gyr were discarded from the sample, because the MSTOs were not resolved. For many intermediate-age and old SMC clusters accurate ages have been determined elsewhere in the literature mostly based on HST data (e.g., Mighell et al. 1998a; Olsen et al. 1998; Rich et al. 2000; Piatti et al. 2001; Glatt et al. 2008a,b).

3. METALLICITY, DISTANCE MODULUS, DEPTH EXTENT

Latest spectroscopical measurements of SMC star clusters by Parisi et al. (2008) showed that the young clusters with ages between ~ 0.9 and 2 Gyr have a spread in metallicity of 0.53 dex. The two youngest clusters in their sample, Lindsay 106 and Lindsay 108, both with ages around 0.9 Gyr, have mean metallicities of [Fe/H]=-0.88 and -1.05, respectively. Studies based on spectroscopy of six supergiants in the young population cluster NGC 330 (age~20-25 Myr) rendered a metallicity of [Fe/H] = -0.69 ± 0.11 dex (Hill & Zaritsky 2006). Venn (1999) analyzed 10 A-type supergiants in the SMC and derived a present-day metallicity of [Fe/H] = -0.70 ± 0.07 dex. This metallicity corresponds to an isochrone models of Z = 0.004, which we used for the age determination.

A distance modulus of (m-M) = 18.90 mag (e.g., Storm et al. 2004) was assumed for the SMC.

There are no direct determinations of the cluster distances along the line of sight, but it is assumed that the SMC has a depth extent of up to 20 kpc (Mathewson et al. 1988; Hatzidimitriou et al. 1993; Crowl et al. 2001; Lah et al. 2005; Glatt et al. 2008b). The clusters analyzed in this study lie in the center region of the SMC main body and the large depth extent should be negligible. Chiosi et al.

ID	E_{B-V} mag	R arcmin	log(age) yr	σ_t	Ra J2000.0	Dec J2000.0	V mag	<i>Cross - ID</i>
SMC0017	0.02	0.25	9.00	2	0.4753	-73.0136	16.95 ± 0.14	BS2
SMC0018	0.01	0.60	8.70	1	0.5000	-73.3792	14.10 ± 0.13	K9, L13
SMC0023	0.01	0.60	9.10	3	0.5447	-72.5814	14.77 ± 0.15	L14
SMC0026	0.03	1.50	8.85	3	0.5489	-73.1161	12.51 ± 0.12	NGC 152, K10, L15, ESO028SC24

TABLE 6.1. SMC cluster catalog including determined ages and V-band luminosities (full Table see Appendix B).

(2006) found a variation in the distance modulus of ~ 0.14 mag assuming an elongation of 4 kpc. The resulting error in log(age) is less than 0.05.

4. CLUSTER AGE DISTRIBUTION

The cluster age distribution of the SMC was obtained by first matching the clusters' central positions adopted from B08 with the MCPS (Zaritsky et al. 2002). Stars within a radius of 10 arcmin around these positions were selected in the MCPS to assure that all cluster stars and surroundings were included. From the apparent major and minor axis in B08 we computed the mean apparent diameter $D_{app} = (a + b)/2$ for each object. All stars within these radii are considered cluster members. Four CMDs were then plotted for each object. Two V vs B-V CMDs and two V vs V-I CMDs showing the cluster and the surrounding field within an annulus between 1 and 2 arcmin around the cluster centers (for examples see Figures 6.1 and 6.2).

4.1. Method

We fitted the CMDs with two different isochrone models: Padova isochrones (Girardi et al. 1995) and Geneva isochrones (Lejeune & Schaerer 2001). Both the Padova and the Geneva isochrone grids have an age resolution of $\log(t)=0.05$. The Dartmouth isochrone models have a youngest age of 250 Gyr (Dotter et al. 2007), which is too old for many of the star clusters in our sample. Therefore, we did not use this model. To fit the isochrones, a constant distance modulus and metallicity were used. The best-fit isochrone was then found by using different combinations of reddening and age. The age and reddening of each cluster are derived by visual inspection. The Geneva isochrone models deviate from the Padova isochrones for ages younger than $\log(\text{age})=6.9$ by about $\log(\text{age})=-0.1$ yr. In our catalog, we give the ages derived with the Padova isochrones.

Many star clusters in the present sample are located in the main body of the SMC, which is highly crowded. Therefore, field star contamination is a severe effect and hinders the age determination. To estimate the location of the SMC field in each CMD in which the ages were determined, concentric annuli with a width of 0.1 arcmin around the cluster center were constructed 0.5 arcmin outside the cluster radii (adopted by B08). The selected stars lying within these annuli were plotted on top of the cluster CMDs to illustrate the location of the SMC field stars. The accuracy of the determined ages depends on the number of cluster member stars and the density of the surrounding field. Many star clusters in the sample could not be age-dated, because they are too sparse or they have very small radii, which include too small a number of stars against the SMC field background for a reliable isochrone fit. In the densest SMC regions, the cluster membership determination on the basis of photometric information is most difficult, and therefore the derived ages are severely uncertain.

In Figures 6.1 and 6.2 two examples are displayed. For NGC 376 we derive an age of ~ 32 Myr and $E_{B-V} = 0.08$. H86-23 is an older object for which we determine an age of ~ 800 Myr and $E_{B-V} = 0.02$. In the respective upper panels, stars that were selected within the cluster radii adopted

from B08 are displayed. The magenta dots represent the field stars within a concentric 0.1 arcmin wide annulus located 0.5 arcmin outside the cluster. The blue solid line shows the best-fitting Geneva (Lejeune & Schaerer 2001) isochrone. The red solid line is the best-fitting Padova (Girardi et al. 1995) isochrone. In the lower panels, SMC field stars selected within an annulus between 1 and 2 arcmin around the cluster centers are shown.

Young cluster ages derived from isochrone fitting are not severely affected by the discreteness of isochrones due to the logarithmic age-steps of the applied isochrone models, which produce a denser grid for small ages. The interstellar extinction, however, can have a severe impact on the determination of the cluster ages. We compared the reddenings found by isochrone fitting to the reddenings adopted from PU99. The standard deviation is of the order of $\sigma_{E_{(B-V)}}=0.03$. In § 3, the uncertainty in the present-day metallicity of the SMC is mentioned. Consequently, for some clusters, the applied isochrone metallicity of $Z=0.004$ might not be the best choice. However, the attempt to fit the clusters with a different metallicity (e.g., $Z=0.008$) provided fits of less quality (age difference of $\sim\log(\text{age})=0.2$). Therefore, the uncertainties of the age determinations are partly a function of interstellar extinction, partly a function of the age itself in the sense that older clusters are more difficult to identify, and partly a function of the cluster density.

An uncertainty that cannot be handled with our data occurs when the clusters are all inside large groups of clusters having small separations along the line of sight or when they are very sparse. Sparse objects usually do not have a well-defined main sequence turn-off. On the other hand, supergiants with their short lifetimes (typically ~ 20 Myr) are well-suited as age tracers if they show a concentration toward the cluster center. We therefore require that our "best" isochrones reproduce the location to the supergiants in the CMDs and use that as a primary criterion for age determinations. The reddenings, on the other hand, are based on the perceived locus of the main sequence. The determination of a certain membership of cluster stars is a very difficult matter (based on only photometric information) and further investigation with e.g., the Hubble Space Telescope or studies based on spectroscopy are necessary. A clear separation between clusters and their surroundings becomes particularly difficult when they are embedded in associations of a very similar age.

For the SMC, ages of 324 clusters have been determined. The full table is shown in Appendix B, but an illustrative excerpt is shown in Table 7. Column 1 gives the cluster identification number. The reddening parameter E_{B-V} is listed in column 2 and the apparent radii in column 3. The derived ages are shown in column 4, while column 5 gives the degree of reliability of our age measurements. Class 1 indicates having errors $\Delta\sigma_{\log(\text{age})} < 0.3$; class 2 indicates objects having errors $0.3 \leq \sigma_{\log(\text{age})} < 0.5$; class 3 indicates objects having errors $\sigma_{\log(\text{age})} \geq 0.5$ as already used by C06. Columns 6 and 7 give the right ascension and the declination, respectively. The calculated V band magnitudes (see § 5) are listed in columns 8 and finally, the cross-identifications are listed in column 9.

4.2. Comparison of our age determination with previous studies

C06 used data from OGLE (Udalski et al. 1998a) for the SMC disk and data obtained at the ESO 2.2 m telescope for the region around NGC 269 that is located at the border of the supershell 37 A to derive ages of 461 SMC clusters and associations. The ages were derived fitting Padova isochrones (Girardi et al. 2002). A distance modulus of $(m-M) = 18.9$ was assumed and the reddening derived by main-sequence fitting. A mean SMC metallicity of $Z = 0.008$ was assumed (in our work we used $Z = 0.004$) as found spectroscopically for young objects by Pagel & Tautvaišienė (1999). An upper age limit was set by the limiting magnitude of the used photometry indicating that clusters which have an MSTO fainter than $V=20$ mag in the OGLE field could not be age-dated. For homogeneity reasons, the study was restricted to clusters younger than 1 Gyr. C06 derived ages within an age range of 4 Myr and 1 Gyr for clusters covering an area of 2.4 deg^2 of the SMC main body. 136 clusters are also included in our study.

In the first panel of Fig. 6.3 cluster ages determined in our work are compared to ages presented by C06. The ages derived in our work tend to be $\sim 0.2-0.3$ in $\log(\text{age})$ older than the ages by C06. The main reason for the difference is the different metallicity of the applied isochrone models as tested for

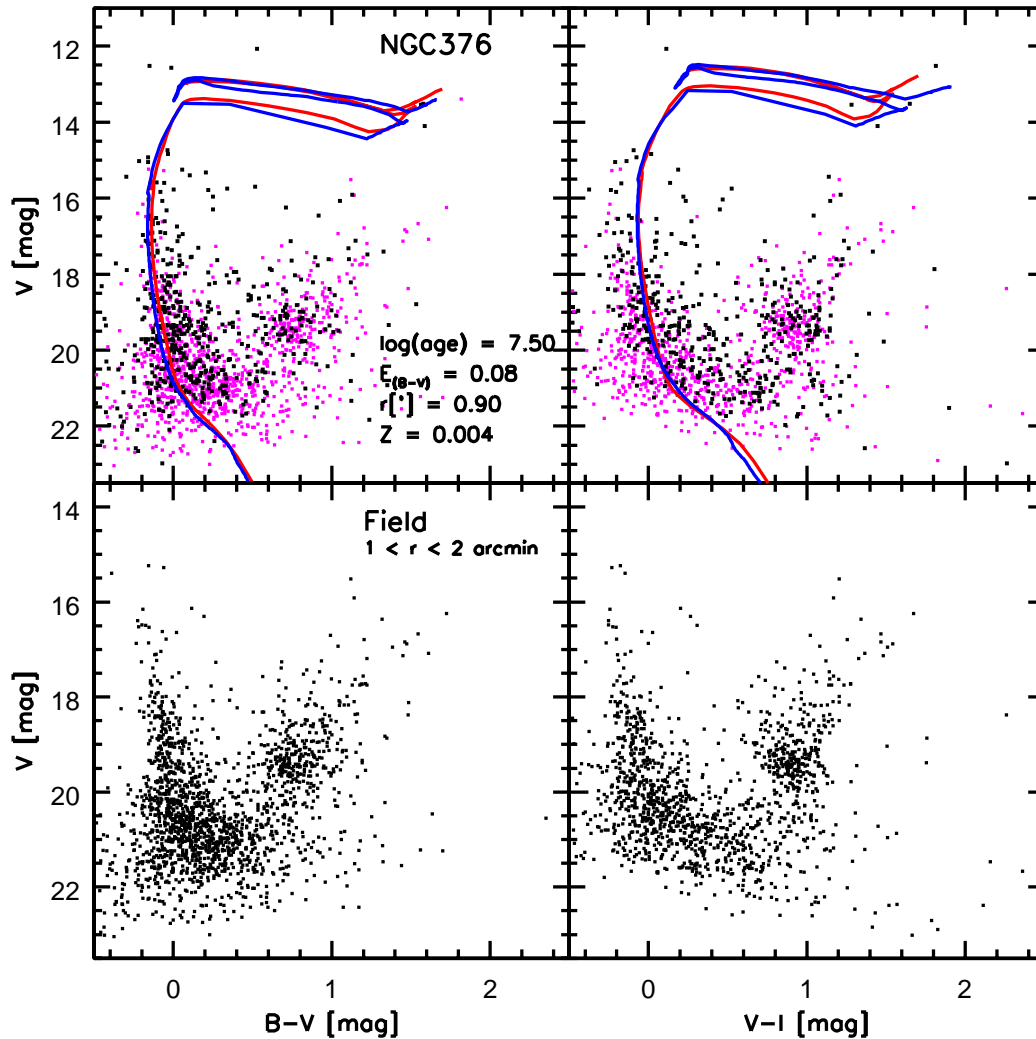


FIGURE 6.1. Color-magnitude diagrams of NGC 376. In the upper panel, V vs $B-V$ and V vs $V-I$ CMDs including stars within a radius of 0.90 arcmin (B08) are shown, and in the lower panel field stars within a concentric annulus between 1 and 2 arcmin are displayed. The blue solid line shows the best-fitting Geneva (Lejeune & Schaerer 2001) isochrone. The red solid line is the best-fitting Padova (Girardi et al. 1995) isochrone. The magenta dots were selected in a 0.10 arcmin concentric annulus that is located 0.50 arcmin away from the cluster center. They indicate the location of the SMC field.

a selection of CMDs. For those clusters with the most significant age deviation large age uncertainties are stated both in their and our work (e.g. BS271, BS272, B114). The dispersion about the 1:1 unity (red solid line) for the sample is $\sigma_{\log(\text{age})} = 0.15$.

RZ05 derived ages of 204 SMC star clusters using integrated colors, of which 112 are included in our sample. The second panel of Fig. 6.3 shows the comparison between our ages and ages adopted by RZ05. The largest deviations are found at the upper and the ends of the upper and the lower age limits. A few clusters having ages younger than 25 Myr and older than 1 Gyr show an age deviation of up to 1 Gyr. Stochastic effects on the number of bright stars, uncertainties on the metallicity, dubious cluster membership, and on the adopted stellar models may contribute to the large uncertainties in the

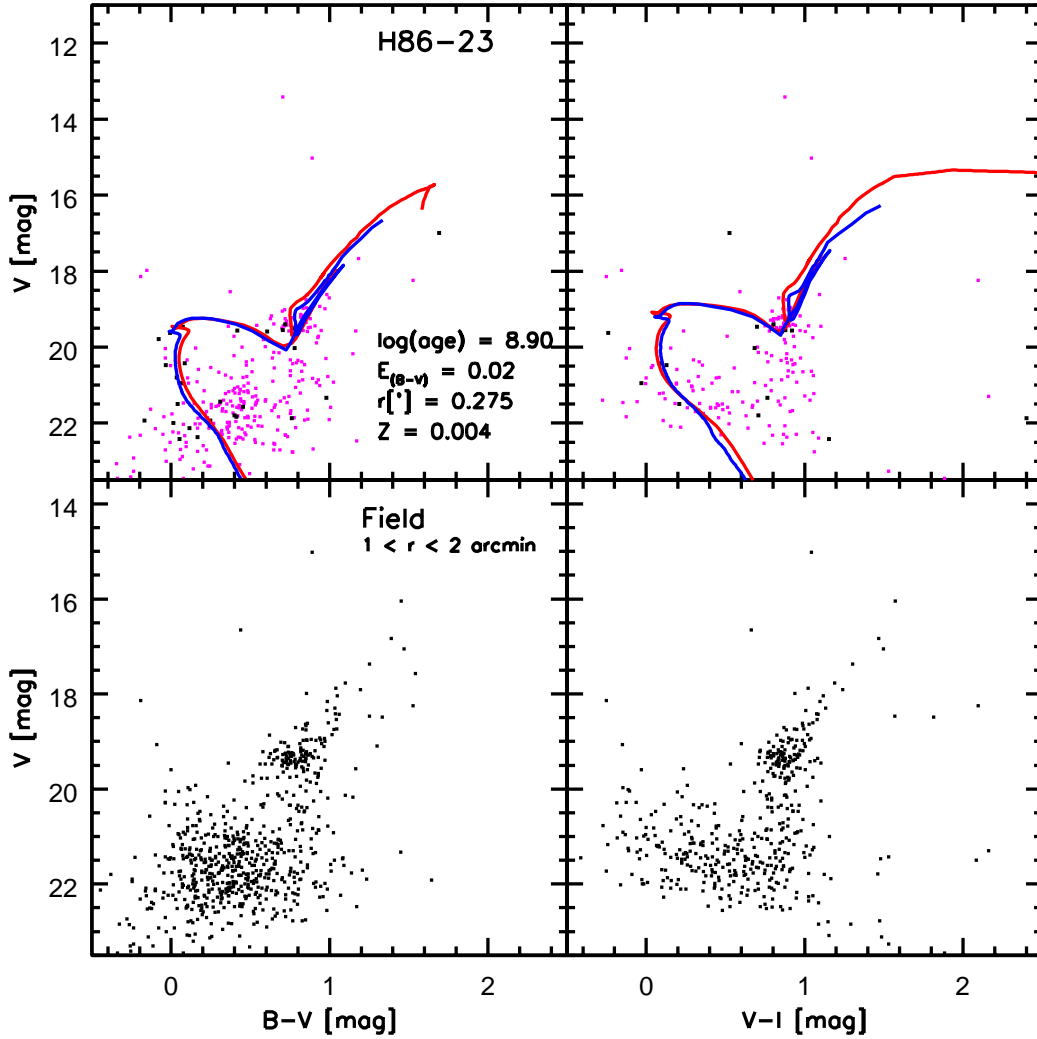


FIGURE 6.2. Color-magnitude diagrams of H86-23. In the upper panel, V vs B-V and V vs V-I CMDs including stars within a radius of 0.275 arcmin (B08) are shown, and in the lower panel field stars within a concentric annulus between 1 and 2 arcmin are displayed. The blue solid line shows the best-fitting Geneva (Lejeune & Schaerer 2001) isochrone. The red solid line is the best-fitting Padova (Girardi et al. 1995) isochrone. The magenta dots were selected in a 0.10 arcmin concentric annulus that is located 0.50 arcmin away from the cluster center. They indicate the location of the SMC field.

conclusion of the cluster age, even though the color of a stellar population usually provides a reliable chronometer to age-date star clusters. RZ05 used a metallicity of $Z = 0.004$. Those clusters with the largest age differences are mostly very sparse objects or objects to which very young isochrones were fitted based on only 2-3 bright stars. Large uncertainties for the oldest clusters are caused by large field contamination and unresolved main-sequence turnoff points. The dispersion about the 1:1 unity (red solid line) for the sample is $\sigma_{\log(\text{age})} = 0.3$.

PU99 determined ages for 93 SMC star clusters from the OGLE catalog (Pietrzynski et al. 1998), of which 51 are included in our sample. They fitted isochrones from the library of Bertelli et al. (1994) applying a distance modulus of $(m - M)_0 = 18.65$ (Udalski 1998b) and a metallicity of $Z = 0.004$. In

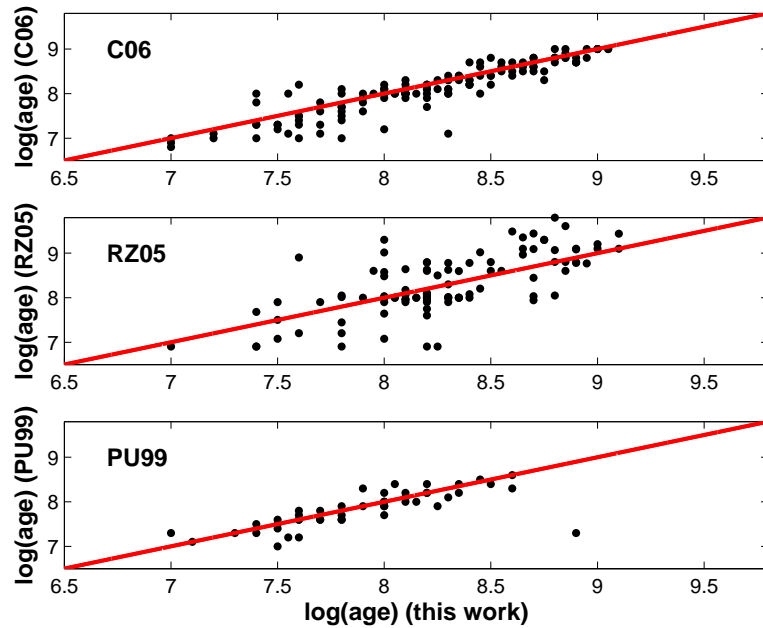


FIGURE 6.3. Cluster ages derived in this work are compared with the ages by C06 (upper panel), RZ05 (middle panel), and PU99 (lower panel) for the clusters in common. The solid line shows the loci of the 1:1 agreement.

their study, they derived ages within an age range of 10 Myr and 1 Gyr. In the third panel of Fig. 6.3 we compare ages presented by PU99 to our study. The ages are in very good agreement and the dispersion about the 1:1 unity (red solid line) is $\sigma_{\log(\text{age})}=0.17$.

4.3. Age Distribution

Uncertainties aside, the age distribution of star clusters is influenced by two effects (Boutloukos & Lamers 2003). The first is fading that occurs through the stellar evolution when the clusters get fainter with time. Therefore, the number of observed star clusters decreases with increasing age for a given magnitude limit since sparse, faint clusters become increasingly harder to detect. This effect is dominant for old objects. Cluster disruption due to the galactic tidal field is the second effect and is relevant for younger clusters.

The cluster age distribution of the SMC is shown in using ages Fig. 6.4 displaying only cluster ages determined in our study (upper panel), by C06 (middle panel), and the combination of this sample with C06 (lower panel). For the clusters common in both samples ages derived in this study were used. Because we age-dated only objects that included a 'C' in the B08 classification, our sample contains only a few objects younger than ~ 20 Myr, which are usually classified as associations or nebulae and were excluded from our sample.

The age distribution of the SMC star clusters derived in our study shows a first peak of enhanced cluster formation around 160 Myr and a second one at around 630 Myr. Only clusters with an age uncertainty smaller than 3 were used. C06 found two main episodes of enhanced cluster formation between 5-15 Myr and at 90 Myr. Their cluster sample contains ages for 164 associations, which is the reason why their sample reaches down to ages of ~ 3.2 Myr. In the combined sample three episodes of enhanced cluster formation are detectable, the youngest around 6.5 Myr, the middle around 160 Myr, and the oldest around 630 Myr. The analysis in the age range of the oldest peak is limited through the depth of the photometry, while the youngest peak mostly comes from the associations adopted from C06. The difference between the second peak found in our study and by C06 are within the given

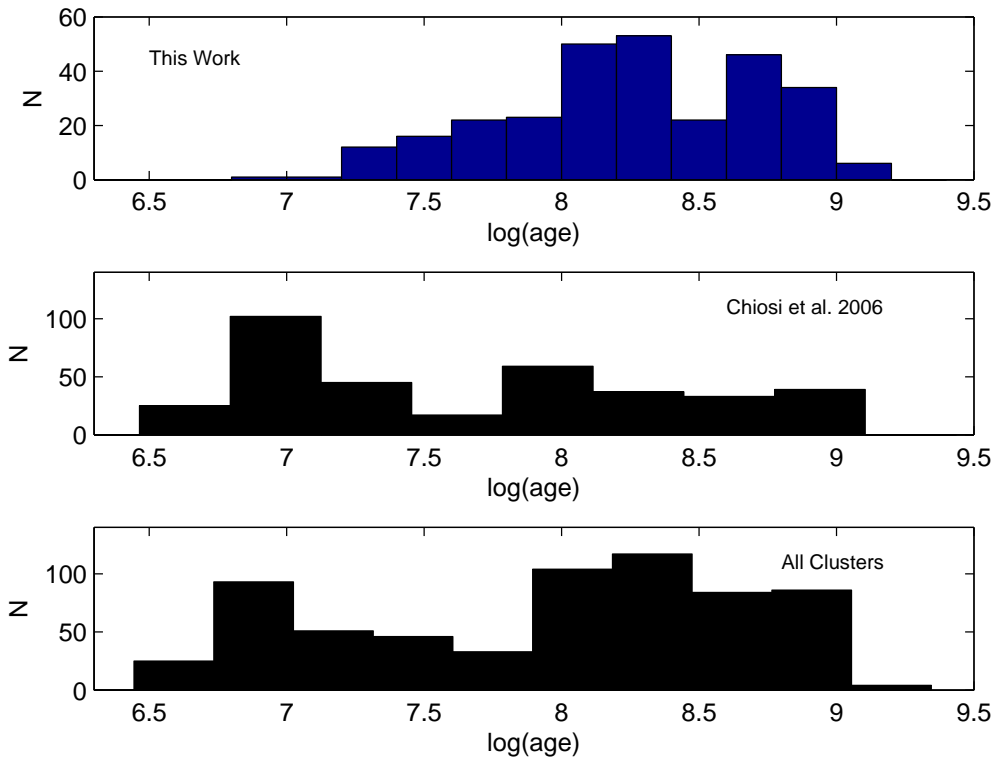


FIGURE 6.4. Cluster age distributions of the SMC. The age distribution derived in this study (upper panel), by C06 (middle panel), and the combined samples (lower panel) of this study and C06 are shown (in total 821 clusters). Only the most reliable ages were considered for this plot (classes 1 and 2 in Table 7 and Appendix B).

uncertainties for the cluster ages ($\sigma_{\log(\text{age})}=0.3$). The first maximum can only be seen in the sample by C06 due to their larger age range.

We find evidence for periods of enhanced cluster formation, which appear to have occurred during the same periods. The peaks at ~ 125 and 160 Myr, respectively, are very pronounced and are most probably correlated with similar peaks found in the cluster formation history in the LMC Girardi et al. (1995); Pietrzynski & Udalski (2000). The difference between the peaks are within the given uncertainties for the cluster ages (difference in $\log(\text{age})=0.1$). Model calculations performed by e.g., Bekki & Chiba (2005) and Kallivayalil et al. (2006a,b) showed that the MW, the LMC, and the SMC have only interacted long enough to produce the Magellanic Stream. According to these models, the last close encounter with the LMC occurred about 100-200 Myr ago. The SMC star formation rate increases, if the LMC orbit leads to a close encounter with the SMC and vice versa. The star formation rate decreases again when the LMC recedes from SMC's proximity, thus leading to episodic cluster formation. The peak at ~ 125 Myr of enhanced cluster formation in the age distribution might have been triggered by a tidal interaction with the neighboring galaxy and coincides with the closest approach of the LMC to the SMC (e.g., Gardiner & Noguchi 1996; Bekki & Chiba 2005; Kallivayalil et al. 2006a,b).

The younger peak, however, might have another origin. High velocity cloud-cloud collisions are another trigger mechanism of cluster formation (Zhang et al. 2001; Bekki et al. 2004) that are particularly effective during galaxy interactions and mergers. High-speed motions may produce a high-pressure environment that in return can trigger turbulences or shocks (Elmegreen & Efremov

1997). Stellar winds and supernova explosions can also trigger the star formation through compression by turbulent motions (Larson 1993).

4.4. Spatial Age Distribution

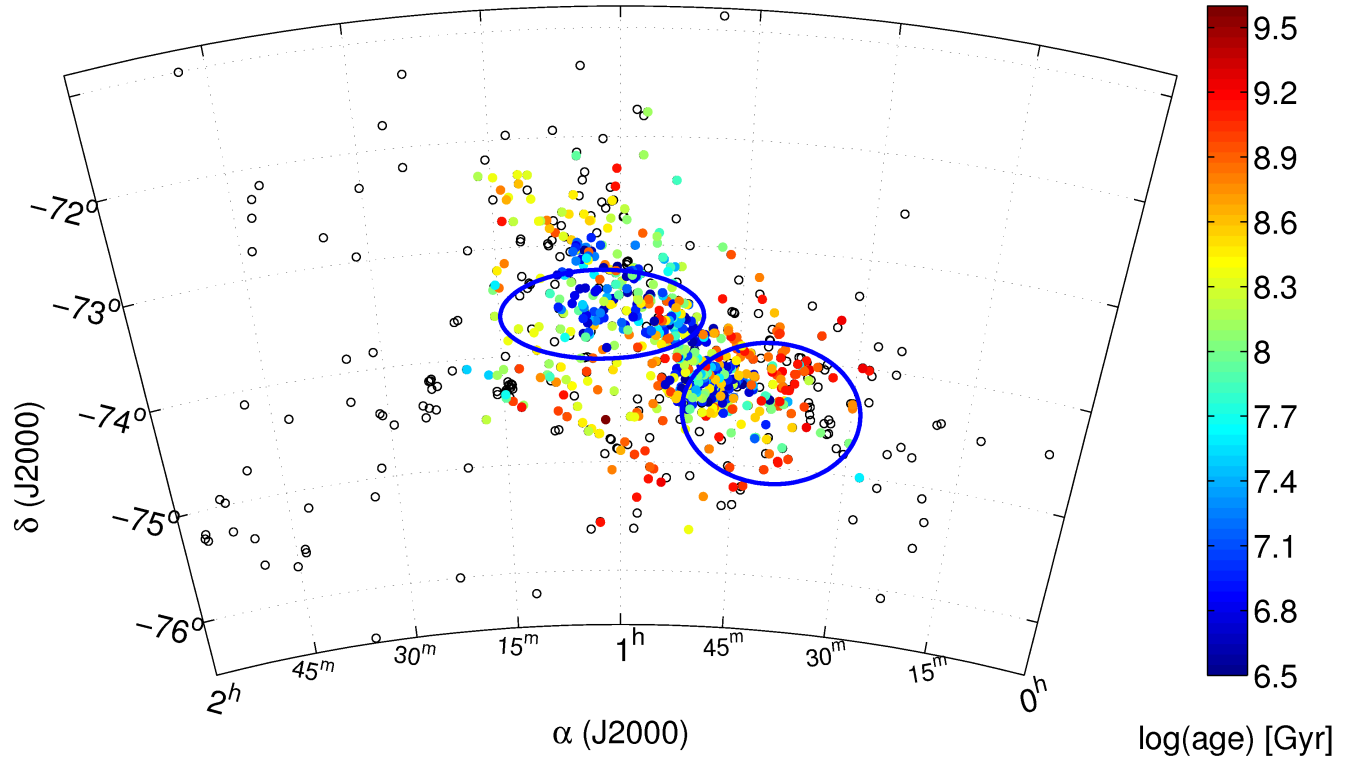


FIGURE 6.5. Spatial Distribution of the combined sample of this work and C06 of the young SMC star clusters. The two blue ellipses indicate the location of the HI super-shells 304 A (middle), and 37 A (right) (Stanimirović et al. 1999). The open circles indicate all objects from B08 including a 'C'-classification (in total 765 objects). North is up, west to the right.

The spatial distribution of the star clusters in Fig. 6.5 clearly shows that the youngest clusters are assembled in the two large HI super-shells 37 A and 304 A (Stanimirović et al. 1999). These features are explained as evolution of an OB association in which the most massive stars become supernovae and/or stellar winds lead to a runaway expansion and the formation of a supergiant shell (e.g., Bruhweiler et al. 1980; Tomisaka et al. 1981; Elmegreen & Chiang 1982). Most of the shells and super-shells are associated with young objects (McCray & Kafatos 1987). Inside the shells, second generation star clusters may form due to supernova explosions in the first generation clusters. Our (or C06) data does not cover the western side of 37 A, but most of the remaining objects are age-dated. We confirm the findings of C06 about the discontinuity in the spatial distribution of younger clusters in the super-shells 37 A and 304 A: That is, the youngest objects are found toward the eastern rim of the shell where gas and dust are located (Staveley-Smith et al. 1997; Stanimirović et al. 1999) and toward regions with a high $H\alpha$ content. $H\alpha$ indicates the presence of evolved massive stars (e.g., OB-stars, supergiants, luminous blue variable stars), supernova remnants, or diffuse ionized nebulae. The youngest objects of the shell 304 A are located toward its northern and western rim (toward 37 A) and also in the central part. The compression of gas due to shell-shell interactions related to the expansion of the shells might have triggered the cluster formation at the opposing rims as well

as in the inter-shell region. $H\alpha$ is concentrated in the northern part of 304 A where we also find the youngest objects.

In Fig. 6.6 four snapshots are shown displaying the spatial distribution of star clusters within different age ranges. In the first snapshot only clusters younger than 16 Myr are shown. The clusters are distributed along the SMC bar in an elongated but narrow area. The two supershells and the inter-shell region are clearly visible in this plot. Clusters with ages between 16 Myr and 63 Myr are also concentrated along the bar, but there are outliers found toward the SMC wing or slightly offset of the bar (second snapshot). The super-shell 304 A is highly populated by clusters of this age range. Widely spread over the entire SMC main-body are clusters with ages between 63 Myr and 315 Myr (third snapshot). Moreover, the northern part of the SMC body is covered with clusters in this age range. Finally, the last snapshot displays clusters older than 315 Myr (up to ~ 1 Gyr). These clusters mainly populate the western part of the SMC main-body and only a few are found in the north or in the east. 304 A contains fewer of these older objects than 37 A and they are mainly located at the western rim of the shell, while in 37 A they are widely distributed. Generally, the cluster distribution in 304 A shows a continuous formation from a few Myr to 1 Gyr.

According to the standard model of shell formation (McCray & Kafatos 1987) the older objects are supposed to be found in the center of the shell while younger objects are distributed around the edge. As mentioned above, the younger objects in 37 A and 304 A are assembled toward the eastern and the western rim of the shells, respectively. One reason for the deviation from the theory might be the extension of the SMC along the line of sight and that the apparent distance of the clusters from the shell center is a projection effect. More probable, however, is that the spatial distribution of young SMC clusters is related to the shell expansion and shell interaction that has triggered the cluster formation in the inter-shell region as well as at the two opposing rims.

We confirm C06's finding that the location of the young SMC clusters is correlated with HI intensities, which decreases with increasing age. C06 also discovered that clusters and associations younger than ~ 10 Myr are associated with the CO clouds in the SW region of the disk, which indicates that the gas content is related to the cluster formation, but that its presence does not automatically imply star formation.

4.5. Dissolution Effects

Due to the different morphology of SMC, LMC, and MW, low-concentration clusters can easily survive in the SMC and LMC, while in the MW halo clusters have to pass the Galactic disk or bulge while orbiting the Galaxy (Hunter et al. 2003; Lamers et al. 2005; Gieles et al. 2007). The biggest dynamical influence on most MW halo clusters is the tidal shocking that occurs as the clusters cross the disk of the MW. Palomar 5 (Odenkirchen et al. 2003) is a classic example of these effects. Galactic open clusters mostly rotate with the Galactic disk and are not affected by tidal shocking. Also in the LMC the clusters appear to rotate with the disk. Therefore, tidal shocking is likely much less effective in the LMC and probably even less so in the SMC. Moreover, in the LMC we observe solid-body rotation while the MW rotates differentially, which leads to shear and interaction with massive molecular clouds that can result in cluster dissolution. Because the SMC has no disk or bulge, the disintegration process of SMC clusters should not have a big influence on the cluster formation history, but is mostly affected by the star formation rate. Parmentier & de Grijs (2008) found for young LMC clusters a cluster formation rate of 0.3 clusters Myr^{-1} 5 Gyr ago to a present rate of ~ 25 clusters Myr^{-1} . For the SMC such studies have not been published yet.

Cluster disruption due to the galactic tidal field is relevant for old objects. The main distinct phases and corresponding typical timescales of cluster disruption in the MCs are: (I.) *infant mortality* ($\sim 10^7$ yr), (II.) mass loss dominated by *stellar evolution* ($\sim 10^8$ yr), and (III.) a phase dominated by *tidal relaxation* ($\sim 10^9$ yr) in which the mass loss is driven by the clusters dynamical evolution and internal influence of the tidal field of the host galaxy (Lamers et al. 2005; Bastian & Gieles 2006, and references therein). Additionally, tidal external perturbations speed up the process of disruption during all three phases, but these effects operate on longer timescales and mostly affect phase III.

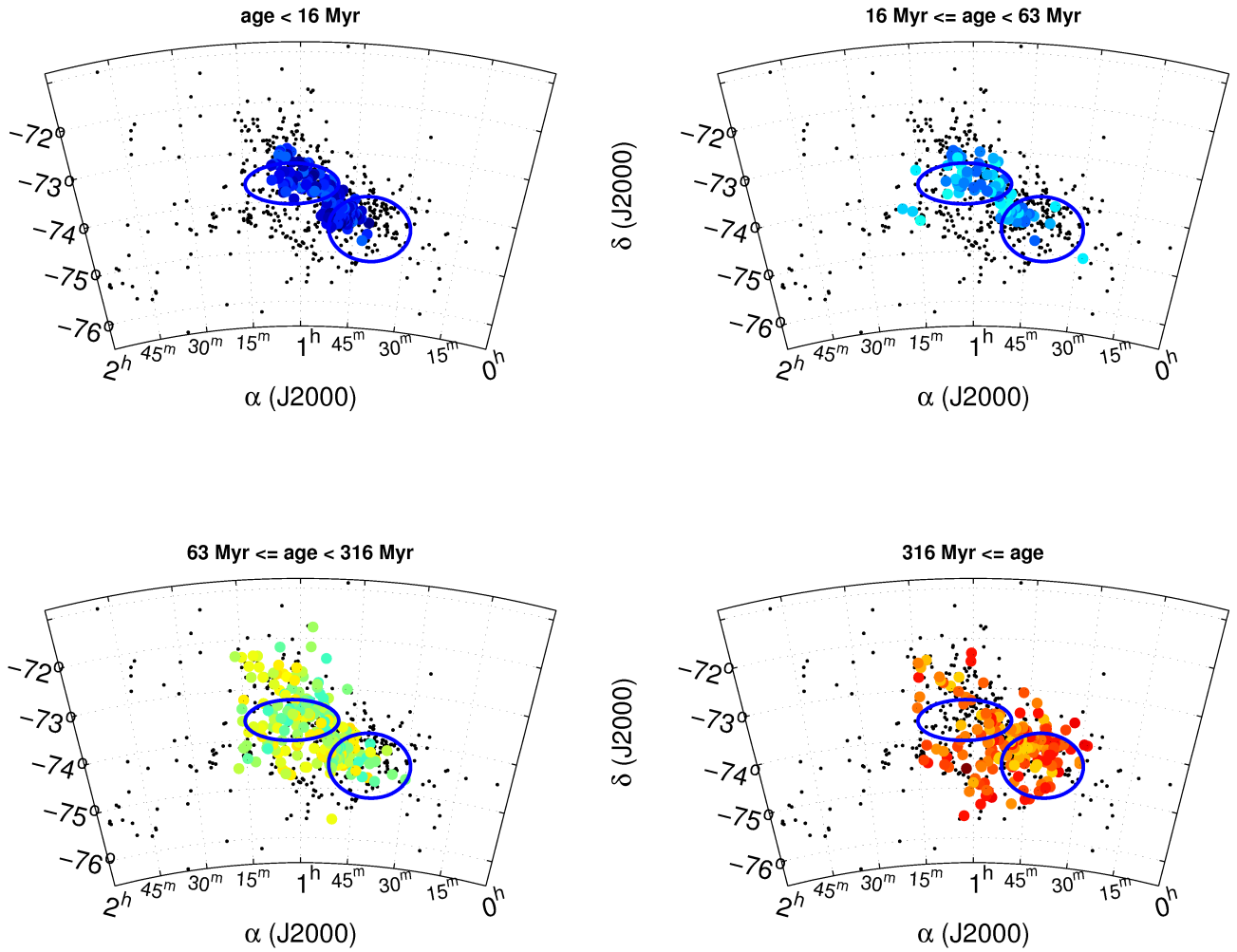


FIGURE 6.6. Spatial distribution of SMC clusters younger than 1 Gyr in different age bins.

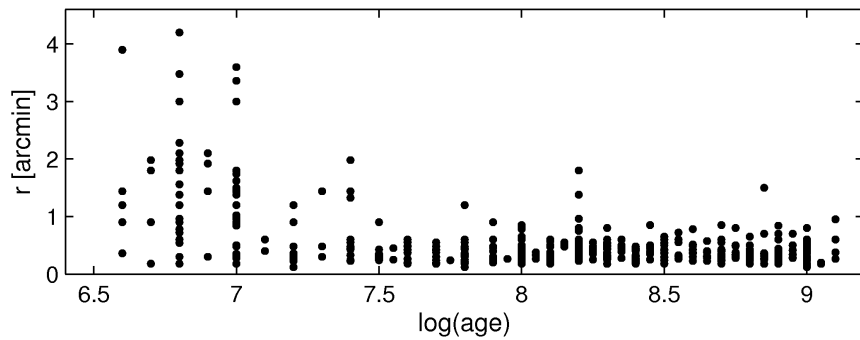


FIGURE 6.7. Age vs radius. No indication of cluster dissolution is visible in our sample. However, the limited depth of the MCPS might cause false decrease in number of older diffuse star clusters, which we cannot take into account without further observations.

Most of the clusters in our sample have survived the first phase and are dominated by the second and third phase. The rate of infant mortality is highly dependent on the ambience of the host galaxy, but is largely mass-independent - at least for masses in excess of $\sim 10^4 M_{\odot}$ (e.g., de Grijs & Goodwin 2008). Infant mortality is driven by two phases: gas expulsion and violent relaxation. This first lifecycle of a cluster results from the expulsion of the intra cluster gas due to explosive expansion driven by stellar winds or supernova activity (e.g., Mengel et al. 2005; Bastian & Goodwin 2006; Goodwin & Bastian 2006). While in spiral galaxies, such as e.g., M 51, clusters younger than ~ 50 Myr suffer from infant mortality, in this phase for clusters in the SMC probably much shorter and around 10 Myr. The clusters in the present sample have an age of 10 Myr and higher, and therefore are in the phase of stellar evolution. The second (mass-dependent) lifecycle of a cluster includes the so-called secular evolution (gas free evolution). This phase is driven by 2-body relaxation and the morphology (ambience) of the host galaxy. Therefore, the disruption time of a cluster is dependent on the internal cluster conditions, such as the initial mass, density, and velocity dispersion, as well as on external conditions, such as the orbit in the galaxy and tidal heating. While the disruption timescale in a spiral galaxy like the MW is rather short and about 90-95% of all star clusters get disrupted, most star clusters in an irregular galaxy can survive (e.g., 70% of all SMC clusters, de Grijs & Goodwin 2008).

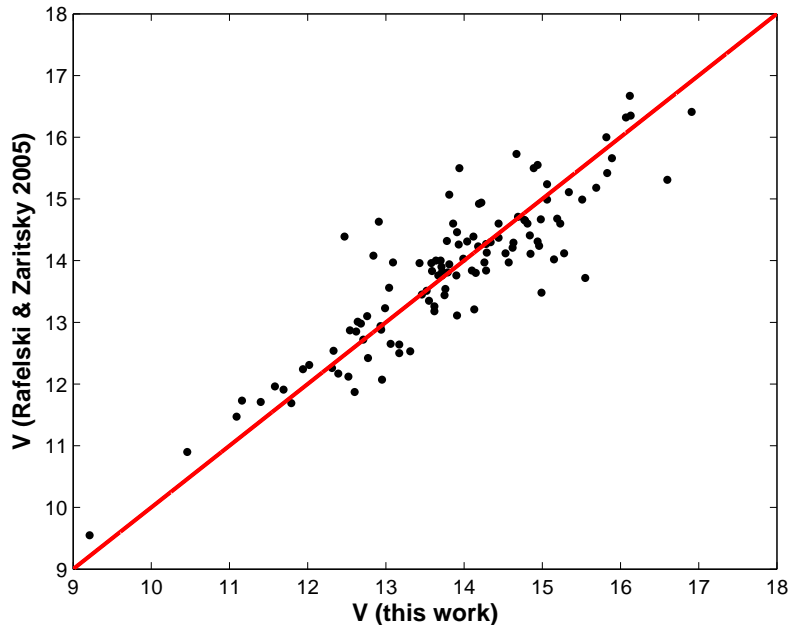


FIGURE 6.8. V band magnitudes derived in this work are compared with the V band magnitudes derived by RZ05 for the clusters in common. The solid line shows the loci of the 1:1 unity.

Fig. 6.7 shows the age-radius relation of the combined SMC cluster sample (this work and C06) with ages between 4 Myr and 1 Gyr. Cluster ages are plotted against their radii from the combined sample derived in this study and C06. The youngest star clusters have radii up to ~ 4 arcmin, but these objects are adopted objects from C06 and are mostly classified as associations. The radii decrease until an age of ~ 25 Myr and then remain relatively constant until 1 Gyr. From this study we conclude that the mass of the SMC star clusters decreases linearly with time, until the clusters finally dissolve. The SMC cluster disruption time derived in the literature is of the order of 8×10^9 Myr (e.g., Boutloukos & Lamers 2003). In Chapter 5 we have shown that clusters with ages older than 1 Gyr have a trend for larger core radii with increasing age. This trend was first found by Mackey & Gilmore (2003b) and is also visible for LMC, Fornax, and Sagittarius clusters (Mackey & Gilmore 2003a,c). In our study only clusters with ages younger than 1 Gyr could be age-dated, which might be the reason

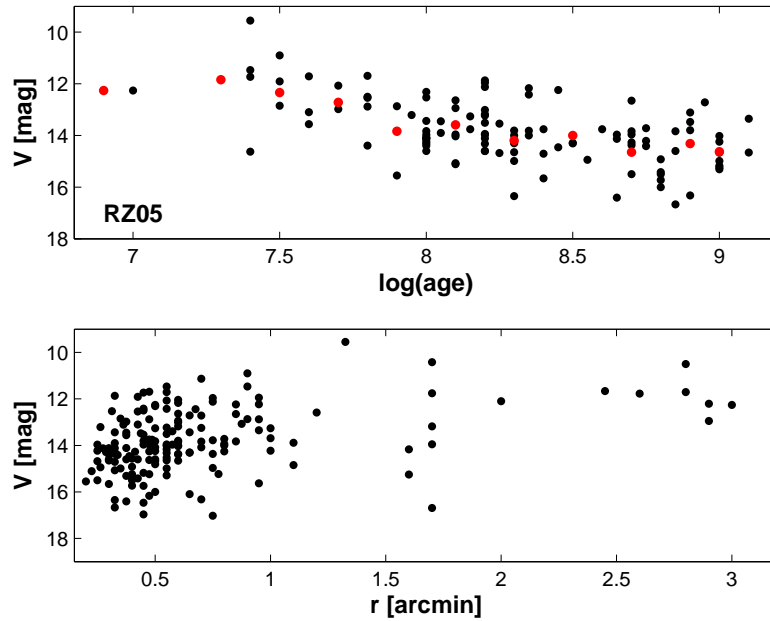


FIGURE 6.9. V vs $\log(\text{age})$ and V vs radius. The luminosities were adopted from RZ05, the ages are from our study. In the upper panel only clusters are shown for which ages have been determined in this study. The red dots represent the mean of the age distribution in magnitude bins of 0.3 mag. A trend for fainter magnitudes with increasing age is visible. The lower panel shows the entire sample of RZ05 with the radii adopted from B08.

that we cannot see this effect in our sample. We conclude that in our sample no obvious dissolution effects of SMC clusters is visible. However, there are two selection effects that may play a major role. The first is the detection limit of the "old" clusters from the MCPS. The number of observed star clusters decreases with increasing age for a given magnitude limit since sparse, faint clusters become increasingly harder to detect. Also a clear separation between sparse and extended clusters and their surroundings becomes particularly difficult when they are embedded in associations of a very similar age or when they are located in a high-density area. Therefore, our sample might not contain any of these older star clusters due to these effects. The second selection effect is real dissolution effects that reduce the number of older clusters. Further investigation with e.g., the Hubble Space Telescope are necessary to illuminate the effect that cluster dissolution has in the SMC.

5. THE CLUSTER LUMINOSITIES

RZ05 published luminosities of 204 SMC star clusters measuring integrated colors from the MCPS. For the age-dated clusters in our sample, we computed luminosities by summing the flux of each star within the individual cluster radii. To correct for field stars, the luminosity of a concentric annulus between 2 and 1 arcmin was calculated for each cluster, area corrected, and subtracted from the cluster luminosity. 112 clusters of our sample are in common with RZ05's sample. The comparison between the V band luminosity derived using this method and the integrated colors by RZ05 (see Fig. 6.8) shows that our V band magnitudes are broadly correlated to each other. A dispersion about the 1:1 correlation (red solid line) for all clusters in common is of $\sigma_V = 0.28$.

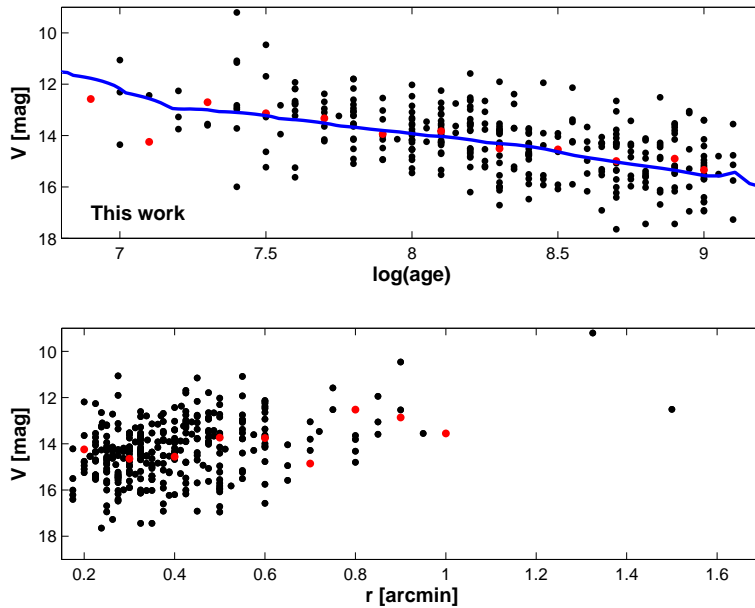


FIGURE 6.10. V vs $\log(\text{age})$ and V vs radius. The luminosities were derived in this study. The red dots represent the mean of the age distribution in magnitude bins of 0.3 mag. The trend for fainter magnitudes with increasing age is also obvious in this plot. The blue solid line represents the GALEVEX model for $Z=0.004$ (Bruzual & Charlot 2003).

The younger the star clusters the brighter they are because young clusters still contain very massive hot stars (e.g. supergiants), which contribute most of the light. The older a cluster gets the more of these massive stars are in their end stage of evolution and no longer contribute to the cluster light. Therefore, clusters become fainter and redder with increasing age. This effect can be seen in the upper panel of Fig. 6.9, in which cluster age is plotted versus luminosity for those clusters that appear in both RZ05 and our sample. The red dots represent the mean of the age distribution in magnitude bins of 0.3 mag. Even though the sample is very small, the trend for fainter magnitudes with increasing age is visible. The lower plot of Fig. 6.9 shows that the SMC star clusters become brighter with increasing radius, which is expected assuming a larger number of stars with the cluster radius contributing to the total cluster luminosity. The trend for fainter magnitudes with increasing age is also obvious when plotting our cluster luminosities versus age (upper panel Fig. 6.10). The mean magnitudes of each age bin (*red dots*) also show a slow declining cluster luminosity. We overplotted a GALEVEX model (Bruzual & Charlot 2003) for $Z = 0.004$, which is in very good agreement with the mean magnitudes. GALEVEX is a model for computing the spectral evolution of stellar populations. The trend for brighter luminosity with increasing radius is also visible in the lower panel of Fig. 6.10 using the cluster luminosities of the present sample. The two clusters with radii larger than 1.20 arcmin are the massive populous star clusters NGC 152 and NGC 330.

6. Summary

We have presented ages and luminosities of 324 populous SMC star clusters. An age range of ~ 10 Myr to 1 Gyr was covered based on isochrone fitting. Using only cluster ages derived in this study, we find two maxima of enhanced cluster formation: the first around 160 Myr and the second around 630 Myr. The first peak appears to be correlated with a peak of enhanced cluster formation found in the LMC. Model calculations predict the last close encounter between LMC and

SMC occurred around 100-200 Myr ago. During a close encounter, the star formation is not expected to be only enhanced in the tidal arms but also in the main body of the galaxy. Therefore, the first peak in the cluster age distribution could have been triggered by this tidal interaction. Extending our sample with cluster ages derived by C06 we find a third pronounced period of enhanced cluster formation. This younger peak of enhanced cluster formation might have a different origin and occurred due to local phenomena.

The youngest objects in the present sample are associated with the two SMC super-shells 37 A and 304 A, the inter-shell region, and toward regions with a high $H\alpha$ content. Their formation is probably related to shell expansion and shell interaction. In the spatial distribution of the clusters younger than ~ 16 Myr the two shells are clearly visible. The older objects are widely spread over the entire SMC main-body, but show a concentration in the western part of the galaxy.

No dissolution effects were found for SMC star clusters younger than ~ 1 Gyr. The morphology of the SMC might be the main reason for this effect. There is no disk or bulge to be passed for SMC clusters unlike clusters in the MW halo, which are subject to much larger tidal effects. SMC clusters do not rotate in the galaxy and therefore do not undergo the process of tidal shocking and have good chances to survive a Hubble time if they are sufficiently strongly bound. This result might be altered when surveys with a deeper detection limit are analyzed detecting also the older clusters, which we might have missed.

The cluster luminosities become fainter with increasing age. Massive stars contribute most of the light in young star clusters. The older a cluster gets the more of these massive stars have evolved away and the fainter the cluster becomes. This trend can be seen in the present sample. The clusters also become brighter with increasing radius.

CHAPTER 7

SUMMARY

“Children are wormholes. They’re portals into the unreachable future and unattainable past.”

Dr. Larry Fleinhardt (Numb3rs)

In my Thesis, I determined ages of Small Magellanic Cloud (SMC) star clusters that have formed during the galaxy's entire lifetime. The youngest cluster ages ($\sim 10 \text{ Myr} < \text{age} < 1 \text{ Gyr}$) were derived using ground-based photometric data. For the six intermediate-age clusters Lindsay 1, Kron 3, NGC 339, NGC 416, Lindsay 38, and NGC 419 and the only old globular cluster (GC), NGC 121, observations obtained with the Hubble Space Telescope exist. This work was part of a ground-based and space-based program to uncover the age-metallicity evolution of the SMC. In the first three parts of my Thesis, I presented accurate ages, distance estimates, and structural parameters for the seven intermediate-age and old SMC star clusters. The cluster ages were determined by fitting different isochrone models to the observed color-magnitude diagrams (CMDs). The CMDs reach at least 3 mag below the main-sequence turnoff-points, which makes it the deepest available photometry for these clusters obtained so far. Only for a few SMC clusters ages had been determined in previous studies using space-based data. The ground-based spectroscopy was obtained with the *Very Large Telescope* (VLT). My photometric results are combined with these spectroscopic metallicity determinations to obtain a well-sampled age-metallicity relation. I measured structural parameters of these seven star clusters and extended the sample of known SMC clusters having accurate age measurements and structural parameters enormously.

The SMC hosts a large number of intermediate-age and young star clusters, but only one ‘old’ GC, NGC 121, for which I determined an age of $\sim 10.5 \text{ Gyr}$. Consequently, NGC 121 is 2–3 Gyr younger than the oldest GCs in the Large Magellanic Cloud (LMC) and the Milky Way (MW). For comparison, the GC system of the MW exhibits a range of ages between ~ 10.5 and 14 Gyr, similar to the LMC, with the oldest populations belonging to the most ancient surviving stellar systems. NGC 121 is similar in age to the youngest GC in the Fornax dSph and to several of the young Galactic halo clusters. On the other hand, NGC 121 is not as young as some of the Sgr dwarf galaxy’s GCs or the youngest Galactic GCs. With the SMC having no ‘truly’ old star cluster, it appears that the SMC has a delayed cluster formation compared to its companions.

The isochrone that fitted best the CMD of NGC 121 was α -enhanced. NGC 121 is the only known α -enhanced star cluster in the SMC, a property that it shares with many of the old outer Galactic halo globulars and which indicates an early rapid chemical enrichment. In a subsequent project additional SMC clusters will be analyzed for possible α -abundances and elements produced through r-processes (rapid neutron capture). These α -elements and r-process elements are synthesized in quickly evolving high-mass stars. The outcoming results can be compared to chemical evolution models, which calculate chemical abundances in detail (e.g., Pagel & Tautvaišienė 1998). With these models the chemical evolution of the SMC can be further constrained and analyzed.

It is also intriguing that NGC 121 is not as metal-poor as the oldest LMC and MW globulars. The SMC must have experienced substantial enrichment prior to the formation of NGC 121. In the LMC, two main epochs of the formation of compact populous clusters are observed. In the first epoch, GCs with ages and metallicities similar to the oldest MW GCs are found, but also very old GCs having a metallicity similar to NGC 121, indicating very early chemical enrichment also in this galaxy. In the

second epoch, numerous stellar populations with ages less than 3-4 Gyr developed. The two epochs are separated by an ‘age gap’ of $\sim 4\text{-}9$ Gyr in which no star cluster has formed. Also the MW contains old GCs that have similarly high metallicities as the younger NGC 121. Evidently, the conditions for and the efficiency of star formation varied in these three galaxies at early epochs. The fact that this cluster is younger than the Galactic mean, relatively metal-rich, and enhanced in α -elements has interesting implications for the early development of the SMC.

The SMC is the only dwarf galaxy in the Local Group in which populous star clusters formed and survived for most of its lifetime. The intermediate-age clusters in the SMC appear to be capable of surviving a Hubble time, due to their high mass and the structure of the SMC (no bulge or disk to be passed). After the formation of NGC 121, there is a gap of ~ 3 Gyr and thus likely in cluster formation activity. The second oldest star cluster is Lindsay 1 for which I determined an age of ~ 7.5 Gyr. Since then compact populous star clusters formed fairly continuously until the present day in the SMC - a contrast to both the LMC and the MW. For the youngest cluster in my sample, NGC 419, me and Elena Sabbi found indication for a multiple stellar population. A more detailed analysis is in progress and the study will be published by Elena Sabbi. Only a few multiple stellar populations are known in the MW, the LMC, and the SMC, but their number is increasing also due to the improved instruments. Combining the newly derived ages with age and metallicity estimates adopted from different sources in the literature, it is possible to present a well-sampled age-metallicity relation (AMR) for the SMC, which is fully based on space-based age determinations and spectroscopic metallicity measurements. The SMC has experienced an early enrichment as can be seen in the relatively metal-rich oldest SMC star cluster NGC 121. The most striking feature in the AMR is the wide metallicity spread for clusters with ages around 6 Gyr indicating that the SMC was not very well mixed in the past. The mean metallicity, however, remains relatively constant for about 4 Gyr, but rises for star clusters that have formed within the past 2–3 Gyr to a present day metallicity of $[\text{Fe}/\text{H}] \approx -0.70$.

From the apparent magnitudes of the cluster’s red clumps, I provided an estimate of direct distances for the clusters. Together with cluster distances from the literature that were obtained using the same approach and that are based on space-based observations, I confirmed the large depth extent of the SMC along the line-of-sight. The three oldest clusters (age > 7 Gyr) are located in the north-western part of the SMC. NGC 361 is a candidate for having an age older than 8 Gyr, but the age determination found in the literature is associated with large uncertainties and new space-based photometry of this cluster is needed. The youngest clusters (age < 1 Gyr) lie near the SMC main body in active star forming regions.

The number of intermediate-age and old SMC clusters having accurate structural parameters and reliable ages was extended enormously in this study. The galactic environment causes external perturbations such as tidal shocking that occurs as star clusters cross the disk or pass near the bulge. These processes tend to decrease the cluster mass and therefore change its structural parameters. I confirmed previous findings (Mackey & Gilmore 2003a,b) that some of the older objects in LMC and SMC have experienced a significant change in core radius, while for other old objects the core radii apparently have almost remained unchanged. The core radii of SMC clusters show a trend of older clusters having a larger spread in core radii than the younger population. Even though I extended the sample with structural parameters from the literature, the sample is highly incomplete, because only for a few intermediate-age clusters both reliable ages and corresponding profiles are available. The analysis of structural parameters of additional SMC clusters is necessary. Clusters in the LMC have experienced a similar evolution, even though the two galaxies show strong differences in various other aspects. The two confirmed Sagittarius clusters as well as the five Fornax clusters show the same spread in core radii. The oldest clusters in the MW, however, modified their original structure during their lifetime and have developed small cores. The largest difference between GCs in the MW, the LMC, and the SMC is that the MW GCs clusters are subject to much larger tidal effects. The biggest dynamical influence on most MW globular halo clusters is the tidal shocking that occurs when they cross the disk of the MW. Tidal shocking is likely much less effective in the LMC and probably even less so in the SMC. Therefore, the main reason for the smaller core radii of MW globulars is the different morphology of the three galaxies.

The different morphologies might also be the reason for the different flattening distributions of star clusters in the SMC, the LMC, and the MW. SMC clusters are more flattened than clusters in the MW and even more flattened than those in the LMC. I found that only NGC 121 and Lindsay 38 exhibit a significant flattening. Galactic GCs modify their original structure and become more spherical with increasing age, while LMC and SMC clusters maintain their original shape. This might be explained with the different dynamical influence and therefore the varying strength of the tidal field of the parent galaxy. The tidal fields of the LMC and SMC might not be strong enough to modify the shape of their clusters significantly. No relation between cluster age, distance from the SMC center, and ellipticity was found, but this point needs further analysis because only for a few SMC star clusters reliable ages, ellipticities and distances are available.

Finally, I provided today's largest catalog of young SMC star clusters containing ages *and* luminosities. The catalog covers an age range between 10 Myr and 1 Gyr. Star clusters are claimed to be produced through strong shock compressions induced by the collision of their host galaxies which causes enhanced star formation during close encounters. The most recent model calculations (e.g., Bekki & Chiba 2005, Kallivayalil et al. 2006a,b) showed that the SMC, the LMC, and the MW have only interacted long enough to produce the Magellanic Stream. The models predict the last close encounter between LMC and SMC around 200 Myr ago due to which enhanced cluster formation can be expected. The cluster age distribution combining my results with the cluster ages provided by Chiosi et al. (2006) shows indeed evidence for episodic star formation. The second of two peaks in the age distribution coincides with the model predicted closest approach of the LMC. The origin of the first peak about 6.5 Myr ago might have been triggered by internal mechanisms. Looking at their spatial distribution, the young clusters are assembled in the two large star forming HI super-shells and in the inter-shell region. Their formation might have been triggered by the expansion of the shells through gas compression. I found no indication of cluster dissolution. As mentioned above, SMC clusters evolve differently from MW clusters. Due to the different morphologies of the parent galaxies, the tidal field of the SMC has no big influence on its star clusters. It is most likely that SMC clusters decrease their mass through stellar evolution with time until the clusters finally dissolve.

Zusammenfassung

In meiner Doktorarbeit habe ich die Alter von Sternhaufen in der Kleinen Magellanschen Wolke (SMC; *engl.* Small Magellanic Cloud) bestimmt, welche sich während ihrer gesamten Lebensdauer gebildet haben. Die SMC ist eine irreguläre Zwerggalaxie, das heisst sie hat keine deutliche Struktur (wie z.B. Spiralarme) und einen hohen Gasgehalt. Die jüngsten von mir untersuchten Sternhaufen haben Alter zwischen ~ 10 Myr und 1 Gyr und wurden mit Hilfe von bodengebundenen Daten untersucht. Für die sechs Sternhaufen mittleren Alters Lindsay 1, Kron 3, NGC 339, NGC 416, Lindsay 38, und NGC 419 habe ich Alter zwischen 1.2 und 7.5 Gyr bestimmt und für den einzig wirklich alten Sternhaufen, NGC 121, ein Alter von ca. 10.5 Gyr. Diese sieben Haufen wurden mit dem Hubble Weltraum Teleskop (HST) beobachtet. Meine Arbeit ist Teil eines Programs, welches mit bodengebundener Spektroskopie und weltraumgebundener Photometrie die Alters-Metallizität Relation der SMC untersucht hat. In den ersten drei Teilen meiner Doktorarbeit diskutiere ich die Altersbestimmung, die Distanzen und Strukturparameter dieser sieben älteren Sternhaufen. Im vierten Teil beschreibe ich die jüngeren Sternhaufen, ihre räumliche Verteilung und berechne ihre Helligkeit. Die Alter aller Haufen wurden mit Hilfe von verschiedenen Isochronenmodellen bestimmt, welche über die Farben-Helligkeits Diagramme (CMDs; *engl.* color-magnitude diagrams) der Sternhaufen gezeichnet wurden. Die von mir erarbeiteten CMDs erreichen mindestens 3 Magnituden schwächere Helligkeiten als je zuvor gemessen, was bedeutet dass meine Arbeit die tiefste Photometrie beinhaltet, welche von diesen sieben Haufen heute existiert. Nur für einige wenige SMC Sternhaufen existieren weltraumgebundene Daten und die Altersbestimmung basierend auf bodengebundenen Beobachtungen sind oft mit grossen Unsicherheiten verbunden. Die bodengebundene Spektroskopie wurde mit dem *Very Large Telescope* der ESO aufgenommen, eines der besten Instrumente die heute existieren. Meine Alter habe ich mit Daten aus der Literatur kombiniert, um eine gut sortierte Alters-Metallizität Relation der SMC zu erhalten. Ausserdem habe ich Strukturparameter (z.B. Kernradius, Gezeitenradius, Elliptizität) dieser sieben Sternhaufen bestimmt und damit die Anzahl Sternhaufen erhöht für welche genaue Alter *und* Strukturparameter existieren. Unser Wissen über die Evolution der SMC kann mit diesen neuen Resultaten deutlich verbessert werden. Für NGC 121 habe ich Anzeichen für Massensegregation gefunden.

Sternhaufen spielen in der Erforschung von Sternentstehungsgeschichten und der chemischen Entwicklung von Galaxien eine sehr wichtige Rolle. Die SMC ist jene Zwerggalaxie, welche von uns am wenigsten weit entfernt ist und in welcher heute aktiv Sterne entstehen. Wegen ihrer Nähe lässt sich die Entstehungsgeschichte und Entwicklung dieser Galaxie mit dem HST genauestens analysieren. Überraschenderweise wurde die SMC bisher nur spärlich mit dem HST beobachtet, obwohl seine Instrumente es ermöglichen einzelne Sterne in den zum Teil sehr dichten Zentrumsregionen von Sternhaufen aufzulösen. Die SMC bildet zusammen mit der Grossen Magellanschen Wolke (LMC; *engl.* Large Magellanic Cloud) und der Milchstrasse (MW; *engl.* Milky Way) ein Dreiersystem, welches miteinander interagiert. Sternentstehung wird durch nahe Durchgänge von Nachbargalaxien ausgelöst deren gravitative Einwirkung die riesigen molekularen Gaswolken zum kollabieren bringen, sodass daraus neue Sterne entstehen.

In der SMC findet man eine grosse Anzahl von Sternhaufen mittleren und jungen Alters, jedoch nur einen alter Kugelsternhaufen (GC; *engl.* globular cluster), NGC 121. Das Alter dieses Haufens wurde mit verschiedenen Methoden in dieser Arbeit bestimmt. Ich zeige, dass NGC 121 2–3 Gyr jünger ist als die ältesten GCs in der LMC und der MW, welche einen Altersbereich von 10–14 Gyr abdecken und deren älteste Exemplare somit zu den ältesten Objekten des Universums gehören. In

der SMC gibt es keine dieser alten Exemplare! Da die SMC keinen klassisch alten Kugelsternhaufen besitzt, hat es den Anschein als habe die SMC verspätet mit ihrer Haufenentstehung begonnen. Interessanterweise zeigt NGC 121 eine erhöhte Häufigkeit in α -Elementen ($Z < 22$: C, N, O, Ne, Mg, Si, S, Ar, Ca, Ti). Einige der alten Haufen im äusseren Galaktischen Halo zeigen dieselbe Eigenschaft, welche auf eine rasche Anreicherung von chemischen Elementen hindeutet (SN II). Die Tatsache, dass NGC 121 der einzig wirklich alte Sternhaufen in der SMC ist, lässt die Frage aufkommen, ob dieses Objekt möglicherweise das einzig überlebende Objekt einer frühen Epoche von Haufenentstehung darstellt. Es ist jedoch schwierig einen GC in einer Zwerggalaxie durch externe Effekte zu zerstören. In der MW müssen Sternhaufen auf ihrer Umlaufbahn die Galaktische Scheibe durchstossen oder kommen nahe am Bulge vorbei, wodurch sie vorzeitig durch die Gezeitenkräfte auseinandergerissen werden und ihre Sterne an die Galaxie verlieren. In der SMC gibt es solche Strukturen nicht und somit ist die Wahrscheinlichkeit einer vorzeitigen Auflösung durch Gezeitenkräfte gering.

Interessanterweise ist NGC 121 nicht so metall arm wie die ältesten LMC und MW GCs. Diese haben in der Regel einen $[Fe/H]$ -Gehalt von ~ -2 dex, während NGC 121 einen Metallgehalt von ~ -1.46 dex aufweist. Dies deutet darauf hin, dass die SMC vor der Entstehung von NGC 121 massiv mit chemischen Elementen angereichert wurde. In der LMC hat man zwei Epochen von Haufenentstehung beobachtet: eine frühe Epoche in welcher GCs mit ähnlichen Eigenschaften wie die der ältesten MW GC entstanden sind, und eine zweite spätere Epoche die vor circa 4 Gyr begonnen hat und bis heute andauert. Dazwischen befindet sich gewissermassen ein "Loch" in welchem kein einziger Sternhaufen entstanden ist. Man findet jedoch in der LMC auch sehr alte Haufen mit einem ähnlichen Metallgehalt wie NGC 121, was auch in dieser Galaxie auf eine frühe Anreicherung chemischer Elemente hinweist. Dieselbe Art von Sternhaufen findet man auch im MW Halo. Ganz offensichtlich waren die Bedingungen und die Effizienz der Sternentstehung in diesen drei Galaxien zu einem sehr frühen Zeitpunkt sehr unterschiedlich und die Tatsache, dass NGC 121 jünger, metall-reicher und in α -Elementen angereichert ist, ermöglicht interessante Rückschlüsse auf die frühe Entwicklung der SMC.

Die SMC ist die einzige Zwerggalaxie in der Lokalen Gruppe, in welcher sich sogenannte *populous* Sternhaufen gebildet und überlebt haben. Wegen ihrer hohen Masse und der Struktur der SMC, scheinen diese Haufen mittleren Alters in der Lage zu sein, eine Hubble Zeit zu überleben. Nach der Entstehung von NGC 121 bildeten sich während ~ 3 Gyr keine Sternhaufen in der SMC. Der zweitälteste SMC Haufen ist Lindsay 1 mit einem Alter von ~ 7.5 Gyr. Seither haben sich kompakte, massereiche Sternhaufen bis zum heutigen Tage kontinuierlich gebildet, was einen Kontrast zur Haufenentstehungsgeschichte der MW und der LMC darstellt. Neben den sehr alten Objekten in der MW, hat man in deren Halo eine Gruppe 'jüngerer' Kugelsternhaufen gefunden, wie zum Beispiel Pal 1, welcher mit einem Alter vom 8 Gyr das jüngste dieser Objekte ist. Der Ursprung dieser "jungen" Haufen ist jedoch ungewiss. Es wird vermutet, dass die MW diese Objekte von der Sagittarius Zwerggalaxie akkreditiert hat, oder dass sie im Zuge naher Durchgänge der Magellanschen Wolken an der MW entstanden sind.

In dieser Arbeit wurden exakte Alter von sechs weiteren SMC Sternhaufen bestimmt, nämlich Lindsay 1, Kron 3, NGC 339, NGC 416, Lindsay 38 und NGC 419. Es gibt Anzeichen, dass es sich bei dem jüngsten Objekt in dieser Serie, NGC 419, nicht um eine einzelne Sternpopulation handelt, sondern dass sich zwei oder mehrere Populationen im Haufen befinden. Dies kann zum Beispiel durch das Vermischen zweier Haufen bei einem Zusammenstoss geschehen. Zwei Haufen können jedoch auch auf der Sichtlinie genau hintereinander liegen, was dann wie eine multiple Sternpopulation aussieht. Eine detaillierte Analyse von NGC 419 wird von Elena Sabbi durchgeführt und wohl im nächsten Jahr veröffentlicht.

Indem meine neuen Resultate mit genauen Altern und Metallizitäten aus der Literatur kombiniert wurden, können wir zum ersten Mal eine Alters-Metallizität Relation präsentieren, welche die gesamte Lebensdauer der SMC abdeckt. An dem relativ hohen Metallgehalt von NGC 121 lässt sich ersehen, dass die SMC eine frühe Anreicherung von chemischen Elementen erfahren hat. Was jedoch am meisten auffällt, ist die grosse Bandbreite von Metallizitäten für Sternhaufen mit einem Alter von ~ 6 Gyr. Dies zeigt deutlich, dass die SMC in der Vergangenheit nicht sehr gut durchmischt wurde,

was bisher weitgehend angenommen wurde. Die Durchschnittsmetallizität jedoch bleibt während etwa 4 Gyr relativ konstant, nimmt dann aber, für Haufen die sich in den letzten 2–3 Gyr gebildet haben, zu.

Ich war in der Lage, die Anzahl von Sternhaufen zu erhöhen für welche exakte Alter *und* Strukturparameter (z.B. Kernradius, Gezeitenradius, Konzentration) vorhanden sind. Ich konnte frühere Erkenntnisse bestätigen, dass einige alte Objekte in der SMC eine signifikante Veränderung des Kernradius erfahren haben, während andere völlig unbeeinflusst geblieben sind. Jedoch ist das Sample sehr unvollständig, auch wenn es wieder mit Werten aus der Literatur ergänzt wurde. Es existieren leider nur sehr wenige Sternhaufen, für welche genaue Strukturparameter *und* Alter existieren. Weitere Analysen sind daher dringend notwendig, um die noch vorhandenen Unsicherheiten zu beseitigen. Interessanterweise weisen die älteren LMC Sternhaufen die gleiche Tendenz auf, obwohl die beiden Galaxien unterschiedliche Strukturen besitzen. Die beiden Sternhaufen in Sagittarius sowie die fünf Fornax Haufen zeigen ebenfalls die gleiche Tendenz. Die ältesten Haufen in der MW hingegen haben ihre ursprüngliche Struktur während ihres Lebens kaum verändert und sind bei ihren kleinen Kernradien geblieben. Der grösste Unterschied zwischen diesen Galaxien ist ihre unterschiedliche Struktur und die damit einhergehenden Gezeiteneffekte, welche auf die Sternhaufen wirken. Den grössten dynamischen Einfluss auf die MW Haufen hat das so-genannte Gezeitenschock welches auftritt, sobald Sternhaufen die Galaktische Scheibe durchqueren müssen. Dieser Prozess ist in der LMC und der SMC vernachlässigbar, da beide keine ausgebildete Scheibe besitzen. Somit lässt sich schliessen, dass die verschiedenen Morphologien der drei Galaxien der Hauptgrund für unterschiedliche Strukturparameter ihrer Sternhaufen sind.

Die Altersbestimmung der jüngeren Sternhaufen wurde mit bodengebundenen Daten durchgeführt. Die ermittelten Alter decken einen Bereich zwischen 10 Myr und 1 Gyr ab. Sternhaufen werden durch starke Kompressionen von Gas geformt, welche durch nahe Galaxiendurchgänge ausgelöst werden können. Befinden sich zwei Galaxien in einer Umlaufbahn umeinander, sollte die Sternentstehungsrate bei einem nahen Durchgang erhöht und während des auseinander driftens erniedrigt sein. Geschieht dies mehrere Male, spricht man von episodischer Sternentstehung. Kürzliche Modellrechnungen haben gezeigt, dass die Magellanschen Wolken wahrscheinlich nur solange miteinander wechselgewirkt haben um den Magellanic Stream zu produzieren. Die letzte Annäherung der LMC an die SMC soll vor circa 200 Myr stattgefunden haben, womit man einen Höhepunkt in der Haufenentstehungsgeschichte zu diesem Zeitpunkt erwarten würde. Die Altersverteilung der SMC zeigt in der Tat Anzeichen für episodische Haufenentstehung mit einem Maximum vor ~ 200 Myr. Wir finden noch ein zweites Maximum vor ~ 6.5 Myr, welches durch interne Effekte hervorgerufen werden konnte. Diese jungen Sternhaufen befinden sich innerhalb der zwei riesigen HI-Wolken sowie in der Region dazwischen. Die Expansion dieser Wolken und die damit verbundene Kompression von Gas könnte der Grund für die Entstehung dieser Haufen sein. Ausserdem finden wir keine Anzeichen von Haufenauflösung. Durch die Gezeitenkräfte in der MW werden viele ihrer Sternhaufen auseinandergerissen während ihrer Umlaufbahn durch die Scheibe oder nahe am Bulge vorbei. Da die SMC keine solchen Strukturen aufweist, ist es nicht verwunderlich, dass die Sternhaufen aller Wahrscheinlichkeit nach nur durch stellare Evolution stetig an Masse verlieren bis sich der Haufen schlussendlich auflöst.

Appendix A

Cluster Ridgelines

On the following pages, the full ridgelines of NGC 121, Lindsay 1, Kron 3, NGC 339, NGC 416, Lindsay 38, and NGC 419 are tabulated.

$m_{555} - m_{814}$	m_{555}	$m_{555} - m_{814}$ CONT.	m_{555} CONT.	$m_{555} - m_{814}$ CONT.	m_{555} CONT.
1.7400	16.6859	1.2500	17.9231	0.7700	22.3380
1.7300	16.6916	1.2400	17.9690	0.7600	22.3480
1.7200	16.7011	1.2300	18.0171	0.7500	22.3570
1.7100	16.7107	1.2200	18.0676	0.7400	22.3670
1.7000	16.7224	1.2100	18.1205	0.7300	22.3770
1.6900	16.7339	1.2000	18.1761	0.7200	22.3880
1.6800	16.7483	1.1900	18.2343	0.7100	22.4010
1.6700	16.7605	1.1800	18.2952	0.7000	22.4120
1.6600	16.7834	1.1700	18.3590	0.6900	22.4260
1.6500	16.8001	1.1600	18.4257	0.6800	22.4520
1.6400	16.8177	1.1500	18.4955	0.6700	22.4710
1.6300	16.8381	1.1400	18.5685	0.6600	22.5020
1.6200	16.8554	1.1300	18.6447	0.6500	22.5190
1.6100	16.8706	1.1200	18.7242	0.6400	22.5410
1.6000	16.8867	1.1100	18.8071	0.6300	22.5720
1.5900	16.9098	1.1000	18.8936	0.6200	22.6240
1.5800	16.9289	1.0900	18.9837	0.6100	22.6890
1.5700	16.9540	1.0800	19.0775	0.6000	22.7610
1.5600	16.9712	1.0700	19.1752	0.5950	22.8500
1.5500	16.9874	1.0600	19.2767	0.5950	23.0310
1.5400	17.0008	1.0500	19.3823	0.6125	23.4000
1.5300	17.0153	1.0400	19.4920	0.6670	24.0000
1.5200	17.0309	1.0300	19.6059	0.7400	24.6000
1.5100	17.0477	1.0200	19.7241	0.8400	25.2000
1.5000	17.0658	1.0100	19.8367	0.9700	25.8000
1.4900	17.0851	1.0000	19.9538	1.1000	26.4000
1.4800	17.1057	0.9900	20.0855		
1.4700	17.1276	0.9800	20.2218		
1.4600	17.1508	0.9700	20.3630		
1.4500	17.1753	0.9600	20.5090		
1.4400	17.2013	0.9500	20.6601		
1.4300	17.2286	0.9400	20.8162		
1.4200	17.2575	0.9300	20.9774		
1.4100	17.2877	0.9200	21.1440		
1.4000	17.3195	0.9100	21.3159		
1.3900	17.3528	0.9000	21.4932		
1.3800	17.3877	0.8900	21.6762		
1.3700	17.4241	0.8800	21.8899		
1.3600	17.4621	0.8700	22.0599		
1.3500	17.5018	0.8600	22.1921		
1.3400	17.5432	0.8600	22.1933		
1.3300	17.5962	0.8500	22.2305		
1.3200	17.6378	0.8400	22.2520		
1.3100	17.6904	0.8300	22.2660		
1.3000	17.7246	0.8200	22.2770		
1.2900	17.7605	0.8100	22.2890		
1.2800	17.7983	0.8000	22.3050		
1.2700	17.8379	0.7900	22.3180		
1.2600	17.8794	0.7800	22.3280		

TABLE 7.1. **Ridgeline of NGC 121**

$m_{555} - m_{814}$	m_{555}	$m_{555} - m_{814}$ CONT.	m_{555} CONT.	$m_{555} - m_{814}$ CONT.	m_{555} CONT.
1.3230	27.1000	0.9690	20.3380	1.4440	17.0550
1.1720	26.5000	0.9780	20.2230	1.4530	17.0410
1.0320	25.9000	0.9880	20.1100	1.4630	17.0100
0.9090	25.3000	0.9980	19.9990	1.4730	16.9830
0.7950	24.7000	1.0080	19.8900	1.4830	16.9540
0.7050	24.1000	1.0180	19.7830	1.4930	16.9350
0.6290	23.5000	1.0280	19.6780	1.5030	16.9160
0.5790	22.9000	1.0380	19.5750	1.5130	16.8850
0.5610	22.5000	1.0480	19.4750	1.5230	16.8660
0.5590	22.4000	1.0580	19.3760	1.5330	16.8480
0.5600	22.2923	1.0670	19.2790	1.5430	16.8220
0.5700	22.1930	1.0770	19.1840	1.5520	16.8070
0.5800	22.1157	1.0870	19.0910	1.5620	16.7830
0.5900	22.0562	1.0970	19.0000	1.5720	16.7550
0.6000	22.0108	1.1070	18.9110	1.5820	16.7360
0.6100	21.9765	1.1170	18.8240	1.5920	16.7110
0.6200	21.9507	1.1270	18.7380	1.6020	16.6920
0.6300	21.9312	1.1370	18.6550	1.6120	16.6790
0.6400	21.9163	1.1470	18.5730	1.6220	16.6500
0.6500	21.9047	1.1570	18.4940	1.6320	16.6310
0.6600	21.8954	1.1670	18.4160	1.6420	16.6120
0.6700	21.8875	1.1760	18.3400	1.6510	16.5900
0.6800	21.8806	1.1860	18.2660	1.6610	16.5780
0.6900	21.8744	1.1960	18.1940	1.6710	16.5620
0.7000	21.8687	1.2060	18.1230	1.6810	16.5480
0.7100	21.8635	1.2160	18.0540	1.6910	16.5350
0.7200	21.8589	1.2260	17.9870	1.7010	16.5220
0.7300	21.8549	1.2360	17.9220	1.7110	16.5150
0.7400	21.8517	1.2460	17.8590	1.7210	16.5020
0.7500	21.8492	1.2560	17.8070	1.7310	16.4940
0.7600	21.8475	1.2650	17.7470	1.7410	16.4880
0.7700	21.8463	1.2750	17.6890	1.7500	16.4820
0.7800	21.8452	1.2850	17.6320	1.7600	16.4780
0.7900	21.8438	1.2950	17.5770	1.7700	16.4760
0.8000	21.8412	1.3050	17.5240	1.7800	16.4640
0.8100	21.8362	1.3150	17.4930	1.7900	16.4600
0.8200	21.8274	1.3250	17.4530	1.8000	16.4550
0.8300	21.8130	1.3350	17.4150		
0.8400	21.7906	1.3450	17.3710		
0.8500	21.7577	1.3550	17.3290		
0.8600	21.7108	1.3640	17.3080		
0.8700	21.6463	1.3740	17.2720		
0.8800	21.5598	1.3840	17.2440		
0.9130	21.0720	1.3940	17.1960		
0.9190	20.9440	1.4040	17.1630		
0.9290	20.8190	1.4140	17.1270		
0.9390	20.6950	1.4240	17.1080		
0.9490	20.5740	1.4340	17.0860		
0.9590	20.4550	1.4440	17.0550		

TABLE 7.2. **Ridgeline of Lindsay 1**

$m_{555} - m_{814}$	m_{555}	$m_{555} - m_{814}$ CONT.	m_{555} CONT.	$m_{555} - m_{814}$ CONT.	m_{555} CONT.
1.1110	26.2000	0.8893	20.8646	1.3644	17.4060
0.9870	25.7000	0.8992	20.7276	1.3743	17.3692
0.8830	25.2000	0.9091	20.5944	1.3842	17.3431
0.7710	24.7000	0.9190	20.4649	1.3941	17.3178
0.6910	24.2000	0.9289	20.3390	1.4040	17.2932
0.6190	23.7000	0.9388	20.2166	1.4139	17.2691
0.5730	23.2000	0.9487	20.0978	1.4238	17.2456
0.5350	22.7000	0.9586	19.9823	1.4337	17.2226
0.5210	22.5000	0.9685	19.8703	1.4436	17.2000
0.5200	22.3000	0.9784	19.7615	1.4535	17.1777
0.5190	22.2000	0.9883	19.6560	1.4634	17.1557
0.5300	22.1000	0.9982	19.5537	1.4733	17.1340
0.5300	22.0620	1.0081	19.4545	1.4832	17.1124
0.5400	22.0023	1.0180	19.3584	1.4931	17.0910
0.5500	21.9529	1.0279	19.2653	1.5030	17.0696
0.5600	21.9120	1.0378	19.1751	1.5129	17.0482
0.5700	21.8782	1.0477	19.0878	1.5228	17.0267
0.5800	21.8501	1.0576	19.0033	1.5327	17.0050
0.5900	21.8269	1.0675	18.9216	1.5426	16.9832
0.6000	21.8076	1.0774	18.8426	1.5525	16.9611
0.6100	21.7918	1.0873	18.7662	1.5624	16.9387
0.6200	21.7789	1.0972	18.6923	1.5723	16.9159
0.6300	21.7688	1.1071	18.6210	1.5822	16.8926
0.6400	21.7612	1.1170	18.5521	1.5921	16.8689
0.6500	21.7561	1.1269	18.4857	1.6020	16.8446
0.6600	21.7533	1.1368	18.4215	1.6308	16.8087
0.6700	21.7529	1.1467	18.3596	1.6525	16.7815
0.6800	21.7549	1.1566	18.2999	1.6795	16.7429
0.6900	21.7591	1.1665	18.2424	1.7110	16.7002
0.7000	21.7655	1.1764	18.1869		
0.7100	21.7739	1.1863	18.1334		
0.7200	21.7838	1.1962	18.0819		
0.7300	21.7948	1.2061	18.0323		
0.7400	21.8063	1.2160	17.9845		
0.7500	21.8175	1.2259	17.9385		
0.7600	21.8271	1.2358	17.8943		
0.7700	21.8340	1.2457	17.8516		
0.7800	21.8363	1.2556	17.8105		
0.7900	21.8323	1.2655	17.7710		
0.8000	21.8195	1.2754	17.7329		
0.8100	21.7954	1.2853	17.6963		
0.8200	21.7569	1.2952	17.6609		
0.8300	21.7004	1.3051	17.6269		
0.8400	21.6220	1.3149	17.5841		
0.8500	21.5174	1.3248	17.5424		
0.8600	21.3814	1.3347	17.5018		
0.8700	21.2087	1.3446	17.4722		
0.8794	21.0054	1.3545	17.4437		
0.8794	21.0054	1.3644	17.4060		

TABLE 7.3. Ridgeline of Kron 3

$m_{555} - m_{814}$	m_{555}	$m_{555} - m_{814}$ CONT.	m_{555} CONT.	$m_{555} - m_{814}$ CONT.	m_{555} CONT.
1.1940	26.6000	0.9566	20.9366	1.3030	17.5360
1.0820	26.0000	0.9636	20.8328	1.3101	17.5043
0.9680	25.4000	0.9707	20.7303	1.3172	17.4740
0.8380	24.8000	0.9778	20.6288	1.3242	17.4449
0.7410	24.2000	0.9848	20.5285	1.3313	17.4171
0.6680	23.6000	0.9919	20.4295	1.3384	17.3906
0.5960	23.0000	0.9990	20.3317	1.3455	17.3652
0.5400	22.4000	1.0061	20.2351	1.3525	17.3411
0.5400	22.3409	1.0131	20.1399	1.3596	17.3180
0.5400	22.2095	1.0202	20.0460	1.3667	17.2961
0.5500	22.1047	1.0273	19.9534	1.3737	17.2752
0.5600	22.0221	1.0343	19.8623	1.3808	17.2554
0.5700	21.9578	1.0414	19.7725	1.3879	17.2365
0.5800	21.9183	1.0485	19.6842	1.3949	17.2186
0.6000	21.8709	1.0556	19.5973	1.4020	17.2016
0.6100	21.8428	1.0626	19.5119	1.4091	17.1854
0.6200	21.8220	1.0697	19.4279	1.4162	17.1701
0.6300	21.8068	1.0768	19.3455	1.4232	17.1555
0.6400	21.7956	1.0838	19.2646	1.4303	17.1417
0.6500	21.7873	1.0909	19.1852	1.4374	17.1225
0.6600	21.7809	1.0980	19.1074	1.4444	17.1060
0.6700	21.7759	1.1051	19.0311	1.4515	17.0940
0.6800	21.7718	1.1121	18.9564	1.4586	17.0826
0.6900	21.7683	1.1192	18.8832	1.4657	17.0616
0.7000	21.7653	1.1263	18.8117	1.4727	17.0411
0.7100	21.7627	1.1333	18.7417	1.4798	17.0189
0.7200	21.7605	1.1404	18.6734	1.4869	17.0080
0.7300	21.7590	1.1475	18.6066	1.4897	17.0022
0.7400	21.7583	1.1545	18.5415	1.4939	16.9883
0.7500	21.7584	1.1616	18.4779	1.5010	16.9719
0.7600	21.7594	1.1687	18.4160	1.5081	16.9525
0.7700	21.7614	1.1758	18.3557	1.5152	16.9333
0.7800	21.7643	1.1828	18.2970	1.5222	16.9140
0.7900	21.7679	1.1899	18.2398	1.5293	16.8998
0.8000	21.7717	1.1970	18.1843	1.5364	16.8852
0.8100	21.7753	1.2040	18.1304	1.5434	16.8755
0.8200	21.7777	1.2111	18.0780	1.5505	16.8656
0.8300	21.7781	1.2182	18.0273	1.5576	16.8553
0.8400	21.7750	1.2253	17.9780	1.5646	16.8446
0.8500	21.7668	1.2323	17.9304	1.5717	16.8334
0.8600	21.7516	1.2394	17.8843	1.5788	16.8217
0.8700	21.7269	1.2465	17.8397	1.5859	16.8093
0.8800	21.6900	1.2535	17.7966	1.5929	16.7962
0.8900	21.6377	1.2606	17.7550	1.6000	16.7824
0.9000	21.5664	1.2677	17.7149		
0.9100	21.4718	1.2747	17.6763		
0.9200	21.3494	1.2818	17.6391		
0.9500	21.0420	1.2889	17.6033		
0.9495	21.0413	1.2960	17.5690		

TABLE 7.4. **Ridgeline of NGC 339**

$m_{555} - m_{814}$	m_{555}	$m_{555} - m_{814}$ CONT.	m_{555} CONT.	$m_{555} - m_{814}$ CONT.	m_{555} CONT.	$m_{555} - m_{814}$ CONT.	m_{555} CONT.
1.0800	25.9920	0.6100	22.3580	1.1100	19.7890	1.7720	16.9890
1.0700	25.9520	0.6200	22.2720	1.1200	19.7040	1.7870	16.9770
1.0600	25.8860	0.6300	22.2120	1.1300	19.5900	1.8010	16.9670
1.0500	25.8390	0.6400	22.1610	1.1400	19.5090	1.8170	16.9570
1.0400	25.7640	0.6500	22.1370	1.1500	19.4090	1.8310	16.9470
1.0300	25.7060	0.6600	22.1180	1.1600	19.3210	1.8460	16.9380
1.0200	25.6560	0.6700	22.1010	1.1700	19.2450	1.8610	16.9300
1.0100	25.6140	0.6800	22.0850	1.1800	19.1700	1.8760	16.9220
1.0000	25.5540	0.6900	22.0750	1.1900	19.0770	1.8910	16.9150
0.9900	25.4860	0.7000	22.0680	1.2000	18.9960	1.9060	16.9080
0.9800	25.4510	0.7100	22.0610	1.2100	18.9170	1.9210	16.9000
0.9700	25.3780	0.7200	22.0560	1.2200	18.8300		
0.9600	25.3150	0.7300	22.0490	1.2300	18.7540		
0.9500	25.2840	0.7400	22.0410	1.2400	18.6700		
0.9400	25.2260	0.7500	22.0380	1.2500	18.5970		
0.9300	25.1680	0.7600	22.0360	1.2600	18.5170		
0.9200	25.1080	0.7700	22.0350	1.2780	18.3990		
0.9100	25.0470	0.7800	22.0350	1.2930	18.3180		
0.9000	24.9850	0.7900	22.0350	1.3080	18.2310		
0.8900	24.9230	0.8000	22.0380	1.3230	18.1460		
0.8800	24.8590	0.8100	22.0410	1.3380	18.0850		
0.8700	24.7950	0.8200	22.0450	1.3530	18.0170		
0.8600	24.7310	0.8300	22.0520	1.3680	17.9320		
0.8500	24.6670	0.8400	22.0620	1.3830	17.8600		
0.8400	24.6020	0.8500	22.0760	1.3980	17.7910		
0.8300	24.5380	0.8600	22.0820	1.4130	17.7350		
0.8200	24.4740	0.8700	22.0910	1.4280	17.6710		
0.8100	24.4100	0.8800	22.0960	1.4430	17.6000		
0.8000	24.3470	0.8900	22.0980	1.4580	17.5510		
0.7900	24.2840	0.9000	22.1040	1.4730	17.5050		
0.7800	24.2210	0.9100	22.1050	1.4880	17.4620		
0.7700	24.1590	0.9200	22.1060	1.5020	17.4200		
0.7600	24.0960	0.9300	22.0970	1.5170	17.3810		
0.7500	24.0320	0.9400	22.0820	1.5320	17.3450		
0.7400	23.9680	0.9500	22.0300	1.5470	17.3100		
0.7300	23.9020	0.9700	21.8510	1.5620	17.2770		
0.7200	23.8340	0.9800	21.6580	1.5770	17.2460		
0.7100	23.7630	0.9900	21.4730	1.5920	17.2170		
0.7000	23.6890	1.0000	21.3080	1.6070	17.1900		
0.6900	23.6100	1.0100	21.1420	1.6220	17.1650		
0.6800	23.5240	1.0200	20.9740	1.6370	17.1410		
0.6700	23.4310	1.0300	20.8100	1.6520	17.1190		
0.6600	23.3300	1.0400	20.6580	1.6670	17.0980		
0.6500	23.2180	1.0500	20.4870	1.6820	17.0790		
0.6400	23.0940	1.0600	20.3590	1.6970	17.0610		
0.6300	22.9550	1.0700	20.2180	1.7120	17.0440		
0.6200	22.8000	1.0800	20.1160	1.7270	17.0290		
0.6100	22.6260	1.0900	20.0050	1.7420	17.0150		
0.6050	22.4800	1.1000	19.8860	1.7570	17.0010		

TABLE 7.5. Ridgeline of NGC 416

$m_{555} - m_{814}$	m_{555}
1.063	26.255
0.974	25.855
0.894	25.455
0.821	25.055
0.755	24.655
0.693	24.255
0.631	23.855
0.582	23.455
0.522	23.055
0.471	22.655
0.457	22.455
0.455	22.255
0.492	22.057
0.586	21.907
0.637	21.850
0.737	21.794
0.838	21.788
0.871	21.715
0.889	21.598
0.919	21.168
0.925	21.073
0.929	20.978
0.935	20.886
0.941	20.794
0.947	20.703
0.956	20.491
0.966	20.345
0.976	20.196
0.986	20.044
0.996	19.894
1.006	19.741
1.016	19.591
1.026	19.441
1.036	19.294
1.046	19.152
1.055	19.012
1.065	18.878
1.075	18.751
1.085	18.630
1.095	18.515
1.105	18.412
1.115	18.316
1.125	18.231
1.135	18.156
1.146	18.094
1.207	17.508

TABLE 7.6. **Ridgeline of Lindsay 38**

$m_{555} - m_{814}$	m_{555}	$m_{555} - m_{814}$ CONT.	m_{555} CONT.	$m_{555} - m_{814}$ CONT.	m_{555} CONT.	$m_{555} - m_{814}$ CONT.	m_{555} CONT.
1.3610	26.7610	0.4910	22.2890	0.3680	20.3100	1.4780	17.4330
1.2240	26.2930	0.4750	22.2290	0.7700	20.2980	1.4970	17.3820
1.1500	25.9550	0.4610	22.1620	0.7600	20.2870	1.5120	17.3320
1.1050	25.7990	0.4440	22.0860	0.7500	20.2670	1.5280	17.2810
1.0950	25.7310	0.4240	22.0000	0.7400	20.2580	1.5430	17.2320
1.0760	25.6670	0.4030	21.9000	0.7300	20.2500	1.5580	17.1820
1.0630	25.6010	0.3850	21.7890	0.7200	20.2380	1.5780	17.1340
1.0500	25.5300	0.3510	21.5970	0.7100	20.2290	1.5980	17.0870
1.0370	25.4550	0.3310	21.4660	1.0270	20.2110	1.6130	17.0410
1.0240	25.3760	0.3140	21.3460	0.6650	20.2010	1.6290	16.9960
1.0110	25.2950	0.2980	21.1580	0.4310	20.2000	1.6440	16.9530
0.9970	25.2120	0.2940	20.9620	0.4520	20.1800	1.6590	16.9120
0.9840	25.1300	0.2950	20.8920	0.6020	20.1680	1.6740	16.8730
0.9710	25.0480	0.2960	20.8330	0.4690	20.1600	1.6890	16.8350
0.9580	24.9670	0.9900	20.7750	0.5070	20.1590	1.7040	16.8000
0.9450	24.8880	1.0000	20.7740	0.4910	20.1570	1.7190	16.7670
0.9320	24.8100	0.9800	20.7670	0.5320	20.1550	1.7340	16.7360
0.9190	24.7340	0.2970	20.7630	0.5730	20.1520	1.7500	16.7080
0.9050	24.6590	0.9700	20.7530	1.0360	19.9910	1.7650	16.6810
0.8920	24.5860	1.0020	20.7410	1.0460	19.7910	1.7800	16.6570
0.8790	24.5130	0.9600	20.7400	1.0610	19.5800	1.7950	16.6350
0.8660	24.4400	0.9500	20.7310	1.0690	19.4460	1.8100	16.6160
0.8530	24.3670	0.9400	20.7120	1.0800	19.2970	1.8250	16.5980
0.8400	24.2940	0.3000	20.7090	1.0930	19.1630	1.8410	16.5820
0.8270	24.2180	0.9300	20.6870	1.1080	19.0400	1.8560	16.5680
0.8140	24.1420	0.9200	20.6660	1.1230	18.9290	1.8660	16.5520
0.8000	24.0620	0.9100	20.6420	1.1390	18.8280	1.8810	16.5400
0.7870	23.9810	1.0090	20.6210	1.1530	18.7350	1.9000	16.5210
0.7740	23.8960	0.9000	20.6180	1.1680	18.6500	1.9150	16.4990
0.7610	23.8090	0.3050	20.6110	1.1820	18.5720	1.9310	16.4870
0.7480	23.7200	0.8900	20.5850	1.1970	18.4990	1.9470	16.4640
0.7350	23.6290	0.8800	20.5550	1.2080	18.4320	1.9620	16.4490
0.7220	23.5360	0.3120	20.5530	1.2210	18.3680	1.9770	16.4380
0.7080	23.4420	0.8700	20.5340	1.2340	18.3080	2.0070	16.4320
0.6950	23.3470	0.8600	20.5150	1.2470	18.2500	1.9920	16.4320
0.6820	23.2530	0.3210	20.4920	1.2610	18.1950	2.0220	16.4290
0.6690	23.1610	0.8500	20.4860	1.2820	18.1120	2.0380	16.4230
0.6560	23.0710	0.8400	20.4640	1.2980	18.0600	2.1350	16.4220
0.6430	22.9840	0.3290	20.4620	1.3140	18.0080	2.2400	16.4210
0.6300	22.9000	1.0150	20.4540	1.3330	17.9380	2.1850	16.4210
0.6160	22.8210	0.8300	20.4420	1.3480	17.8880		
0.6030	22.7470	0.3350	20.4250	1.3610	17.8380		
0.5900	22.6790	0.8200	20.4180	1.3760	17.7880		
0.5770	22.6150	0.8100	20.3910	1.3910	17.7380		
0.5640	22.5550	0.3390	20.3900	1.4050	17.6880		
0.5510	22.5000	0.8000	20.3730	1.4190	17.6370		
0.5380	22.4470	0.3480	20.3600	1.4380	17.5870		
0.5250	22.3950	0.7900	20.3390	1.4520	17.5360		
0.5120	22.3430	0.7800	20.3190	1.4660	17.4840		

TABLE 7.7. Ridgeline of NGC 419

Appendix B

Star cluster catalog

In the following tables, parameters, ages, and luminosities determined for the young SMC star clusters ($t < 1$ Gyr) are listed. In the first column (1) we give the clusters' identification as used in this work. The reddening values E_{B-V} and the apparent radii (diameters adopted by (Bica & Schmitt 1995)) are listed in columns (2) and (3). Column (4) and (5) show the derived ages and the errors in logarithmic scale. Error class 1 indicates having errors $\Delta\sigma_{\log(\text{age})} < 0.3$; class 2 indicates objects having errors $0.3 < \sigma_{\log(\text{age})} < 0.5$; class 3 indicates objects having errors $\sigma_{\log(\text{age})} > 0.5$. In column (6) the integrated cluster luminosities in the V band is shown. Right ascension and declination are given in columns (7) and (8), and finally in column (9) the cross identification with other catalogs are listed.

ID	E_{B-V}	R_{app} [ARCMIN]	LOG(τ)	LOG(σ_τ)	V MAG	R.A. (J2000.0)	Dec. (J2000.0)	Cross-ID.
SMC0017	0.02	0.250	9.00	2	16.94 ± 0.13	0.47528	-73.01361	BS2
SMC0018	0.01	0.600	8.70	1	14.09 ± 0.12	0.50000	-73.37917	K9,L13
SMC0023	0.01	0.600	9.10	3	14.76 ± 0.15	0.54472	-72.58139	L14
SMC0026	0.03	1.500	8.85	3	12.51 ± 0.12	0.54889	-73.11611	NGC152,K10,L15,ESO28SC24
SMC0028	0.05	0.850	8.00	1	13.58 ± 0.12	0.56278	-73.63306	HW8
SMC0037	0.03	0.950	9.10	1	13.55 ± 0.12	0.59472	-73.59806	K13,L17,ESO29SC1
SMC0039	0.10	0.600	8.20	1	12.64 ± 0.11	0.59944	-73.16611	NGC176,K12,L16,ESO29SC2
SMC0044	0.08	0.475	>9.00	3	15.06 ± 0.11	0.60861	-72.98694	HW10
SMC0048	0.08	0.650	8.50	2	14.04 ± 0.12	0.62583	-73.61194	HW11,SOGLE2
SMC0052	0.06	0.400	9.00	2	13.40 ± 0.11	0.62889	-73.21111	B10,SOGLE4
SMC0054	0.07	0.275	8.95	2	13.11 ± 0.11	0.63083	-73.12111	H86-43
SMC0058	0.05	0.400	8.70	1	14.35 ± 0.11	0.64750	-73.37417	HW12,SOGLE163
SMC0063	0.08	0.275	8.65	1	15.40 ± 0.11	0.64361	-73.80583	BS14,SOGLE165
SMC0064	0.10	0.375	8.75	2	15.70 ± 0.11	0.65472	-72.90333	H86-53
SMC0066	0.07	0.200	9.05	1	14.79 ± 0.11	0.65722	-73.10639	H86-55,SOGLE167
SMC0067	0.05	0.338	8.95	1	14.53 ± 0.11	0.65861	-73.42389	HW13,SOGLE168
SMC0068	0.06	0.275	8.70	1	16.40 ± 0.11	0.65972	-73.38278	H86-54
SMC0069	0.03	0.300	8.90	1	13.52 ± 0.11	0.66806	-73.14278	H86-58
SMC0070	0.05	0.550	8.70	1	13.77 ± 0.12	0.67000	-72.69889	K15,L21
SMC0071	0.06	0.800	8.75	2	14.32 ± 0.12	0.67056	-73.87222	HW14
SMC0073	0.08	0.600	8.00	1	12.46 ± 0.11	0.67528	-73.40278	NGC220,K18,L22,ESO29SC3,SOGLE8
SMC0074	0.04	0.425	8.80	1	15.48 ± 0.12	0.67583	-72.73972	K16,L23
SMC0075	0.10	0.175	9.05	1	15.49 ± 0.11	0.67861	-73.11806	H86-60
SMC0076	0.10	0.200	7.80	1	15.09 ± 0.11	0.67889	-73.06167	B19
SMC0077	0.06	0.450	8.45	1	14.37 ± 0.12	0.67917	-73.74056	B26,SOGLE169
SMC0079	0.06	0.600	8.10	1	12.24 ± 0.11	0.67889	-73.38333	NGC222,K19,L24,ESO29SC4
SMC0081	0.10	0.300	8.60	1	14.97 ± 0.11	0.68000	-73.08806	H86-62,SOGLE10
SMC0082	0.04	0.438	8.90	1	13.58 ± 0.12	0.67972	-74.02167	HW15
SMC0083	0.08	0.263	7.95	1	14.13 ± 0.11	0.68194	-73.40194	B23,SOGLE170
SMC0084	0.04	0.550	8.55	2	13.37 ± 0.12	0.68361	-72.57222	K17,L26
SMC0086	0.10	0.900	7.90	1	12.53 ± 0.11	0.68500	-73.35194	NGC231,K20,L25,ESO29SC5,SOGLE11

TABLE 7.8. K = Kron (1956); L = Lindsay (1958); HW = Hodge & Wright (1974); H86 = Hodge (1986); BS95 = Bica & Schmitt (1995); B = Bruck (1976)

ID	E_{B-V}	R_{app} [ARCMIN]	LOG(T)	LOG(σ_T)	V MAG	R.A. (J2000.0)	DEC. (J2000.0)	Cross-ID.
SMC0090	0.07	0.550	>9.00	3	15.15 ± 0.12	0.71056	-72.45583	H86-68
SMC0094	0.10	0.475	8.25	1	12.65 ± 0.11	0.72583	-73.44028	NGC241,K22w,L29W,ESO29SC6w
SMC0095	0.05	0.500	8.95	1	16.94 ± 0.13	0.72417	-74.18444	HW19
SMC0098	0.02	0.225	8.90	1	15.44 ± 0.11	0.72722	-72.98000	BS20,SOGLE20
SMC0101	0.14	0.300	8.70	1	14.28 ± 0.11	0.74778	-73.00194	B34,SOGLE176
SMC0104	0.20	0.325	8.00	1	13.75 ± 0.10	0.75389	-73.21917	H86-74,SOGLE25
SMC0105	0.08	0.275	8.65	1	14.29 ± 0.11	0.75722	-73.48139	B39,SOGLE27
SMC0106	0.10	0.250	8.00	1	14.18 ± 0.12	0.75750	-73.70306	B41
SMC0110	0.14	0.325	8.30	1	14.27 ± 0.12	0.76222	-72.84306	B36
SMC0112	0.20	0.450	7.80	1	12.16 ± 0.11	0.76500	-73.50667	NGC256,K23,L30,ESO29SC11,SOGLE32
SMC0117	0.10	0.487	8.60	1	13.66 ± 0.12	0.77639	-72.74222	L31,SOGLE36
SMC0118	0.08	0.350	8.45	1	15.54 ± 0.12	0.77611	-72.77389	H86-83,SOGLE35
SMC0120	0.08	0.300	8.85	3	14.44 ± 0.12	0.77889	-72.06306	HW22
SMC0123	0.08	0.275	8.40	1	15.68 ± 0.11	0.78222	-73.42361	H86-85,SOGLE186
SMC0124	0.16	0.363	8.10	1	13.14 ± 0.10	0.78361	-73.39306	H86-86,SOGLE40
SMC0127	0.09	0.600	8.35	2	12.38 ± 0.11	0.78667	-73.47722	NGC265,K24,L34,ESO29SC14,SOGLE39
SMC0129	0.15	0.450	8.00	2	13.08 ± 0.11	0.79028	-72.84083	L33,SOGLE41
SMC0130	0.12	0.275	8.40	1	16.47 ± 0.11	0.79028	-73.45722	H86-90
SMC0131	0.07	0.800	>9.00	3	14.80 ± 0.11	0.79139	-72.47500	HW24
SMC0133	0.10	0.225	8.10	2	13.92 ± 0.10	0.79278	-73.33167	H86-92
SMC0134	0.10	0.350	8.85	1	14.36 ± 0.11	0.79722	-73.47833	BS35,SOGLE42
SMC0136	0.08	0.250	8.45	1	15.69 ± 0.12	0.79806	-73.53139	H86-94
SMC0137	0.10	0.600	8.35	1	13.70 ± 0.11	0.80028	-73.48611	K25,L35,SOGLE45
SMC0138	0.08	0.850	8.70	1	13.05 ± 0.12	0.80361	-73.86278	K27,L36
SMC0140	0.15	0.250	8.30	2	15.99 ± 0.11	0.80889	-72.76167	H86-101
SMC0143	0.20	0.225	8.65	1	15.53 ± 0.13	0.81194	-74.30306	HW25
SMC0144	0.06	0.250	9.00	1	15.60 ± 0.12	0.81444	-73.56139	B49
SMC0145	0.08	0.275	7.00	1	11.06 ± 0.11	0.81722	-73.36222	B50
SMC0149	0.08	0.313	8.00	1	13.31 ± 0.11	0.82167	-73.37222	L39,SOGLE54
SMC0150	0.10	0.275	8.75	2	15.56 ± 0.12	0.82306	-73.53028	H86-102
SMC0152	0.17	0.225	8.60	1	15.47 ± 0.11	0.82917	-72.86611	H86-109,SOGLE58
SMC0153	0.25	0.475	8.20	1	12.86 ± 0.11	0.83444	-73.38444	B53,SOGLE197
SMC0156	0.15	0.325	8.05	1	13.71 ± 0.11	0.83944	-73.38778	B55,SOGLE60
SMC0157	0.18	0.325	8.10	1	13.81 ± 0.11	0.84111	-73.20333	B54,SOGLE62
SMC0158	0.15	0.350	8.20	1	14.64 ± 0.11	0.84222	-72.65250	H86-114
SMC0159	0.17	0.225	8.65	1	14.06 ± 0.11	0.84194	-73.33639	H86-106w
SMC0160	0.15	0.250	7.55	1	13.94 ± 0.11	0.84361	-73.33639	H86-106e
SMC0161	0.05	0.325	8.30	1	16.12 ± 0.13	0.84222	-74.61417	HW27
SMC0163	0.20	0.250	8.10	1	13.18 ± 0.11	0.84444	-72.96528	H86-116,SOGLE64
SMC0164	0.20	0.325	8.20	1	12.60 ± 0.11	0.84889	-72.72778	L41,SOGLE67
SMC0167	0.10	0.550	7.60	3	11.92 ± 0.11	0.85389	-73.16139	NGC290,L42,ESO29SC19,SOGLE69
SMC0170	0.08	0.375	8.30	1	13.53 ± 0.11	0.85889	-72.97917	H86-124,SOGLE205
SMC0171	0.10	0.300	<7.2	1	13.74 ± 0.10	0.86028	-72.54194	H86-119
SMC0174	0.08	0.225	8.20	2	14.69 ± 0.12	0.86139	-73.53111	H86-117
SMC0180	0.05	0.225	8.10	1	14.36 ± 0.11	0.86611	-73.46139	H86-122
SMC0184	0.08	0.338	7.80	1	12.79 ± 0.11	0.87139	-73.01778	H86-130,SOGLE78
SMC0185	0.10	0.350	8.25	1	13.53 ± 0.11	0.87500	-73.04972	B64,SOGLE210
SMC0189	0.08	0.750	8.20	3	12.51 ± 0.11	0.87639	-72.19306	K30,L45
SMC0191	0.10	0.400	7.90	1	13.02 ± 0.11	0.87833	-72.92556	BS60,SOGLE82
SMC0193	0.23	0.375	7.70	1	12.68 ± 0.11	0.87889	-72.98000	B65,SOGLE83
SMC0194	0.13	0.263	8.55	2	14.22 ± 0.12	0.88000	-72.79611	B66,SOGLE85
SMC0196	0.03	0.225	8.70	1	14.33 ± 0.11	0.87972	-73.40694	BS63,SOGLE84
SMC0198	0.03	0.225	7.20	1	12.25 ± 0.12	0.88083	-72.73528	BS254
SMC0204	0.10	0.850	8.45	1	11.94 ± 0.12	0.88500	-73.38028	NGC294,L47,ESO29SC22,SOGLE90
SMC0208	0.10	0.238	7.75	1	13.23 ± 0.11	0.88806	-72.73417	BS256,SOGLE215
SMC0209	0.10	0.425	7.50	1	11.68 ± 0.12	0.88833	-72.76667	B71,SOGLE92
SMC0211	0.10	0.450	7.40	1	11.15 ± 0.11	0.89028	-72.19639	NGC299,K32,L49,ESO51SC5
SMC0212	0.02	0.475	7.80	1	12.94 ± 0.17	0.89111	-71.39861	L48,ESO51SC6
SMC0213	0.08	0.600	7.60	1	12.16 ± 0.11	0.89056	-72.68250	B72
SMC0215	0.04	0.225	7.80	1	13.55 ± 0.11	0.89361	-72.34972	H86-145
SMC0216	0.08	0.450	8.00	1	13.36 ± 0.11	0.89417	-72.48528	H86-142
SMC0217	0.08	0.600	8.55	2	12.13 ± 0.11	0.89722	-72.89639	H86-147,SOGLE216
SMC0218	0.03	0.250	8.90	1	13.67 ± 0.11	0.89861	-72.66889	H86-148
SMC0219	0.04	0.550	7.80	3	13.07 ± 0.11	0.89944	-72.20056	B74
SMC0220	0.10	0.275	8.35	2	15.31 ± 0.12	0.90056	-73.32639	H86-144

TABLE 7.9. Table 7 continued.

ID	E_{B-V}	R_{app} [ARCMIN]	LOG(τ)	LOG(σ_r)	V MAG	R.A. (J2000.0)	DEC. (J2000.0)	Cross-ID.
SMC0221	0.04	0.550	7.70	1	12.95 ± 0.11	0.90417	-72.24139	NGC306,K33,L50,ESO29SC23
SMC0222	0.12	0.250	8.80	1	14.11 ± 0.11	0.90528	-72.51472	H86-149
SMC0225	0.05	0.250	8.85	1	16.68 ± 0.12	0.90778	-73.61806	HW30
SMC0226	0.05	0.600	9.10	1	15.74 ± 0.13	0.90861	-74.18528	BS75
SMC0227	0.01	0.475	7.40	1	12.91 ± 0.12	0.91250	-72.12944	B78
SMC0228	0.04	0.363	8.90	2	13.91 ± 0.12	0.91306	-73.22361	B80,SOGLE98
SMC0229	0.05	0.350	7.50	1	13.13 ± 0.11	0.91333	-72.46611	B79,SOGLE99
SMC0232	0.07	0.438	7.80	1	13.05 ± 0.12	0.91500	-72.11278	L51,ESO51SC7
SMC0233	0.02	0.263	7.90	1	14.48 ± 0.11	0.91528	-72.44194	BS259
SMC0237	0.03	0.250	8.80	1	14.89 ± 0.13	0.92000	-73.29667	H86-155,SOGLE101
SMC0238	0.22	0.375	8.20	1	14.85 ± 0.12	0.92139	-73.50806	L52
SMC0239	0.08	0.350	7.80	2	14.91 ± 0.12	0.92306	-71.88528	B81
SMC0242	0.06	0.300	8.00	1	13.54 ± 0.11	0.92667	-71.98250	B82
SMC0244	0.08	0.350	8.10	1	15.52 ± 0.12	0.92750	-71.92167	BS76
SMC0245	0.03	0.388	8.90	1	15.25 ± 0.13	0.92583	-74.06361	HW31
SMC0247	0.05	0.225	8.70	1	15.34 ± 0.12	0.92972	-73.46278	H86-157
SMC0251	0.10	1.325	7.40	1	9.20 ± 0.11	0.93861	-72.46389	NGC330,K35,L54,ESO29SC24
SMC0252	0.10	0.325	8.10	1	13.53 ± 0.11	0.93778	-72.51639	B86,SOGLE222
SMC0258	0.10	0.700	8.95	2	13.04 ± 0.12	0.94556	-73.89889	L55
SMC0259	0.05	0.225	8.10	1	15.33 ± 0.13	0.94889	-70.77333	B88
SMC0262	0.10	0.250	8.10	2	14.29 ± 0.11	0.95583	-72.57528	H86-173
SMC0263	0.11	0.475	7.80	1	11.79 ± 0.11	0.95861	-72.26444	L56,S26,SOGLE109
SMC0264	0.11	0.263	7.60	1	12.71 ± 0.11	0.96278	-72.70583	H86-178,SOGLE110
SMC0270	0.08	0.275	8.30	1	11.90 ± 0.11	0.96472	-72.49667	H86-176
SMC0271	0.02	0.500	>9.00	3	14.95 ± 0.13	0.96306	-74.32667	K37,L58
SMC0272	0.08	0.200	7.60	1	12.18 ± 0.11	0.96528	-72.29111	B90
SMC0273	0.08	0.500	8.80	2	15.82 ± 0.11	0.96444	-73.54528	HW34
SMC0275	0.10	0.300	7.30	3	13.60 ± 0.11	0.97056	-72.00389	B92
SMC0276	0.12	0.700	8.90	1	13.80 ± 0.12	0.96889	-73.93278	B91
SMC0278	0.10	0.325	7.40	1	12.82 ± 0.11	0.97194	-72.29917	H86-181,SOGLE228
SMC0280	0.10	0.425	8.25	1	13.07 ± 0.11	0.97833	-73.58389	HW35
SMC0285	0.13	0.375	8.05	1	13.45 ± 0.12	0.98750	-71.76889	HW37
SMC0286	0.12	0.475	8.30	1	13.93 ± 0.11	0.98722	-72.60806	B96,SOGLE117
SMC0287	0.07	0.375	8.20	1	14.51 ± 0.12	0.99194	-71.66944	HW39
SMC0288	0.07	0.400	8.80	1	14.67 ± 0.11	0.99028	-73.81722	HW38
SMC0291	0.05	0.750	8.20	1	11.58 ± 0.11	0.99667	-72.33389	IC1611,K40,L61,ESO29SC27
SMC0292	0.10	0.300	8.20	1	13.58 ± 0.11	0.99917	-72.37333	H86-186,SOGLE119
SMC0293	0.13	0.500	8.00	1	12.02 ± 0.11	1.00028	-72.36889	IC1612,K41,L62,ESO29SC28
SMC0294	0.05	0.450	>9.00	3	15.69 ± 0.13	1.00694	-71.29472	HW40
SMC0295	0.03	0.325	8.10	1	13.72 ± 0.12	1.00639	-72.08472	B100
SMC0297	0.10	0.600	>9.00	3	16.57 ± 0.12	1.00972	-71.46083	HW41
SMC0300	0.01	0.200	<7.9	3	14.94 ± 0.12	1.00917	-72.25861	H86-190,SOGLE230
SMC0302	0.15	0.425	7.80	1	12.60 ± 0.11	1.00944	-72.36556	K42,L63,SOGLE124
SMC0304	0.05	0.600	8.20	2	13.62 ± 0.12	1.01361	-73.34889	K43,L64
SMC0305	0.08	0.388	8.45	1	13.90 ± 0.12	1.01556	-73.15250	B103
SMC0306	0.15	0.400	8.40	1	13.76 ± 0.11	1.01611	-72.54028	H86-191,SOGLE231
SMC0307	0.02	0.550	8.20	2	13.78 ± 0.11	1.01722	-72.75139	L65,H86-192,SOGLE126
SMC0308	0.10	0.400	8.20	1	16.20 ± 0.12	1.01889	-71.75472	HW43
SMC0311	0.08	0.275	8.40	2	14.51 ± 0.11	1.02167	-72.22833	H86-193,SOGLE127
SMC0313	0.07	0.375	<8.00	3	13.86 ± 0.11	1.02694	-72.40694	B105,SOGLE128
SMC0314	0.05	0.550	7.40	1	11.08 ± 0.11	1.02917	-72.56444	L66,SOGLE129
SMC0315	0.03	0.400	8.70	1	13.94 ± 0.11	1.03111	-72.18278	B108,SOGLE130
SMC0317	0.03	0.350	9.40	3	15.39 ± 0.11	1.03222	-73.61278	B109
SMC0319	0.03	0.250	8.00	1	14.81 ± 0.11	1.03639	-72.00306	B110
SMC0321	0.04	0.400	7.10	1	12.43 ± 0.11	1.03972	-72.00306	B112
SMC0322	0.02	0.250	8.40	1	14.64 ± 0.11	1.04583	-73.73861	K45w,L69w
SMC0323	0.02	0.200	8.40	2	14.75 ± 0.11	1.04694	-73.74028	K45e,L69w
SMC0324	0.02	0.300	8.75	1	14.62 ± 0.12	1.04889	-73.33611	B113
SMC0325	0.08	0.375	7.60	2	13.03 ± 0.11	1.05333	-72.27250	K47,L70,SOGLE134
SMC0326	0.10	0.425	7.60	2	12.76 ± 0.11	1.05639	-72.65167	B115,SOGLE137
SMC0327	0.08	0.900	7.50	1	10.46 ± 0.11	1.06472	-72.82611	NGC376,K49,L72,ESO29SC29
SMC0332	0.08	0.325	8.30	1	14.34 ± 0.12	1.07000	-73.25528	B117
SMC0333	0.05	0.450	8.40	1	14.70 ± 0.12	1.07167	-71.71500	B122

TABLE 7.10. Table 7 continued.

ID	E_{B-V}	R_{app} [ARCMIN]	LOG(T)	LOG(σ_t)	V MAG	R.A. (J2000.0)	DEC. (J2000.0)	Cross-ID.
SMC0337	0.05	0.300	8.90	1	15.17 ± 0.12	1.07194	-73.16500	B119
SMC0338	0.04	0.325	8.00	1	14.53 ± 0.11	1.07500	-72.61917	B121,SOGLE237
SMC0340	0.08	0.500	7.00	3	12.30 ± 0.11	1.07667	-72.16056	K50,L74,ESO51SC15,SOGLE142
SMC0342	0.02	0.300	7.30	2	13.55 ± 0.11	1.08222	-72.04556	B125
SMC0343	0.02	0.325	8.40	1	14.69 ± 0.12	1.08278	-73.63750	HW48
SMC0344	0.08	0.275	8.10	1	14.25 ± 0.11	1.08389	-73.04278	B124
SMC0345	0.04	0.450	8.35	2	12.76 ± 0.11	1.08944	-72.04306	IC1624,K52,L76,ESO51SC17
SMC0346	0.10	0.550	8.25	1	15.23 ± 0.11	1.09278	-73.48722	BS128
SMC0347	0.02	0.287	8.50	1	14.63 ± 0.11	1.09722	-71.95111	B128
SMC0349	0.02	0.500	8.45	2	15.92 ± 0.12	1.10083	-71.71139	HW50
SMC0351	0.05	0.500	8.35	2	13.72 ± 0.11	1.10361	-73.29694	IC1626,K53,L77,ESO29SC30
SMC0352	0.03	0.450	7.55	3	12.82 ± 0.11	1.11333	-72.27361	K54,L79,ESO29SC31,SOGLE153
SMC0353	0.08	0.800	8.20	1	13.81 ± 0.12	1.11472	-71.69111	L78
SMC0354	0.02	0.250	8.20	1	14.57 ± 0.11	1.11583	-73.23583	HW52
SMC0355	0.02	0.325	8.85	1	16.12 ± 0.12	1.11611	-73.57833	HW53
SMC0357	0.08	0.500	9.00	3	14.40 ± 0.11	1.12222	-73.37750	HW55
SMC0358	0.05	0.500	8.00	1	12.84 ± 0.10	1.12444	-72.49333	K56,SOGLE155
SMC0359	0.10	0.600	8.10	1	12.93 ± 0.11	1.12444	-72.76944	L80,SOGLE156
SMC0361	0.15	0.475	8.40	1	13.72 ± 0.11	1.12556	-73.11972	K55,L81,SOGLE157
SMC0362	0.15	0.700	8.85	1	14.28 ± 0.12	1.12889	-71.88083	HW57
SMC0365	0.02	0.575	8.65	2	14.28 ± 0.11	1.13722	-73.25722	K57,L86
SMC0367	0.02	0.325	8.55	1	14.26 ± 0.12	1.14028	-71.83806	H86-196
SMC0368	0.02	0.413	8.70	1	14.27 ± 0.12	1.14472	-71.76278	B136
SMC0369	0.05	0.475	8.10	1	13.42 ± 0.11	1.15083	-73.08667	K61,SOGLE161
SMC0371	0.10	0.500	8.15	1	13.62 ± 0.12	1.15694	-71.76667	NGC422,K62,L87,ESO51SC22
SMC0372	0.02	0.238	8.00	2	14.26 ± 0.11	1.15528	-73.18750	B135
SMC0373	0.12	0.350	8.30	1	15.06 ± 0.12	1.16083	-71.76861	IC1641,HW62,ESO51SC21
SMC0374	0.06	0.325	8.30	1	14.42 ± 0.11	1.16194	-72.29528	HW61
SMC0375	0.06	0.388	8.25	1	14.53 ± 0.11	1.16917	-72.74028	BS276
SMC0376	0.10	0.375	8.65	2	16.91 ± 0.11	1.17028	-73.20917	HW63
SMC0377	0.12	0.300	8.30	1	14.78 ± 0.12	1.17444	-71.56139	B139
SMC0378	0.12	0.300	8.40	1	14.92 ± 0.11	1.17500	-72.95639	B137
SMC0379	0.10	0.450	8.25	1	13.76 ± 0.12	1.17917	-71.33833	HW64
SMC0381	0.05	0.450	8.30	1	13.78 ± 0.12	1.18000	-72.79361	K63,L88
SMC0383	0.09	0.800	8.30	1	13.64 ± 0.12	1.19806	-71.33139	IC1655,L90,ESO51SC23
SMC0386	0.06	0.550	8.20	1	13.52 ± 0.12	1.21056	-71.76139	IC1660,K64,L89,ESO51SC24
SMC0387	0.08	0.600	8.10	1	13.99 ± 0.12	1.20917	-73.45667	IC1662,L92,ESO29SC37
SMC0388	0.05	0.250	8.25	1	15.18 ± 0.11	1.21167	-72.75194	B143
SMC0389	0.05	0.550	9.00	1	15.51 ± 0.12	1.21333	-73.47389	L93
SMC0390	0.09	0.600	8.90	2	14.15 ± 0.12	1.21417	-73.11944	L91
SMC0392	0.06	0.275	8.90	1	16.02 ± 0.12	1.23111	-73.41639	HW68
SMC0395	0.05	0.500	8.30	1	15.55 ± 0.13	1.24583	-71.34694	L95
SMC0397	0.05	0.300	8.40	1	15.88 ± 0.12	1.24861	-72.20583	HW70
SMC0401	0.10	0.300	<8.00	3	15.28 ± 0.11	1.25917	-72.38056	HW71se
SMC0402	0.07	0.500	8.20	1	15.22 ± 0.12	1.25917	-72.62361	K68,L98
SMC0405	0.15	0.475	8.15	1	13.89 ± 0.13	1.27389	-71.32611	HW73
SMC0406	0.08	0.263	7.50	1	14.63 ± 0.12	1.28000	-73.16000	HW74
SMC0408	0.05	0.275	7.50	1	15.23 ± 0.12	1.32500	-73.09389	B156
SMC0460	0.02	0.275	8.90	1	16.17 ± 0.14	0.58167	-72.74417	H86-23
SMC0461	0.02	0.375	9.10	1	15.13 ± 0.11	0.60056	-73.06778	H86-31
SMC0463	0.02	0.500	8.75	2	15.97 ± 0.11	0.66056	-72.92972	H86-56
SMC0465	0.05	0.250	>9.00	3	15.22 ± 0.11	0.66306	-72.98222	H86-57
SMC0466	0.05	0.413	8.95	1	15.29 ± 0.12	0.66889	-72.75833	BS13
SMC0468	0.05	0.338	8.75	2	14.84 ± 0.11	0.68917	-72.98083	B24
SMC0469	0.12	0.213	8.00	3	14.53 ± 0.12	0.70306	-73.73083	B29
SMC0470	0.15	0.238	8.70	1	12.65 ± 0.11	0.71417	-73.17556	BS249
SMC0471	0.05	0.350	8.70	1	16.01 ± 0.12	0.71944	-72.25667	B28
SMC0472	0.05	0.363	8.85	1	14.83 ± 0.11	0.72056	-73.01194	BS17,SOGLE174
SMC0474	0.02	0.425	8.30	2	16.00 ± 0.11	0.74611	-72.89806	BS25
SMC0475	0.02	0.500	>9.00	3	14.14 ± 0.13	0.74556	-74.20167	B37
SMC0476	0.02	0.325	8.75	1	14.39 ± 0.11	0.75306	-72.87528	BS28,SOGLE178
SMC0477	0.20	0.425	8.50	1	13.91 ± 0.10	0.78278	-73.33583	H86-88
SMC0478	0.02	0.175	9.00	3	16.40 ± 0.12	0.78361	-73.74861	BS34
SMC0479	0.02	0.275	8.00	3	15.45 ± 0.12	0.79639	-71.99889	B45

TABLE 7.11. Table 7 continued.

ID	E_{B-V}	R_{app} [ARCMIN]	LOG(τ)	LOG(σ_T)	V MAG	R.A. (J2000.0)	DEC. (J2000.0)	CROSS-ID.
SMC0483	0.02	0.600	7.90	1	13.36 ± 0.11	0.81028	-73.41472	B48,SOGLE49
SMC0486	0.15	0.325	7.40	1	15.99 ± 0.11	0.82889	-72.85389	H86-110
SMC0490	0.25	0.425	7.40	1	12.98 ± 0.11	0.84889	-73.28917	BS40,SOGLE68
SMC0492	0.10	0.525	8.30	1	15.82 ± 0.12	0.85806	-73.69139	BS52
SMC0493	0.10	0.313	8.40	2	13.92 ± 0.11	0.87139	-73.37556	H86-125,SOGLE79
SMC0495	0.07	0.450	8.20	1	14.50 ± 0.11	0.89528	-72.38778	H86-146
SMC0496	0.12	0.413	8.40	1	13.87 ± 0.12	0.89500	-73.35889	BS68,SOGLE95
SMC0501	0.12	0.300	8.10	1	14.25 ± 0.11	0.93361	-72.36389	H86-166
SMC0502	0.02	0.450	>9.00	1	16.91 ± 0.13	0.93722	-74.15667	BS80
SMC0503	0.05	0.325	8.10	1	14.66 ± 0.13	0.95556	-71.17056	HW32
SMC0504	0.05	0.300	8.80	1	15.61 ± 0.11	0.95611	-71.89139	BS265
SMC0505	0.05	0.250	8.70	1	15.07 ± 0.11	0.96056	-73.57972	BS86
SMC0506	0.11	0.325	8.30	1	13.81 ± 0.11	0.96944	-73.58722	B93
SMC0507	0.11	0.175	8.30	3	16.00 ± 0.12	0.97194	-72.21944	BS269
SMC0508	0.08	0.263	8.05	1	14.24 ± 0.12	0.97306	-72.21194	BS270
SMC0509	0.10	0.512	8.60	1	14.23 ± 0.11	0.99972	-73.89500	BS97
SMC0510	0.10	0.425	8.70	2	15.70 ± 0.12	1.01889	-74.07361	HW42
SMC0513	0.02	0.500	9.00	2	15.70 ± 0.14	1.04611	-74.55778	BS108
SMC0514	0.02	0.388	8.35	2	15.21 ± 0.12	1.05806	-71.77278	BS111
SMC0515	0.02	0.350	8.80	1	15.38 ± 0.11	1.05806	-73.04417	BS110
SMC0516	0.02	0.325	8.40	2	15.51 ± 0.11	1.06306	-73.69417	BS113
SMC0517	0.03	0.475	8.20	1	13.50 ± 0.12	1.07000	-73.71583	BS120
SMC0519	0.07	0.487	7.60	3	12.65 ± 0.11	1.07444	-72.18500	BS123
SMC0521	0.02	0.425	8.40	1	14.79 ± 0.12	1.09167	-71.53444	B127
SMC0524	0.07	0.350	8.25	2	14.99 ± 0.11	1.11333	-71.91528	BS136
SMC0525	0.10	0.550	8.20	1	12.98 ± 0.11	1.11722	-72.62167	B129,SOGLE154
SMC0526	0.08	0.275	8.90	2	15.48 ± 0.11	1.13472	-73.52361	B132
SMC0529	0.02	0.338	7.80	2	14.51 ± 0.11	1.15028	-73.20667	B134
SMC0531	0.04	0.300	8.55	1	15.89 ± 0.12	1.19667	-71.41694	BS150
SMC0533	0.03	0.375	>9.00	3	16.59 ± 0.12	1.23306	-71.75306	B151
SMC0534	0.03	0.425	8.20	2	14.81 ± 0.12	1.29139	-73.56917	HW75
SMC0547	0.05	0.475	7.60	2	15.62 ± 0.15	0.46583	-74.00139	HW2
SMC0549	0.01	0.263	9.10	1	17.27 ± 0.13	0.48944	-73.00000	H86-6
SMC0550	0.03	0.650	8.00	3	14.94 ± 0.13	0.49833	-73.70083	HW3
SMC0552	0.03	0.313	8.65	1	15.31 ± 0.12	0.50111	-73.34306	H86-2
SMC0555	0.06	0.350	8.80	2	17.44 ± 0.11	0.58389	-73.03722	BS9
SMC0557	0.05	0.338	8.80	1	16.02 ± 0.11	0.61389	-73.07111	H86-36
SMC0558	0.06	0.287	8.95	1	15.99 ± 0.12	0.67083	-72.76722	BS248
SMC0562	0.01	0.325	8.90	1	15.64 ± 0.12	0.75611	-74.02250	BS29
SMC0565	0.08	0.275	8.20	2	13.35 ± 0.11	0.85833	-73.33556	BS252
SMC0569	0.05	0.325	8.90	2	15.19 ± 0.12	0.89222	-73.35083	BS67
SMC0570	0.07	0.363	7.80	3	14.15 ± 0.11	0.89333	-72.64167	BS257
SMC0571	0.08	0.650	8.80	1	15.57 ± 0.13	0.93444	-74.04500	BS79
SMC0572	0.15	0.350	7.00	3	14.35 ± 0.11	0.95167	-72.54556	BS83
SMC0574	0.08	0.375	8.50	2	15.91 ± 0.11	0.96333	-72.53944	BS87
SMC0575	0.07	0.287	8.10	1	14.18 ± 0.12	0.96639	-72.23444	BS267
SMC0579	0.03	0.500	8.50	1	16.08 ± 0.12	1.06083	-71.77778	HW45
SMC0581	0.03	0.463	7.90	2	14.92 ± 0.13	1.08444	-71.17444	B126
SMC0587	0.05	0.500	8.30	1	16.71 ± 0.11	1.21778	-71.53639	BS155
SMC0588	0.01	0.425	8.60	1	16.16 ± 0.11	1.22167	-71.55778	BS156
SMC0589	0.03	0.388	8.70	1	16.22 ± 0.12	1.23194	-71.46444	BS158
SMC0590	0.01	0.238	8.70	1	17.64 ± 0.12	1.23333	-72.14306	BS277
SMC0591	0.01	0.550	8.30	2	14.40 ± 0.12	1.23472	-72.85500	B148
SMC0592	0.01	0.487	8.75	1	13.42 ± 0.11	1.24639	-72.36417	BS163
SMC0593	0.01	0.400	7.90	3	13.94 ± 0.12	1.24583	-73.38167	BS165
SMC0594	0.05	0.575	8.10	1	13.60 ± 0.12	1.24778	-73.11778	B147
SMC0641	0.07	0.287	8.30	1	14.33 ± 0.12	0.97694	-72.22417	BS271
SMC0642	0.01	0.325	8.00	1	14.16 ± 0.12	0.97694	-72.23389	BS272
SMC0647	0.02	0.263	8.40	1	14.29 ± 0.12	1.01611	-71.59167	SMC-N71,L61-372,SMC-DEM109,MA1234
SMC0650	0.02	0.225	8.40	1	14.75 ± 0.12	1.02528	-71.84639	SMC-N72
SMC0653	0.05	0.425	7.80	1	13.23 ± 0.10	1.04861	-72.41306	B114
SMC0654	0.05	0.325	7.50	2	13.27 ± 0.11	1.05194	-72.10722	SMC-N76B,SMC-DEM120,MA1361

TABLE 7.12. Table 7 continued.

ID	E_{B-V}	R_{app} [ARCMIN]	LOG(τ)	LOG(σ_t)	V MAG	R.A. (J2000.0)	DEC. (J2000.0)	Cross-ID.
SMC0658	0.20	0.175	7.70	3	14.21 ± 0.11	1.08472	-71.99528	SMC-N78B
SMC0659	0.10	0.238	7.20	2	13.27 ± 0.11	1.08556	-71.99611	MA1520
SMC0678	0.12	0.200	7.70	3	13.64 ± 0.12	1.24639	-73.35111	BS166
SMC0681	0.12	0.300	7.80	2	14.12 ± 0.12	0.70583	-73.73556	HW16
SMC0682	0.18	0.225	7.40	2	13.71 ± 0.10	0.76944	-73.39167	H86-78n
SMC0683	0.05	0.213	8.00	1	14.54 ± 0.10	0.76944	-73.39528	H86-78s
SMC0686	0.05	0.200	7.60	1	15.24 ± 0.11	1.25417	-72.33639	BS279
SMC0687	0.05	0.250	8.10	1	14.70 ± 0.12	1.26167	-73.16667	HW72
SMC0689	0.12	0.400	9.00	1	13.39 ± 0.11	0.65611	-73.25778	SOGLE5
SMC0690	0.12	0.400	8.65	2	14.43 ± 0.11	0.65917	-73.17694	SOGLE6
SMC0693	0.20	0.500	8.10	1	12.72 ± 0.11	0.71500	-73.29361	SOGLE15
SMC0697	0.25	0.375	8.60	3	14.51 ± 0.10	0.75917	-73.10750	SOGLE30
SMC0701	0.16	0.500	8.20	3	13.53 ± 0.10	0.86167	-73.22972	B60,SOGLE50
SMC0707	0.22	0.415	7.70	1	12.37 ± 0.11	0.86167	-73.22972	SOGLE72
SMC0708	0.10	0.550	8.15	1	12.74 ± 0.11	0.92861	-72.88000	H86-165,SOGLE105
SMC0709	0.05	0.425	8.30	1	13.88 ± 0.13	0.93583	-73.20611	SOGLE106
SMC0710	0.10	0.425	7.80	1	11.80 ± 0.11	0.95861	-72.26444	L56,SMC-S26,SOGLE109
SMC0712	0.10	0.340	8.10	1	13.83 ± 0.11	0.98472	-72.78667	SOGLE116
SMC0713	0.10	0.375	8.10	1	13.81 ± 0.11	1.01306	-72.92806	SOGLE125
SMC0715	0.10	0.325	8.70	2	14.43 ± 0.11	1.03694	-72.96639	SOGLE132
SMC0716	0.08	0.400	8.80	2	14.18 ± 0.11	1.04194	-72.31833	SOGLE133
SMC0717	0.02	0.720	8.55	1	13.46 ± 0.11	1.05472	-72.74083	SOGLE135
SMC0718	0.15	0.325	8.00	2	13.98 ± 0.10	1.05611	-72.46583	SOGLE136
SMC0719	0.05	0.425	<7.80	1	13.53 ± 0.11	1.05639	-72.65167	B115,SOGLE137
SMC0720	0.05	0.420	7.60	1	13.23 ± 0.11	1.07056	-72.64694	SOGLE140
SMC0721	0.05	0.300	7.70	1	14.15 ± 0.11	1.06806	-72.12083	SOGLE144,SOGLE236
SMC0722	0.02	0.240	7.70	3	13.09 ± 0.11	1.08778	-71.99472	SOGLE146
SMC0723	0.02	0.370	7.60	2	12.79 ± 0.11	1.08556	-71.99583	SOGLE147
SMC0724	0.05	0.475	7.90	3	14.01 ± 0.11	1.08611	-72.60222	SOGLE148
SMC0725	0.02	0.600	8.30	2	13.74 ± 0.11	1.10361	-72.79417	SOGLE151
SMC0727	0.08	0.325	7.80	1	13.64 ± 0.10	1.14361	-72.43917	SOGLE160
SMC0728	0.08	0.400	8.40	2	14.33 ± 0.11	0.64750	-73.37417	HW12,SOGLE163
SMC0730	0.05	0.275	8.70	1	15.36 ± 0.11	0.65333	-73.24611	BS14,SOGLE165
SMC0732	0.07	0.270	8.85	1	14.90 ± 0.11	0.65861	-73.42389	HW13,SOGLE168
SMC0739	0.07	0.175	8.85	1	16.21 ± 0.11	0.75639	-72.92861	SOGLE180
SMC0740	0.08	0.300	8.65	1	14.31 ± 0.11	0.75778	-72.88583	SOGLE181
SMC0754	0.10	0.250	7.80	2	13.21 ± 0.11	0.88806	-72.73417	BS256,SOGLE215
SMC0761	0.05	0.425	7.70	1	13.30 ± 0.10	1.04806	-72.41472	B114,SOGLE234
SMC0763	0.04	0.300	7.90	1	14.15 ± 0.11	1.06806	-72.12083	SOGLE144,SOGLE236

TABLE 7.13. Table 7 continued.

IMPORTANT ABBREVIATIONS

ACS	Advanced Camera for Surveys
AGB	Asymptotic giant branch
AMR	Age-metallicity relation
CMD	Color magnitude diagram
dE	Dwarf elliptical galaxy
dIrr	Dwarf irregular galaxy
dSph	Dwarf spheroidal galaxy
EFF	Elson-Fall-Freeman
GC	Globular cluster
Gyr	Giga year
H	Hydrogen
HB	Horizontal branch
He	Helium
HRC	High Resolution Camera
HST	Hubble Space Telescope
ISM	Interstellar Medium
kpc	Kilo parsec
KS-test	Kolmogorov-Smirnov-test to compare 2 distributions
LMC	Large Magellanic Cloud
LG	Local Group
M_{\odot}	Solar mass
MCs	Magellanic Clouds
MS	Main-sequence
MSTO	Main-sequence turnoff point
MW	Milky Way
NGC	New General Catalogue
RB	Red bump
RC	Red clump
RGB	Red giant branch
SGB	Sub-giant branch
SMC	Small Magellanic Cloud
SFH	Star formation history
SN	Supernova
WFPC2	Wide Field Planetary Camera 2

Bibliography

- Adelberger, E. C. et al. 2002, *Rev. Mod. Phys.*, 70, 1265
- Ahumada, A. V., Clariá, J. J., Bica, E., & Dutra, C. M. 2002, *A&A*, 393, 855
- Alcaino, G., Liller, W., Alvarado, F., Kravtsov, V., Ipatov, A., Samus, N., & Smirnov, O. 1996, *AJ*, 112, 2004
- Alcaino, G. 2003, *A&A*, 407, 919
- Alexander, D. R., & Ferguson, J. W. 1994, *ApJ*, 437, 879
- Alves, D. R., & Sarajedini, A. 1999, *ApJ*, 511, 225
- Alves, D. R. 2004, *New Astronomy Review*, 48, 659
- Angulo, C., et al. 1999, *Nuclear Physics A*, 656, 3
- Ashman, K. M., & Zepf, S. E. 1992, *ApJ*, 384, 50
- Bailyn, C. D. 1995, *ARA&A*, 33, 133
- Bastian, N., & Gieles, M. 2006, *Cluster Disruption: Combining Theory and Observations*, to appear in the ASP Conf. Proc., arXiv:astro-ph/0609669
- Bastian, N., & Goodwin, S. P. 2006, *MNRAS*, 369, L9
- Bedin, L. R., Piotto, G., Anderson, J., Cassisi, S., King, I. R., Momany, Y., & Carraro, G. 2004, *ApJ*, 605, L125
- Bekki, K., Couch, W. J., Beasley, M. A., Forbes, D. A., Chiba, M., & Da Costa, G. S. 2004, *ApJ*, 610, L93
- Bekki, K., & Chiba, M. 2005, *MNRAS*, 356, 680
- Bekki, K., & Stanimirović, S. 2008, *ArXiv e-prints*, 807, arXiv:0807.2102
- Bellazzini, M., Fusi Pecci, F., Ferraro, F. R., Galletti, S., Catelan, M., & Landsman, W. B. 2001, *AJ*, 122, 2569
- Bellazzini, M., Fusi Pecci, F., Messineo, M., Monaco, L., & Rood, R. T. 2002, *AJ*, 123, 1509
- Bertelli, G., Mateo, M., Chiosi, C., & Bressan, A. 1992, *ApJ*, 388, 400
- Bertelli, G., Bressan, A., Chiosi, C., Fagotto, F., & Nasi, E. 1994, *A&AS*, 106, 275
- Bertin, E., & Arnouts, S. 1996, *A&AS*, 117, 393
- Besla, G., Kallivayalil, N., Hernquist, L., Robertson, B., Cox, T. J., van der Marel, R. P., & Alcock, C. 2007, *ApJ*, 668, 949
- Bica, E., Dottori, H., Pastoriza, M. 1986, *A&A*, 156, 261
- Bica, E. L. D., & Schmitt, H. R. 1995, *ApJS*, 101, 41
- Bica, E., & Dutra, C. M. 2000, *AJ*, 119, 1214
- Bica, E., Bonatto, C., Barbuy, B., & Ortolani, S. 2006, *A&A*, 450, 105
- Bica, E., Bonatto, C., Dutra, C., & Santos, J. F. C., Jr 2008a, *MNRAS*, 389, 678
- Bica, E., Santos, J. F. C., Jr., & Schmidt, A. A. 2008b, *MNRAS*, 389, 678
- Binney, J., & Tremaine, S. 1987, *Galactic Dynamics*, Princeton, NJ, Princeton University Press, 1987, 747 p.,
- Binney, J., & Merrifield, M. 1998, *Galactic astronomy / James Binney and Michael Merrifield*. Princeton, NJ : Princeton University Press, 1998. (Princeton series in astrophysics) QB8
- Bonatto, C., & Bica, E. 2008, *A&A*, 479, 741
- Boutloukos, S. G., & Lamers, H. J. G. L. M. 2003, *MNRAS*, 338, 717
- Brown, T. M., et al. 2007, *ApJ*, 658, L95
- Bruck, M. T. 1976, *Occasional Reports of the Royal Observatory Edinburgh*, 1, 1
- Bruhweiler, F. C., Gull, T. R., Kafatos, M., & Sofia, S. 1980, *ApJ*, 238, L27

- Bruzual, G., & Charlot, S. 2003, MNRAS, 344, 1000
- Brüms, C., et al. 2005, A&A, 432, 45
- Buonanno, R., Corsi, C. E. & Fusi Pecci, F. 1989, A&A, 216, 80
- Buonanno, R., Corsi, C. E., Fusi Pecci, F., Richer, H. B., & Fahlman, G. G. 1993, AJ, 105, 184
- Buonanno, R., Corsi, C. E., Buzzoni, A., Cacciari, C., Ferraro, F. R., & Fusi Pecci, F. 1994, A&A, 290, 69
- Buonanno, R., Corsi, C. E., Pulone, L., Fusi Pecci, F., Richer, H. B., & Fahlman, G. G. 1995a, AJ, 109, 663
- Buonanno, R., Corsi, C. E., Fusi Pecci, F., Richer, H. B., & Fahlman, G. G. 1995b, AJ, 109, 650
- Buonanno, R., Corsi, C., Bellazzini, M., Ferraro, F. R., & Fusi Pecci, F. 1997, AJ, 113, 706
- Buonanno, R., Corsi, C. E., Pulone, L., Fusi Pecci, F., & Bellazzini, M. 1998a, A&A, 333, 505
- Buonanno, R., Corsi, C. E., Zinn, R., Fusi Pecci, F., Hardy, E., & Suntzeff, N. B. 1998b, ApJ, 501, L33
- Buonanno, R., Corsi, C. E., Castellani, M., Marconi, G., Fusi Pecci, F., & Zinn, R. 1999, AJ, 118, 1671
- Canuto, V. 1970, ApJ, 159, 641
- Carraro, G., Zinn, R., & Moni Bidin, C. 2007, A&A, 466, 181
- Carraro, G., Vazquez, R. A., & Moitinho, A. 2008, A&A, 482, 777
- Carrera, R., Gallart, C., Aparicio, A., Costa, E., Méndez, R. A., & Noël, N. E. D. 2008, ArXiv e-prints, 806, arXiv:0806.4465
- Carretta, E., & Gratton, R. G. 1997, A&AS, 121, 95
- Carroll, B. W., & Ostlie, D. A. 2006, An introduction to modern astrophysics and cosmology / B. W. Carroll and D. A. Ostlie. 2nd edition. San Francisco: Pearson, Addison-Wesley
- Carvalho, L., Saurin, T., Bica, E., Bonatto, C., & Schmidt, A. 2008, A&A, 485, 71
- Cassisi, S., & Salaris, M. 1997, MNRAS, 285, 593
- Catelan, M., Ferraro, F. R., & Rood, R. T. 2001a, ApJ, 560, 970
- Catelan, M., Bellazzini, M., Landsman, W. B., Ferraro, F. R., Fusi Pecci, F., & Galleti, S. 2001b, AJ, 122, 3171
- Catelan, M. 2005, ArXiv Astrophysics e-prints, arXiv:astro-ph/0507464
- Caughlan, G. R., Fowler, W. A., Harris, M. J., & Zimmerman, B. A. 1985, Atomic Data and Nuclear Data Tables, 32, 197
- Caughlan, G. R., & Fowler, W. A. 1988, Atomic Data and Nuclear Data Tables, 40, 283
- Chaboyer, B., Demarque, P., & Sarajedini, A. 1996a, ApJ, 459, 558
- Chaboyer, B., Demarque, P., Kernan, P. J. & Krauss, L. M. 1996b, Science, 271, 957
- Chaboyer, B., Demarque, P., & Sarajedini, A. 1996c, ApJ, 459, 558
- Chaboyer, B., Demarque, P., Kernan, P. J., Krauss, L. M., & Sarajedini, A. 1996d, MNRAS, 283, 683
- Chiosi, E., Vallenari, A., Held, E. V., Rizzi, L., & Moretti, A. 2006, A&A, 452, 179
- Clementini, G., Held, E. V., Baldacci, L., & Rizzi, L. 2003, ApJ, 588, L85
- Cole, A. A., Tolstoy, E., Gallagher, J. S., III, & Smecker-Hane, T. A. 2005, AJ, 129, 1465
- Cole, A. A., et al. 2007, ApJ, 659, L17
- Cox, J. P., & Giuli, R. T. 1968, Principles of Stellar Structure, Vol. II, New York: Gordon and Breach, 590 pp.
- Crowl, H. H., Sarajedini, A., Piatti, A. E., Geisler, D., Bica, E., Clariá, J. J., & Santos, J. F. C., Jr. 2001, AJ, 122, 220
- Da Costa, G. S., Armandroff, T. E. & Norris, J. E. 1992, AJ, 104, 154
- Da Costa, G. S. & Hatzidimitriou, D. 1998, AJ, 115, 1934
- Da Costa, G. S. 2002, in IAU Symp. 207, Extragalactic Star Clusters, ed. D. Geisler, E. K. Grebel, & D. Minniti (San Francisco: ASP), 83
- D'Antona, F., Bellazzini, M., Caloi, V., Pecci, F. F., Galleti, S., & Rood, R. T. 2005, ApJ, 631, 868
- De Angeli, F., Piotto, G., Cassisi, S., Busso, G., Recio-Blanco, A., Salaris, M., Aparicio, A., & Rosenberg, A. 2005, AJ, 130, 116
- de Grijs, R., & Goodwin, S. P. 2008, MNRAS, 383, 1000

- Dean, J. F., Warren, P. R., & Cousins, A. W. J. 1978, *MNRAS*, 183, 569
- de Vaucouleurs, G., de Vaucouleurs, A., Corwin, H. G., Jr., Buta, R. J., Paturel, G., & Fouque, P. 1991, *Third Reference Catalog of Bright Galaxies*, Vol. 1-3, XII, Springer-Verlag Berlin Heidelberg New York (RC3)
- Dickey, J. M. 1996, *The Minnesota Lectures on Extragalactic Hydrogen*, ed. E. D. Skillman (San Francisco: ASP), 106, p. 187
- Djorgovski, S., & Meylan, G. 1994, *AJ*, 108, 1292
- Dirsch, B., Richtler, T., Geisler, D., Forte, J. C., Bassino, L. P., & Gieren, W. P. 2003, *AJ*, 125, 1908
- Dolphin, A. E., Walker, A. R., Hodge, P. W., Mateo, M., Olszewski, E. W., Schommer, R. A., & Suntzeff, N. B. 2001, *ApJ*, 562, 303
- Dotter, A., Chaboyer, B., Jevremović, D., Baron, E., Ferguson, J. W., Sarajedini, A., & Anderson, J. 2007, *AJ*, 134, 376
- Duc, P.-A., Brinks, E., Springel, V., Pichardo, B., Weilbacher, P., & Mirabel, I. F. 2000, *AJ*, 120, 1238
- Dufton, P. L., Ryans, R. S. I., Thompson, H. M. A., & Street, R. A. 2008, *MNRAS*, 385, 2261
- Durand, D., Hardy, E., Melnick, J. 1984, *AJ*, 283, 552
- Dutra, C., M., Bica, E., Clariá, J. J., Piatti, A. E. 1999, *MNRAS*, 305, 373
- Elmegreen, B. G., & Chiang, W.-H. 1982, *ApJ*, 253, 666
- Elmegreen, B. G., & Efremov, Y. N. 1997, *ApJ*, 480, 235
- Elson, R. A. W., & Fall, S. M. 1985, *AJ*, 299, 211
- Elson, R. A. W., Fall, S. M., & Freeman, K. C. 1987, *ApJ*, 323, 54
- Elson, R. A. W. 1991, *ApJS*, 76, 185
- Ferguson, J. W., Alexander, D. R., Allard, F., Barman, T., Bodnarik, J. G., Hauschildt, P. H., Heffner-Wong, A., & Tamanai, A. 2005, *ApJ*, 623, 585
- Ferraro, I., Ferraro, F. R., Fusi Pecci, F., Corsi, C. E. & Buonanno, R. 1995, *MNRAS*, 275, 1057
- Ferraro, F. R., Sills, A., Rood, R. T., Paltrinieri, B., & Buonanno, R. 2003, *ApJ*, 588, 464
- Fiorentino, G., Contreras, R., Clementini, G., Glatt, K., Sabbi, E., Sirianni, M., Grebel, E., & Gallagher, J. 2008, arXiv:0801.2713
- Forbes, D. A., Brodie, J. P., & Grillmair, C. J. 1997, *AJ*, 113, 1652
- Fulbright, J. P. 2002, *AJ*, 123, 404
- Fusi Pecci, F., Bellazzini, M., Cacciari, C. & Ferraro F. R. 1995, *AJ*, 110, 1664
- Fusi Pecci, F., Bellazzini, M., Ferraro, F. R., Buonanno, R., & Corsi, C. E. 1996, in *ASP Conf. Ser. 92, Formation of the Galactic Halo - Inside and Out*, ed. H. L. Morrison & A. Sarajedini (San Francisco: ASP), 221
- Gallart, C., Zoccali, M., & Aparicio, A. 2005, *ARA&A*, 43, 387
- Gardiner, L. T., Sawa, T., & Fujimoto, M. 1994, *MNRAS*, 266, 567
- Gardiner, L. T., & Noguchi, M. 1996, *MNRAS*, 278, 191
- Gascoigne, S. C. B. 1966, *MNRAS*, 134, 59
- Gascoigne, S. C. B. 1980, *Star clusters*, ed. by J. E. Hesser (Reidel Dordrecht), *IAU Symp.*, 85, 305
- Gebhardt, K., & Kissler-Patig, M. 1999, *AJ*, 118, 1526
- Georgiev, I. Y., Goudfrooij, P., Puzia, T. H., & Hilker, M. 2008, *AJ*, 135, 1858
- Geyer, E. H., Nelles, B., & Hopp, U. 1983, *A&A*, 125, 359
- Gieles, M., Lamers, H. J. G. L. M., & Portegies Zwart, S. F. 2007, *ApJ*, 668, 268
- Gieles, M., & Bastian, N. 2008, *A&A*, 482, 165
- Girardi, L., Chiosi, C., Bertelli, G., & Bressan, A. 1995, *A&A*, 298, 87
- Girardi, L., Bressan, A., Bertelli, G., & Chiosi, C. 2000, *A&AS*, 141, 371
- Girardi, L., & Salaris, M. 2001, *MNRAS*, 323, 109
- Girardi, L., Bertelli, G., Bressan, A., Chiosi, C., Groenewegen, M. A. T., Marigo, P., Salasnich, B., & Weiss, A. 2002, *A&A*, 391, 195
- Girardi, L., et al. 2008, *PASP*, 120, 583
- Glatt, K., et al. 2008a, *AJ*, 135, 1106
- Glatt, K., et al. 2008b, *AJ*, 136, 1703
- Gnedin, O. Y., & Ostriker, J. P. 1997, *ApJ*, 474, 223

- Gonzalez, G., & Wallerstein, G. 1999, *AJ*, 117, 2286
- Goodwin, S. P. 1997, *MNRAS*, 286, L39
- Goodwin, S. P., & Bastian, N. 2006, *MNRAS*, 373, 752
- Goudfrooij, P., Gilmore, D., Whitmore, B. C., & Schweizer, F. 2004, *ApJ*, 613, L121
- Graham, J. A. 1975, *PASP*, 87, 641
- Grebel, E. K., & Richtler, T. 1992, *A&A*, 253, 359
- Grebel, E. K., Roberts, W. J., & Brandner, W. 1996, *A&A*, 311, 470
- Grebel, E. K. 1997, *Reviews in Modern Astronomy*, 10, 27
- Grebel, E. K. 1999, *The Stellar Content of the Local Group*, IAU Symp. 192, eds. P. Whitelock & R. Cannon (San Francisco: ASP), 17
- Grebel, E. K. 2001, *Astrophysics and Space Science Supplement*, 277, 231
- Grebel, E. K., Gallagher, J. S., III, & Harbeck, D. 2003, *AJ*, 125, 1926
- Grebel, E. K., & Gallagher, J. S., III 2004, *ApJ*, 610, L89
- Haft, M., Raffelt, G., & Weiss, A. 1994, *ApJ*, 425, 222
- Han, C., & Ryden, B. S. 1994, *ApJ*, 433, 80
- Harbeck, D., et al. 2001, *AJ*, 122, 3092
- Harbeck, D., Gallagher, J. S., Grebel, E. K., Koch, A., & Zucker, D. B. 2005, *ApJ*, 623, 159
- Harris, W. E. 1996, *AJ*, 112, 1487
- Harris, J., & Zaritsky, D. 2001, *ApJS*, 136, 25
- Harris, W. E., Whitmore, B. C., Karakla, D., Okoń, W., Baum, W. A., Hanes, D. A., & Kavelaars, J. J. 2006, *ApJ*, 636, 90
- Hatzidimitriou, D., Cannon, R. D., & Hawkins, M. R. S. 1993, *MNRAS*, 261, 873
- Held, E. V., Clementini, G., Rizzi, L., Momany, Y., Saviane, I., & Di Fabrizio, L. 2001, *ApJ*, 562, L39
- Hill, V. 1999, *A&A*, 345, 430
- Hill, V., François, P., Spite, M., Primas, F., & Spite, F. 2000, *A&A*, 364, L19
- Hill, A., & Zaritsky, D. 2006, *AJ*, 131, 414
- Hodge, P. W., & Wright, F. W. 1974, *AJ*, 79, 858
- Hodge, P. W. 1983, *ApJ*, 264, 470
- Hodge, P. 1986, *PASP*, 98, 1113
- Hodge, P., & Flower, P. 1987, *PASP*, 99, 734
- Holtzman, J. A., et al. 1997, *AJ*, 113, 656
- Holtzman, J. A. 1999, *AJ*, 118, 2262
- Hubbard, W. B., & Lampe, M. 1969, *ApJS*, 18, 297
- Hunter, D. A., Elmegreen, B. G., Dupuy, T. J., & Mortonson, M. 2003, *AJ*, 126, 1836
- Iben, I. J., & Faulkner, J. 1968, *ApJ*, 153, 101
- Iglesias, C. A., & Rogers, F. J. 1996, *ApJ*, 464, 943
- Imbriani, G., et al. 2004, *A&A*, 420, 625
- Itoh, N., & Kohyama, Y. 1983, *ApJ*, 275, 858
- Itoh, N., Adachi, T., Nakagawa, M., Kohyama, Y., & Munakata, H. 1989, *ApJ*, 339, 354
- Johnson, J. A. Bolte, M., Stetson, P. B., Hesser, J. E., & Somerville, R. S. 1999, *ApJ*, 527, 199
- Johnson, J. A., Bolte, M., Hesser, J. E., Ivans, I. I., & Stetson, P. B. 2004, *Abundances in LMC and SMC Globular Clusters*, eds. A. McWilliam & M. Rauch (Pasadena: Carnegie Observatories)
- Johnson, J. A., Ivans, I. I., & Stetson, P. B. 2006, *ApJ*, 640, 801
- Kallivayalil, N., van der Marel, R. P., Alcock, C., Axelrod, T., Cook, K. H., Drake, A. J., & Geha, M. 2006a, *ApJ*, 638, 772
- Kallivayalil, N., van der Marel, R. P., & Alcock, C. 2006b, *ApJ*, 652, 1213
- Karachentsev, I. D., Karachentseva, V. E., Huchtmeier, W. K., & Makarov, D. I. 2004, *AJ*, 127, 2031
- Kayser, A., Grebel, E. K., Harbeck, D. R., Cole, A. A., Koch, A., Gallagher, J. S., & Da Costa, G. S. 2006, *ArXiv Astrophysics e-prints*, arXiv:astro-ph/0607047
- Kayser, A., Grebel, E. K., Harbeck, D. R., Cole, A. A., Koch, A., Glatt, K., Gallagher, J. S., & Da Costa, G. S. 2007, *Stellar Populations as Building Blocks of Galaxies*, IAU Symp. 241, eds. A.

- Vazdekis & R. F. Peletier (Cambridge: Cambridge University Press), 351
- Keller, S. C., & Wood, P. R. 2006, *ApJ*, 642, 834
- King, I. 1962, *AJ*, 67, 471
- Kippenhahn, R., Thomas, H. C., & Weigert, A. 1965, *Zeitschrift fur Astrophysik*, 61, 241
- Koch, A., Grebel, E. K., Odenkirchen, M., Martínez-Delgado, D., & Caldwell, J. A. R. 2004, *AJ*, 128, 2274
- Koch, A., Wilkinson, M. I., Kleyna, J. T., Gilmore, G. F., Grebel, E. K., Mackey, A. D., Evans, N. W., & Wyse, R. F. G. 2007, *ApJ*, 657, 241
- Koekemoer, A. M., Fruchter, A. S., Hook, R. N., & Hack, W. 2002, in *Hubble after the Installation of the ACS and the NICMOS Cooling System*, eds. S. Arribas, A. Koekemoer & B. Whitmore (Baltimore: STScI), 337
- Kontizas, M., Danezis, E., & Kontizas, E. 1982, *A&AS*, 49, 1
- Kontizas, E., & Kontizas, M. 1983, *A&AS*, 52, 143
- Kontizas, M., Theodossiou, E., & Kontizas, E. 1986, *A&AS*, 65, 207
- Kontizas, E., Kontizas, M., Sedmak, G., & Smareglia, R. 1989, *AJ*, 98, 590
- Kontizas, E., Kontizas, M., Sedmak, G., Smareglia, R., & Dapergolas, A. 1990, *AJ*, 100, 425
- Krauss, L. M., & Chaboyer, B. 2003, *Science*, 299, 65
- Kron, G. E. 1956, *PASP*, 68, 125
- Kroupa, P., & Boily, C. M. 2002, *MNRAS*, 336, 1188
- Kundu, A., & Whitmore, B. C. 2001, *AJ*, 121, 2950
- Kunz, R., Fey, M., Jaeger, M., Mayer, A., Hammer, J. W., Staudt, G., Harissopulos, S., & Paradellis, T. 2002, *ApJ*, 567, 643
- Kurucz, R. L. 1991, *Stellar Atmospheres - Beyond Classical Models*, NATO ASIC Ser. C, Vol. 341, ed. L. Crivellari, I. Hubeny, D. G. Hummer, pp.441-48. Dordrecht: Kluwer
- Lanfranchi, G. A., & Matteucci, F. 2003, *MNRAS*, 345, 71
- Lah, P., Kiss, L. L., & Bedding, T. R. 2005, *MNRAS*, 359, L42
- Lamers, H. J. G. L. M., Gieles, M., & Portegies Zwart, S. F. 2005, *A&A*, 429, 173
- Landre, V., Prantzos, N., Aguer, P., Bogaert, G., Lefebvre, A., & Thibaud, J. P. 1990, *A&A*, 240, 85
- Larsen, S. S., Brodie, J. P., Huchra, J. P., Forbes, D. A., & Grillmair, C. J. 2001, *AJ*, 121, 2974
- Larson, R. B. 1993, in *The Globular Cluster-Galaxy Connection*, ed. G. H. Smith, & J. P. Brodie, ASP Conf. Ser., 48 (ASP: San Francisco), 675
- Lee, Y.-W., Demarque, P., & Zinn, R. 1994, *ApJ*, 423, 248
- Lejeune, T., & Schaerer, D. 2001, *A&A*, 366, 538
- Lindsay, E. M. 1958, *MNRAS*, 118, 172
- McCray, R., & Kafatos, M. 1987, *ApJ*, 317, 190
- Mackey, A. D., & Gilmore, G. F. 2003a, *MNRAS*, 338, 85
- Mackey, A. D., & Gilmore, G. F. 2003b, *MNRAS*, 338, 120
- Mackey, A. D., & Gilmore, G. F. 2003c, *MNRAS*, 340, 175
- Mackey, A. D. & Gilmore, G. F. 2004, *MNRAS*, 352, 153
- Mackey, A. D., Payne, M. J., & Gilmore, G. F. 2006, *MNRAS*, 369, 921
- Mackey, A. D., & Broby Nielsen, P. 2007, *MNRAS*, 379, 151
- Mackey, A. D., Broby Nielsen, P., Ferguson, A. M. N., & Richardson, J. C. 2008, *ApJ*, 681, 17L
- Makarova, L. N., et al. 2002, *A&A*, 396, 473
- Mathewson, D. S., Ford, V. L., & Visvanathan, N. 1986, *ApJ*, 301, 664
- Mathewson, D. S., Ford, V. L., & Visvanathan, N. 1988, *ApJ*, 333, 617
- McConnachie, A., et al. 2008, *ArXiv e-prints*, 806, arXiv:0806.3988
- McKee, C. F., & Ostriker, E. C. 2007, *ARA&A*, 45, 565
- McLaughlin, D. E., Harris, W. E., & Hanes, D. A. 1994, *ApJ*, 422, 486
- McLaughlin, D. E., Secker, J., Harris, W. E., & Geisler, D. 1995, *AJ*, 109, 1033
- McLaughlin, D. E., & van der Marel, R. P. 2005, *ApJS*, 161, 304
- Mengel, S., Lehnert, M. D., Thatte, N., & Genzel, R. 2005, *A&A*, 443, 41
- Mighell, K. J., Sarajedini, A., & Frenck, R. S. 1998a, *AJ*, 116, 2395

- Mighell, K. J., Sarajedini, A., & French, R. S. 1998b, *ApJ*, 494, L189
- Mihalas, D., Hummer, D. G., Mihalas, B. W., & Daepfen, W. 1990, *ApJ*, 350, 300
- Milone, A. P., Bedin, L. R., Piotto, G., & Anderson, J. 2008, arXiv:0810.2558
- Moore, B., Diemand, J., Madau, P., Zemp, M., & Stadel, J. 2006, *MNRAS*, 368, 563
- Mould, J. R., Jensen, J. B., & Da Costa, G. S. 1992, *ApJS*, 82, 489
- Muller, E., Staveley-Smith, L., & Zealey, W. J. 2003, *MNRAS*, 338, 609
- Munakata, H., Kohyama, Y., & Itoh, N. 1985, *ApJ*, 296, 197
- Murai, T., & Fujimoto, M. 1980, *PASJ*, 32, 581
- O'Donnell, J. E. 1994, *ApJ*, 422, 158
- Odenkirchen, M., et al. 2003, *AJ*, 126, 2385
- Olsen, K. A. G., Hodge, P. W., Mateo, M., Olszewski, E. W., Schommer, R. A., Suntzeff, N. B., & Walker, A. R. 1998, *MNRAS*, 300, 665
- Olszewski, E. W. 1987, *AJ*, 93, 565
- Olszewski, E. W., Schommer, R. A., Suntzeff, N. B., & Harris, H. C. 1991, *AJ*, 101, 515
- Olszewski, E. W., Suntzeff, N. B. & Mateo, M. 1996, *ARA&A*, 34, 511
- Pagel, B. E. J., & Tautvaišienė, G. 1998, *MNRAS*, 299, 535
- Pagel, B. E. J., & Tautvaišienė, G. 1999, *Ap&SS*, 265, 461
- Parisi, M. C., Grocholski, A. J., Geisler, D., Sarajedini, A., & Claria, J. J. 2008, ArXiv e-prints, 808, arXiv:0808.0018
- Parmentier, G., & de Grijs, R. 2008, *MNRAS*, 383, 1103
- Parmentier, G., & Fritze, U. 2008, ArXiv e-prints, 809, arXiv:0809.2416
- Piatek, S., Pryor, C., & Olszewski, E. W. 2008, *AJ*, 135, 1024
- Piatti, A. E., Santos, J. F. C., Clariá, J. J., Bica, E., Sarajedini, A. & Geisler, D. 2001, *MNRAS*, 325, 792
- Piatti, A. E., Sarajedini, A., Geisler, D., Seguel, J., & Clark, D. 2005a, *MNRAS*, 358, 1215
- Piatti, A. E., Santos, J. F. C., Jr., Clariá, J. J., Bica, E., Ahumada, A. V., & Parisi, M. C. 2005b, *A&A*, 440, 111
- Piatti, A. E., Sarajedini, A., Geisler, D., Gallart, C., & Wischnjewsky, M. 2007a, *MNRAS*, 382, 1203
- Piatti, A. E., Sarajedini, A., Geisler, D., Gallart, C., & Wischnjewsky, M. 2007b, *MNRAS*, 381, L84
- Piatti, A. E., Sarajedini, A., Geisler, D., Gallart, C., & Wischnjewsky, M. 2007c, *MNRAS*, 382, 1203
- Pietrinferni, A., Cassisi, S., Salaris, M., & Castelli, F. 2004, *AJ*, 612, 168
- Pietrzynski, G., Udalski, A., Kubiak, M., Szymanski, M., Wozniak, P., & Zebrun, K. 1998, *Acta Astronomica*, 48, 175
- Pietrzynski, G., & Udalski, A. 1999, *Acta Astronomica*, 49, 157
- Pietrzynski, G., & Udalski, A. 2000, *Acta Astronomica*, 50, 355
- Pipino, A., Puzia, T. H., & Matteucci, F. 2007, *ApJ*, 665, 295
- Piotto, G., et al. 2005, *ApJ*, 621, 777
- Piotto, G., Bedin, L. R., Anderson, A., King, I. R., Cassisi, S., Milone, A. P., Villanova, S., Pietrinferni, A. & Renzini, A. 2007, *ApJ*, 661, L53
- Piotto, G. 2008, in *XXI Century Challenges for Stellar Evolution*, *Memorie della Societa Astronomica Italiana*, vol. 79/2, eds: S. Cassisi, M. Salaris (arXiv:0801.3175)
- Potekhin, A. Y. 1999, *A&A*, 351, 787
- Prialnik, D. 2000, *An Introduction to the Theory of Stellar Structure and Evolution*, by D. Prialnik. ISBN 052165937X. <http://www.cambridge.org/us/catalogue/catalogue.asp?isbn=052165937X>. Cambridge, UK: Cambridge University Press, 2000.,
- Pritzl, B. J., Armandroff, T. E., Jacoby, G. H., & Da Costa, G. S. 2004, *AJ*, 129, 2232
- Pritzl, B. J., Venn, K. A., & Irwin, M. I. 2005, *AJ*, 130, 2140
- Puzia, T. H., Kissler-Patig, M., Brodie, J. P., & Huchra, J. P. 1999, *AJ*, 118, 2734
- Puzia, T. H., Zepf, S. E., Kissler-Patig, M., Hilker, M., Minniti, D., & Goudfrooij, P. 2002, *A&A*, 391, 453
- Rafelski, M., & Zaritsky, D. 2005, *AJ*, 129, 2701
- Ratnatunga, K. U., & Bahcall, J. N. 1985, *ApJS*, 59, 63

- Rich, R. M., Da Costa, G. S., & Mould, J. R. 1984, *ApJ*, 286, 517
- Rich, R. M., Shara, M., Fall, S. M., & Zurek, D. 2000, *AJ*, 119, 197
- Rogers, F. J., & Iglesias, C. A. 1992, *ApJS*, 79, 507
- Rolleston, W. R. J., Venn, K., Tolstoy, E., & Dufton, P. L. 2003, *A&A*, 400, 21
- Rosenberg, A., Saviane, I., Piotto, G., Aparicio, A. & Zaggia, S. R. 1998, *AJ*, 115, 648
- Rosenberg, A., Saviane, I., Piotto, G., & Aparicio, A. 1999, *AJ*, 118, 2306
- Roy, J.-R., & Kunth, D. 1995, *A&A*, 294, 432
- Rutledge, G. A., Hesser, J. E., Stetson, P. B., Mateo, M., Simard, L., Bolte, M., Friel, E. D., & Copin, Y. 1997, *PASP*, 109, 883
- Sabbi, E., et al. 2007, *AJ*, 133, 44
- Salaris, M., & Girardi, L. 2002a, *MNRAS*, 337, 332
- Salaris, M., & Weiss, A. 2002b, *A&A*, 388, 492
- Salaris, M., & Cassisi, S. 2005, *Evolution of Stars and Stellar Populations*, (New York: Wiley)
- Sandage, A. 1990, *ApJ*, 350, 603
- Sarajedini, A., & Demarque, P. 1990, *ApJ*, 365, 219
- Sarajedini, A., Lee, Y.-W. & Lee, D.-H. 1995, *ApJ*, 450, 712
- Sarajedini, A. 1997, *AJ*, 113, 682
- Sarajedini, A., Geisler, D., Harding, P., & Schommer, R. 1998, *ApJ*, 508, L37
- Sarajedini, A. 1999, *AJ*, 118, 2321
- Sarajedini, A., et al. 2002, *ApJ*, 567, 915
- Sawa, T., Fujimoto, M., & Kumai, Y. 1999, in *IAU Symp. 190: New Views of the Magellanic Clouds*, 499
- Schaller, G., Schaerer, D., Meynet, G., & Maeder, A. 1992, *A&AS*, 96, 269
- Schlegel, D. J., Finkbeiner, D. P., & Davis, M. 1998, *ApJ*, 500, 525
- Schommer, R. A., Suntzeff, N. B., Olszewski, E. W., & Harris, H. C. 1992, *AJ*, 103, 447
- Schweizer, F. 1987, in *Proc. Santa Cruz Summer Workshop in Astronomy & Astrophysics 8, Nearly Normal Galaxies. From the Planck Time to the Present*, ed. S. M. Faber (New York: Springer), 18-25
- Searle, L., & Zinn, R. 1978, *ApJ*, 225, 357
- Shapley, H., & Wilson, H. H. 1925, *Harvard College Observatory Circular*, 276, 1
- Shara, M. M., Fall, S. M., Rich, R. M., & Zurek, D. 1998, *AJ*, 508, 570
- Sharina, M. E., Puzia, T. H., & Makarov, D. I. 2005, *A&A*, 442, 85
- Shetrone, M. D., Côté, P., & Sargent, W. L. W. 2001, *ApJ*, 548, 592
- Sirianni, M., et al. 2005, *PASP*, 117, 1049
- Smecker-Hane, T. A., Cole, A. A., Gallagher, J. S., III, & Stetson, P. B. 2002, *ApJ*, 566, 239
- Sparke, L. S., & Gallagher, J. S., III 2000, *Galaxies in the Universe*, by Linda S. Sparke and John S. Gallagher, III, pp. 416. ISBN 0521592410. Cambridge, UK: Cambridge University Press
- Stanimirović, S., Staveley-Smith, L., Dickey, J. M., Sault, R. J., & Snowden, S. L. 1999, *MNRAS*, 302, 417
- Stanimirović, S., Staveley-Smith, L., & Jones, P. A. 2004, *ApJ*, 604, 176
- Staveley-Smith, L., Sault, R. J., Hatzidimitriou, D., Kesteven, M. J., & McConnell, D. 1997, *MNRAS*, 289, 225
- Storm, J., Carney, B. W., Gieren, W. P., Fouqué, P., Latham, D. W., & Fry, A. M. 2004, *A&A*, 415, 531
- Straniero, O. 1988, *A&AS*, 76, 157
- Stryker, L. L., Da Costa, G. S. & Mould, J. R. 1985, *ApJ*, 298, 544
- Suntzeff, N. B., Olszewski, E. W. & Walker, A. R. 1992, *AJ*, 104, 1743
- Tamura, N., Sharples, R. M., Arimoto, N., Onodera, M., Ohta, K., & Yamada, Y. 2006, *MNRAS*, 373, 588
- Thackeray, A. D. 1958, *MNRAS*, 118, 117
- Tomisaka, K., Habe, A., & Ikeuchi, S. 1981, *Ap&SS*, 78, 273
- Trager, S. C., King, I. R., & Djorgovski, S. 1995, *AJ*, 109, 218

- Udalski, A., Szymanski, M., Kubiak, M., Pietrzynski, G., Wozniak, P., & Zebrun, K. 1998a, *Acta Astronomica*, 48, 147
- Udalski, A. 1998b, *Acta Astronomica*, 48, 383
- VandenBerg, D. A., Bolte, M., & Stetson, P. B. 1990, *AJ*, 100, 445
- VandenBerg, D. A. 2000a, *ApJS*, 129, 315
- VandenBerg, D. A., Swenson, F. J., Rogers, F. J., Iglesias, C. A., & Alexander, D. R. 2000b, *ApJ*, 532, 430
- van den Bergh, S. 2008, *AJ*, 135, 1731
- Venn, K. A. 1999, *ApJ*, 518, 405
- Walker, A. R. 1991, *The Magellanic Clouds*, IAU Symp. 148, eds. R. Haynes & D. Milne (Los Angeles: ASP), 307
- Walker, A. R. 1992, *ApJ*, 390, L81
- Weaver, T. A., & Woosley, S. E. 1993, *Phys. Rep.*, 227, 65
- White, R. E., & Shawl, S. J. 1987, *ApJ*, 317, 246
- Whitmore, B. C., & Schweizer, F. 1995, *AJ*, 109, 960
- Whitmore, B. C. 1999, in *IAU Symp. 186, Galaxy Interactions at Low and High Redshift*, ed. J. E. Barnes & D. B. Sanders (Dordrecht: Kluwer), 251
- Yoshizawa, A.M. & Noguchi, M. 2003, *MNRAS*, 339, 1135
- Zaritsky, D., Harris, J., Thompson, I. B., Grebel, E. K., & Massey, P. 2002, *AJ*, 123, 855
- Zhang, Q., Fall, S. M., & Whitmore, B. C. 2001, *ApJ*, 561, 727
- Zinn, R., & West, M. J. 1984, *ApJS*, 55, 45
- Zinn, R. 1993, *The Globular Cluster-Galaxy Connection*, ASP Conf. Ser. 48, eds. Smith, G. H. & Brodie, J. P. (San Francisco: ASP), 302

Acknowledgements

Sowohl während meiner Zeit in Basel, als auch in Heidelberg war ich Teil eines wunderbaren Teams bei welchem ich mich hiermit gerne bedanken möchte:

Allen voran möchte ich mich bei meiner Doktormama Eva Grebel bedanken, dass ich unter ihrer Führung meine Doktorarbeit schreiben durfte. Auch in der schwierigen Zeit als unser Instiut von der Schliessung bedroht wurde und wir nach Heidelberg umzogen, war sie immer da um mich mit wissenschaftlichem und freundschaftlichem Rat zu unterstützen.

My warmest thanks go to "uncle" Jay Gallagher for his hospitality and becoming my second supervisor in difficult times. I enjoyed my visits in Madison enormously and I am very grateful for our not only scientific, but also political and economical discussions. Of course I also have to thank him for introducing me to "*Steep & Brew*"!

E riesigs Danggschön goht an min lanjöhriige BüroKumpel Katrin Jordi. Ohni sie wäri nie sowit cho. Ihri Geduld, ihri Fründschaft und ihr offnigs Ohr in allne Läbenslage hän mi immer unglaublich unterstützt. Messi Katrin!!!

Mein besonderer Danke gilt Thorsten Lisker für die zahllosen fruchtbaren Gespräche, seine Geduld und die Möglichkeit mehr über *blue cores* zu erfahren und im Zuge dieser Zusammenarbeit zum VLT nach Chile zu fahren. *Live long and prosper!*

Weiter bedanke ich mich ganz fest bei Andreas Koch, der allfällige Fragen immer schnell und umfassend beantwortet hat. *Metal for ever!*

Ich möchte Daniel Harbeck sehr herzlich danken für seine kostbaren Kommentare und für meinen Aufenthalt in Tuscon, Arizona.

Herzlich danken möchte ich Gernot Burkhardt, der sich die Zeit genommen hat Teile meiner Doktorarbeit aufmerksam durchzulesen.

Meinen Eltern, Hugo & Maria Glatt-Matt, gebührt mein besonderer Dank, da sie mich bei all meinen Entscheidungen unterstützt haben. Meiner Schwester, Sabine Glatt, danke ich für ihre Ehrlichkeit und ihre Vielseitigkeit für die ich sie immer bewundert habe.

Ich möchte mich für die Unterstützung des Schweizerischen Nationalfonds und der Schweizerischen Gesellschaft für Astrophysik und Astronomie bedanken, die mir diese Doktorarbeit, sowie die Teilnahme an Konferenzen und wissenschaftlichen Meetings ermöglicht haben.

I'm very grateful for the wonderful and supporting team that I was working with during my time in Basel and Heidelberg and whose members have accompanied and beared me for such a long time: Dr. Karin Ammon, Prof. Dr. Bruno Binggeli, Denija Crnojevic, Dr. Peter Engelmeier, Raoul Haschke, Dr. Shoko Jin, Baybars Külebi, Dr. Wolfgang Löffler, Johannes Ludwig, Dr. Sarah Martell, Xiaoying Pang, Dr. Stefano Pasetto, Dr. Niranjan Sambhus, Dr. Pieter Westera, and last but not least Prof. Dr. Gustav Andreas Tammann. You all are responsible for the wonderful atmosphere I was working in.

Schliesslich und endlich muss ich mich bei den drei wahren Helden meines Büros bedanken: Elchi, Nasi und Ägypto-Hypo. Die gute Laune, welche diese drei immer verbreiteten, die Aufmunterung in Stresssituationen, sowie ihre aufopfernde Hilfe beim Schreiben der Doktorarbeit (" ,m") waren eine immense Hilfe. Manchmal wurde jedoch ein ziemlicher Radau veranstaltet und das montägliche Aufräumen des Büros nach einem von ihnen durchgefeierten Wochenende war für Katrin und mich nicht immer einfach. Trotzdem werden diese drei Rabauken immer einen besonderen Platz in meinem Herzen besitzen. Sollten Katrin und ich uns jemals in einem Altersheim wiedersehen, so werden diese drei sicher auch mit von der Partie sein. Vielleicht ist dann auch Nihli-Pink wieder mit dabei, welcher das Dream Team verlassen musste und mit Tatjana in Basel geblieben ist.



CURRICULUM VITAE

Stand vom 12.Juli 2009

Persönliche Daten:

Name Katharina Glatt
Anschrift Magdenerstrasse 20
CH-4310 Rheinfelden
Email kaglatt@yahoo.com
Telefon +49 (0) 61 831 37 23 (privat)
+49 (0) 61 267 38 22 (office)
+41 (0) 79 718 20 33 (mobil)
Geburtsdatum 31.10.1978
Geburtsort Rheinfelden/Schweiz
Staatangehörigkeit Schweiz
Familienstand ledig



Ausbildung:

seit 10/2005 Wissenschaftliche Mitarbeiterin
Departement Physik, Universität Basel, Schweiz und
Astronomisches Rechen-Institut, Universität Heidelberg, Deutschland

10/2005 – 02/2009 Promotion im Fach Astronomie
Departement Physik, Universität Basel, Schweiz
Abschluss: Dr. phil. nat.
Abschlussnote: **magna cum laude**
Titel der Arbeit: *Star Clusters as Age Tracers of the Age-Metallicity
Relation of the Small Magellanic Cloud*
Betreuer: Eva K. Grebel, Jay Gallagher

09/2000 – 10/2005 Studium der Physik und Astronomie
Departement Physik, Universität Basel, Schweiz
Abschluss: Diplom Physikerin
Abschlussnote: **5.3**
Titel der Diplomarbeit: *Sternhaufen in der Grossen Magellanschen Wolke*

10/1999 – 08/2000 Studium der Physik und Astronomie
ETH Zürich, Schweiz

1998 – 1999 Zwischenjahr: Küchenhilfe im Kantonsspital Basel

1994 – 1998 Gymnasium Muttenz, Schweiz
Abschluss: Matur (Typus: E)

Berufspraktische Erfahrung:

1999-2006 20% Stelle als Schalterangestellte bei der Migros Bank Basel (Samstagskassier).
In den Semesterferien habe ich ausserdem im Notenhandel, der Hypotheken- und der Firmenkundenabteilung gearbeitet.

Sprachen:

Deutsch	Muttersprache
Englisch	flüssig in Sprache und Schrift: 2005-2009 während der Diplomarbeit und der Promotion täglich in Anwendung, 2006/2007 jeweils 3 Monate an der University of Wisconsin, USA
Französisch	Schulkenntnisse
Spanisch	Grundkenntnisse
Norwegisch	Grundkenntnisse
Russisch	Anfängerkenntnisse

Aktivitäten während der Ausbildung:

Veröffentlichungen	13 Veröffentlichungen in internationalen Fachzeitschriften, 6 davon als Erstautorin
Präsentationen	zahlreiche Präsentationen auf internationalen Konferenzen und an in- und ausländischen Universitäten
Auslandsaufenthalte	Astronomy Department, University of Wisconsin, Madison, USA, Januar 14, - Januar 26, 2008 April 10, - Juni 26, 2007 April 18, - März 3, 2006 mit Prof. J. Gallagher Cerro Paranal, Chile: ESO VLT + FORS2 März 15, - März 24, 2007 National Optical Astronomy Observatory, Tuscon, USA, Mai 7, - Mai 12, 2007 mit Dr. Daniel Harbeck INAF - Osservatorio Astronomica di Bologna, Bologna, Italien, Januar 29, - Februar 7, 2007, mit Prof. M. Tosi Space Telescope Science Institute, Baltimore, Maryland, USA, Mai 4, - Juli 28, 2006 mit Dr. M. Sirianni & Dr. E. Sabbi
Lehre	2006/7: Tutor für Astronomie, Physikalisches Institut der Universität Basel

EDV-Kenntnisse:

Betriebssysteme	UNIX/Linux, Mac OSX, Windows
Wissenschaftliches Programmieren/Scripting	Unix shell Skripte, MATLAB, C++, Latex, Supermongo, IRAF und CL scripting

Persönliche Interessen:

Reisen und Natur**Sport**

Schwimmen, Wandern, Radfahren, Nordic Walking

Musik

Geige, Bratsche, Guggen, Grüttrabe Geischer Rhyfælde

Kultur

Bücher, Kino, Museumsbesuche

Publikationsliste

Referierte Publikationen

- **Glatt, K.**; Grebel, E.K.; Gallagher, J.S.; Nota, A.; Sabbi, E.; Sirianni, M.; Clementini, G.; Tosi, M.; Harbeck, D.; Koch, A.; Kayser, A. 2008, *Structural Parameters of Seven SMC Intermediate-Age and Old Star Clusters*, (submitted to the Astronomical Journal)
- **Glatt, K.**; Gallagher, J.S.; Grebel, E.K.; Nota, A.; Sabbi, E.; Sirianni, M.; Clementini, G.; Tosi, M.; Harbeck, D.; Koch, A.; Kayser, A. 2008, *An Accurate Age Determination for Six SMC Star Clusters with HST/ACS*, The Astronomical Journal, 136, 1703
- **Glatt, K.**; Gallagher, J.S.; Grebel, E.K.; Nota, A.; Sabbi, E.; Sirianni, M.; Clementini, G.; Tosi, M.; Harbeck, D.; Koch, A.; Cracraft, M. 2008, *An Accurate Age Determination for the SMC Star Cluster NGC121 with HST/ACS*, The Astronomical Journal, 135, 1106
- Lisker, T.; Grebel, E.K.; Binggeli, B.; **Glatt, K.** 2007, *Virgo Cluster Early-Type Dwarf Galaxies with the Sloan Digital Sky Survey. III. Subpopulations: Distributions, Shapes, Origins*, The Astrophysical Journal, 660, 1186
- Lisker, T.; **Glatt, K.**; Westera, P.; Grebel, E.K. 2006, *Virgo Cluster Early-Type Dwarf Galaxies with the Sloan Digital Sky Survey. II. Early-Type Dwarfs with Central Star Formation*, The Astronomical Journal 132, 2432

Andere Publikationen

- Sabbi, E.; Tosi, M.; Gallagher, J.S.; Anderson, J.; Nota, A.; Grebel, E.K.; Cignoni, A.A.; Da Costa G.S.; Harbeck, D.; **Glatt, K.**; & Marconi, M. 2009, *Star Formation History of the SMS: six HST/ASC fields*, (submitted to the Astronomical Journal)
- Tosi, M.; Gallagher, J.S.; Sabbi, E.; **Glatt, K.**; Grebel, E.K.; Christian, C.; Cignoni, M.; Clementini, G.; Cole, A.; Da Costa, G.; Harbeck, D.; Marconi, M.; Meixner, M.; Nota, A.; Sirianni, M.; Smecker-Hane, T. 2008 *SMC in space and time: a project to study the evolution of the prototype interacting late-type Dwarf Galaxy*, IAU Symposium, 255, (in press)
- Fiorentino, G.; Contreras, R.; Clementini, G.; **Glatt, K.**; Sabbi, E.; Sirianni, M.; Grebel, E.K.; Gallagher, J.S. 2008, *Detection of new variable stars in the SMC cluster NGC 121*, Mem. S. A. It. Vol. 79, 3
- **Glatt, K.**; Gallagher, J.S.; Grebel, E.K.; Nota, A.; Sabbi, E.; Sirianni, M.; Clementini, G.; Tosi, M.; Harbeck, D.; Koch, A.; Cracraft, M. 2007, AAS Meeting, 2008
- Lisker, T.; Grebel, E.K.; Binggeli, B.; Vodicka, M.; **Glatt, K.**; Westera, P. 2007, *The many faces of early-type dwarf galaxies*, IAU Symposium, 241, 409
- Kayser, A.; Grebel, E.K.; Harbeck, D.R.; Cole, A.A.; Koch, A.; **Glatt, K.**; Gallagher, J.S.; da Costa, G.S. 2007, *A spectroscopy-based Age-Metallicity Relation of the SMC*, IAU Symposium, 241, 351

- Lisker, T.; **Glatt, K.**; Westera, P.; Grebel, E.K. 2007, *The Last Stages of Star Formation in dEs?*, IAU Symposium, 235, 317
- **Glatt, K.**; Grebel, E. K.; Koch, A. *Star clusters in the Large Magellanic Cloud*, 2005, Astron. Nachr., 326, 651-652

Publikationen in Vorbereitung

- **Glatt, K.**; Grebel, E.K.; Koch, A. 2009, *Ages Determination of Young SMC Star Clusters*, (to be submitted)
- Tosi, M.; Gallagher, J.S.; Sabbi, E.; **Glatt, K.**; Grebel, E.K.; Christian, C.; Cignoni, M.; Clementini, G.; Cole, A.; Da Costa, G.; Harbeck, D.; Marconi, M.; Meixner, M.; Nota, A.; Sirianni, M.; Smecker-Hane, T. 2009
SMC in space and time: a project to study the evolution of the prototype interacting late-type Dwarf Galaxy, (to be submitted to the Astronomical Journal 2009)
- Kayser, A.; Grebel, E.K.; Harbeck, D.; Cole, A.A.; Koch, A.; Glatt, K.; Gallagher, J.S.; Da Costa, G.S. 2009, *New Clues on the Chemical Evolution of the Small Magellanic Cloud from Star Clusters*, (to be submitted)

Teilnahmen und Vorträge an Konferenzen und Kolloquien

Konferenzen

- 10/2008 Konferenz: General Assembly of the SGAA, Zürich, Schweiz
- 01/2008 Konferenz: 211th AAS Meeting, Austin, TX, USA
Poster: *Old and Intermediate-Age Star Clusters in the SMC*
- 10/2007 Konferenz: General Assembly of the SGAA, Bern, Schweiz
- 03/2007 Saas Fee Advanced Lectures, Mürren, Schweiz
Thema: *The Origin of the Galaxy and the Local Group*
- 04/2007 Saas Fee Advanced Lectures, Les Diablerets, Schweiz
Thema: *First Light in the Universe*
- 03/2006 Konferenz: Globular Clusters - Guides to Galaxies, Concepcion, Chile
Poster: *Star Clusters in the SMC*
- 11/2005 Rhine Stellar Dynamics Network Meeting (Hoher List Observatory, Deutschland)
- 09/2005 Jährliches Treffen der Astronomischen Gesellschaft, Köln, Deutschland
Poster: *Star Clusters in the LMC*

Kolloquien

- 11/2007 Zentrum für Astronomie (Heidelberg/D)
Star clusters in the Small Magellanic Cloud
- 10/2007 SGAA-Tagung, Bern, CH *Star clusters in the Small Magellanic Cloud*
- 06/2007 University of Wisconsin (Madison/USA) *Star clusters in the Small Magellanic Cloud*
- 03/2007 NOAO, Tuscon, AZ, USA *Star clusters in the Small Magellanic Cloud*

Referenzen:

- Prof. Dr. Eva K. Grebel
Astronomisches Rechen-Institut
Mönchhofstrasse 12-14
D-69120 Heidelberg
Germany
grebel@ari.uni-heidelberg.de
- Prof. Dr. John S. Gallagher
Department of Astronomy
University of Wisconsin
475 North Charter Street
Madison, WI 53706-1582
USA
jsg@astro.wisc.edu
- Iris Mondelli
Personalchefin Migros Bank Basel
Aeschenvorstadt 72
4002 Basel
Schweiz
iris.mondelli@migrosbank.ch

